ISSN: 1715-9997

Canadian Journal of pure & applied sciences

an International Journal

SENRA
Academic Publishers
Burnaby, British Columbia

The Canadian Journal of Pure and Applied Sciences (CJPAS-ISSN 1715-9997) is a peer reviewed multi-disciplinary specialist journal aimed at promoting research worldwide in Agricultural Sciences, Biological Sciences, Chemical Sciences, Computer and Mathematical Sciences, Engineering, Environmental Sciences, Medicine and Physics (all subjects).

Editorial Office
E-mail: editor@cjpas.ca
: editor@cjpas.net

SENRA Academic Publishers
7845 15th Street Burnaby
British Columbia V3N 3A3 Canada
www.cjpas.net
E-mail: senra@cjpas.ca

Print ISSN 1715-9997
Online ISSN 1920-3853

Volume 4, Number 1
Feb 2010

CANADIAN JOURNAL OF PURE AND APPLIED SCIENCES

Board of Editorial Advisors

Canadian Journal of pure & applied sciences

Volume 4, Number 1
February 2010

CONTENTS

LIFE SCIENCES

PHYSICAL SCIENCES

SENRA Academic Publishers, Burnaby, British Columbia
Vol. 4, No. 1, pp. 1003-1009, 2010
ISSN: 1715-9997

Canadian Journal of pure&applied sciences

INFLUENCE OF COPPER AND COBALT STRESS ON MEMBRANE FLUIDITY OF *STACHYBOTRYS CHARTARUM*

*Mohamed A Hefnawy[1], Mohamed I Ali[2] and Salah Abdul-Ghany[1]
[1]Department of Botany, Faculty of Science, Menoufia University, Shebin El-kom
[2]Department of Botany, Faculty of Science, Cairo University, Giza, Egypt

ABSTRACT

The growth of *S. chartarum* markedly decreased with elevated concentrations of Cu and Co in the growth medium. Total lipids and proteins in isolated plasma membrane were increased at 400mg Cu or Col^{-1} and decreased above this concentration while, carbohydrates markedly increased with elevated concentrations of both metals. The total amount of detected phospholipids in the membranes was decreased at 800mg l^{-1} of both metal ions. However, Phosphatidyl ethanolamine and phosphatidyl glycerol showed an increase at this concentration. Moreover, most of the detected fatty acids (C16:0, C16:1, C18:1 and C18:2) in the plasma membrane were increased with elevated concentrations of both metals to approximately 1.5-2 fold higher than in the control except C16:1 at 800mg Cu l^{-1} highly increased to 24.9 times higher than in the control. Whereas, C16:0 was the only fatty acid which decreased at 800mg Col^{-1}. The unsaturation index of fatty acids at 400mg l^{-1} exhibited a slight decrease while, at this concentration the fluorescence polarization value of DPH in the plasma membranes markedly increased. On the other hand, at 800mgl^{-1} the unsaturation index was increased while, fluorescence polarization value of DPH markedly decreased. This refers that the membrane at 400mgl^{-1} might be less fluid and at 800mgl^{-1} more fluid and cannot able to control the entry of toxic metals.

Keywords: *S. chartarum*, lipid composition, membrane fluidity, copper and cobalt stress.

INTRODUCTION

Living organisms are exposed in nature to heavy metals, commonly present in their ionized species. These ions exert diverse toxic effects on microorganisms. Metal exposure selects and maintains microbial variants able to tolerate their harmful effects. Varied and efficient metal resistance mechanisms have been identified in diverse species of bacteria, fungi and protists (Cervantes *et al*., 2006).

Fungal survival and tolerance to toxic metals depend on intrinsic biochemical and structural properties, physiological and genetical adaptation (Gadd and Griffiths, 1978; Gadd, 1993). Heavy metals (cobalt, nickel, cadmium and chromium) at different concentrations were toxic and inhibited the growth of *Rhizoctonia solani* in both solid and liquid media. Total inhibition was observed upon treatment with 1000ppm of each tested heavy metal. Nickel was the most toxic to the fungus, followed by cadmium, cobalt and chromium (Singh and Singh, 2002).

Metal resistant fungi belonged to the genera *Aspergillus, Penicillium, Alternaria, Geotrichum, Fusarium, Rhizopus, Monilia* and *Trichoderma* were isolated from wastewater-treated soil. The minimum inhibitory concentration (MIC) for Cd, Ni, Cr, Cu and Co was determined. The MIC ranged from 0.2-0.5mg l^{-1} for Cd, followed by Ni 0.1-4mg l^{-1}, Cr 0.3-7mg l^{-1}, Cu 0.6-9mg l^{-1} and Co 0.1-5mg l^{-1} (Zafar *et al*., 2007).

Much work has been done on the biosorbtion of heavy metals by fungal cell wall and also the chemical changes that have happened to cell wall in presence of toxic metals. However, there is spare information on changes in chemical composition of plasma membrane of fungi cultured in toxic concentrations of metals. The effect of some metals such as aluminum on membrane proteins and lipids of plants has been described (Haug and Caldwell, 1985). Total proteins and sugars in isolated plasma membrane of *Penicillium expansum* were slightly increased at 20mg Se l^{-1} and decreased above this concentration. Whereas, total lipids was increased at higher concentrations of selenium in the growth medium. The fungus responds to selenium stress by increasing the biosynthesis of phospholipids, fatty acids and unsaturation index of fatty acids in plasma membrane (Hefnawy, 2002). Addition of different levels of lead, zinc and barium acetates in the growth medium of *Neurospora indica* [*Tilletia indica*], revealed that lead acetate and zinc acetate inhibited the synthesis of both lipids and proteins in the membrane, while barium acetate only had a mild effect. Among phosphatides, phosphatidic acid, phosphatidyl inositol and phosphatidyl ethanolamine progressively accumulated while phosphatidyl choline declined by increasing the concentrations of all 3 metal salts (Sushma *et al*., 1996).

*Corresponding author email: Hef3000@yahoo.com

The changes in phospholipids composition and its content may play a crucial role in fungal tolerance to toxic metals. It was observed that cells of *Microsporum gypseum* grown in the presence of Ca exhibited increased content of phospholipids and enhances its synthesis. The rise in the levels of phospholipids was found to be due to increased synthesis of Fatty acids. Moreover, the changes in the phospholipids composition increased the membrane fluidity (Giri *et al*., 1995).

Aluminum (10mM Al^{3+}) stimulated mycelial growth and increased membrane fluidity of *Lactarius piperatus* (Zel and Gogala, 1989). While, in *Amanita muscaria*, aluminum (10mM Al^{3+}) inhibited mycelial growth and decreased membrane fluidity (Zel *et al*., 1993). Hefnawy (1999) found that copper stress increased total lipids and proteins in plasma membrane of *Fusarium oxysporium* and decreased its fluidity.

This work aims at investigation of the changes in the plasma membrane composition as a response of toxic metals and also gives light on the role of the membrane in metal tolerance by fungal cells.

MATERIALS AND METHODS

Organism and culture conditions. *S. chartarum* was isolated from heavy metal contaminated Egyptian soil, on Dox agar medium amended with 400 mgl^{-1} $CuSO_4.5H_2O$ and $CoSO_4.7H_2O$ separately. The isolated fungus was identified according to Domsch *et al*. (1980).

The fungus was grown on Dox liquid medium supplemented separately with different concentrations of Cu^{2+} and Co^{2+} (0, 200, 400, 600, 800, 1000mgl^{-1}), incubating in an orbital incubating shaker (120 rpm) at 28ºC ± 2ºC for 7 days. The mycelial pellets were harvested, washed several times with distilled water and blotted with tissue paper prior to biochemical analysis. While, for dry mass determination the harvested pellets after washing were dried at 85ºC until constant weight was obtained.

Isolation of plasma membrane enriched fraction. The method was based on that described by Touze-Soluet *et al.* (1990) and Umura and Yoshida (1983). A known weight of fresh mycelia was ground using a Bead- Beater homogenizer with 0.5 mm diameter glass beads in 0.05M Tris-HCl (pH 7.4) buffer containing 0.25 M sucrose, 1mM EDTA, 0.1 mM $MgCl_2$, chloramphenicol (200mgl^{-1}) and cycloheximide (200mgl^{-1}). The homogenate were subjected to differential centrifugation (1000g for 10 minutes, 6000g for 15minutes and 105000 g for 20minutes), using a Beckman centrifuge (L5 50 SW 28) Ultra-Centrifuge. The homogenate was fractionated, the supernatant was retained and re-centrifuged. After the final centrifugation the pellet containing the crude microsomal fraction was washed once with a 10mM phosphate buffer (pH 7.4) containing 0.25M sucrose and 30mM NaCl, and resedimented by recentrifugation at 105000g for 20minutes. The washed microsomes were subjected to phase partition for further purification by placing it on the top of polyethylene glycol (PEG 400) and dextran T500 (5.6:5.6% W/W), mixed and centrifuged at 400g for 3min. The upper layer was removed and placed on top of freshly prepared lower phase and centrifuged as before. The upper layer from the second centrifugation was plasma membrane enriched fraction.

Extraction and estimation of total lipids, proteins and carbohydrates. Lipids were extracted from plasma membrane enriched fraction by chloroform methanol mixture (2:1, v/v) at 40ºC with occasional manual stirring for 1h. The extract was filtered and the non-lipid materials were removed by adding 1ml of 0.88% (w/v) KCl (Hunter and Rose, 1972), the upper phase was removed and discarded. While, the lower phase was evaporated to dryness under nitrogen and the total amount of lipids were determined, using the method of Barnes and Blackstock (1973). Protein was determined according to the methods of Lowry *et al*. (1951), after extraction with 1 M NaOH. Sugar determination was carried out using the anthrone technique as described by Umbriet *et al*. (1959).

Phospholipids determination. Phospholipids were extracted from plasma membrane enriched fraction obtained from (1g fresh weight) according to the method of Bligh and Dayer (1959) as detailed by Kates (1972).

Polar lipids were resolved by thin layer chromatography (TLC) on silica gel plates or commercially prepared plates in two dimension chromatography according to the method described by Nichols (1964). The spots were revealed by iodine vapor and outlined with a pencil. The iodine was removed in a vacuo and the chromatogram sprayed with fine mist of cupric acetate (3% w/v) in sulphric acid (8% w/v). The Plates were sprayed until translucent and then heated to approximately 170ºC for 30min. Phospholipids spots appeared dark brown and were identified by comparing R_F values with standard phospholipids. The content of each spot was measured calorimetrically according to the method of Miller (1985).

Fatty acid methyl ester analysis. Lipids were extracted from plasma membrane enriched fraction obtained from 1 g fresh weight mycelium in chloroform/ methanol (2:1), the extract was removed by shaking with 0.2 volumes of distilled water. The chloroform layer was separated by centrifugation or allowing the tubes to stand over night, this layer was then removed and washed once with methanol / water (1:1, v/v). Butylated hydroxytoluene (0.005% w/v) was added as antioxidant. The chloroform was then evaporated under nitrogen. Lipids were converted into fatty acid methyl esters by adding 5 ml of

methylation reagent (conc. H_2SO_4: toluene: methanol 1: 10:20 by vol.) to each sample. The mixture was refluxed for 1 h at 90ºC. The resulting fatty acid methyl esters were extracted with hexane and analyzed by GLC using a (Chrompack CP 9000 with a column packed with CP-Sil-58 Support Chromsorb WHP). The degree of unsaturation was expressed as unsaturation index, defined by Kates and Hagen (1964) as : Δ mol^{-1} = 1x (% monoenes)/100 +2 x (% dienes)/100 + 3 x (% trienes)/100

Measurement of plasma membrane fluidity. To monitor the fluidity of lipid regions in the plasma membrane1, 6-diphenyl 1, 3, 5- hexatriene (DPH) was used as a probe (Shinitzky and Inbar, 1976; Shinitzky and Barenholz, 1978). A solution of 2mM DPH in tetrahydrofuran was diluted 1000 fold with 50mM Tris/ HCl pH (7.4) containing NaCl (0.9%, w/v). Freshly prepared membranes with 3 ml of diluted DPH were incubated for 30minutes at 30ºC. Fluorescence polarization measurements were made in a Fluorescence Spectrophlorometer F-2000 at 30ºC. DPH was excited at 340nm while the emission was measured at 440nm. The degree of fluorescence polarization (P), was calculated, according to the equation P = (I//- I$^{\perp}$) / (I//+ I$^{\perp}$), where I//and I$^{\perp}$ are the fluorescence emission intensities measured at right angles to the excitation beam, with the analyzer polarization axis parallel to, and perpendicular to, the polarization axis of the polarizer respectively.

RESULTS

Growth, Total carbohydrate, protein and lipid content in plasma membrane. *S. chartarum* was able to tolerate elevated concentrations of Cu and Co in the growth medium up to 800mg l^{-1}. The dry mass was markedly decreased with increasing both metal ion concentrations in the medium. At 800mg Cu and Co l^{-1} the growth was decreased to approximately 85%. Total carbohydrate content in isolated plasma membrane were markedly increased with elevate concentrations of both metal ions. Where, total protein and lipid were increased at 400mgl^{-1} and decreased at 800mg^{-1} comparing with the control (Table 1).

Polar phospholipids composition in plasma membranes. It is clear that phospholipid composition of *S. chartarum* membranes markedly changed in the presence of both Cu and Co in the growth medium. Some of the detected phospholipids slightly increased in the presence of 800mg Cu l^{-1} except that phosphatidyl coline, cardiolipin and phosphatidic acid showed a decrease at this concentration (Table 2 and Fig. 1). At 800mg Cu l^{-1}, phosphatidyl ethanolamine and phosphatidyl glycerol showed an increase to approximately 2.4, 1.1 fold

Table 1. Dry mass (mg/50ml culture medium), total carbohydrate, protein and lipid (mg g^{-1} fresh mycelium weight) in plasma membrane fraction obtained from 1 gm fresh weight of *Stachybotrys chartarum* grown in the presence of different concentrations of heavy metals. ± SE of three determinations.

Metals	Conc. (mgl^{-1})	Dry mass	Carbohydrate	Protein	Lipids
Cu	0.0	167±3.4	3.9±0.4	2.2±0.4	2.9±0.22
	400	112±4.1	4.4±0.5	3.3±0.2	3.9±0.4
	800	24±0.5	7.4±0.6	2.0±0.1	2.3±0.42
Co	0.0	160±4.2	3.4±0.4	2.4±0.2	2.8±0.2
	400	57±2.4	3.8±0.6	2.8±0.1	3.2±0.32
	800	21±0.2	6.3±0.5	1.4±0.12	2.2±0.4

Table 2. Phospholipid composition in plasma membrane fraction of *Stachybotrys chartarum* grown in absence and in the presence of 800mg Cu or Co l^{-1}.

Phospholipids	control	Cu	Co
PI	152.1±4.2	180.4±4.6	ND
PS	82.2±2.6	155.2±4.2	ND
PC	320.6±8.4	230.4±6.8	250.5±11.4
PE	45.2±2.2	110.4±8.2	87.7±4.2
PG	135.5±4.6	148.4±4.5	160.5±6.2
CL	175±5.6	trace	ND
CMH	170.5±8.4	165±4.4	175.6±4.8
PA	250.4±10.6	128.6±4.6	ND
Total	1331.5	1118.4	674.3

Data are expressed as nM of phospholipids/ gm of fresh weight mycelium ±SE of three investigations. PI, phosphtidyl inositol; PS, phosphatidyl serine; PC, phosphatidyl choline; PE, phosphatidyl ethanol amine; PG, phosphatidyl glycerol; CL, cardiolipin; CMH, ceramide monohexoside; PA, phosphatidic acid. ND, not detected.

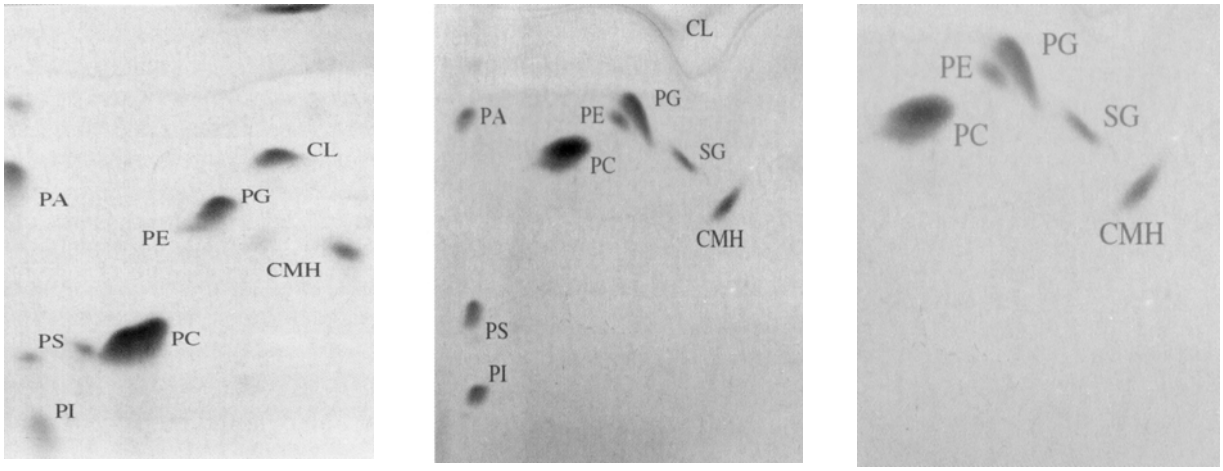

(A) (B) (C)

Fig. 1. Two-dimensional TLC plates of polar lipid classes of *Stachybotrys chartarum* (A) control; (B) 800mg Cu l^{-1} and (C) 800mg Co l^{-1}. (PA, phosphatidic acid; PC, phosphatidyl choline; PE, phosphatidyl ethanolamine; PG, phosphatidyl glycerol; PI, Phosphatidyl inositol; PS, phosphatidyl serine; CMH, ceramide monohexoside; SG, steryl glycoside; CL, cardiolipin).

Table 3. Fatty acids composition of total lipids extracted from isolated plasma membrane fraction obtained from 1 g fresh weight of *Stachybotrys chartarum* grown at different concentrations of Cu and Co.

Metal	Conc. mgl^{-1}	Fatty acids						
		C14:0	C16:0	C16:1	C18:1	C18:2	C18:3	Δmol^{-1}
Cu	0.0	0.4±0.02 (0.66%)	17.6±0.8 (29.28%)	1.4±0.2 (2.32%)	25.8±1.2 (42.92%)	14.9±0.3 (24.79%)	Tr.	0.948
	400	0.6±0.1 (0.7%)	23.8±1.4 (27.93%)	14.9±0.6 (17.48%)	28.7±3.3 (33.68%)	15.8±0.5 (18.54%)	1.4±0.02 (1.6%)	0.929
	800	3.8±0.2 (2.37%)	34.6±4.2 (21.6%)	34.9±0.8 (21.6%)	50.2±2.4 (31.4%)	33.7±1.5 (21.06%)	2.8±0.22 (1.75%)	1.001
Co	0.0	Tr.	17.9±1.1 (25.21%)	14.8±1.2 (20.84%)	27.9±1.4 (39.29%)	9.0±0.8 (12.67%)	1.4±0.12 (1.97%)	0.914
	400	0.4±0.1 (0.36%)	38±3.1 (35.05%)	9±0.3 (8.3%)	34.6±2.5 (31.91%)	23.9±2.2 (22.04%)	2.5±0.24 (2.3%)	0.912
	800	Tr.	15.4±3.4 (14.3%)	27.9±0.4 (25.9%)	41.4±4.2 (38.47%)	20.9±0.6 (19.4%)	2.0±0.21 (1.8%)	1.115

Data are expressed as μg g^{-1} fresh weight mycelium. ± SE of three investigations. Values in parenthesis are percentages.

respectively higher than in the control while, at 800mg Col l^{-1}, they also increased to approximately 1.9, 1.2 fold respectively higher than in the control. It was also observed that phospholipids biosynthesis was highly affected by the presence of Co in the growth medium where phosphatidyl inositol, phosphatidyl serine, cardiolipin and phosphatidic acid not detected at 800mg Col l^{-1}. In general, the total amount of phospholipids in the plasma membrane decreased at 800mg Cu or Co l l^{-1}.

Fatty acids composition of pure plasma membrane. Most of the detected fatty acids in the plasma membrane of *S. chartarum* showed a marked increase with increasing both Cu and Co concentrations in the growth medium. Fatty acids with carbon number (16:0, 16:1, 18:1 and 18:2) were the major detected fatty acid in membranes and represented the highest percentage. At 800mg Cu l^{-1}, C18:1 represented the highest amount while C16:1 represented the highest increase to approximately 24.9 times higher than in the control. While, at 800mg Co l^{-1}, C16:1 and C18:1 showed the highest amount and increased to approximately 1.8 and 1.5 times higher than in the control. Whereas, C16:0 increased at 400mg and decreased at 800mg Co l^{-1} (Table 3).

The unsaturation index of the identified fatty acids of the plasma membrane of *S. chartarum* decreased at 400mg Cu or Co l^{-1}. This may indicate that the plasma membrane may become less fluid or more rigid at this concentration. While, at 800mg Cu or Co l^{-1} it markedly increased over

the control. This may refer that the membrane is more fluid or less rigid than the control and the membrane may becomes unable to control the entry of metal ions into the cells.

Plasma membrane fluidity. The plasma membranes were labeled with a fluorescence probe (DPH), to measure the fluorescence polarization of isolated plasma membrane of *S. chartarum*. P value (fluorescence polarization) of DPH in the plasma membrane markedly increased at 400 mg Cu or Co l^{-1}. While, it sharply decreased at 800mg Cu or Co l^{-1} (Table 4). The result indicated that the plasma membranes might be more rigid or less fluid at 400mg Cu or Co $l^{-1}$and might aid in controlling entry of metal ions to the fungal cells. While, it might be more fluid at 800mg Cu or Co l^{-1} and therefore, the membrane may be disordered and can not retard the entry of metal ions across the membrane.

Table 4. Fluorescence polarization values (P) of isolated plasma membrane of *Stachybotrys chartarum* grown at different concentrations of Cu and Co. ± SE of three investigations.

Heavy Metals	Conc. (mgl^{-1})	Fluorescence polarization (P)
Cu	0.0	0.12±0.02
	400	0.24±0.05
	800	0.08±0.01
Co	0.0	0.1±0.01
	400	0.35±0.06
	800	0.06±0.04

DISCUSSION

Copper and cobalt were toxic to *S. chartarum.* However, it tolerated both metal ions up to a concentration of 800mg l^{-1}. In other work, it was found that *Streptomyces anulatus* and *Penicillium citrinum* were able to tolerate copper in the growth medium up to 1000 and 400 mgl l^{-1} respectively (Azab and Hefnawy, 1999). Other fungal species such as *Thelephora terrestris* proved high tolerance to Cu at 100 and 500ppm in agar plates (Jones and Muehlchen, 1994). Toxic effects include the blocking of functional groups of biologically important molecules (e.g. enzymes and transport system for nutrients), denaturation and inactivation of enzymes and disruption of cellular organellar membrane integrity (Ochiai, 1987).

Total carbohydrates content in *S. chartarum* plasma membrane were increased with increasing Cu and Co concentrations in the growth medium whereas, total proteins and lipids slightly increased at 400mg l^{-1} and decreased at 800mg l^{-1}. The increasing amount of lipid and carbohydrate and proteins at 400mg l^{-1} may important in maintenance of the membrane integrity and retard the entry of toxic metals. Much work has been done on the role of protein, especially metallothioneine in metal tolerant fungi and yeasts whereas, lipids have been neglected in this regard. The role of lipids in fungi are generally not well understood. Phospholipids are important structural components of biological membranes. Some phospholipids have been implicated in the active transport of ions across membranes and are also essential for the activity of some membrane bound enzymes (Weete, 1980). There is a direct relationship between lipid composition and metal tolerance by fungi. Most phospholipids in *S. chartarum* were increased under Cu and Co stress. Phosphatidyl ethanolamine and phosphatidyl glycerol exhibited an increase at 800mg Cu or Co l^{-1}. Similar observation was also found in *Fusarium oxysporum* grown under Cu stress, total phospholipids of the whole mycelium were increased with increasing copper concentrations in the growth medium. Phosphatidyl ethanolamine and cardiolipin showed the greatest increase under copper stress (Hefnawy, 1996). It was also reported that *Microsporum gypseum* respond to calcium stress by increasing the content of phospholipids due to increased fatty acids biosynthesis (Giri *et al*., 1995). Phosphatidyl ethanolamine showed the greatest increase in plasma membrane of *Fusarium oxysporum* with increased copper in the medium, it increased at 600mg Cu l^{-1} to approximately 2 fold higher than in the relevant control (Hefnawy, 1999). It was also found that Phosphatidyl ethanolamine in the plasma membranes of *Penicillium expansum* grown under selenium stress increased at 200mg Se l^{-1} to approximately 2.37 times higher than in the control (Hefnawy, 2002).

The tested fungus may respond to the effect of copper and cobalt stress by increased synthesis of some phospholipids which are membrane components and these may be important in repairing the injured membranes and might be one of the mechanisms involved in heavy metal tolerance by fungi. It was also reported that 300mg Zn l^{-1} inhibit the growth of *Candida utilis* and at this concentration the content of protein, RNA, DNA and polysaccharides fell while, lipid content increased (Andreeva *et al*., 1983).

It has been found that environmental conditions affect the fatty acid compositions of the fungal cells. The detected fatty acids in the plasma membranes of *S. chartarum* were markedly increased with increasing Cu and Co in growth medium. Fatty acids C16:0, C16:1 C18:1 and C18:2 were the major detected fatty acids in the plasma membranes and represented the highest amounts and percentages. Quite similar observation was also found in the whole mycelium of *Fusarium oxysporum* grown under copper stress, the major fatty acids detected were oleic acid (C18:1) and palmitic acid (C16:0) (Hefnawy, 1996). It was also observed that most of the detected fatty acids increased in plasma membranes of *Fusarium oxysporum* at all tested copper concentrations. The highest amounts

were obtained at 200mg Cu l^{-1} and the major fatty acids at this concentration were C18:1 and C17:0 (Hefnawy, 1999). Quite similar observations were also found in membranes of *Penicillium expansum* grown under different concentrations of Selenium. The major detected fatty acids were C16:0, C18:1, C18:2 which showed the greatest increase in the presence of 100mg Se l l^{-1} in the growth medium (Hefnawy, 2002). In contrast, to these observations it was reported that phospholipids fatty acids composition of soil contaminated with copper was decreased consistently with increasing levels of copper (Yao *et al*., 2006).

The unsaturation index of fatty acids in plasma membranes of *S. chartarum* showed a decrease at 400mgl^{-1} Cu and Co while, it increased at 800mg. These observations may indicate that the membrane is less fluid or more rigid at 400mg and more fluid at 800mg of Cu and Co. To confirm these observations the plasma membrane fluidity was measured by labeling the membranes by DPH and the fluorescence polarization values (P) were measured. The P value was record to be increased at 400 mg and sharply decreased at 800mg Cu and Co concentration in the medium. This indicates that the membrane fluidity decreased and increased at both concentrations respectively. This result was in contrast to that found by Zel and Gogala (1989), they found that aluminum stimulated mycelial growth of *Lactarius piperatus* and increased membrane fluidity. Whereas, (Zel *et al*., 1993) reported that aluminum stress decreased membrane fluidity of *Amanita muscari*. Also, Hefnawy (1999) found that copper stress decreased membrane fluidity of a copper tolerant strain of *Fusarium oxysporum*. It was also found that the membranes of *Penicillium expansum* becomes less fluid or more rigid under selenium stress (Hefnawy, 2002). The rigidity of plasma membranes of *S. chartarum* might aid in retarding the flux of metal ions into the fungal cells and enable the fungi to tolerate Cu and Co in the growth medium to a certain limit.

In conclusion, fungal cells may respond to heavy metal stress by increasing the synthesis of some membrane phospholipids and its fatty acids acyl chain. Decreasing the unsaturation index of the membrane fatty acids indicate that the membrane becomes less fluid or more rigid, this may enable the organism to tolerate toxic metals to certain concentration and might be one of the tolerance mechanisms to heavy metals stress by filamentous fungi.

REFERENCES

Andreeva, EA., Biriuk, AI., Khovrychev, MP. and Robotnova, IL. 1983. Chemical composition and morphological changes in the cells in a chemostat *Candida utilis* culture inhibited by zinc ions. Mikrobiologiia (52):924-928.

Azab, AM. and Hefnawy, MA. 1999. Copper metal-protein in *Streptomyces anulatus* and *Penicillium citrenium*. J. Union Arab Biol, Cairo. B- Microbiol. and Viruses. 8:403-415.

Barnes, H. and Blackstock, J. 1973. Estimation of lipids in marine animals and tissue: detailed investigation of total lipids. J. Exp. Mar. Biol. Ecol. (12):101-118

Bligh, EG. and Dayer, WJ. 1959. A rapid method of total lipid extraction and purification. Can. J. Biochem. Physiol. (37):911-917.

Cervantes, C., Espino-Saldana, AE., Acevedo-Aguilar, F., Leon-Rodriguez, IL., Rivera-Cano, ME., Avila-Rodríguez, M., Wróbel-Kaczmarczyk, K., Wrobel-Zasada, K., Gutierrez-Corona, JF., Rodriguez-Zavala, JS. and Moreno-Sánchez, R. 2006. Microbial interactions with heavy metals. Rev Latinoam Microbiol. (48):203-210.

Domsch, KH., Game, W. and Anderson, T H. 1980. Compendium of soil fungi. Academic Press, London.

Gadd, GM. 1993. Interactions of fungi with toxic metals. New Phytologist (124):25-60.

Gadd, GM. and Griffiths, AJ. 1978. Microorganisms and heavy metal toxicity. Microbiol. Ecology (4**)**:303-317.

Giri, S., Bindra, A. and Khuller, GK. 1995. Calcium induced alterations in structural and functional role of phospholipids in *Microsporum gypseum*. Indian J. Biochem. Biophys. (32):166-169.

Haug, AA. and Caldwell, CR. 1985. Aluminum toxicity in plants: The role of the root plasma membrane and calmodulin. In Frontiers of Membrane Research in Agriculture. Eds. John, JBST., Berlin, F. and Jackson, PC. Rowman and Allenheld, Ottawa. 359-381.

Hefnawy, MA. 1996. Phospholipids and fatty acids composition in copper tolerant *Fusarium oxysporum*. Proceedings of the First International Conference on Fungi: Hopes & Challenges Cairo, 2-5 Sept. (1):21-30.

Hefnawy, MA. 1999. Effect of copper stress on membrane fluidity and lipid composition of a copper tolerant strain of *Fusarium oxysporium*. Egyptian J. Microbiol. (34):201-215.

Hefnawy, MA. 2002. Influence of Selenium Stress on Plasma Membrane Fluidity and Lipid Composition of *penicillium expansum*. Egypt J Microbiol. (37):117-133.

Jones, D. and Muehlchen, A. 1994. Effect of the potentially toxic metals, aluminium, zinc and copper on ectomycorrhizal fungi. J. Environ Sci. (29):949-966.

Kates, M. 1972. Techniques of Lipidology: Isolation, Analysis and Identification of Lipids. North-Holland Publishing Co. Amsterdam 349-352.

Kates, M. and Hagen, PO. 1964. Influence of temperature on fatty acid composition of psychrophilic and mesophilic Serratia species. Can J. of Biochem. (22):481-488.

Lowery, OH., Rosebrough, NJ., Furr, AL. and Randell, J. 1951. Protein measurement with folin phenol reagents. J Biol. Chem. (193):265-275.

Miller, KJ. 1985. Effect of temperature and sodium chloride concentration on the phospholipids and fatty acid composition of a halotolerant *Planococcus* sp. J of Bacteriol. (162):263-270.

Nichols, BW. 1964. Separation of plant phospholipids and glycolipids. In: New Biochemical Separations. Eds. James, AT. and Morris, LJ. Van Nostrad, London, U.K. 221-237.

Ochiai, EI. 1987. General principles of biochemistry of the elements. Plenum press, New York, USA.

Shinitzky, M. and Inbar, M. 1976. Microviscosity parameters and protein mobility in biological membranes. Biochim Et Biophys Acta. (433): 133-149.

Shinitzky, M. and Barenholz, Y. 1978. Fluidity parameters of lipid regions determined by fluorescence polarization. Biochim Et Biophys Acta. (515):367-394.

Singh, LP. and Singh, S. 2002. In vitro growth of fungus Rhizoctonia solani in relation to heavy metals treatment. Bionotes. (4**)**:101-104.

Sushma, P., Arneja, JS. and Phutela, S. 1996. Effect of heavy metal ions on the synthesis of membrane lipids and proteins in *Neovossia indica*. Indian J Microbiol. (36):227-228.

Touze- Soleut, JM., Weet, JD., Sancholle, M., Rami, J. and Dargent, R. 1990. Influence of biotin on lipid composition of plasma membranes of Hyphomyces chlorines. Biochem. Cell Biol. (68):138-144.

Umbriet, RH., Burris, J F., Stauffer, PP., Cohen, WJ., Johnse, GA., Leepage, UR. and Patler Scheider, WC. 1959. Manometric techniques, a manual describing methods applicable to the study of tissue metabolism. Burgess publishing company. p. 239.

Umura, M. and Yoshida, S. 1983. Isolation and identification of plasma membrane from light-grown winter rye seedlings (Secale cereale L. ov Puma). Plant Physiol. (73):586-596.

Weete, JD. 1980. Lipid Biochemistry of fungi and Other Organisms. Plenum Press. New York, NY, USA.

Yao, HY., Liu, YY., Xue, D. and Huang, CY. 2006. Effect of copper on phospholipids fatty acid composition of microbial communities in two red soils. J. environ Sci. (18):503-509.

Zafar, S., Aqil, F. and Ahmad, I. 2007. Metal tolerance and biosorption potential of filamentous fungi isolated from metal contaminated agricultural soil. Bioresour. Technol. (98):2557-2561.

Zel, J. and Gogala, N. 1989. Influence of aluminum on mycorrhiza. Aric Ecosyst Environ. (28):569.

Zel, J., Svetek, J., Crne, H. and Schara, M. 1993. Effects of aluminum on membrane fluidity of mycorrhizal fungus *Amanita muscaria*. Physiol Plantarum. (89):172-176.

Received: June 15, 2009; Accepted: Jan 6, 2010

SENRA Academic Publishers, Burnaby, British Columbia
Vol. 4, No. 1, pp. 1011-1019, 2010
ISSN: 1715-9997

Canadian Journal of pure&applied sciences

GROWTH AND HEAVY METAL UPTAKE IN *B. JUNCEA* L. SEEDLINGS AS AFFECTED BY BINARY INTERACTIONS BETWEEN NICKEL AND OTHER HEAVY METALS

Rupinder Kaur, Renu Bhardwaj and *Ashwani K Thukral
Department of Botanical and Environmental Sciences
Guru Nanak Dev University, Amritsar, 143005, India

ABSTRACT

Interactive effects of Ni in binary combinations with other heavy metals (Mn, Co, Cu, Cr and Zn) were investigated on the growth of *B. juncea* L. seedlings. There was a decline in germination percentage, root and shoot lengths and dry weight of the seedlings with increase in concentrations of the metals in the growth medium. Multiple regression interaction models revealed that in all the binary combinations of Ni with other heavy metals, both the metals were detrimental to the seedling growth. However, the metals in combinations mutually decreased the toxicity of each other. Zn acted antagonistic to Ni and increased the germination percentage of *B. juncea* seeds. Zn and Mn were accumulated to the extent of 0.531 and 0.445 mg g^{-1} dw respectively at 100mg l^{-1} concentration of these metals, whereas the lowest uptake was observed for Ni (0.135 mg g^{-1} dw) at a concentration of 100 mg l^{-1}. In binary combinations, (Ni+Cr), (Ni+Mn), (Ni+Co), (Ni+Cu) and (Ni+Zn), both the metals mutually inhibited the uptake of each other.

Keywords: Heavy metal interactions, synergism, antagonism, Mn, Co, Cu, Cr and Zn.

INTRODUCTION

Industrial wastes impregnated with heavy metals, besides being detrimental to the health of man and animals, extensively damage the living and natural resources of the environment. Heavy metals like Cd, Cu, Pb, Cr, Ni, Hg *etc*. pose a major occupational and environmental hazard, as they are non-biodegradable and have a long biological half life (Barbier *et al.,* 2005). Global awareness of underlying detriments of heavy metals in the environment has gained considerable public attention and brought monumental changes in societies to curtail environmental pollution through pollution control technologies. Phytoremediation is an innovative green clean technology involving the use of plants for pollution abatement. Researchers have been successfully delineating the molecular mechanism of metal uptake and the physiology of metal tolerance by hyperaccumulator species used in phytoremediation (Kochian, 2000). It is well known that in natural environment, contamination by a single pollutant rarely occurs. Metal smelting, mining, manufacturing processes and industrial wastes more often result in contamination of environment with a mixture of toxic metals. Recently, it is more widely realized that examining the effects of heavy metals in various combinations is more representative than single metal studies (Krupa *et al*., 2002). Earlier studies have revealed that the combined metal toxicity of pollutants present in multiple contaminated sites, directly or indirectly affects the phytoremediation potential of hyperaccumulators. It was reported that during the uptake of heavy metals in the plants, there are various positive or negative interactions occurring among different metal ions (Martin-Prevel, 1987), which influence the rate of uptake, transfer, accumulation and their subsequent translocation in the plant body. Therefore, thorough understanding of metal interactions is necessary to streamline the technique of phytoremediation to be used successfully for the remediation of soils impregnated with a variety of pollutants at varying concentrations.

B. juncea is considered as a model system to investigate the biochemistry and physiology of hyperaccumulation of various metal ions (Ebbs and Kochian, 1998). Dushenkov *et al.* (1997) reported *B. juncea* as being particularly effective in sorbing divalent cations of toxic metals from soil solution. Since interactions between two or more metal ions have consistently been shown to result in their altered behavior and mode of action inside the plant body, the mechanism of metal interactions needs to be fully explored for improving the practical effectiveness of phytoremediation according to the current changes in the contaminated environment. Some heavy metals like Zn, Mn, Ni, Co and Cu are essential in small quantities for the metabolic activities of the organisms, but these prove to be toxic beyond certain limits. Ni is considered as an essential micronutrient for plants, but is strongly phytotoxic at higher concentrations (Boominathan and Doran, 2002). Ni induced deactivation of proteins involved in antioxidative enzymes and membrane function has been reported in numerous plants. The present investigation was therefore undertaken to study

*Corresponding author email: akthukral@rediffmail.com

the interactive effects of Ni in binary combinations with Cr, Mn, Co, Cu and Zn on the growth and metal uptake in *B. juncea* seedlings.

MATERIALS AND METHODS

Certified seeds of *B. juncea* L. *cv* PBR 91 were procured from Punjab Agricultural University, Ludhiana, India. The seeds were surface sterilized with 0.1% $HgCl_2$ solution, washed and rinsed thoroughly with distilled water. These seeds were then cultured in Petri plates containing different concentrations of heavy metals, single or in binary combinations of Ni.

i) Single metal treatments –0, 25, 50 and 100mg l^{-1} of each metal (Cr, Mn, Ni, Co, Cu and Zn).
ii) Binary treatments – Ni treatments in combination with other metals at 0, 25, 50 and 100mg l^{-1}.

The surface sterilized seeds were germinated on Whatman filter paper No. 1, lined inside (9cm diameter) sterilized Petri plates containing 5 ml of aqueous solutions of heavy metals. The solutions were prepared using AR grade K_2CrO_4, $MnSO_4.H_2O$, $NiSO_4.6H_2O$, $CoCl_2.6H_2O$, $CuSO_4.5H_2O$ and $ZnSO_4.7H_2O$ procured from Sigma aldrich, Qualigens and Loba chemie. Sterilized seeds grown in double distilled water served as the controls. Petri plates in triplicates, each containing 50 seeds were kept at 25± 0.5 °C temperature and 16 h/8 h dark and light photo period (1700 Lux), for 7 days of the growth period. The rate of germination was recorded daily for 7 days and root and shoot lengths were measured. Thereafter, the harvested seedlings were washed thoroughly with double distilled water and kept in oven for 48 h at 80ºC, and the dry weights were recorded. The dried seedlings of different treatments were ground and digested in H_2SO_4: HNO_3: $HClO_4$ (1:5:1) digestion mixture (Allen, 1976). The samples were diluted with double distilled water and filtered. The concentrations of Cr, Mn, Ni, Co, Cu and Zn were determined using atomic absorption spectrophotometer (Model 6200, Shimadzu, Japan). All the analyses were carried out in triplicate, and the data was analyzed for descriptive statistics, standard error, ANOVA, Tukey's multiple comparison test, multiple regression and correlation, and β-regression coefficients (Sokal and Rholf, 1981; Bailey, 1995). Self coded software developed in MS-Excel was used. The multiple regression interaction model used for binary combinations was $Y = a + b_1X_1 + b_2X_2 + b_3X_1X_2$

Where, Y is the studied parameter, X_1 and X_2 are metals in binary combinations, b_1 and b_2 are partial regression coefficients due to the effects of X_1 and X_2 respectively, and b_3 is the partial regression coefficient due to interaction between X_1 and X_2. β_1 and β_2 are the unitless β-regression coefficients due to X_1 and X_2. Metal interaction was interpreted as described in table 1.

Table 1. Interaction in terms of β regression coefficients.

Variables			Interaction
X_1	X_2	$X_1 X_2$	
β regression coefficients			
β_1	β_2	β_3	
+	+	+	Synergistic
-	-	-	Synergistic
+	+	-	Antagonistic
-	-	+	Antagonistic
+	-	+	Mixed: X_1 antagonistic to X_2, but X_2 synergistic to X_1
+	-	-	Mixed: X_1 synergistic to X_2, but X_2 antagonistic to X_1
+/-	+/-	0	Additive

Table 2. IC_{50} values of different heavy metals calculated on the basis of inhibition of root length of *B. juncea* seedlings.

Metals	IC_{50} (mg l^{-1})
Cr	0.524
Mn	73.739
Ni	28.881
Co	47.803
Cu	0.563
Zn	77.882

RESULTS AND DISSCUSSION

Individual and combined effects of Ni with Zn, Mn, Co, Cu and Cr on the germination parameters of *B. juncea* are presented in figure 1 and tables 2-5. It was observed that there was a reduction in germination percentage with increase in metal concentration in the medium. Maximum reduction was observed in case of Cr, followed by Ni. With increase in Ni concentration in the medium from 25 to 100 mg g^{-1}, germination decreased to 65%, compared to the control (94.6%). Multiple regression equations for combinations, Ni+Zn, Ni+Mn, Ni+Co, Ni+Cu and Ni+Cr showed that both the metals in binary combinations exerted negative influence on the percentage germination as indicated by their negative β-regression coefficients. However, better correlations were obtained when an interaction model was used (Table 4). Additions of Cr, Mn, Co, Cu and Zn even at low concentration of 25 mg l^{-1} further declined the germination percentage with respect to the control. Maximum decline in germination (41%) was caused at (Ni25+Cr25) mg l^{-1} followed by (Ni25+Cu25) mg l^{-1} The interactive effects of all the binary combinations of Ni were observed to be negative except for Ni+Zn, thereby implying that Mn, Co, Cu and Cr are synergistic to Ni in further retarding the percentage germination of *Brassica* seeds. 2-way ANOVA for germination percentage of *B. juncea* seeds for Ni and

Table 3. Percentage change in root length of *B. juncea* seedlings grown in binary combinations of Ni with other heavy metals, with respect to Ni controls.

Metal conc.	Ni in solution (mg l^{-1})			
(mg l^{-1})	0	25	50	100
	% Change with respect to control			
Control 0	0	0	0	0
Cr	Ni + Cr			
25	-86.9	-62.5	-56.9	-3.9
50	-91.3	-78.2	-70.3	-44.7
100	-98.6	-93.8	-95.0	-80.3
Mn	Ni + Mn			
25	-18.787	42.773	29.707	182.895
50	-26.541	73.156	67.782	305.263
100	-61.133	12.389	16.736	201.316
Co	Ni + Co			
25	-39.463	-4.720	27.197	165.789
50	-58.549	-15.339	0.418	153.947
100	-77.137	-39.823	-28.033	135.526
Cu	Ni + Cu			
25	-83.8	-29.5	-29.5	123.7
50	-93.8	-44.5	-28.3	63.2
100	-97.7	-56.6	-54.9	25.0
Zn	Ni + Zn			
25	-12.1	85.5	143.9	509.2
50	-26.8	84.1	135.9	581.6
100	-58.2	20.1	47.7	255.3

Table 4. Multiple regression with interaction for different parameters of *B. juncea* grown in binary combinations of Ni (X_1, mg l^{-1}) and other metals (X_2 mg l^{-1}).

Treatments	Mutiple regression with interaction								r	β regression coefficients		
	Germination percentage (Y)									(β_1)	(β_2)	Interaction (β_3)
Ni+Cr	Y=	80.7	-0.25	X_1-	0.46	X_2-	$1.7x10^{-4}$	X_1X_2	0.8780*	-0.42	-0.75	-0.02
Ni+Mn	Y=	91.26	-0.21	X_1-	0.12	X_2-	$6.8x10^{-4}$	X_1X_2	0.8956*	-0.67	-0.37	-0.15
Ni+Co	Y=	87.78	-0.32	X_1-	0.29	X_2-	$1.5x10^{-4}$	X_1X_2	0.8740*	-0.64	-0.57	-0.02
Ni+Cu	Y=	86.50	-0.31	X_1-	0.14	X_2-	$1.6x10^{-3}$	X_1X_2	0.8951*	-0.64	-0.28	-0.23
Ni+Zn	Y=	93.50	-0.31	X_1-	0.12	X_2+	$2.5x10^{-4}$	X_1X_2	0.9073*	-0.89	-0.33	0.05
	Root length (cm)(Y)											
Ni+Cr	Y=	5.32	-0.05	X_1-	0.06	X_2+	$6.7x10^{-4}$	X_1X_2	0.7573*	-0.82	-1.00	0.75
Ni+Mn	Y=	8.04	-0.08	X_1-	0.04	X_2+	$6.2x10^{-4}$	X_1X_2	0.8570*	-1.18	-0.57	0.69
Ni+Co	Y=	7	-0.07	X_1-	0.05	X_2+	$7x10^{-4}$	X_1X_2	0.8529*	-1.15	-0.81	0.87
Ni+Cu	Y=	5.49	-0.05	X_1-	0.06	X_2+	$7x10^{-4}$	X_1X_2	0.7245*	-0.84	-1.00	0.85
Ni+Zn	Y=	8.35	-0.06	X_1-	0.04	X_2+	$5.9x10^{-4}$	X_1X_2	0.7309*	-1.03	-0.58	0.68
	Shoot length (cm)(Y)											
Ni+Cr	Y=	2.64	$-1.4x10^{-2}$	X_1	$-1.8x10^{-2}$	X_2+	$1.1x10^{-4}$	X_1X_2	0.9240*	-0.78	-1.01	0.45
Ni+Mn	Y=	2.7	-8.8	X_1	$-6x10^{-3}$	X_2+	$1.9x10^{-4}$	X_1X_2	0.8010*	-0.75	-0.49	0.12
Ni+Co	Y=	2.7	-0.01	X_1	$-1.4x10^{-2}$	X_2+	$1.2x10^{-4}$	X_1X_2	0.8757*	-0.83	-1.06	0.63
Ni+Cu	Y=	2.7	-0.01	X_1	$-1.7x10^{-2}$	X_2+	$1.3x10^{-4}$	X_1X_2	0.8789*	-0.75	-1.06	0.56
Ni+Zn	Y=	2.85	-0.01	X_1	$-5.2x10^{-3}$	X_2+	$9.9x10^{-5}$	X_1X_2	0.7891*	-1.14	-0.56	0.77
	Dry weight (mg/seedling)(Y)											
Ni+Cr	Y=	6.48	-0.02	X_1	$-2.3x10^{-2}$	X_2-	$1.2x10^{-5}$	X_1X_2	0.9180*	-0.54	-0.72	-0.03
Ni+Mn	Y=	7.52	-0.02	X_1	$-1.1x10^{-2}$	X_2+	$8.4x10^{-5}$	X_1X_2	0.7178*	-0.8	-0.4	0.22
Ni+Co	Y=	6.86	-0.02	X_1	$-1.7x10^{-2}$	X_2+	$1.2x10^{-4}$	X_1X_2	0.8963*	-0.89	-0.85	0.42
Ni+Cu	Y=	6.6	-0.02	X_1	$-1.3x10^{-2}$	X_2+	$9.9x10^{-5}$	X_1X_2	0.8139*	-0.85	-0.75	0.41
Ni+Zn	Y=	7.88	-0.02	X_1	$-9x10^{-3}$	X_2+	$4.4x10^{-5}$	X_1X_2	0.7463*	-0.78	-0.27	0.1

*$p \leq 0.05$

other metals in binary combinations (Table 5) shows that there are statistically significant differences among mean germination percentage values on treatment with both the metals. The interaction between Ni and Mn was also found to be significant.

Table 5. ANOVA for different parameters of *B. juncea* seedlings grown in binary combinations of Ni and other metals.

		Germination percentage		Root lengths		Shoot lengths		Dry weights	
	Cr+Ni								
Source of variation	df	F-ratio	HSD	F-ratio	HSD	F-ratio	HSD	F-ratio	HSD
Treatment	3	108.2*	24.93	1814.1*	0.48	229.2*	0.37	39.8*	1.48
Dose	3	30.8*		700.4*		103.2*		14.5*	
Treatment x Dose	9	1.3		555.7*		13.5*		7.01*	
	Ni+Mn								
Source of variation	df	F-ratio	HSD	F-ratio	HSD	F-ratio	HSD	F-ratio	HSD
Treatment	3	31.7*	21.47	1258.9*	0.68	87.2*	0.4	16.6*	1.51
Dose	3	11.5*		150.5*		32.5*		16.4*	
Treatment x Dose	9	2.4*		131.8*		11.5*		10.9*	
	Co+Ni								
Source of variation	df	F-ratio	HSD	F-ratio	HSD	F-ratio	HSD	F-ratio	HSD
Treatment	3	49.8*	22.92	368.0*	0.48	97.01*	0.4	8.55*	1.12
Dose	3	57.0*		1248.5*		51.22*		12.27*	
Treatment x Dose	9	1.7		295.1*		13.93*		7.15*	
	Cu+Ni								
Source of variation	df	F-ratio	HSD	F-ratio	HSD	F-ratio	HSD	F-ratio	HSD
Treatment	3	18.5*	30.5	786.6*	0.48	131.98*	0.4	16.21*	2.21
Dose	3	36.7*		273.1*		69.86*		12.97*	
Treatment x Dose	9	1.1		465.7*		16.82*		6.64*	
	Ni+Zn								
Source of variation	df	F-ratio	HSD	F-ratio	HSD	F-ratio	HSD	F-ratio	HSD
Treatment	3	56.2*	19.9	759.6*	0.68	90.15*	0.31	20.91*	2.06
Dose	3	13.7*		416.0*		22.44*		20.65*	
Treatment x Dose	9	1.1		146.0*		19.43*		6.59*	

*$p \leq 0.05$

Table 6. Multiple regression equations for uptake of metals in *B. juncea* grown in binary combinations of Ni (X_1, mg l^{-1}) and other metals (X_2 mg l^{-1}).

Treatments (mg l^{-1})	Uptake of metals (mg g^{-1} dw)(Y)								r	β regression coefficients	
	Multiple regression equations									β_1	β_2
Cr+Ni	Y (Cr) =	0.083	+	$7.5x10^{-4}$	X_1	-	$7.9x10^{-4}$	X_2	0.9088*	0.569	-0.708
	Y (Ni) =	0.083	+	$6.1x10^{-4}$	X_1	-	$4.4x10^{-4}$	X_2	0.9139*	0.698	-0.590
Mn+Ni	Y (Mn) =	0.157	+	$3.2x10^{-3}$	X_1	-	$1.4x10^{-3}$	X_2	0.9298*	0.824	-0.431
	Y (Ni) =	0.100	+	$4.4x10^{-5}$	X_1	-	$2.9x10^{-4}$	X_2	0.5113	0.065	-0.507
Ni+Co	Y (Ni) =	0.099	+	$2.8x10^{-4}$	X_1	-	$3.1x10^{-4}$	X_2	0.6467*	0.391	-0.516
	Y (Co =	0.135	+	$8.5x10^{-4}$	X_1	-	$9.8x10^{-4}$	X_2	0.7524*	0.443	-0.608
Ni+Cu	Y (Ni) =	0.083	+	$3.9x10^{-4}$	X_1	-	$3.9x10^{-4}$	X_2	0.6933*	0.446	-0.531
	Y (Cu) =	0.102	+	$5.3x10^{-4}$	X_1	-	$6.8x10^{-4}$	X_2	0.5470	0.302	-0.456
Ni+Zn	Y (Ni) =	0.102	+	$-1.6x10^{-5}$	X_1	-	$2.6x10^{-4}$	X_2	0.4021	-0.021	-0.402
	Y (Zn) =	0.218	+	$1.9x10^{-3}$	X_1	-	$1.8x10^{-3}$	X_2	0.8133*	0.535	-0.612

*$p \leq 0.05$

The data corresponding to root and shoot growth of the seedling versus the treatment of heavy metals is presented in figures 2-3. It was found that the inhibitory effects of metals on the growth of the seedlings were more pronounced at the higher concentration, thereby demonstrating a dose dependent inhibition of the shoot and root growth. The IC_{50} values calculated on the basis of root length inhibition were given in table 2. Cr (VI) was found to be most toxic metal as the lowest observed value of root length is 0.14 cm at the concentration of Cr

Table 7. ANOVA for metal uptake (mg g^{-1} dw) by the seedlings of *B. juncea* grown in water cultures containing different binary combinations of Ni with other metals.

		Cr+Ni		Ni+Cr	
		Ni uptake (mg g^{-1} dw)		Cr uptake (mg g^{-1} dw)	
Source of variation	df	F-ratio	HSD	F-ratio	HSD
Treatment	3	3.9*	0.097	3.5*	0.177
Dose	2	9.3*		3.3	
Treatment x Dose	6	0.09		0.5	
		Mn+Ni		Ni+Mn	
		Ni uptake (mg g^{-1} dw)		Mn uptake (mg g^{-1} dw)	
Source of variation	df	F-ratio	HSD	F-ratio	HSD
Treatment	3	6.2*	0.079	6.1*	0.25
Dose	2	0.2		34.5*	
Treatment x Dose	6	1.1		1.4	
		Co+Ni		Ni+Co	
		Ni uptake (mg g^{-1} dw)		Co uptake (mg g^{-1} dw)	
Source of variation	df	F-ratio	HSD	F-ratio	HSD
Treatment	3	2.7	0.008	21.5*	0.105
Dose	2	3		11.8*	
Treatment x Dose	6	1.8		5.2*	
		Cu+Ni		Ni+Cu	
		Ni uptake (mg g^{-1} dw)		Cu uptake (mg g^{-1} dw)	
Source of variation	df	F-ratio	HSD	F-ratio	HSD
Treatment	3	6.1*	0.079	66.1*	0.056
Dose	2	2.7		15.6*	
Treatment x Dose	6	1.6		14.5*	
		Zn+Ni		Ni+Zn	
		Ni uptake (mg g^{-1} dw)		Zn uptake (mg g^{-1} dw)	
Source of variation	df	F-ratio	HSD	F-ratio	HSD
Treatment	3	5.6*	0.097	13.7*	0.217
Dose	2	0.03		26.4*	
Treatment x Dose	6	1.4		1.9	

*$p \leq 0.05$

100 mg l^{-1}. The IC_{50} value for Ni was found to be 28.88 mg l^{-1}. The effects of heavy metals on root growth were more pronounced as compared to shoot growth. All the binary combinations of Ni had inhibitory effects on the seedling growth at all the tested concentrations. Percentage change in root lengths of *B. juncea* seedlings in binary combinations of Ni with other metals is given in table 3. Maximum inhibitory effect was caused by Cr followed by Cu. Even at low concentration of these metals in the medium, there was a decline in root length by 62% in case of (Ni25+Cr25) and by 29% in case of (Ni25+Cu25) mg l^{-1}as compared to the control. Similarly shoot length was also adversely affected by all the binary combinations with respect to the controls. The shoot lengths of the seedlings were most affected by (Ni25+Cr25) and (Ni25+Co25) which decreased the shoot length by 52% and 31% respectively. The multiple regression interaction models (Table 4) for both root and shoot growth of the seedlings showed that, although all the metals exerted negative influence on the seedling growth, the interactive effects of Ni in combination with Cr, Mn, Co, Cu, and Zn are antagonistic. 2-way ANOVA for root and shoot growth of *B. juncea* seedlings for Ni and other metals in binary combinations (Table 5) showed that there are statistically significant differences among mean root and shoot lengths on treatment with both the metals. The interactions between Ni and the other metal in all binary treatments were also found to be significant.

The effects of heavy metals on the seedling biomass varied with different concentrations, applied individually or in combination with Ni (Fig. 4). Since all the metals induced negative effects on the seedling growth, corresponding dry weight was also greatly reduced. Both Ni and Cr at a concentration of 100 mg l^{-1} caused maximum reduction by 66% as compared to the control. However, in the presence of Zn and Mn, there was a slight increase in the biomass, by 17% at (Ni25+Zn50) and by 6% at (Ni25+Mn50) concentrations as compared to the control (Ni 25 mg l^{-1}). However, at (Ni25+Cu25)

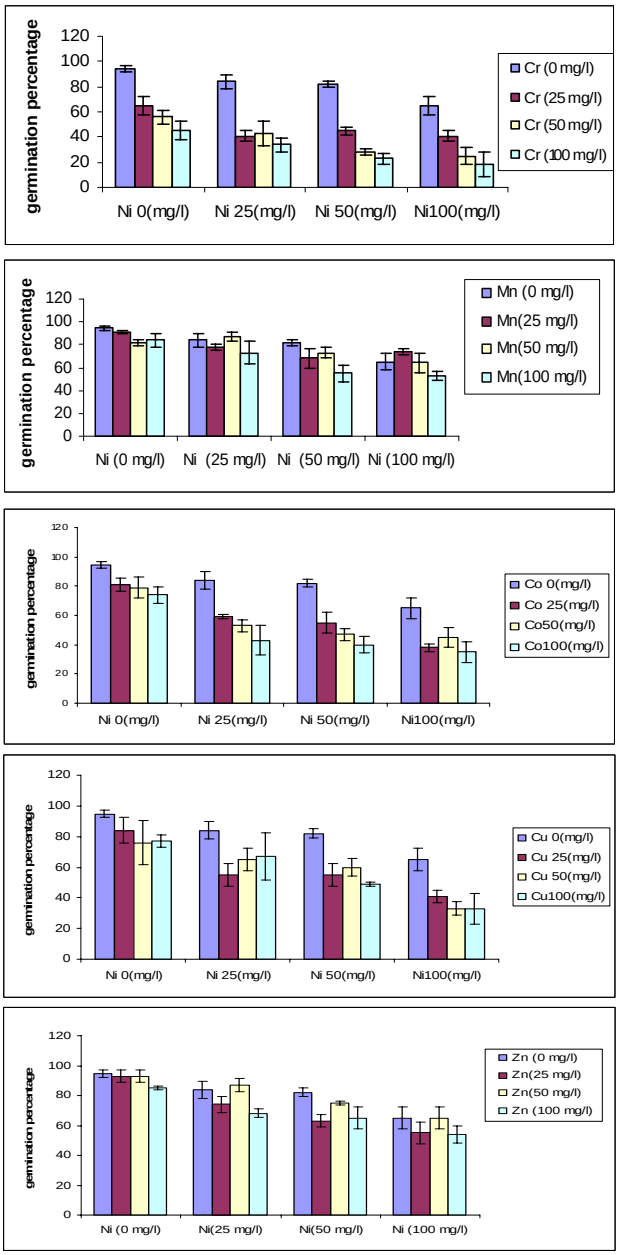

Fig.1. Germination percentage (mean±SD) of *B. juncea* grown in binary combinations of Ni with other heavy metals.

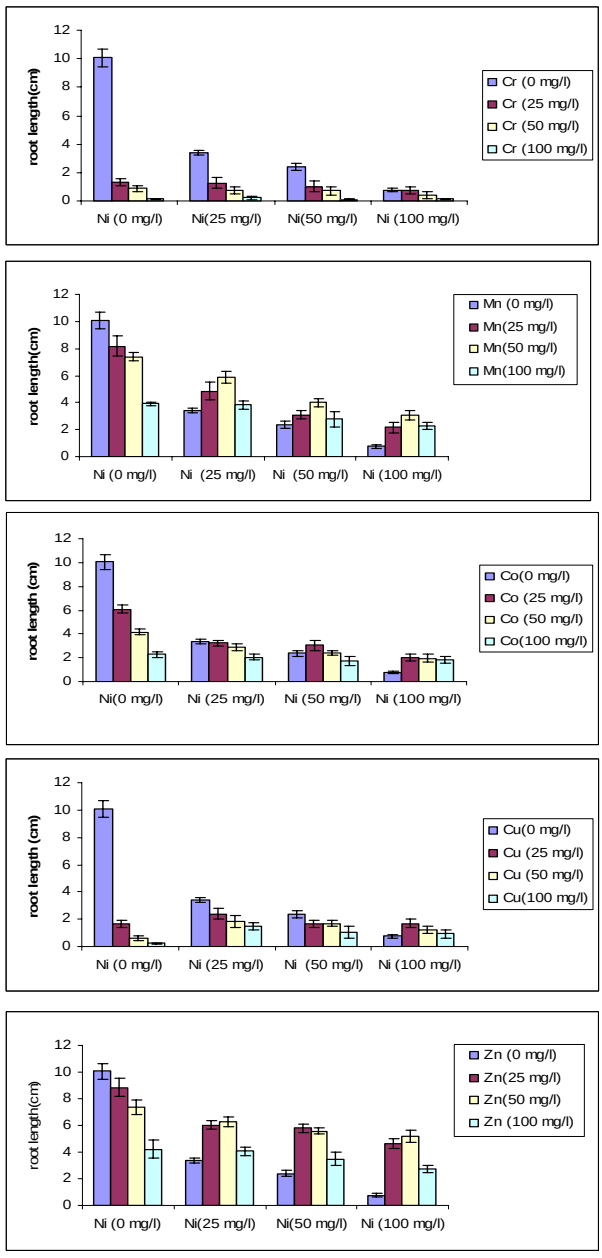

Fig. 2. Root length (cm) (mean±SD) of *B. juncea* seedlings grown in binary combinations of Ni with other heavy metals.

and (Ni25+Co25), the dry weight of the seedlings was further reduced by 6% and 5% respectively. The multiple regression interaction model (Table 4) for the dry weight of the seedlings depicted that in binary combinations, Ni along with the other metal ions exerted negative influence on the dry weight as represented by their negative β-regression coefficients. However, the interactive effect of Ni with Mn, Co, Cu and Zn, was observed to be positive, showing mutual decrease in the toxicities caused by the antagonistic interaction of the metal ions in binary combinations. 2-way ANOVA for dry weight of *B. juncea* seedlings for Ni and other metals in binary combinations (Table 5) showed that there are statistically significant differences among mean dry weight values on treatment with both the metals in all binary combinations. The interaction of Ni with Cu, Cr, Co and Zn was also found to be significant.

Figure 5 gives the uptake potential of all the six metals in the *B. juncea* seedlings, applied singly or in binary combinations of Ni with other heavy metals at various concentrations. The results fairly indicated that the uptake

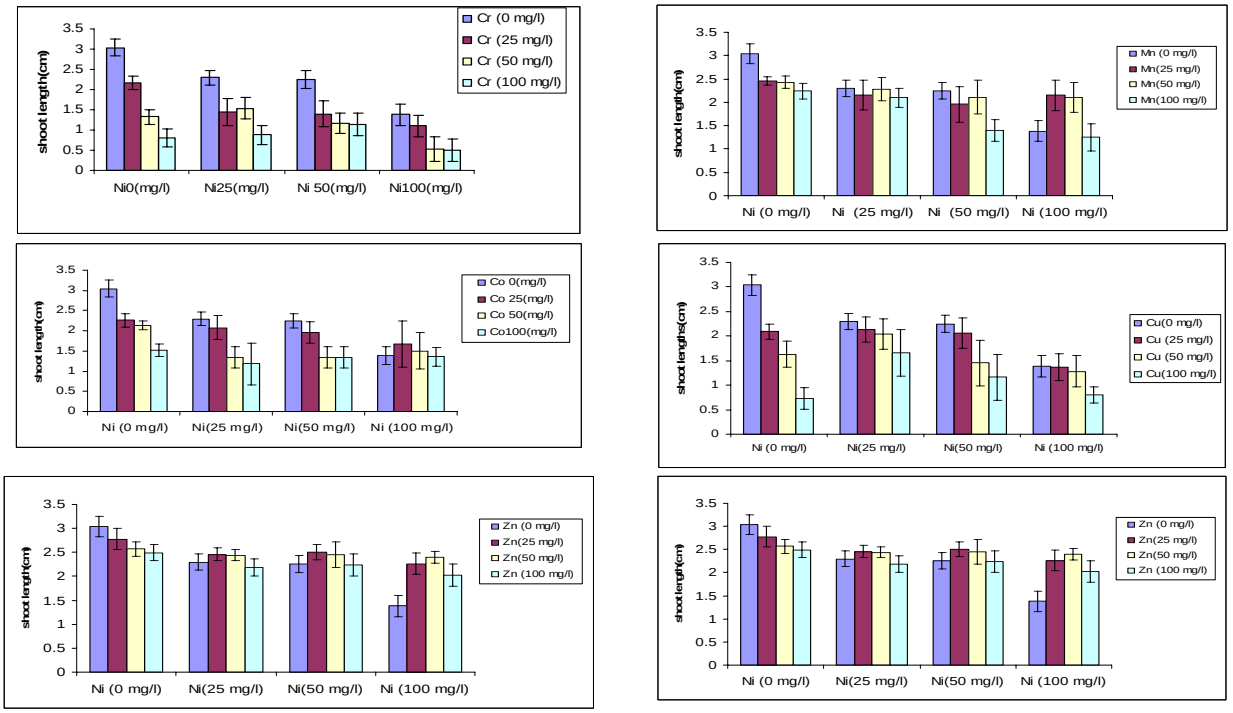

Fig. 3. Shoot length (cm) (mean±SD) of *B. juncea* seedlings grown in binary combinations of Ni with other heavy metals.

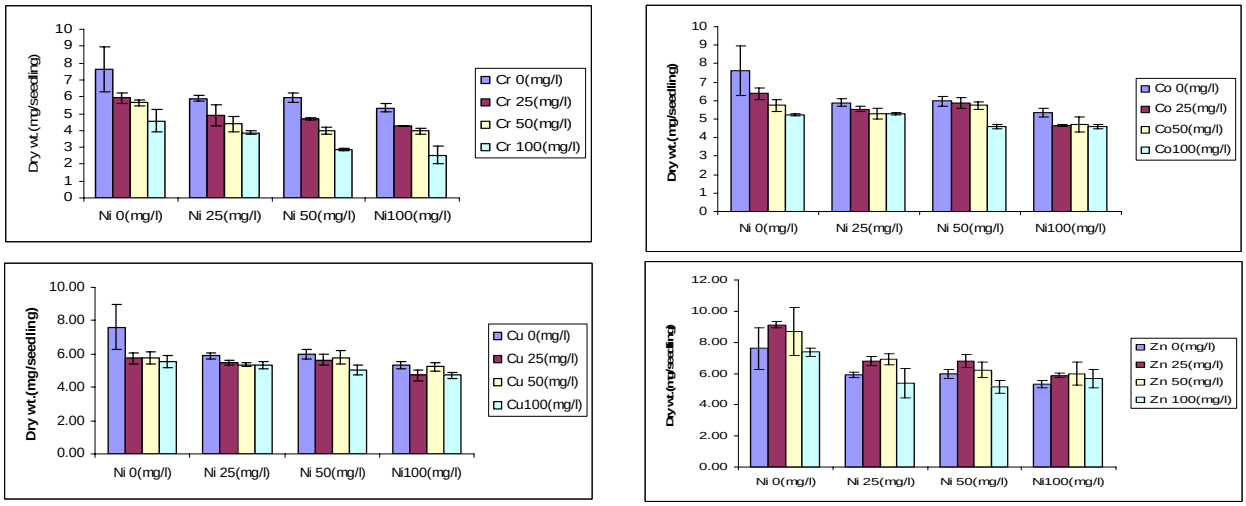

Fig. 4. Dry weight (mg/seedling) (mean±) of *B. juncea* seedlings grown in binary combinations of Ni with other heavy metals.

potential of each metal was directly proportional to its concentration in the medium. As the concentration of the metal ion increases from 25 mg l^{-1} to 100 mg l^{-1}, there is a corresponding increase in the uptake of metal ions, thereby showing dose dependent linear relation of metal uptake in the seedlings. The data obtained revealed that the *B. juncea* seedlings showed maximum uptake of Zn (0.531 mg g^{-1}dw) followed by Mn (0.446 mg g^{-1}dw), and the lowest uptake by Ni (0.135 mg g^{-1}dw) at the highest applied treatment of 100 mg l^{-1} to the seedlings. As given in table 6, uptake of each ion was not only affected by the concentration of the element in the medium but also by the presence of other elements. In binary combinations of Ni with Cr, Mn, Co, Cu and Zn both the metal ion mutually inhibited the uptake of each other. 2-way ANOVA for the uptake of Ni and other metals in binary combinations (Table 7) showed that there are statistically significant differences among mean uptake values on treatment with both the metals in all binary combinations.

Therefore, the results of the present study elucidate various positive and negative interactions among metal ions in binary combination of Ni. Inhibitory effects of Ni in plant growth and development has been reported by

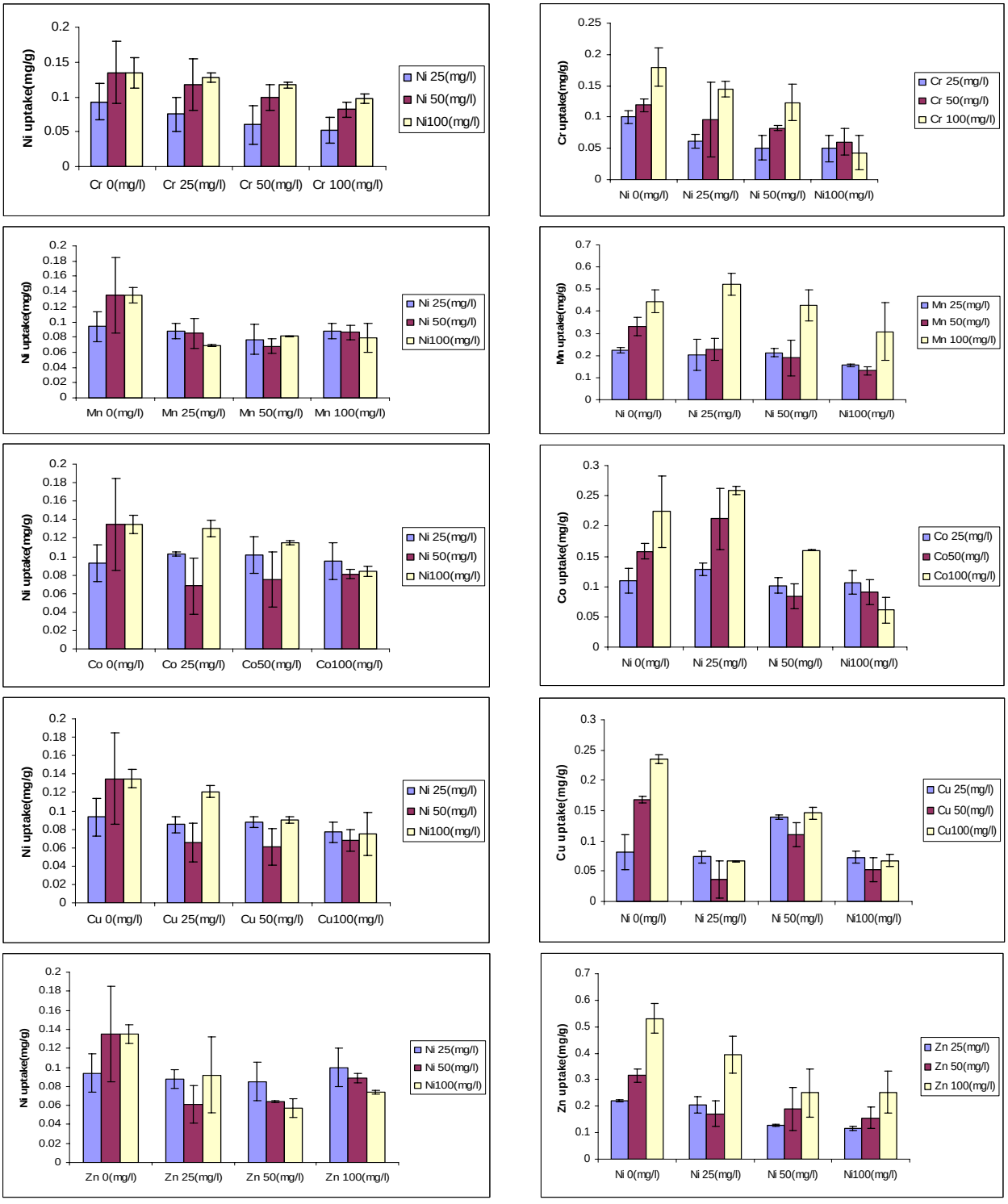

Fig. 4. Metal uptake (mean±) by *B. juncea* seedlings grown in binary combinations of Ni with other heavy metals.

many researchers (Gajweska *et al.*, 2008). Ni is not considered to be an essential element in plant nutrition, yet its uptake behavior is characteristic of nutrients, suggesting thereby that Ni^{2+} may be acting as an analog of an essential species for which effective transport mechanism are operating. Korner *et al.* (2008) studied free space uptake and influx of Ni^{2+} in excised barley roots. Ni inhibits the uptake of Mn, Cr, and Cu probably due to the complexes or allosteric interactions with the carrier complex or proteins which could affect their

uptake. It was further observed that Zn and Cu increased Ni uptake which is not consistent with the results of Catalado *et al.* (1978), who showed Cu and Zn are competitive inhibitors with respect to Ni^{2+} uptake. Generally the interaction of metal ions with biological surfaces such as cell membranes, affects the transport, chemistry, bioaccumulation and toxicity of metals. Different surface functional groups such as carbonyl, sulphydryl, hydroxide, oxides and amines act as sites of interactions among metals ions (Dirilgen, 2001). Also the various reactions occurring between surface groups and metal ions are numerous, complicating the aqueous chemistry of metals, their interactions and toxicological properties. The proposed model can be used to investigate critically the phytotoxicity and interactive aspects of metal mixtures to the plant. It was observed that Cr, Mn, Ni, Co Cu and Zn, when applied individually, are toxic to growth of *B. juncea* seedlings beyond the threshold values but in binary combinations, Ni and other studied heavy metals are antagonistic to each other for their effects on the growth of seedlings. The uptake of Ni was inhibited in combinations, (Ni+Mn), (Ni+Co), (Ni+Cu) and (Ni+Zn) due to competitive inhibition of metals. The present study therefore, highlights the importance of understanding the basic mechanism involved in uptake and accumulation of metal ions in a phytoremediator undergoing multiple metal stress which is essential for genetic engineering approaches aimed at improving the cellular defence mechanism, and hence the efficiency of a phytoremediator.

ACKNOWLEDGEMENTS

Thanks are due to the Head of Department of Botanical & Environmental Sciences, Guru Nanak Dev University Amritsar, and to the Ministry of Environment and Forests, Government of India, for providing research facilities and financial assistance.

REFERENCES

Allen, SE., Grimshaw, HM., Pakinson, JA., Quarmby, C. and Roberts, JD. 1976. Chemical analysis. In: Methods in plant ecology. Ed. Chapman, SB. Blackwell Scientific Publishers, Oxford, London. 424-426.

Bailey NTJ. 1995. Statistical Methods in Biology. Cambridge University Press, Cambridge. pp. 255

Barbier, O., Jacquillet, G., Tauc, M., Cougnon, M. and Poujeol, P. 2005. Effect of Heavy Metals on, and Handling by, the Kidney. Nephron Physiology. 99:105-110.

Boominathan, R. and Doran, PM. 2002. Ni-induced oxidative stress in roots of the Ni hyperaccumulator, *Alyssum bertolonii*. New Phytologist. 26:424-426.

Catalado, DA., Garland, TR. and Wildung, RE. 1978. Nickle in plants. Plant Physiology. 62:563-565.

Dirilgen, N. 2001. Accumulators of heavy metals in fresh water organism: Asssessment of toxic interactions. Turkish Journal of Chemistry. 25:173-179.

Dushenkov, S., Vasudev, D., Kapulnik, Y., Gleba, D., Fleisher, D., Ting, KC. and Ensley, B. 1997. Removal of uranium from water using terrestrial plants. Environmental Science and Technology. 31:3468-3474.

Ebbs, SD. and Kochian, LV. 1998. Phytoextraction of zinc by oat (*Avena sativa*), barley (*Hordeum vulgare*), and Indian mustard (*Brassica juncea*). Environmental Science and Technology. 32:802-806.

Gajewska, E. and Sklodowska, M. 2008. Differential biochemical responses of wheat shoots and root to nickel stress: antioxidative reactions and proline accumulation. Plant Growth Regulation. 54:179-188.

Kochian, LV. 2000. Molecular physiology of mineral nutrient acquisition, transport and utilization. In: Biochemistry and Molecular Biology of Plants. Eds. Buchanan, BB., Gruissem, W. and LJ, Russell. American Society of Plant Physiologists.1204-1249.

Korner, LE., Moller, IM. and Jensen, P. 2008. Free space uptake and influx of Ni^{2+} in excised barley roots. Physiologia Plantarum. 68:583-588.

Krupa, Z., Siedlecka, A., Skorzynska-Polit, E. and Maksymiec, W. 2002. Heavy metal interactions. In: Physiology and biochemistry of metal toxicity and tolerance in plants. Ed. Prasad, MNV. Kluwar Academic Publishers, Netherlands. 287-301.

Martin-Prevel, P., Gagnard, J. and Gautier, P. 1987. Plant Analysis: As a Guide to the Nutrient Requirements of Temperate and Tropical Crops. Lavoisier Publishing Inc., New York. pp. 722.

Sokal, RR. and Rholf, FJ. 1981. Biometry: The Principles and Practice of Statistics in Biological Research. WH Freeman and Co., San Francisco. pp. 859.

Received: March 4, 2009; Revised: Jan 4, 2010; Accepted: Jan 5, 2010

SENRA Academic Publishers, Burnaby, British Columbia
Vol. 4, No. 1, pp. 1021-1026, 2010
ISSN: 1715-9997

Canadian Journal of pure&applied sciences

LARVICIDAL ACTIVITY OF EXTRACELLULAR SECONDARY METABOLITES OF *STREPTOMYCES MICROFLAVUS* AGAINST *CULEX PIPIENS*

Magda A El-Bendary, *Hala M Rifaat and Abeer A Keera
Department of Microbial Chemistry, National Research Centre, Cairo, Egypt

ABSTRACT

Eight isolates of actinomycetes were isolated from sand samples of underground spring at Giza Governorate, Egypt. The extracellular secondary metabolites of one isolate (Act-1) showed larvicidal activity against *Culex pipiens*. The morphological, physiological and chemotaxonomical characteristics of this isolate revealed that it belongs to *Streptomyces* sp. However, according to the 16S rDNA sequencing analysis, it was identified as *Streptomyces microflavus*. Twenty five ml of peptone-beef extract-yeast extract-glucose medium under static condition showed the best conditions for the production of secondary metabolites from Act-1 against mosquito larva. Addition of NaCl, $FeSO_4$ and $CaCO_3$ to the medium increased the produced mosquitocidal metabolites twelve times more than the original. The LC_{50} value of *Streptomyces microflavus* metabolites was 77.3 ppm with 95% fiducial limits (62.6-95.7).

Keywords: *Culex pipiens*, larvicidal, secondary metabolites, *Streptomyces.*

INTRODUCTION

Mosquitoes are the oldest human enemy and are the most medically important arthropod vectors of disease. Mosquitoes transmit many dreadful diseases like malaria, filariasis, Japanese encephalitis and dengue fever affecting the socio-economical status of many nations (Service, 1983). Mosquitoes are also an important pest of humans, causing allergic responses that include local skin reaction and systemic reaction such as angioedema and urticaria (Peng *et al*., 1999). *Culex pipiens* is the most widely distributed species in the world and is predominantly found in all Egyptian governorates (El-Kady *et al*., 2008).

Actinomycetes and its derived products are highly toxic to mosquitoes, yet have low toxicity to non target organisms (Vijayan and Balaraman, 1991). Accordingly, the use of actinomycetes may be a promising approach for biological control of mosquitoes (Liu *et al*., 2008). The filamentous actinomycetes are Gram-positive bacteria with a high G+C content and are well known as prolific producers of biologically active secondary metabolites. Some genera were reported as producer of extracellular secondary metabolites that have larvicidal activity against mosquitoes (Rao *et al*., 1990). Microbial insecticides are being considered as alternative to chemical insecticides because of their selective toxicity and ready decomposability in the ecosystem. Also, unlike the inherent dangers associated with the process of production of synthetic insecticides, the process for the manufacture of microbial products is safe and less pollution (Misato, 1983).

*Corresponding author email: halamohamed6@yahoo.com

The present study has been undertaken to identify the actinomycete isolate which isolated from sand of underground spring in Egypt and showed a larvicidal activity against *Culex pipiens* to species level. Moreover, the efficiency of extracellular secondary metabolites of the actinomycete isolate under laboratory conditions was studied.

MATERIALS AND METHODS

Microorganism and culture conditions

During the isolation of mosquitocidal bacteria from sand samples of underground spring at Giza Governorate, Egypt, eight isolates of actinomycetes were isolated. One of them showed promising mosquitocidal activity against *Culex pipiens* and it was designated as Act-1. It was cultured on starch-nitrate agar medium (Küster and Williams, 1964) and incubated at 28°C.

Identification of Act-1

The cultural characteristics of Act-1 were studied on the basis of the International *Streptomyces* Project (ISP) recommended by Shirling and Gottlieb (1966). The morphological characters of this isolate were examined by the light and transmission electron microscopy (Tresner *et al*. 1961). The enzyme activities (proteolytic, lipolytic, lecithinase and pectinase) of Act-1were performed according to the method of Nitsch and Kutzner (1969) and Hankin *et al*. (1971). The utilization of nitrate and H_2S production were examined adopting the method of Williams *et al*. (1989). Arbutin decomposition was determined by the method of Kutzner (1976). Utilization of carbohydrates was investigated with a basal carbon nutrient medium (Pridham and Gottlieb, 1948). The antimicrobial activities of the culture broth of Act-1 were

examined by the agar diffusion method (Wu, 1984). The tested microorganisms were obtained from MIRCEN Faculty of Agriculture, Ain Shams University, Cairo, Egypt. The cell wall composition including diaminopimelic acid (DAP) isomers and sugars were determined according to the methods of Hasegawa *et al*. (1983). Partial 16S rDNA analysis has been performed for the identification of Act-1 (De Soete, 1983 and Ludwig and Strunk, 1997).

Cultivation of actinomycete Act-1

A loopful of actinomycete isolate growth from starch-nitrate agar slop was transferred to 25 ml of growth medium in 250 ml Erlenmeyer conical flasks and incubated under static or shaking conditions at 28^{o}C for 5 days and harvested by centrifugation. The mycelial mass and the culture filtrate were bioassayed for toxicity against larva of *Culex pipiens.*

Effect of medium type

Five culture media of varying composition were tested for their ability to support the secondary metabolites production by Act-1 against larvae of *Culex pipiens* namely, (M1) peptone-beef extract-yeast extract-glucose medium (Greorgieva *et al*., 1966), (M2) has the same composition as M1 but without glucose, (M3) is the starch-nitrate medium, (M4) has the same composition of M3 but using glucose instead of starch and (M5) nutrient broth medium (Atlas, 1993).

Determination of the nutritional requirements for mosquitocidal metabolites production by Act-1 in M1 medium

One or more constituents of M1 medium were removed to study its/their effects on mosquitocidal metabolites production by Act-1.

Bioassay of mosquitocidal activity

Bioassay of mosquitocidal activity of Act-1 was detected according to the method of Ampofo (1995). Serial dilutions of the tested solution were prepared and the dilutions were placed into 100 ml beakers in triplicate along with *Culex pipiens* larvae. Uninoculated culture medium was served as control. The mortality percentage was recorded after 48 hours and corrected using appropriate control and adopting Abbott's formula (Abbott, 1925).

Statistical analysis

The data obtained statistically analyzed according to SPSS system using one-way analysis and the Duncan's multiple range test (Duncan, 1955) to determine the significance between means. Data were expressed as mean values ± standard errors. LC_{50} value was calculated by probit regression analysis (Proban version 1.1, Jedrychowski, 1991 shareware).

RESULTS AND DISCUSSION

The microscopic examination of Act-1 revealed that aerial mycelia were morphologically straight sporophore (Fig. 1). Each spore chain consisted of 10-20 turns with white and smooth surface (Fig. 2).

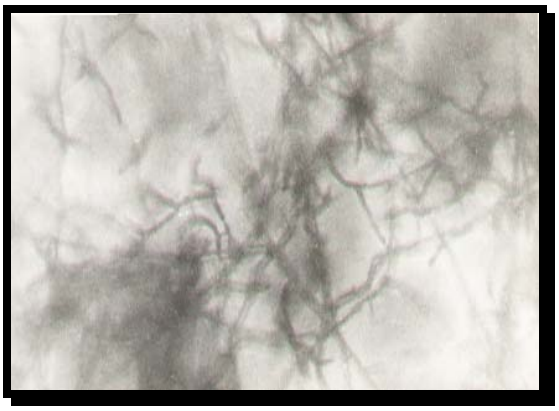

Fig. 1. Photograph showing spore chains of Act-1.

Fig. 2. Electron micrograph of spores of Act-1.

The cultural properties of Act-1 on various media are presented in Table 1. Act-1 grew well on most of the tested organic and synthetic media. The colonies were elevated, spreading and covered with white aerial mycelia and spores. Diffusable pigment was not produced.

The physiological characteristics of the tested isolate were listed in Table 2. Act-1 did not produce melanoid pigments on peptone-yeast extract-iron and tyrosine agars media. No proteolytic, lipolytic and lecithinase activity detected by Act-1 but moderate activity was showed for pectinase and arbutin degradation. Also Act-1 highly reduces nitrate with H_2S production. The utilization of various carbohydrates by Act-1 suggests a good pattern of carbon sources assimilation (Table 3). All of the sugars were utilized except inositol. Act-1 showed a narrow antimicrobial spectrum against the target microorganisms (Table 4).

Table 1. Culture characteristics of Act-1

Agar media used	Characteristics			
	Growth	Substrate mycelia	Aerial mycelia	Soluble pigment
Starch nitrate	Moderate	Yellow grey	White	-
Glycerol asparagine	Moderate	Light grey	White	-
Sucrose nitrate	Moderate	Slightly orange	White	-
Fish meal extract	Moderate	Medium brown	White	-
Soya bean meal	Moderate	Brown orange	White	-
Oat meal	Moderate	Light yellow brown	White	-
Malt-yeast extract	Moderate	Light yellow brown	White	-

Table 2. Physiological characteristics of Act-1

Reaction	Medium	Response
Melanin pigment production	PYI	-
	T	-
Enzyme activity		
Protyoltic	Egg-yolk	-
Lipolytic	Egg-yolk	-
Lecithinase	Egg-yolk	-
Pectinase	Hankin *et al*. (1971)	+
Nitrate reduction	Nitrate broth	+++
H_2S production	Nitrate broth	+
Degradation of arbutin	Kutzener *et al*. (1976)	+

PYI: peptone-yeast extract-iron medium, T: tyrosine medium, +++: good, +: moderate, -: negative

Analysis of the whole-cell hydrolysate of the tested isolate showed the presence of chemotype I cell wall characterized by LL-DAP acid. No diagnostic sugars were found.

Table 3. Utilization of carbohydrates by Act-1

Carbon sources	Response
No carbon	-
Glucose	+
Fructose	+
L-arabinose	+
Galactose	+
I-inositol	-
D-mannitol	+
L-rhamnose	++
Sucrose	++
D-xylose	+
Raffinose	+
Maltose	+

Trough morphological observations and chemotaxonomic characteristics, strain Act-1 could be characterized as belonging to the genus *Streptomyces*. In an attempt to identify it up to species level, a computerized database was used to compare the biological properties of Act-1 with those of other *Streptomyces* sp. Moreover, the partial sequence of Act-1 was applied to show the similarities to the closest relative in the 16S rDNA database. The obtained results showed that Act-1 has been enrolled into a cluster containing *Streptomyces microflavus*. By checking the similarity percentages, Act-1 is equidistant to *Streptomyces microflavus* (99.8%), based also to ABI database of partial and full sequence. The same equidistance to *Streptomyces microflavus* could be calculated using the MEDLINE database. These results suggest that Act-1 belong to *Streptomyces microflavus*. It was concluded that the use of genotypic and phenotypic techniques (polysporic approach) gives a better resolution in the species level identification (Stackebrandt and Wose, 1981).

Effect of Act-1 on *Culex pipiens* larvae

The clarified solution of Act-1 produced under static conditions was toxic to mosquito larvae of *Culex pipiens*. The precipitated part produced under both shaking and static conditions and clarified solution produced under shaking conditions did not show any activity against larva of *Culex pipiens*. Many workers reported that the secondary metabolites of actinomycetes produced by *Streptomyces aureus*, *Streptomyces avermitilis*, *Streptosporangium albidum*, *Streptomyces griseus*, *Micromonospora*, *Actinomandura*, *Actinoplanes*, *Micropolyspora*, *Nocardiopsis*, *Oerskonia*, *Thermomonospora*, *Streptoverticillium*, *Saccharopolyspora* and *Chainia* were toxic to mosquitoes (Ando, 1983; Zizka *et al*., 1989;

Anonymous, 1990; Rao *et al*., 1990 and Govindarajan *et al*., 2007).

Table 4. Antimicrobial activities of Act-1

Microorganisms	Zone of inhibition (mm)
Bacillus cereus	0
Bacillus subtilus	24
Escherichia coli	0
Candida albicans	0
Rhodotorula minuta	±
Debaryomces hansenii	±
Aspergillus niger	0
Asperagillus flavus	0
Asperagillus terrus	0
Trichoderma viride	0
Macrophomena phseoli	13
Fusarium vasenfectum	0
Botrytis alli	0
Alternaria humicola	13
Diplodia oryzae	20
Geotrichum candidum	0

Table 5. Effect of medium type on mosquitocidal activity of the metabolite of Act-1 against larvae of *Culex pipiens*

Medium type	Mortality % at 2000 ppm*
M1	95.4 ± 1.0 a
M2	78 ± 1.7 b
M3	31.7 ± .0.9 c
M4	20.8 ± 1.0 e
M5	27.5 ± 1.0 d

*Mortality % is presented as means ± SE. Values for each treatment followed by different letters are significantly different at $P = 0.05$.

Table 6. Effect of medium quantity on mosquitocidal activity of the metabolite of Act-1 against second instar larvae of *Culex pipiens*

Medium type/quantity (ml) of medium in 250 ml flask	Mortality % at 2000 ppm*
M1/	
25	97.5 ± 1.0 a
50	62.1 ± 1.6 b
75	13.8 ± 1.3 c
100	3.8 ± 0.7 d
M2/	
25	76.3 ± 2.1 a
50	62.9 ± 1.7 b
75	18.8 ± 0.9 c
100	2.9 ± 0.7 d

*Mortality % is presented as means ± SE. Values for each treatment followed by different letters are significantly different at $P = 0.05$.

Effect of culture media on production of secondary metabolites by Act-1

As shown in Table 5, M1 and M2 media were good media for production of mosquitocidal secondary metabolites of Act-1. The toxicity of the metabolites produced in M1 was 22% higher than that produced in M2 medium. M1 and M2 media contains peptone, beef extract and yeast extract which support the medium with a wide variety of amino acids, minerals and vitamins. M1 medium was enhanced the production of Act-1 secondary metabolites more than M2 medium because it contains glucose. Glucose was found to be an important nutrient for mycelium growth, secondary metabolites synthesis and control the fermentation of various antibiotics (Chen and Zhang, 2002). Increase of glucose concentration could promote the mycelium growth and spinosad production

Table 7. Effect of medium composition on mosquitocidal activity of the metabolite of Act-1 against second instar larvae of *Culex pipiens*

Medium composition	Mortality % at *		
	1000 ppm	500 ppm	100 ppm
1	83.8 ± 1.6 b	25.4 ± 1.3 d	4.2 ± 1.0 d
2	47.5 ± 1.7 e	13.8 ± 1.1 f	2.9 ± 0.7 de
3	100 ± 0.0 a	99.2 ± 0.6 a	27.5 ± 1.0 bc
4	100 ± 0.0 a	99.6 ± 0.4 a	25.4 ± 1.1 c
5	100 ± 0.0 a	98.8 ± 0.7 a	29.6 ± 1.3 b
6	75.4 ± 1.3 c	17.9 ± 1.3 e	2.9 ± 0.7 de
7	100 ± 0.0 a	33.3 ± 1.1 b	2.1 ± 0.7 de
8	100 ± 0.0 a	98.8 ± 0.7 a	50.4 ± 1.6 a
9	64.6 ± 1.1 d	30.0 ± 1.1 c	3.3 ± 0.7 d
Control (M1)	17.9 ± 0.7 f	1.3 ± 0.7 g	0.0 ± 0.0 e

*Mortality % is presented as means ± SE. Values for each treatment followed by different letters are significantly different at $P = 0.05$.

by *Saccharopolyspora spinosa* as reported by Zhihua *et al*. (2006).

Effect of medium quantity on mosquitocidal secondary metabolites produced by Act-1

Quantity of the medium is a critical factor for production of mosquitocidal secondary metabolites by Act-1 as shown in Table 6. The most favourable quantity of the medium for mosquitocidal secondary metabolites production was 25 ml in both media M1 and M2. Increasing the quantity of the medium, mosquitocidal secondary metabolites decreased gradually and disappeared at 100 ml. This indicated that 25 ml of the medium provides sufficient aeration to maximum mosquitocidal metabolites production by Act-1. As reported by Yengneswaran *et al*. (1991), the reduction in oxygen supply is an important limiting factor for growth and the secondary metabolites production of streptomycetes.

Effect of different combinations of M1 constituents on mosquitocidal metabolites production

A numbers of combinations of the constituents of M1 medium were tested to determine the effect of each constituent alone or in combination to other constituents on the mosquitocidal metabolites production by Act-1. As shown in Table 7, nine combinations enhanced the production of mosquitocidal secondary metabolites by Act-1. In all cases peptone, beef, yeast extracts and glucose were present in the medium (core). When $CaCO_3$ (1) or $MgSO_4$ (2) or K_2HPO_4 (3) or NaCl and $FeSO_4$ (4) added to the core, the produced toxicity was enhanced against *Culex pipiens* larvae. However, addition of $CaCO_3$ and NaCl (5) to the core enhanced the secondary metabolite production by Act-1 more than that of the first combination seven times. Addition of NaCl and $MgSO_4$ (6) or NaCl and K_2HPO_4 (7) or NaCl, $MgSO_4$ and $FeSO_4$ (9) to the core did not enhance the mosquitocidal metabolites production by tested organism. Addition of NaCl, $FeSO_4$ and $CaCO_3$ (8) to the core enhanced the produced mosquitocidal metabolites twelve times more than that of the first combination. This combination was found to be the most favourable combination for the metabolite production.

Streptomycetes are usually grown in complex media containing compounds such as peptone, beef or yeast extracts. These media are quite satisfactory for growth and production of secondary metabolites (Liu *et al*. 2008). Rapidly utilized sugars like glucose support increased growth rates at the expense of antibiotic production (Escalante and Ramos, 1999; Chen and Zhang, 2002; Zhihua *et al*., 2006). Increase in biomass production was not necessarily correlated with the increase of secondary metabolites production. Generally, a quickly metabolised substance like glucose is responsible for catabolite repression (Marwick *et al*., 1999).

Metal ions are essentially required for both growth and antibiotic formation, although their optimal concentrations for growth and antibiotic biosynthesis were different. It is known that NaCl added to the media of microorganisms enhance the availability of soluble protein in the medium (Morris *et al*., 1996). Maximum activity of antibiotic biosynthesis by *Streptomyces anulatus* was detected with Fe^{2+} and slightly decreased with Ca^{2+} (Marwick *et al*., 1999). Calcium was essentially required for both growth and antibiotic formation, although its optimal concentration for growth and antibiotic biosynthesis were different. Calcium was found to promote cellular growth **(**Morris *et al*., 1996).

In conclusion, the combinations of peptone, beef, yeast extracts, glucose, NaCl, $FeSO_4$ and $CaCO_3$ was the most suitable for mosquitocidal metabolites production by Act-1 with LC_{50} of about 77.3 ppm with 95% fiducial limits (62.6-95.7).

REFERENCES

Abbott, WS. 1925. A method of computing effectiveness of insecticide. Journal of Economical Entomology. 18:265-267.

Ampofo, JA. 1995. Use of local raw materials for the production of *Bacillus sphaericus* insecticides in Ghana. Biocontrol Science Technology. 5:417-423.

Ando, K. 1983. How to discover new antibiotics for insecticidal use. In: Pesticide chemistry: Human welfare and the environment, (vol. 2), Natural Products. Eds. Takahashi, T., Yoshioka, H., Misato, T. and Matusunaka, S. Pergman Press, New York. 253-259.

Anonymous, T. 1990. Biologically active KSB-1939L3 compound and its production. Pesticide with insecticide and acaricide activity production by *Streptomyces* sp. culture. Biotechnology Abstract 9 (19), 58. (Japan patent, no 273961, 1988).

Atlas, R.M. 1993. Hand book of microbiological media. Lawrence C. Parks, CRC Press, Boca Raton, Ann Arbor, London, Tokyo. 666-789.

Chen, JF. and Zhang, YX. 2002. Studies on the effect of phosphate concentration in sisomicin fermentation. Chinese Journal of Antibiotics. 27:452-455.

De Soete, G. 1983. A least square algorithm for fitting trees to proximity data. Psychometrica. 48:621-625.

Duncan, DB. 1955. Multiple range and multiple F-test. Biometrics. 11:1.

El-Kady, GA., Kamal, NH., Mosleh, YY. and Bahgat, IM. 2008. Comparative toxicity of two bio-insecticides (spinatoran and vertemic) compared with methomyl against *Culex pipiens* and *Anopheles multicolour*. World Journal of Agricultural Sciences. 4:198-205.

Escalante, I. and Ramos, I. 1999. Glucose repression of anthracyclin formation in *Streptomyces peucetius* var *caesius*. Applied Microbiology and Biotechnology. 52: 572-578.

Greorgieva, I., Sheikova, G. and Isov, P. 1966. Biosynthesis of antibiotic 255 under laboratory conditions. Antibiotiki. 11:1067-1079.

Grovindarajan, M., Jebanesan, A. and Reetha, D. 2007. Larvicidal efficacy of extracellular metabolites of actinomycetes against dengue vector mosquito *Aedes aegypti* Linn. (Diptera: Culicidae). Research and Reviews in Biosciences. 1:1-10.

Hankin, L., Zucker, M. and Sands, DC. 1971. Improved solid medium for the detection and enumeration of pectolytic bacteria. Applied Microbiology. 22:205-209.

Hasegawa, T., Takizawa, M. and Tanida, S. 1983. A rapid analysis for chemical grouping of aerobic actinomycetes. Journal of General and Applied Microbiology. 29:319-322.

Küster, E. and Williams, ST. 1964. Selection of media for isolation of streptomycetes. Nature. 202:928-929.

Kutzner, HJ. 1976. Methoden zur Untersuchung von Streptomyceten und einigen anderen Actinomyceten. Darmstadt: Teilsammlung Darmstadt am Institut für Mikrobiologie der Technischen Hochschule. TU Darmstadt. 1-154.

Liu, H., Qin, S., Wang, Y., Li, W. and Zhang, J. 2008. Insecticidal action of quinomycin A from *Streptomyces* sp. KN-0647, isolated from a forest soil. World Journal of Microbiology and Biotechnology. 24:2243-2248.

Ludwig, W. and Strunk, D. 1997. ARB-A software environment for sequence data. TU Munchen. 1-127 .

Marwick, JD., Wright, PC. and Burgess, TG. 1999. Bioprocess intensification for production of novel marine bacterial antibiotics through bioreactor operation and design. Biotechnology. 1:495-507.

Misato, T. 1983. Recent status and future aspects of agricultural antibiotics. In: Pesticides chemistry: Human welfare and Environment, (vol. 2). Natural Products. Pergman Press. Oxford. 241-246.

Morris, ON., Converse, V., Kanagaratnam, P. and Davies, JS. 1996. Effect of cultural conditions on spore-crystal yield and toxicity of *Bacillus thuringiensis* subsp. a*izawai* (HD 133). Journal of Invertebrate Pathology. 67:129-136.

Nitsch, B., and Kutzner, HJ. 1969. Egg-yolk as a diagnostic medium for streptomycetes. Experientia. 25:113.

Peng, Z., Yang, J., Wang, H. and Simons, FER. 1999. Production and characterization of monoclonal antibodies to two new mosquito *Aedes aegypti* salivary proteins. Insect Biochemistry and Molecular Biology. 29:909-914.

Pridham, TG. and Gottlieb, D. 1948. The utilization of carbon compounds by some actinomycetes as an aid for species determination. Journal of Bacteriology. 56:107-114.

Rao, KV., Chattopadhyay, SK. and Reddy, GC. 1990. Flavonoids with mosquito larval toxicity. Tangeration, daidzein and genistein crystal production, isolation, and purification, *Streptomyces* spp culture, insecticide. Journal of Agriculture and Food Chemistry. 38:1427-1430.

Service, MW. 1983. Management of vectors. In: Pest and Vectors Management in Tropics. Eds. Youdeowei, A. and Service, MW. Longman Group Ltd., England. 7-20.

Shirling, EB. and Gottlieb, D. 1966. Methods for characterization of *Streptomyces* species. International Journal of Systematic Bacteriology. 16:313-340.

Stackebrandt, E. and Woese, C. R. 1981. Towards a phylogeny of actinomycetes and related organisms. Current Microbiology. 5:197.

Tresner, HD., Davies, MC. and Backus, EJ. 1961. Electron microscopy of *Streptomyces* spore morphology and its role in species differentiation. Journal of Bacteriology. 81:70-80.

Vijayan, V., and Balaraman, K. 1991. Metabolites of fungi and actinomycetes active against mosquito larvae. Industrial Journal of Medical Research. 93:115-117.

Williams, S.T., Sharp, M.E. and Holt, J.G. 1989. Bergey's Manual of Determinative Bacteriology (vol. 4). The Williams and Wilkins. Co. Baltimore, London.

Wu, RY. 1984. Studies on the *Streptomyces* SC4. II Taxonomic and biological characteristics of *Streptomyces* strain SC4. Botanica Bulltein Academic Sinica 25:111-123.

Yengneswaran, PK., Gray, MR. and Thompson, BG. 1991. Effect of dissolved oxygen control on growth and antibiotic production in *Streptomyces clavuligerus* fermentations. Biotechnology Progress. 7:246-250.

Zhihua, J., Xiu, C. and Peilin, C. 2006. Effects of glucose and phosphate on spinosad fermentation by *Saccharopolyspora spinosa*. Chinese Journal of Chemical Engineering. 14:542-546.

Zizka, Z., Weiser, J., Blumauerova, M. and Jizba, J. 1989. Ultra structural effects of macroterrolides of *Streptomyces grieseus* LKS-1 in tissues of *Culex pipiens* larvae-monactin, dinactin, triactin and nonactin preparations, insecticide activity. Cytobios. 58:85-91.

Received: Oct 1, 2009; Accepted: Nov 11, 2009

SENRA Academic Publishers, Burnaby, British Columbia
Vol. 4, No. 1, pp. 1027-1031, 2010
ISSN: 1715-9997

Canadian Journal of pure&applied sciences

HETEROLOGOUS PRODUCTION OF SYNTHETIC CATIONIC ANTIMICROBIAL PEPTIDE IN NOVEL OSMOTICALLY INDUCIBLE *E.COLI GJ1158*

*K Haritha[1], P Udayasri, J Madhavi, KK Pulicherla[2] and KRS Sambasiva Rao
[1]Center for Biotechnology, Acharya Nagarjuna University, Guntur-522510
[2]Department of Biotechnology, R.V.R. and J.C College of Engineering, Guntur, India

ABSTRACT

Cationic antimicrobial peptides are the upcoming therapeutic molecules as alternative drugs to the antibiotics. These peptides have a good scope in current antibiotic research. In the present study *E. coli* strain GJ1158 host was chosen for the expression of gene for Insilco designed synthetic peptide, Using Modified M9 medium. Various trails were carried out to optimize the recombinant peptide production in modified M9 medium by following the Placket Burman model. The optimal media was chosen for further expression studies and the expressed antimicrobial peptide was purified using Immobilized Metal Affinity Chromatography (IMAC) system. The product was visualized on 16% Tricine SDS-PAGE. It was identified that 30% of the bacterial proteins as the recombinant protein. The expressed antimicrobial peptide was purified using Immobilized Metal Affinity Chromatography (IMAC) system. The antimicrobial activity of purified peptide using Top agar assay showed that the recombinant antimicrobial peptide has high antibacterial activity against both Gram-positive and -negative bacteria.

Keywords: Cationc synthetic peptide, immobilized metal affinity chromatography system, placket burman model, antibacterial activity.

INTRODUCTION

Many diseases are becoming difficult to treat because of the emergence of drug-resistant organisms, including bacteria, fungi, viruses and parasites (Anthony and Fauci, 1999). The pharmaceutical industry has continuously met this need by modifying existing antibiotics and developing newer antibiotics in a timely fashion. However, the rapid emergence of resistance is even a greater problem for life-threatening viral infections. Cationic antimicrobial peptides are the upcoming therapeutic molecules as alternative drugs to the antibiotics, they are widespread in nature, occur in animals, plants and bacterial species, and represent a major defence mechanism for bacteria, plants and lower animals. Recent reports have suggested that their antibiosis against bacteria is due to their positive charge and ability to adopt amphipathic conformations. Natural CPs show considerable sequence diversity, but share certain common structural features, including a high of basic amino acid content and the dispersion of hydrophobic and hydrophilic residues, which gives the peptides their amphipathic character under hydrophobic conditions (Merrifield *et al*., 1999). Even though the natural CP's so far used as a potent alternative to antibiotics they are undesirable due to fast proteolysis after application; a poor absorption due to their hydrophilicity. For these reasons there is a strong interest to develop synthetic substances that mimic the properties of AMPs, but are not as damageable as AMPs. On the other hand commercial production of natural or synthetic peptides at large scale is very expensive because it includes various extractions and purification strategies. Hence Recombinant DNA technology has been used to clone natural or synthetic genes in bacteria, fungi, plants, or yeast cells for increased production of many eukaryotic and prokaryotic proteins. Many different host/vector systems have been used to produce antimicrobial peptides through recombinant DNA technology. *E.coli* has been utilized most often due to the low cost of fermentation compared to mammalian cells, and its ability to produce inclusion bodies, which aid in the purification process (Haught *et al*., 1998). In this paper, we report the production and optimization of M9 media and purification of a synthetic antimicrobial peptide in prokaryotic strain GJ 1158 of *E. coli.*

*Corresponding author email: harithabio@gmail.com

MATERIALS AND METHODS

Strains and Plasmids

Pseudomonas aeruginosa (MTCC 424), Klebsiella pneumonia (MTCC 2405) and Streptococcus species (MTCC 389), E. coli (MTCC 1687), were procured from Microbial Type Culture Collection (MTCC), Institute of Microbial Technology, Chandigarh, India. *E. coli* GJ1158 was procured from Genei Bangalore, India. Plasmid Cloning Vector pRSET-A was procured from Invitrogen.

Culture Media

Luria-Bertani (LB) medium was used in seed culture. The expression studies used Glucose yeast extract medium [GYE: yeast extract (5g/l), NH4Cl (1g/l), NaCl (0.5g/l), KH2PO4 (3g/l), K2HPO4 (6g/l), 1M MgSO4 (2ml/l), Trace element mix (1ml/l)]. 2% D-Glucose was supplemented to the media that required Glucose. Modified M9 media (MM9) was used for the production of recombinant antimicrobial peptide from *E. coli* expression host GJ1158. The medium was prepared as per the given composition. Na_2HPO_4(6 g/l), KH_2PO_4(3 g/l), NH_4Cl(2 g/l), Yeast Extract(4 g/l), Glucose(4 g/l), 1M $CaCl_2$-0.1ml,1M $MgSO_4$-1ml, Trace Metal Mix-1ml, pH-7.4-7.5

Analysis of antimicrobial peptide expression

For the expression of gene for *insilico* designed synthetic cationic antimicrobial peptide, it is required to transform the rDNA (synthetic gene-pRSET-A*)* in to the expression host system. In the present study *E. coli* strain GJ1158 host was chosen for the expression of synthetic gene. The rDNA was transformed into the competent bacterial system by heat shock method. Recombinant synthetic gene bearing GJ1158 bacterial expression host was grown in GYE and MM9 media till the OD_{600} reaches 1.0. GJ1158 culture grown in various media, was induced with NaCl (50 mM, 100 mM, 200 mM, and 500 mM) respectively. Induction was carried out at 37^{o}C for various time intervals (3, 4, and 5 hours). 2ml of bacterial culture was taken and centrifuged at 7000rpm for 10 minutes to harvest the bacterial cells. The pellet was suspended in 100µl Phosphate Buffered Saline. To this, 100µl of 2X Sample Solubilizing Buffer was added and used for the protein analysis.

Optimization studies for recombinant protein production from GJ1158

Modified M9 medium was chosen for the production of recombinant antimicrobial peptide from GJ1158.The medium was chosen with the literature support of Janardhan *et al*. (2007). In addition to the reported modified M9 medium tryptone was also added to the medium. The media was prepared with the composition described earlier. To optimize the media and to find out the key regulators in the growth and production of the desired protein molecules, 9 sets of media were designed by following the Placket Burman model. All 9 sets of media were inoculated with 5% of freshly grown culture and at regular time intervals of time, samples were collected to analyze the parameters viz., OD, dry cell weight, substrate reduction, and product formation.

Purification of the expressed peptide

The cloning vector pRSET-A used in the present study has given the opportunity to easily purify the expressed protein by containing the 6X *His* tag at the N-terminal end. The purification strategy is based on the natural affinity of Histidine towards the nickel ion. In the present study, Immobilized metal affinity chromatography (IMAC) system containing Nickel-Sepharose column provided by Bangalore Genei was used to purify the desired expressed antimicrobial peptide. With this system, by inducing the gene with NaCl can give the product of fusion protein containing desired antimicrobial peptide with 6X His tag at the N-terminal end. Bacterial lysate was prepared using either frozen or fresh bacterial pellet from 100ml of culture in 10ml of equilibration buffer by sonication. The lysate was centrifuged at 14,000rpm for 30 minutes to get rid of cell debris. Nickel CL Agarose column was equilibrated with 10ml of 1x equilibration buffer by removing the cap at the top of the column and pour off the storage solution. The clarified lysate was applied from step 2 of the column to allow the flow of the sample completely in to the gel bed. Then the column was washed with 1 ml of 1x equilibration buffer. Again wash the column with 20ml of 1x equilibration buffer. The column was eluted with 10ml of 1x elution buffer to collect the samples as fractions. Firstly 0.5ml was collected as the first fraction and the rest was collected as 1ml fraction. The eluted His tag protein was now analyzed by means of tricine SDS-PAGE.

Quantification of the purified peptide

The purified peptide was quantified by the standard Bradford's method to identify right fraction of the eluate containing the peptide and also to determine the expression level of the cloned antimicrobial peptide. The experiment was carried out as per the given protocol.

Antimicrobial assays

Antimicrobial activity was tested by an by top agar assay described by Kim *et al.* (2005) and also by radial diffusion method which was developed by Asoodeh *et al.* (2004) on both Gram-positive (*Streptococcus)* and Gram-negative *(Pseudomonas aeruginosa,and Klebsiella pneumonia)* bacteria. Bacteria were first grown in LB broth to an OD_{600} nm of 0.8. A 10µl aliquot of the bacteria was then taken and added to 8ml of fresh LB broth with 0.7% agar and poured over a 90mm Petri dish containing 25ml of 1.5% agar in LB broth. After the top agar hardened, a 20µL aliquot of the test sample filtered on a 0.22µm Millipore filter was dropped onto the surface of the top agar and completely dried before being incubated overnight at 37°C. If the designed peptide contained antimicrobial activity, a clear zone formed on the surface of the top agar representing inhibition of bacterial growth and ampicillin was used as a control.

RESULTS AND DISCUSSIONS

In the present work the prokaryotic strain GJ 1158 of *E. coli* host was used for the recombinant AMP expression. GJ1158 is a salt inducible expression system developed by Gowrishankar, and proven to be a good expression

Table 1. Media design by Placket Burman method for the optimal production of cationic peptide.

Flask No	Glucose (%)	Yeast Extract (%)	Tryptone (%)	Na_2HPO_4 (%)	KH_2PO_4 (%)	NH_4Cl (%)	1M $MgSO_4$ (ml/100ml)	1M $CaCl_2$ (ml/100ml)	Trace Metal Mix (ml/100ml)
1	H 1	H 0.8	H 0.8	L 0.5	H 0.3	L 0.1	L 0.1	0.01	0.1
2	L 0.4	H 0.8	H 0.8	H 0.7	L 0.3	H 0.4	L 0.1	0.01	0.1
3	L 0.4	L 0.2	H 0.8	H 0.7	H 0.3	L 0.1	H 0.1	0.01	0.1
4	H 1	L 0.2	L 0.2	H 0.7	H 0.3	H 0.4	L 0.1	0.01	0.1
5	L 0.4	H 0.8	L 0.2	L 0.5	H 0.3	H 0.4	H 0.1	0.01	0.1
6	H 1	L 0.2	H 0.8	L 0.5	L 0.3	H 0.4	H 0.1	0.01	0.1
7	H 1	H 0.8	L 0.2	H 0.7	L 0.3	L 0.1	H 0.1	0.01	0.1
8	L 0.4	L 0.2	L 0.2	L 0.5	L 0.3	L 0.1	L 0.1	0.01	0.1
9	0.4	0.4	0.4	0.6	0.3	0.2	0.1	0.01	0.1

host for heterologous protein production compared to BL21 (DE3) (Jawahar *et al.,* 2008). The rDNA was extracted from the DH5α bacterial cells and was successfully transformed into GJ1158 bacterial cells. The expression host containing the synthetic gene was grown up to 1 OD in different sets of media which were designed as per the Placket Burman model (Table 1). Various growth parameters like OD, Dry cell weight, Substrate consumption and product formation rate were analyzed (data not shown). Based on the results, it was identified that the flask no. 2 media composition was the optimal combination of nutrients suitable for the expression of AMP. The optimal media was chosen for further expression studies. The bacterial cultures were grown in the selected media and induced with various concentrations of NaCl as described in materials and methods for different intervals of time at 37°C in order to optimize the inducer concentration and time required for the production of recombinant protein. The protein expressions were resolved in 15% SDS-PAGE. As we failed to clearly visualize the desired band size of 11 KDa on 15 % SDS-PAGE, technique of Tricine SDS-PAGE was adapted for our present investigation. The Synthetic gene product was visualized on 16% Tricine SDS-PAGE (Fig. 1), and in turn the inducer concentration of 200mM NaCl for GJ1158 was identified as the optimal inducer concentration. And the time of induction was also optimized and the induction time of 4 hours was identified as the optimal time required for the inducer for the maximal production of recombinant synthetic gene (Fig. 1).

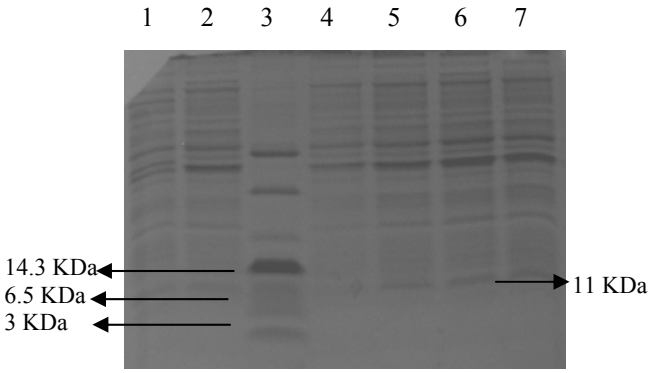

Fig. 1 Tricine SDS – PAGE analysis of recombinant peptide expression from GJ1158 host at different time intervals.

1= GJ1158 uninduced.
2= GJ1158 induced.
3= Low molecular weight protein marker.
4=Syn g pRSET-A GJ1158 uninduced.
5= Syn g pRSET-A GJ1158 induced-2 hours.
6= Syn g pRSET-A GJ1158 induced-4 hours.
7= Syn g pRSET-A GJ1158 induced-6 hours.

Purification of the peptide

Polyhistidine tags on the other hand are extremely small and therefore do not in most cases affect the folding of the attached protein. It also has very strong reversible binding attributes allowing for a very rapid and single-step purification. The tag usually consists of six consecutive histidine residues, but can vary in length from 2 to 10. Indeed, there has been great debate with regard to the length of the polyhistidine repeat and their

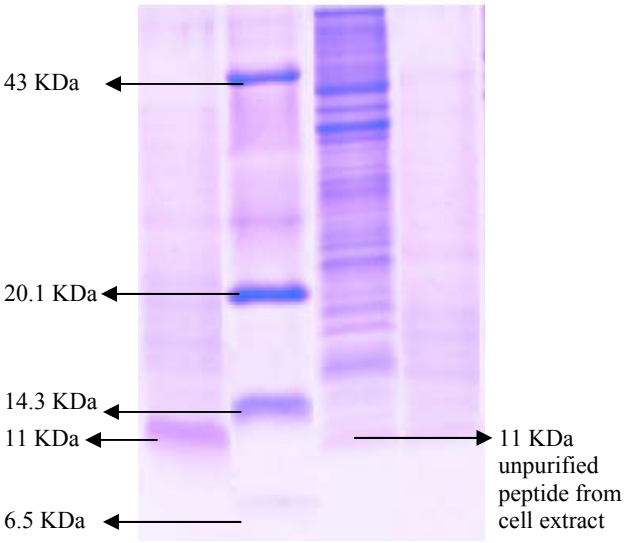

Fig. 2. Tricine SDS-PAGE analysis of IMAC purified Cationic antimicrobial peptide.
1= Purified peptide
M=Low molecular weight protein marker
2= Cell extract of syn g pRSET-A GJ1158 induced

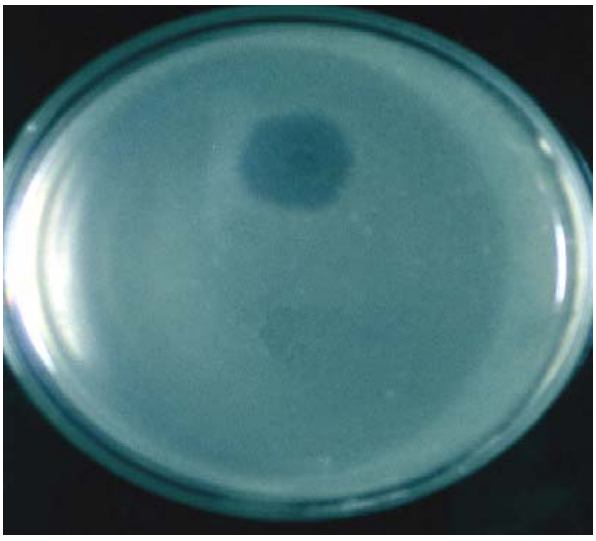

Fig. 3. Activity analysis of antimicrobial peptide by Top agar assay on *Pseudomonas aureginosa*.

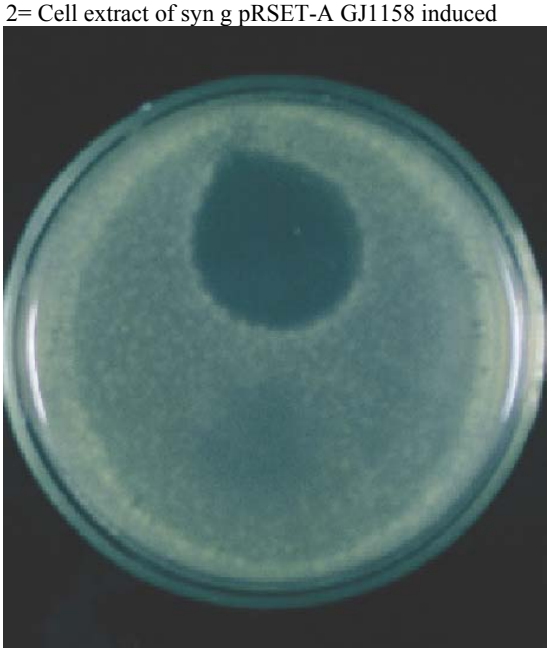

Fig. 4. Activity analysis of antimicrobial peptide by Top agar assay on *Klebsiella pneumonia.*

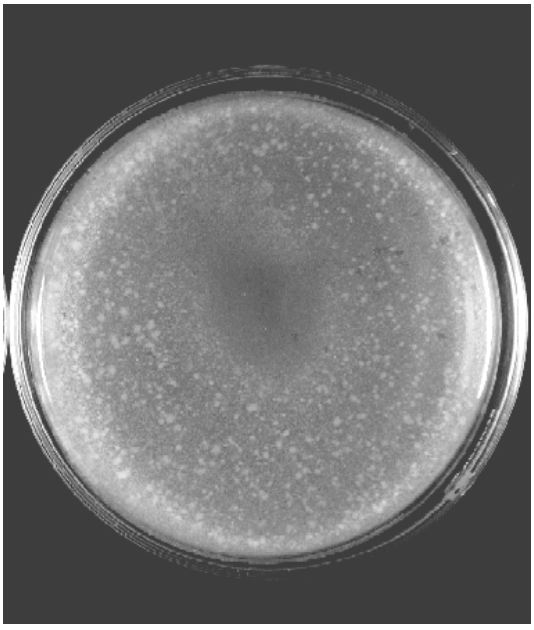

Fig. 5. Activity analysis of antimicrobial peptide by Top agar assay on *Streptococcus species.*

respective capacities to bind metal affinity resins. Recent data however appear to show there is no difference between the length of the repeat and the purification level (Mohanty *et al*., 2004). Polyhistidine tags can be placed on either the N or C-termini of recombinant proteins, although the optimal location does vary depending on the folding and biochemical characteristics of the adjacent recombinant protein. The hexahistidine tag enables the uses of immobilized metal affinity chromatography (Cao *et al.,* 2005; Marzena pazier and Jack Lubkowski, 2006; Moon *et al.,* 2007; Zhou *et al.,* 2007) for the purification of the recombinant peptides. This affinity chromatography is based upon interaction of immobilized metal ions with amino acids residues such as tryptophan, histidine, and cysteine, exposed on the protein surface. The use of immobilized metal affinity chromatography with expanded bed adsorption technology was recently described for recombinant His-tag proteins (Clemmitt *et al*., 2000; Sahin *et al*., 2005) further, the expressed peptide was purified by means of immobilized metal ion

affinity chromatography and purified sample was confirmed on Tricine SDS-PAGE (Fig. 2). It was identified that 30% of the bacterial proteins as the recombinant protein. The N- terminal histidine tag of the peptide facilitated the purification by binding to the immobilized nickel ion in the column. The same procedure was followed for the purification of Sterptolysin O (Camprubi *et al.,* 2006) the purified peptide concentration was estimated as 23mg/l by using Bradford's method by comparison with a standard curve of known amounts of bovine serum albumin (Mattos Areas *et al*., 2002). The antimicrobial assay of CP revealed that it was active against both Gram-positive and -negative bacteria (Figs. 3-5).

CONCLUSION

Towards the end of the present investigation a novel synthetic cationic peptide having broad spectrum of antimicrobial activity was produced to satisfactory levels. Further Clinical trails could prove this synthetic cationic antimicrobial peptide to be an effective antimicrobial agent and it can be effectively used on a commercial scale for control of several human pathogenic microorganisms.

REFERENCES

Anthony, S. and Fauci, MD. 1999. Antimicrobial resistance: the NIH response to a growing problem <http://www3.niaid.nih.gov/about/directors/congress/1999/0225.htm>.

Asoodeh, A., Naderi, MH., Mirshahi, M. and Ranjbar, B. 2004. Purification and characterization of antimicrobial and antifungal and non haemolytic peptide from Rana Ridibunda. Journal of sciences,Islamic republic of Iron.15(4):303-9.

Camprubi, S., Bruguera, M. and Canalias, F. 2006. Purification of recombinant histidine-tag streptolysin O using immobilized metal affinity expanded bed adsorption (IMA-EBA). International journal of biological macromolecules. 38(2):134-9.

Cao W., Zhou, Y., Ma, Y., Luo, Q. and Wei, D. 2005. Expression and purification of antimicrobial peptide adenoregulin with C-amidated terminus in *Escherichia coli***.** Protein Expression Purif. 40:404-410.

Clemmitt, RH. and Chase, HA. 2000. Immobilised metal affinity chromatography of beta-galactosidase from unclarified Escherichia coli homogenates using expanded bed adsorption. J. Chromatography A. 874:27-43.

Haught, C., Davis, G., Subramanian, R., Jackson, K. and Harrison, R. 1998. Recombinant Production and Purification of Novel Antisense Antimicrobial Peptide in *Escherichia coli*. Biotechnology and Bioengineering. 57:55-61.

Jawahar, BP., Pulicherla, KK., Rekha, VPB., Nelson, R. and Sambasiva, Rao KRS. 2008. Studies on Designing, Construction, Cloning and Expression of a novel synthetic antimicrobial peptide Current Trends in Biotechnology and Pharmacy. 2(2):334 -340.

Kim, B. 2006. Antimicrobial peptides: pore formers or metabolic inhibitors in bacteria? Nat Rev Microbiol. 3:238-250.

Marzeena, P. and Jacek, L. 2006. Expression and purification of recombinant human a-defencins in *Escherichia coli,* Protein Expression and Purification.49(1):1-8.

Mattos Arêas Ana Paula de., Maria Leonor Sarno de Oliveira., Celso Raul Romero Ramos, Maria Elisabete Sbrogio-Almeida, Isaías, Raw. and Paulo Lee Ho. 2002. Synthesis of cholera toxin B subunit gene: cloning and expression of a functional 6XHis-tagged protein in *Escherichia coli,* Protein Expression and Purification. 25 (3):481-487.

Mohanthy, AK. and Weiner, MC. 2004. Membrane protein expression and production:effect of poly His taglenth and position. Protein Expression and Purification. 33:311-325.

Moon, WJ., Hwang, Dk., Park, EJ., Kim, YM. and Chae, YK. 2007. Recombinant expression, isotope labeling, refolding, and purification of an antimicrobial peptide. Protein Expr Purif. 51(2):141.

Sahin, A., Tetaud, E., Merlin, G. and Santarelli, X. 2005. Chromatogr. J. 818:19-22.

Zhou, QF., Luo, XG., Ye, L. and Xi, T. 2007. High level production of a novel antimicrobial peptide perinerin in *Escherichia coli* by fusion expression. 54(5):366-70.

Received: Sept 18, 2009; Accepted: Dec 17, 2009

SENRA Academic Publishers, Burnaby, British Columbia
Vol. 4, No. 1, pp. 1033-1037, 2010
ISSN: 1715-9997

Canadian Journal of pure&applied sciences

IN VIVO ANTI-MALARIAL EVALUATION OF *OCIMUM SANCTUM* LINN. AND *O. BASILICUM* LINN

*Balbir Singh[1], Tilak Raj[1], MPS Ishar[1], S Sateesh Kumar[2], RK Jaggi[2] and Anupam Sharma[2]
[1]Department of Pharmaceutical Sciences, Guru Nanak Dev University, Amritsar 143005 Punjab
[2]University Institute of Pharmaceutical Sciences, Panjab University Chandigarh-160014, India

ABSTRACT

Different extractives from leaves and roots of *Ocimum sanctum* Linn. and *O. basilicum* Linn. have been evaluated for *in vivo* anti-malarial activity using Peter's 4-day suppressive test against *Plasmodium berghei* in mice. Ethanol extracts of roots of both plants exhibited maximum anti-malarial activity amongst various extracts viz., petroleum ether, chloroform, ethanol and water at the dose of 800 mg/kg in mice. The results were observed on the 4th and 7th day. Ethanolic extract of *O. sanctum* roots showed maximum antiplasmodial activity of 3.2 ± 0.74 at dose of 800mg/kg on day 4th. However, *O. basilicum* root extract showed maximum activity of 4.9 ± 0.96 at dose 800mg/kg on day 4th. Maximum activity of ethanoic extract was observed on day 4th.

Keywords: *Ocimum sanctum*, *O. basilicum*, anti-malarial activity, *Plasmodium berghei*.

INTRODUCTION

Malaria is a public health problem in more than 90 countries inhabited by 2.4 billion people. It is responsible for >500 million clinical cases and 1.5–2.7 million deaths per year, most of whom are children under 5 years of age and pregnant women (WHO, 1996; Schwartlander, 1997). Every year, 10% of the global population is infected with malaria, and many (99.4%) of them survive after 10–20 days of illness. *Plasmodium* species are protozoan parasites responsible for malaria, an illness killing about millions of people per year (WHO, 2005). With the absence of an operational vaccine for malaria or leishmaniasis in the immediate horizon, chemotherapy and chemoprophylaxis remain the main methods for disease control. Current anti-protozoal drugs are inadequate due to parasite resistance, toxicity, lack of efficacy and inability to eliminate all stages of parasites from the host (Tasdemir *et al*., 2005). However, with the increase in cases of drug resistance and failure, there is an increase in the use of herbal medicine. Approximately 80% of the people in the developing countries depend on traditional medicine for the management of disease conditions (Phillipson and Wright, 1991).

The discovery of quinine and artemisinin from *Cinchona succiruba* (Rubiaceae) and *Artemisia annua*, respectively, followed by their development into powerful anti-malarial drugs represent milestones in the history of anti-parasitic drugs from plants (Kayser *et al*., 2003).

Today's researchers are exploring the plant kingdom to lay hands on the bioactive phyto-moieties, which can be used to cure malaria. *Ocimum sanctum* Linn. (Family Labiatae) commonly known as 'Sacred Basil' or 'Holy Basil' (Tulsi in Hindi) is an herbaceous annual plant indigenous to India. *O. sanctum* has been utilised as a general promotor for health in herbal medicine (Rai, 1993) and most of its properties like antistress (Ashok and Vaidya, 1997), adaptogenic (Sembulingam *et al*., 1999), anticancer (Aruna *et al*., 1992), anti-inflammatory (Chattopadhyay *et al*., 1994; Singh *et al*., 1996), anti-hyperlipidemic (Rai and Mani, 1997), antihyper-cholesteremic (Sarkar *et al*., 1994), hepatoprotective (De, S. Ravishankar *et al*., 1993), radioprotective (Uma Devi *et al*., 1998) and antimicrobial (Rajendhran and Arun, 1998) have been examined scientifically. It has been used traditionally to cure malarial fever (Chopra *et al*., 1956; Usha Devi *et al*., 2001). The present study has been undertaken with an objective to evaluate leaves and roots of *O. sanctum* and *O. basilicum* for their i*n vivo* anti-malarial activity in mice.

MATERIALS AND METHODS

Plant material and extraction: The leaves and roots of *O. sanctum* and *O. basilicum* used for the present study were collected from the plants grown locally in the Medicinal Plants Garden of the University Institute of Pharmaceutical Sciences (UIPS), Panjab University, Chandigarh. The leaves and roots of *O. sanctum* and *O. basilicum* were dried in shade. Each portion was reduced to moderately coarse powder (# 10) and separately extracted with petroleum ether (60-80^{o}C), chloroform, ethanol and distilled water successively using soxhlet apparatus. All the extracts were dried under reduced pressure.

*Corresponding author email: balbir_gndu@yahoo.com

Chemical study: Different extractives obtained above were tested chemically for the presence or absence of alkaloids, saponins, sterols, triterpenoids, proteins, flavonoids, carbohydrates and tannins (Evans, 1996; Farnsworth, 1966).

Animals: Adult Swiss mice BALB /c strain (25-28 g) of either sex, bred in the Central Animal House of Panjab University, Chandigarh were used. Animals were fed on the standard diet and water *ad libitum*.

Tested material: Petroleum ether, Chloroform, ethanol and water extractives of leaves and stems of *O. sanctum* and *O. basilicum.*

Vehicle and preparation of doses: Tween 80 (2.5 %) in distilled water was used as control (vehicle). The extractives obtained were suspended in distilled water using suspending agent, i.e, Tween 80. The doses were so adjusted as to administer 0.25 ml in each mouse; chloroquine diphosphate in vehicle was used as standard.

Antimalarial activity

4 days suppressive test model

The 4-day test developed by Peter's was used to determine *in vivo* antimalarial activity (Peters, 1975). The mice were randomly divided into three different [control (1), standard (2) and test (3)] groups of 5 animals each. On day 0 the test animals in all the groups were inoculated with $1x10^7$ *Plasmodium berghei* infected RBC's. The animal in-group 3 was treated with the test substance on all the four days, while animals of group 1 and 2 received the vehicle and chloroquine diphosphate, respectively, at the same time on the similar days. Blood smears from all the animals were prepared on day-4 and percentage parasitaemia was recorded and compared with that of control animals. On day 4 thin blood smears were prepared from the tail vein of all the animals and stained with Giemsa's solution to monitor the parasitaemia and the reduction of parasitaemia was calculated. Any mortality within 24h of drug administration was considered as toxicity of the drug. The percent parasitaemia was calculated using the following expression:

$$\% \text{ Parasitaemia} = \frac{\text{Number of parasitized cells}}{\text{Total number of cells}} \text{ x } 100$$

Statistical analysis

Results were expressed as mean±S.E.M. and all the extractives were compared with chloroquine diphosphate (standard) and control separately using one way analysis of variance (ANOVA) followed by Dunnett's test. $P < 0.05$ was considered statistically significant.

RESULTS AND DISCUSSION

After removal of solvents from various extracts in vacuo, the percentage of various extractives obtained was obtained (Table 1). Phytochemical screening gave positive tests for saponins, sterols, triterpenoids, carbohydrates, tannins, proteins and flavonoids.

Table 1. Yield of various extracts.

Extract	Yield (% w/w)			
	Ocimum sanctum		*Ocimum basilicum*	
	Leaf	Root	Leaf	Root
Petroleum ether	6.34	0.97	5.88	1.12
Chloroform	5.42	2.18	6.15	1.98
Ethanol	6.61	2.65	6.52	2.16
Water	7.18	3.97	6.85	3.10

Antiplasmodial activity was observed for the leaves and roots extracts of *O. sanctum* and *O. basilicum* (Table 2 and 3). All the extracts i.e., PE, CE, EE and WE were given to the infected mice at doses of 100, 200, 400 and 800mg/kg using chloroquine diphosphate as positive control. Ethanolic extract of leaves and roots showed maximum antiplasmodial activity on the 4^{th} and 7^{th} day at two dose levels of 400 and 800 mg/kg. Ethanolic extract of *O. sanctum* leaves exhibited maximum antiplasmodial activity of 7.8 ± 1.54 (400 mg/kg) on 4^{th} day and 25 ± 3.97 (400 mg/kg) on 7^{th} day (Table 2). However, maximum activity of 6.2 ± 1.32 on 4^{th} day and 20.2 ± 3.24 (800 mg/kg) on 7^{th} day was observed at a dose of 800mg/kg. Ethanolic extract of *O. sanctum* roots exhibited maximum antiplasmodial activity of 5.8 ± .87 (400 mg/kg) and 19.0 ± 3.39 (400 mg/kg) on 4^{th} day and 7^{th} day, respectively. At a dose of 800mg/kg maximum antiplasmodial activity of 3.2 ± 0.74 on 4^{th} day followed by 15.7 ± 5.00 (800 mg/kg) on day 7^{th}. All other extracts were found to be inactive.

In case, of plant *O. basilicum* (Table 3) maximum activity was observed for ethanolic extract of leaves and roots at dose of 400 mg/kg and 800 mg/kg. Leaves extract exhibit 7.8 ± 1.21 followed by 6.6 ± 0.91 on day 4^{th} at a dose of 400 and 800 mg/kg, respectively. On day 7^{th} maximum activity of 27.6 ± 4.39 (400 mg/kg) followed by 22.0 ± 6.14 (800 mg/kg). Ethanolic extracts of roots exhibited maximum growth inhibition of 5.9 ± 0.85 and 4.9 ± 0.96 at dose 400mg/kg and 800 mg/kg, respectively on day 4^{th}. While on day 7^{th} maximum antiplasmodial activity of 20 ± 3.90 (400 mg/kg) and 17.8 ± 2.95 (800mg/kg) was observed.

CONCLUSIONS

All the extracts were prepared and there *in vivo* antimalarial activity was evaluated using Swiss mice BALB /c strain. The results were observed on the 4th and 7th day. Ethanolic extract of *O. sanctum* roots showed maximum antiplasmodial activity of 3.2 ± 0.74 at dose of 800mg/kg on day 4th. However, *O. basilicum* root extract showed maximum activity of 4.9 ± 0.96 at dose 800 mg/kg on day 4th. Maximum activity of ethanoic extract was observed on day 4th.

Table 2. *In vivo* anti-malarial effect of various extracts of *Ocimum sanctum* Linn. Leaves and roots.

Treatment	Dose (mg/kg)	Mean percent parasitaemia ± S.D.			
		O. sanctum leaves		*O. sanctum* roots	
		Day 4	Day 7	Day 4	Day 7
Control	-	11.2 ± 1.90	41.4 ± 5.72	11.2 ± 1.90	41.4 ± 5.72
Standard	5	1.9 ± 0.71	5.3 ± 1.40	1.9 ± 0.71	5.3 ± 1.40
Pet. Ether Extract	100	11.4 ± 1.26	41.9 ± 2.69	11.4 ± 1.26	41.2 ± 4.58
	200	11.2 ± 2.45	39.6 ± 4.18	10.9 ± 1.68	40.8 ± 4.16
	400	10.7 ± 1.31	36.8 ± 3.90	10.5 ± 1.06	39.4 ± 2.85
	800	9.8 ± 1.25	35.9 ± 4.80	9.6 ± 1.60	38.9 ± 5.50
Chloroform Extract	100	11.6 ± 1.86	42.9 ± 5.44	11.0 ± 2.70	42.0 ± 3.43
	200	11.3 ± 1.93	41.0 ± 6.38	10.7 ± 1.82	41.6 ± 5.95
	400	10.6 ± 2.42	40.5 ± 6.89	10.0 ± 2.06	39.8 ± 2.93
	800	9.8 ± 1.96	39.1 ± 3.69	9.8 ± 1.53	37.4 ± 3.14
Ethanol Extract	100	9.7 ± 1.28	34.0 ± 2.53	9.6 ± 1.46	33.8 ± 4.70
	200	8.1 ± 1.11	30.5 ± 5.01	8.0 ± 1.30	28.9 ± 4.11*
	400	7.8 ± 1.54*	25.0 ± 3.97 *	5.8 ± 0.87*	19.0 ± 3.39*
	800	6.2 ± 1.32*	20.2 ± 3.24*	3.2 ± 0.74*	15.7 ± 5.00*
Water Extract	100	10.7 ± 1.26	38.5 ± 3.43	10.0 ± 1.05	35.9 ± 5.05
	200	9.5 ± 0.83	35.8 ± 3.59	9.3 ± 2.09	31.6 ± 3.68
	400	8.7 ± 1.39	32.5 ± 4.03	8.6 ± 1.30	31.4 ± 3.16
	800	8.3 ± 1.00	32.1 ± 3.90	8.4 ± 1.50	30.6 ± 3.35*

Table 3. *In vivo* anti-malarial effect of various extracts of *Ocimum basilicum* Linn. Leaves and roots.

Treatment	Dose (mg/kg)	Mean percent parasitaemia ± S.D.			
		O. basilicum leaves		*O. basilicum* roots	
		Day 4	Day 7	Day 4	Day 7
Control	-	11.2 ± 1.90	41.4 ± 5.72	11.2 ± 1.90	41.4 ± 5.72
Standard	5	1.9 ± 0.71	5.3 ± 1.40	1.9 ± 0.71	5.3 ± 1.40
Pet. Ether Extract	100	11.2 ± 1.19	42.4 ± 8.7	11.3 ± 1.42	41.7 ± 5.48
	200	10.9 ± 1.51	40.6 ± 8.1	10.2 ± 1.47	39.6 ± 6.26
	400	10.7 ± 1.30	39.1 ± 5.01	10.1 ± 1.00	37.5 ± 5.17
	800	9.9 ± 1.70	38.1 ± 6.06	9.3 ± 1.30	36.9 ± 6.19
Chloroform Extract	100	11.5 ± 1.34	39.3 ± 5.68	11.4 ± 1.48	40.4 ± 1.85
	200	11.1 ± 1.76	38.2 ± 4.83	9.7 ± 1.46	39.1± 2.08
	400	10.4 ± 1.55	38.1 ± 4.23	9.4 ± 1.46	39.8 ± 1.36
	800	10.1 ± 1.95	36.7 ± 5.11	8.6 ± 1.27	38.1 ± 2.60
Ethanol Extract	100	9.4 ± 1.55	33.5 ± 5.52	8.7 ± 1.65	34.2 ± 4.32
	200	8.4 ± 1.17	32.8 ± 4.77	8.3 ± 1.00	29.3 ± 4.22*
	400	7.8 ± 1.21*	27.6 ± 4.39 *	5.9 ± 0.85*	20.9 ± 3.90*
	800	6.6 ± 0.91*	22.0 ± 6.14*	4.9 ± 0.96*	17.8 ± 2.95*
Water Extract	100	11.0 ± 1.10	37.6 ± 4.53	10.9 ± 1.16	37.9 ± 4.42
	200	10.6 ± 1.07	34.1 ± 4.45	10.1 ± 1.20	32.8 ± 7.23
	400	9.3 ± 1.35	33.5 ± 2.83	9.3 ± 1.00	30.6 ± 3.54
	800	8.9 ± 1.24	31.0 ± 3.08	8.2 ± 0.87*	28.8 ± 2.66*

Since the different extractives showed reduction of parasitaemia it suggested that leaf and roots of *O. sanctum* and *O. basilicum* contain the active compounds which inhibited *P. berghei*. Phytochemical investigations demonstrated the presence of saponins, sterols, triterpenoids, carbohydrates, tannins, proteins and flavonoids.

Some of the plants such as *Brunsvigia littoralis* [Campbell *et al*., 1998), *B.* radulosa (Likhitwitayawuid *et al*., 1993), *Alstonia macrophylla* (Keawpradub *et al*., 1999) and *Peschiera fuchsiaefolia* (Federici *et al*., 2000) have exhibited antimalarial activity due to the presence of alkaloidal compounds. On the other hand *Rhus retinorrhoea* (Ahmed *et al.*, 2001) possesed antimalarial activity due to the presence of flavonoids. Therefore, the significant antimalarial activity of *O. sanctum* and *O. basilicum* extracts may be attributed to the presence of the alkaloidal and/or flavonoidal constituents. Thus, ethanolic extracts of roots and leaves of *O. sanctum* and *O. basilicum* may be used for further development.

ACKNOWLEDGEMENTS

We are thankful to Prof. HS. Banyal, from Zoology Department, Panjab University, Chandigarh for providing us with *P. berghei* strain and for their kind cooperation. The financial assistance provided by the University Grants Commission of India, New Delhi is duly acknowledged.

REFERENCES

Ahmed, MS., Galal, AM., Ross, SA., Ferreira, D., Elsohly, MA., Ibrahim, ARS., Mossa, JS. and El-Feraly, FS. 2001. A weakly antimalarial biflavanone from Rhus retinorrhoea. Phytochemistry. 58:599-602.

Aruna, K. and Sivaramakrishnan, VM. 1992. Anticarcinogenic effects of some Indian plant products. Food and Chemical Toxicology. 30:953-56.

Campbell, WE., Nair, JJ., Gammon, DW., Bastida, J., Codina, C., Viladomat, F., Smith, PJ. and Albrecht, CF. 1998. Cytotoxic and Antimalarial Alkaloids from *Brunsvigia littoralis*. Planta Medica. 64 (01):91-93.

Chattopadhyay, RR., Sarkar, SK., Ganguly, S. and Basu, TK. 1994. A comparative evaluation of some anti-inflammatory agents of plant origin. Fitoterapia. 65:146-48.

Chopra, RN, Nayar, SL. and Chopra IC. 1956. Glossary of Indian Medicinal Plants. CSIR, New Delhi. p.179.

De S. Ravishankar, B. and Bhassar, GC. 1993. Plants with hepatoprotective activity- a review. Indian Drugs. 30:355-60.

Evans, WC. 1996. Alkaloids. In Trease and Evans' Pharmacognosy, (14th ed.). Gopsons papers Limited, Noida, UP. India. p. 340.

Evans, WC. 1996. Carbohydrates. In Trease and Evans' Pharmacognosy, (14th ed.) Gopsons papers Limited, Noida, UP. India. p. 191.

Evans, WC. 1996. Phenols and phenolic glycosides. In Trease and Evans' pharmacognosy, 14th Edn. Gopsons papers Limited, Noida, UP. India. p. 218.

Farnsworth, RN. 1966. Biological and phytochemical screening of plants. Journal of Pharmaceutical Sciences. 55:225.

Federici, E., Palazzino, G., Nicoletti, M. and Galeffi, C. 2000. Antiplasmodial activity of the alkaloids of Peschiera fuchsiaefolia. Planta Medica. 66(1):93-95.

Kayser, O., Kiderlen, AF. and Croft, SL. 2003. Natural products as potential anti-parasitic drugs. Parasitology Research. 87 (Suppl. 2): S55-62.

Keawpradub, N., Kirby, GC., Steele, JCP. and Houghton, PJ. 1999. Antiplasmodial Activity of Extracts and Alkaloids of Three *Alstonia* Species from Thailand. Planta Medica. 65 (08):690-694.

Likhitwitayawuid, K., Angerhofer, CK., Chai, H., Pezzuto, JM. and Cordell, GA. 1993. Cytotoxic and Antimalarial Alkaloids from the Bulbs of Crinum amabile. Journal of Natural Product. 56: 331-38.

Peters, W. 1975. The chemotherapy of rodent malaria, XXII- The value of drug-resistant strains of *P. berghei* in screening for blood schizontocidal activity. Annals of Tropical Medicine and Parasitology. 69:155-171.

Phillipson, JD., Wright, CW. 1991. Can ethnopharmacology contribute to the development of antimalarial agents? Journal of Ethnopharmacology. 32:155-165.

Rajendhran, J. and Arun, MM. 1998. Antibacterial activity of some selected medicinal plants. Geobios. 25:280-82.

Rai, MK. 1993. Herbal medicine in India: reterospect and prospect. Fitoterapia. 65:485.

Rai, V. and Mani, UV. 1997. Effect of *Ocimum sanctum* leaf powder on blood lipoproteins glycated proteins and total amino acids in patients with non – insulin - dependent diabetes mellitus. Journal of Nutritional and Environmental Medicine. 7:113-118.

Sarkar, A., Lavania, SC., Pandey, DN. and Pant, MC. 1994. Changes in blood lipid profileafter admininistration of *Ocimum sanctum* (Tulsi) leaves in the normal albino rabbits. Indian Journal of Physiology and Pharmacology. 38:311-12.

Schwartlander, B. 1997. Global burden of disease. Lancet. 350:141-142.

Sembulingam, R., Sembulingam, P. and Namasivayam, A. 1999. A. Effect of *O. sanctum* Linn. on changes in leukocytes of albino rats induced by acute noise stress. Indian Journal of Physiology and Pharmacology. 43:137-40.

Singh, S., Majumdar, DK. and Rehan, HMS. 1996. Evaluation of anti-inflammatory potential of fixed oil of *Ocimum sanctum* (Holybasil) and its possible mechanism of action. Journal of Ethanopharmacol. 54:9-26.

Tasdemir, D., Guner, ND., Perozzo, R., Brun, R., Donmez, AA., Calis, I. and Ruedi, P. 2005. Anti-protozoal and plasmodial FabI enzyme inhibiting metabolites of *Scrophularia lepidota* roots. Phyto-chemistry. 66:355-362.

Uma Devi, P., Bist, KS. and Vinitha, M. 1998. A comparative study of radioprotection by *Ocimum* flavanoids and synthetic aminothiol protectors in the mouse. British Journal of Radiology. 71:782-84.

Usha Devi, C., Neena, V., Atul, PK. and Pillai, CR. 2001. Antiplasmodial effect of three medicinal plants: A preliminary study. Current science. 80:917-919.

Vaidya AB. 1997. The status and scope of Indian medicinal plants acting on CNS. Indian Journal of Pharmcology. 29:S-340.

WHO. 1996. Investing in Health Research and Development. WHO Document TDR/Gen/96.1. Report of the Ad Hoc Committee of Health Research Relating to Future Intervention Options. WHO, Geneva.

World Health Organisation (WHO), 2005. World Malaria Report www. who.malariareport 2005.org.

Received: Sept 25, 2009; Accepted: Dec 21, 2009

SENRA Academic Publishers, Burnaby, British Columbia
Vol. 4, No. 1, pp. 1039-1044, 2010
ISSN: 1715-9997

Canadian Journal of pure&applied sciences

EVALUATION OF THE ANTIMALARIAL ACTIVITY OF *BRIDELIA FERRUGINEA* BENTH BARK

*Kolawole, OM[1,2] and Adesoye, AA[1]
[1]Malaria Research Laboratory, Department of Microbiology, Faculty of Science, University of Ilorin, Ilorin, Nigeria
[2]Malaria Laboratory - I, Department of Molecular Parasitology
Bernhard Nocht Institute for Tropical Medicine, Bernhard-Nocht-Str. 74, 20359 Hamburg, Germany

ABSTRACT

The antimalarial activity of the methanolic extract of *Bridelia ferruginea* benth bark was evaluated at varying doses of 200mg/kg, 400mg/kg and 800mg/kg body weights in mice (*Mus musculus*) infected with chloroquine -sensitive *Plasmodium berghei*. The antimalarial activity of the extract during Prophylactic (pre-treatment before infection with the parasite), Suppressive (co-treatment with the infection of the parasite on day zero) and Rane test (established infection which involves post treatment after 72hours infection with the parasite) were investigated. Phytochemical screening revealed the presence of alkaloids, glycosides, phenolics, saponins, steroids, anthraquinones and tannins in the extract. The extract demonstrated a dose-dependent suppression of parasitaemia following administration to infected mice. An optimum dose of 400mg/kg body weight with established infection mode of treatment demonstrated 100% total clearance of parasitaemia comparing favourably with chloroquine, the reference drug over the 28 days period of observations. Conclusively, the bark extract has exhibited promising antimalarial activity which can be exploited in malaria therapy.

Keywords: *Bridelia ferruginea*, methanolic extract, phytochemicals, antimalarial.

INTRODUCTION

Malaria is an infection of the blood that is carried from person to person by mosquitoes. The disease has been recognized for thousands of years and once was found almost every where except in the most northern areas of the world (Wirth, 1998). Over the past hundred years, malaria has been one of the most serious and complex health problems facing humanity. Malaria remains the most important parasitic disease of humans, affecting approximately 40% of the human populations in tropical and subtropical areas of the world, as numbers of travelers of these areas increase (Sachs, 2002).

The disease is caused by *Protozoan* parasites of the subphylum *Apicomplexa,* belonging to the genus *Plasmodium* which is transmitted by female mosquitoes of the genus *Anopheles*. The major burden of approximately two million deaths annually occurs in sub-saharan Africa where 90% of all deaths are from *Plasmodium falciparum. Plasmodium falciparum* is the most lethal, accounting for over 90% of malaria associated deaths (Mesia *et al*., 2005).

The *Plasmodium* life cycle starts with a blood meal of an infected *Anopheles* mosquito and the coincident injection of sporozoites into human skin. After breaching blood vessels of the skin (Amino *et al.,* 2006) sporozoites are transported by the blood stream to the liver. There, the parasite infects liver parenchyma cells (hepatocytes) and differentiates into thousands of merozoites. To access the bloodstream, liver-derived merozoites must leave their host cell and cross the endothelium of the liver blood vessels. Within red blood cells (RBCs) each parasite replicates, depending on the *Plasmodium* species, into 16 or 32 merozoites, which then get released to directly infect other RBCs (Sturm and Heussler, 2007).

Although traditional medicine is widely used to treat malaria and is often more available and affordable than orthodox medicine, there are few clinical data on safety and efficacy. All cultures from ancient times to the present day have used plants as a source of medicine (Elujoba, 2005). Today, according to the World Health Organization (WHO), as many as 80% of the people of the world depend on traditional medicine for their primary health care needs. The greater part of traditional therapy involves the use of plant extracts or their active principles (Farnsworth and Soejarto, 1985). However, there is no consensus, even among traditional healers, on which plants, preparations, and dosages are the most effective. On the whole, medicinal plants are just taken based on local reputation; one such plant is *Bridelia ferruginea.*

Bridelia ferruginea of the family Euphorbiaceae is usually a gnarled shrub, which sometimes reaches the size of a tree in suitable condition. The down curved tip of the leaf is distinctive. In Nigeria, its common names are

*Corresponding author email: tomak74@yahoo.com

Iralodan (Yoruba), Ola (Igbo) and Kizni (Hausa). The plant has a geographical spread that runs from Guinea to Zaire and Angola. Its habitat is the savannah especially in the moister regions (Kolawole and Olayemi, 2003). Kolawole *et al.,* 2006, 2007 reported its efficacy in the reduction of total bacterial and coliform counts in river water and wastewater treatments. A decoction of the leaves is used to treat diabetes. It is also used as a purgative and a vermifuge (Cimanga *et al.,* 1999; De Bruyne *et al*., 1997). In Nigeria, the Yoruba people of Idofian, Ilorin South Local Government Area of Kwara State claimed that when the bark of *Bridelia ferruginea* is boiled in sizeable drinkable water and allowed to cool, it has been in use traditionally as antimalarial drug for more than a century ago. Recently, studies have reported the trypanocidal potentials of the methanolic extract (Ekanem *et al.,* 2008). Although this plant is used in the traditional treatment of malaria, there is no documented study of its antimalarial activity. This study was prompted in view of this to investigate the potency of the plant against blood stage of the plasmodium parasite using varying doses of the extract with different regime of treatments.

MATERIALS AND METHODS

Chemicals

Absolute methanol (Riedel-de Haën) was obtained from Sigma-Aldrich Laborchemikalien GmbH, Germany. Giemsa stain was obtained from Anosantec Laboratories, UK. Chloroquine diphosphate salt was obtained from Sigma Chemical Company, St. Louis, MO, USA. Other reagents used were of analytical grade and were prepared in all glass-distilled water.

Experimental Animals

Fifty five adult Swiss albino mice (*Mus musculus*) with an average weight of 20 ±2g were obtained from the animal breeding unit of the Department of Pharmacology, University of Ibadan, Oyo state. The mice were housed in plastic cages and maintained under standard laboratory conditions with free access to rat pellets and tap water *ad-libitum*. The research adhered to the Principles of Laboratory Animal Care (NIH publication #85−23, revised in 1985).

Parasite strain

A chloroquine-sensitive strain of *Plasmodium berghei* (NK-65) was obtained from the Institute for Advanced Medical Research and Training (IAMRAT), College of Medicine, University of Ibadan, Oyo state. The parasites were maintained by weekly blood passage in mice.

Plant source and Identification

The barks of Bridelia ferruginea benth were obtained from Idofian town of Kwara state, Nigeria in October, 2008 and were authenticated at Forestry Research Institute of Nigeria (FRIN), Ibadan, Oyo state.

Plant extract preparation and phytochemical screening

Fresh bark of *Bridelia ferruginea* were dried in the shade at room temperature and pulverized to powder using an electric blender. The extraction was done using the solvent methanol at ambient temperature (cold extraction) according to the method of Kolawole *et al., 2003.* Preliminary qualitative phytochemical screening of the plant extract was carried out employing standard procedures (Odebiyi and Sofowora, 1978).

Animal grouping and extract administration

The animals were divided into eleven groups A_a, A_b, A_c, B_a, B_b, B_c, C_a, C_b, C_c, D, and E of five mice each. The percentage parasitaemia of the donor mouse was first determined using a haemocytometer and an appropriate dilution of the infected blood with isotonic saline was done. Animals in all the infected groups were inoculated intraperitoneally with 0.2ml of infected blood containing about 1×10^7 *Plasmodium berghei* parasitized red blood cells depending on the regime of extract treatment. All the animals were infected from the same donor mouse. This study involved three regime of extract administration; the prophylactic (A_a, A_b and A_c), which involved pre-treatment stage (5 days before infection with parasite), the 4-day test or suppressive treatment (B_a, B_b and B_c) involving co-treatment starting on the day of infection with parasite and continued for 5-days; and Rane test or test of established infection (C_a, C_b and C_c) which involved post treatment after 72hours of infection with parasite. The test was conducted according to the method described by Ryley and Peters (1970).

Groups A_a, B_a, and C_a were given 800mg/kg body weight of the extract for 5 days.

Groups A_b, B_b, and C_b were given 400mg/kg body weight of the extract for 5 days;

Groups A_c, B_c, and C_c were given 200mg/kg body weight of the extract for 5 days;

Group D animals were infected with parasite but not treated.

Group E animals were given 4mg/kg body weight of the chloroquine diphosphate for 5 days, 72 hours after infection with parasite. All drugs administration was done orally with canula.

Sample collection and analyses

Daily blood films were screened for malaria parasites in tail blood of all the infected animals after fixing in methanol, stained with Giemsa and the percentage of parasites in the blood was determined through microscopic examination. The blood was screened from the fourth to the twenty eight days of post infection.

In calculating the percentage parasitaemia, the slide prepared in thin blood film was used. The parasitized red blood cells were then counted using the ×100 objective

lens (oil immersion). To calculate the percentage parasitaemia, the following formula was used

$$\% \text{ Parasitaemia} = \frac{\text{Total number of PRBC}}{\text{Total number of RBC}} \times 100$$

Where: PRBC = Parasitized Red Blood Cells
RBC = Total Red Blood Cells

Percentage chemosuppression
The percentage chemosuppression was calculated by subtracting the average percentage parasitemia in treated group from the average percentage parasitemia in control group and the value obtained was expressed as a percentage of the average percentage parasitemia in control group.

Mean survival time
The mean survival time for each group was determined arithmetically by finding the average of the survival time (days) of the mice post inoculation in each group over a period of 28 days (D0 to D28).

Statistical analysis
Values are expressed as mean ± SEM. Data from the test groups were compared with their respective controls and differences at $p<0.05$ were considered significant.

RESULTS

Some of the phytochemicals present in the methanolic extract of *Bridelia ferruginea* bark are shown in Table 1. The screening revealed the presence of alkaloids, flavonoids, glycosides, phenolics, saponins, steroids, anthraquinones and tannins.

Table 1. Some phytochemicals in the methanolic extract of *Bridelia ferruginea* bark.

Phytochemicals	Status
Alkaloids	++
Tannins	++
Phenolics	++
Glycosides	++
Saponins	++
Flavonoids	+
Steroids	++
Anthraquinones	+

++ Strongly present, + Fairly present

Parasitaemia levels in infected untreated mice, infected mice treated with 800mg/kg, 400mg/kg, 200mg/kg body weight of methanolic extract of *Bridelia ferruginea* bark administered as prophylactic treatment, co-treatment (comparative with infected mice treated with 4mg/kg body weight of chloroquine) and post-treatment from the fourth to the twenty-eighth day of post infections are shown in Figures 1, 2, and 3. The results of the prophylactic treatment revealed that on day 4, groups treated with 800mg/kg, 400mg/kg and 200mg/kg had 1.45%, 2.02%, and 2.16% parasitaemia respectively. By day eight, there was percentage decrease in parasitaemia for 800mg/kg and 400mg/kg but with a progressive percentage parasitaemia increase for 200mg/kg along with the infected untreated mice continually till the end of the experiment. On day eight, all the remaining mice that received 800mg/kg of extract died, while those with 400mg/kg continued to experience a steady decrease in percentage parasitaemia compared to the infected untreated mice throughout the observation periods (Fig. 1).

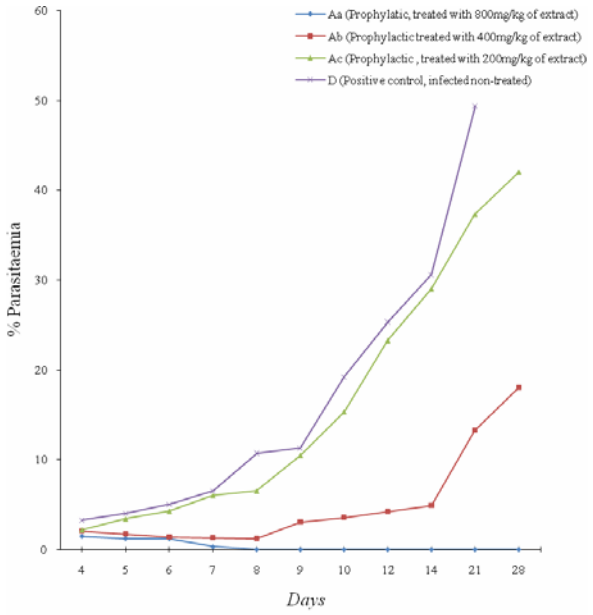

Fig. 1. Dose-dependent percentage parasitaemia of mice placed on prophylactic treatment. Each point is an average count from five infected mice (±SEM).

In the suppressive treatment, on day four, the percentage parasitaemia were 800mg/kg (1.50%), 400mg/kg (1.66%) and 200mg/kg (3.09%). By day eight, there was continual increase in percentage parasitaemia for all the treated groups but with considerable decrease compared to the infected untreated mice throughout the experimental period. It must be noted that at the fourteenth day, all the mice treated with 800mg/kg died (Fig. 2).

The results of established infection treatment shown in Figure 3 revealed that on day four the percentage parasitaemia were 800mg/kg (2.05%), 400mg/kg (2.98%) and 200mg/kg (3.02%). There was increase in parasitaemia in all groups for days 5, 6 and 7. By day 8, there was steady decline for 800mg/kg (2.03%) and 400mg/kg (2.01%) whereas 200mg/kg and infected

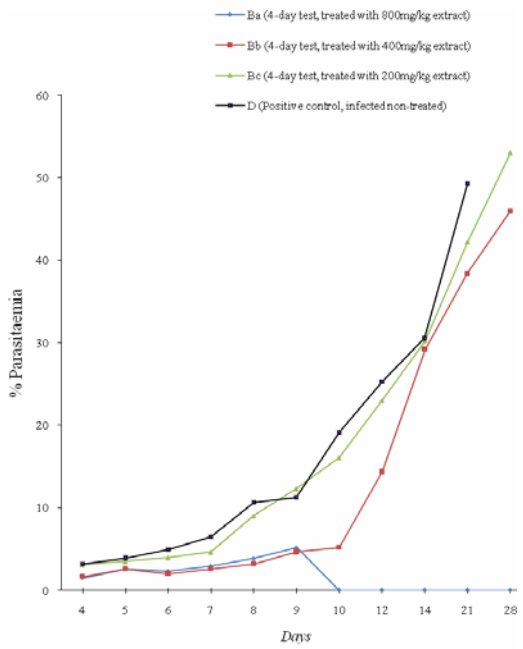

Fig. 2. Dose-dependent percentage parasitaemia of mice placed on 4-day/suppressive treatment. Each point is an average count from five infected mice (±SEM).

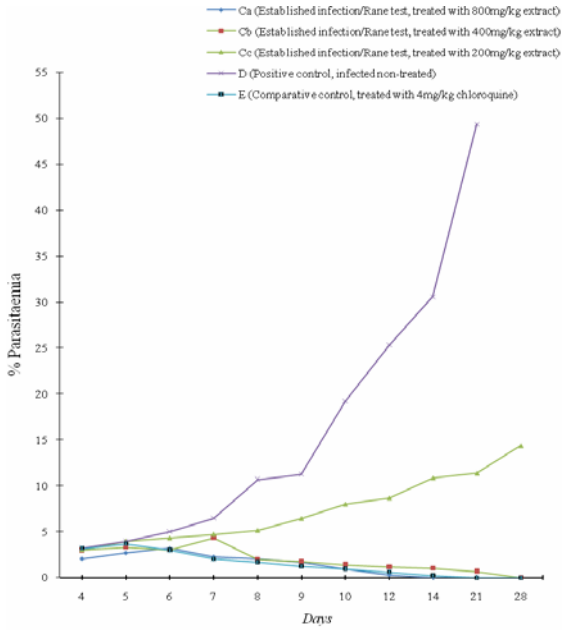

Fig. 3. Dose-dependent percentage parasitaemia of mice placed on established infection/ Rane treatment. Each point is an average count from five infected mice (±SEM).

Table 2. Percentage Chemosuppression at Optimum dose (400mg/kg) of methanolic extract of *Bridelia ferruginea* benth bark**.**

Group Treatment		Day 4 (%)	Day 5 (%)	Day 6 (%)	Day 7 (%)	Day 8 (%)	Day 10 (%)	Day 12 (%)	Day 14 (%)	Day 21 (%)	Day 28 (%)
Treated with Extract (Prophylaxis)	A_1	24.6	48.2	73.2	82.1	88.4	82.2	87.9	90.5	73.0	-
Treated with Chloroquine 4mg/kg (Prophylaxis)	A_2	44.4	46.6	77.1	88.5	95.5	100	-	-	-	-
Treated with Extract (4-Day test)	B	71.4	67.6	82.6	57.9	64.1	72.9	61.3	46.4	15.2	-
Treated with Extract (Established infection)	C	1.6	1.9	6.3	70.2	84.1	91.7	95.4	97.6	98.1	100
Treated with Chloroquine 4mg/kg (Established infection)	E	1.2	2.9	18.0	70.8	85.5	94.1	98.0	99.3	100	100

untreated experienced continual increased (5.13% and 11.19%) respectively. On day 14, all the mice for 800mg/kg died with 400mg/kg (1.00%) and 200mg/kg (10.86%) percentage parasitaemia. On day 21, 400mg/kg recorded 0.69% competing favourably with the positive control (4mg/kg chloroquine) recording 0.65%. However, the infected untreated mice experienced a continual increased (49.5%) percentage parasitaemia throughout the study.

The same trend was observed from the numerical values of percentage chemosuppression caused by treatment with the extract and chloroquine with the different regime of treatments. The established infection treated with extract and chloroquine respectively recorded 100% clearance of parasitaemia at the 28th day of the study while other mode of treatments recorded steady decline in the rates of parasite clearance (Table 2).

Table 3. Mean Survival Times (MST) of mice placed on different treatment at optimum dose (400mg/kg).

Group Treatments		MST (DAY 0 to 28)
Treated with Extract (Prophylaxis)	A_1	26.2 Days
Treated with Chloroquine 4mg/kg (Prophylaxis)	A_2	27.8 Days
Treated with Extract (4-Day test)	B	16.8 Days
Treated with Extract (Established infection)	C	27.4 Days
Infected Untreated (Positive Control)	D	10.6 Days
Treated with Chloroquine 4mg/kg (Established infection)	E	27.9 Days

The values for mean survival time of animals in the infected untreated group, infected extract-treated groups and infected chloroquine-treated groups for the three regimes of treatments over a period of twenty eight days is shown in Table 3. The animals in the extract-treated group for prophylactic and established infection test survived for a favourably comparable number of days as did the chloroquine-treated group.

DISCUSSION

The phytochemical screening of the methanolic extract of *Bridelia ferruginea* bark revealed the presence of alkaloids, flavonoids, glycosides, phenolics, saponins, steroids, anthraquinones and tannins.

The observed antimalarial activity (Figs. 1 to 3) may be attributed to these compounds. Abo *et al.*, 1999 and Okokon *et al.,* 2005 have previously reported the antimalarial activities of these compounds in some medicinal plants. The antimalarial activity observed in this study could be attributed to a single or combined effect of these compounds although the isolation and structural identification of the active principle has not been carried out. The results revealed that the prophylactic treated mice recorded significant (p<0.05) decrease in percentage parasitaemia compared to the infected untreated over the period of observation. On the other hand, suppressive treated mice exhibited significant (p>0.05) increase in percentage parasitaemia slightly lowered than the infected untreated group over 28 days of observation. However, the established infection (Rane test) treated mice showed a gradual percentage parasitaemia increase at the onset with a later significant decrease (p<0.05) tending to total clearance of parasite at the 28th day comparing favourably with chloroquine treated mice, the reference drug.

The initial low percentage chemosuppression observed in the extract-treated group and the chloroquine-treated group (Table 2) may be due to the fact that the extract at the dose administered had not accumulated sufficiently to bring about considerable chemosuppression (Adebayo *et al.,* 2003). However, the prolonged administration of the extract led to the total clearance of the parasites. This result from accumulation of enough active compounds to effect total clearance of the parasites. Also, the calculated mean survival times suggests that the extract had an antimalarial activity which compared favourably to that of the reference drug (Table 3).

The finding from this study have been able to revealed that the optimum dose of extract to achieve total clearance of parasite with a mean survival time comparing favourably with the reference drug is 400mg/kg body weight (Tables 2 and 3). Although, 800mg/kg recorded significant (p<0.05) parasite clearance but was toxic to the animals and they could not live to the end of the observation period. This could possibly be due to the fact that the animals were overdosed at that concentration.

It is noteworthy that the extract exhibited antimalarial activity at all doses with all the regime of treatments but the established infection (Rane test) gave the best performance achieving 100% parasite clearance at the end of the experiment comparing favourably with chloroquine, the reference drug. This finding is contrary to the work of Okokon *et al.,* 2005 who reported that 5mg/kg of chloroquine and 200mg/kg of ethanolic leaf extract of *Croton zambesicus* respectively could not achieve 100% parasite clearance at 28th day of experimental observations.

The mechanism of action of methanolic bark extract of *Bridelia ferruginea* has not been elucidated. The extract could have exerted its action by causing elevation of red blood cell oxidation or by inhibiting protein synthesis (Etkin, 1997; Kirby *et al.,* 1989).

In conclusion, the plant has exhibited promising antimalarial activity confirming forklore report of its traditional use in the treatment of malaria. Therefore, it would be interesting to investigate its in vitro activity against *Plasmodium* parasite thereby establishing the isolation and structural identification of the active principle for possible exploitation in malaria therapy.

ACKNOWLEDGEMENTS

We thanked the Institute for Advanced Medical Research and Training (IAMRAT) for the provision of the parasite and Laboratory space for some aspect of the experimental work.

REFERENCES

Abo, KA., Ogunleye, VO. and Ashidi JS. 1999. Antimicrobial potential of *Spondias mombin, Croton zambesicus,* and *Zygotritonia crocea.* Phytotherapy Research. 13:494-497.

Adebayo, JO., Yakubu, MT., Egwim, EC., Owoyele, B V. and Enaibe, U. 2003. Effect of ethanolic extract of *Khaya senegalensis* stem bark on some biochemical parameters on rat Kidney. Journal of Ethnopharmacology. 88:69-72.

Amino, R., Thiberge, S., Martin, B., Celli, S., Shorte, S., Frischknecht, F. and Menard, R. 2006. Quantitative imaging of *Plasmodium* transmission from mosquito to mammal. Nat Med. 12:220-224.

Cimanga, K., De Bruyne, T., Apers, S., Pieters, L., Totte, J., Kambu, K., Tona, L., Bakana, P., Van Ufford, LQ., Beukelman, C., Labadie, R. and Vlietinck, AJ. 1999. Compliment-Inhibiting constituents of *Bridelia ferruginea* Stem Bark. Planta Med. 65:213-217.

De Bruyne, T., Cimanga, K., Pieters, L., Claeys, M., Dominisse, R. and Vlietinck, A. 1997. Galocatechin ($4' \rightarrow 0 \rightarrow 7$)-Epigallocatechin. A New Biflavonoid Isolated from *Bridelia ferruginea*. Nat. Prod. Let. 11:47-52.

Ekanem, JT., Abbah, OC. and Kolawole, OM. 2008. Trypanocidal Potential of Methanolic Extract of *Bridelia ferruginea* benth Bark in *Rattus novergicus.* African Journal of Biochemistry Research. 2(2):45-50.

Elujoba, AA., Odeleye, OM. and Ogunyemi, CM. 2005. Traditional medicine development for medical and dental primary health care delivery system in Africa. African Journal of Traditional CAM. 2 (1): 46-61.

Etkin, NL. 1997. Antimalarial Plants used by Hausa in Northern Nigeria. Trop Doct. 27:12-6.

Farnsworth, NR. and Soejarto, DD. 1985. Potential consequence of plant extinction in the United States on the current and future availability of prescription drugs. Economic botany. 39:231-240.

Kirby, GC., O'Neill, MJ., Philipson, JD. and Warhurst, DC. 1989. In vitro studies on the mode of action of quassionoids with activity against chloroquine-resistant *Plasmodium falciparum.* Biochem Pharmacol. 38:4367-74.

Kolawole, OM., Oguntoye, SO., Agbede, O. and Olayemi, AB. 2007. Studies on the Efficacy of *Bridelia ferruginea* benth Bark Extract for Domestic Wastewater Treatment. Bulletin of Chemical Society of Ethiopia. 21 (2): 205-211.

Kolawole, OM., Oguntoye, SO., Agbede, O. and Olayemi, AB. 2006. Studies on the Efficacy of *Bridelia ferruginea* in Reducing the Coliform Load and BOD_5 of Domestic Wastewater. Ethnobotanical Leaflets. 10:228-238.

Kolawole, OM. and Olayemi, AB. 2003. Studies on the Efficacy of *Bridelia ferruginea* benth Bark in Water Purification. Nigerian Journal of Pure and Applied Sciences. 18:1387-1394.

Mesia, GK., Tona, L., Penge, O., Lusakibanza, M., Nanga, TM., Cimanga, RK., Apers, S., Van Miert, S., Totte, J., Pieters, L. and Vlieetinck, AJ. 2005. Antimalarial activities of three plants used as traditional remedies for malaria in the Democratic Republic of Congo.

NIH, 1985. Guide for the care and use of laboratory animals. NIH publication No. 85-23, Revised 1985.

Odebiyi, A. and Sofowora, AE. 1978. Phytochemical Screening of Nigeria. Medicinal plants. Part III, Lyodia. 41:23-246.

Okokon, JE., Ofodum, KC., Ajibesin, KK., Danladi, B. and Gamaniel, KS. 2005. Pharmacological screening and evaluation of antiplasmodial activity of *Croton zambesicus* against Plasmodium berghei berghei infection in mice. Indian Journal of Pharmacology. 37:243-246.

Ryley, JF. and Peters, W. 1970. The antimalarial activity of some quinolone esters. American Journal of Tropical Medicine and Parasitology. 84:209-222.

Sachs, JD. 2002. A new global effort to control malaria. Science 298: 122-124.

Sturm, A. and Heussler, V. 2007. Live and let die: manipulation of host hepatocytes by exoerythrocytic *Plasmodium* parasites. Med Microbiol Immunol 196:127-133.

Wirth, D. 1998. Malaria: a 21st century solution for an ancient disease. Nat. Med. 4:1360-1362.

Received: Dec 2, 2009; Revised: Dec 16, 2009; Accepted: Jan 2, 2010

SENRA Academic Publishers, Burnaby, British Columbia
Vol. 4, No. 1, pp. 1045-1051, 2010
ISSN: 1715-9997

Canadian Journal of pure&applied sciences

PRODUCTION, PURIFICATION AND CHARACTERIZATION OF THE ANTIMICROBIAL SUBSTANCES FROM *STREPTOMYCES VIRIDODIASTATICUS* (NRC1)

Nadia H Abd El-Nasser, Samia M Helmy, Amal M Ali, Abeer A Keera and *Hala M Rifaat
Department of Microbial Chemistry, National Research Centre, Cairo, Egypt

ABSTRACT

Streptomyces viridodiastaticus isolated from Qalubiya soil of Egypt is capable to produce antibacterial and antifungal compounds. It showed the highest level of antimicrobial activity in the shaken culture broth after 7 days of incubation at neutral pH value using starch, potassium nitrate and dipotassium hydrogen phosphate amended medium. Two active fractions from the antimicrobial substance were extracted by diethyl ether at acidic pH and purified by Sephadex G-100 column chromatography. Elementary analysis indicated the absence of nitrogen from the two fractions. The empirical formulas for the two fractions (A) and (B) were $C_6H_{13}O$ and C_5H_7O while the molecular formulas were $C_{30}H_{65}O_5$ and $C_{20}H_{28}O_4$ respectively. The ultraviolet, infrared and mass spectra of the purified substance (A) indicated the presence of hydrogen bond, methyl group, diketones, aliphatic compound, alkenes and hydroxyl group. The purified substance (B) contained all the groups present in substance (A) except hydroxyl group.

Keywords: Antimicrobial substances, characterization, production, *Streptomyces.*

INTRODUCTION

The actinomycetes represent a large and heterogeneous group of microorganisms comprising several families and numerous species (Waksman, 1959 and Krassilinikov, 1970). Streptomycetes (Class Actinobacteria, Order *Actinomycetales*, Suborder *Streptomycineae*, Family *Streptomycetaceae*) are Gram-positive, filamentous soil bacteria that undergo morphological differentiation during their life cycle (Dworkin *et al*., 2006). They are considered to be one of the major groups of soil bacteria. *Streptomyces* produce a wide range of secondary metabolites, including antibiotics, many of which are of clinical importance in the treatment of infectious diseases or diseases caused by the proliferation of malignant cells (Pelczar *et al*., 1986; Innes and Allan, 2001). They are noteworthy as antibiotic producers making three quarter of all known products; the *Streptomyces* species are especially prolific and can produce many antibiotics and other classes of biologically active secondary metabolites (Waksman, 1959; Demain, 1999).

The evolution and spread of antibiotic-resistant pathogens remains a major clinical problem (Silver and Bostian, 1993). Although the discovery of new antimicrobial agents has become increasingly more difficult, the search for unique metabolites from microorganisms remains an attractive venture (Bull *et al*., 1992; Omura, 1992). The isolation of antibiotic from microorganisms is relatively easy as compared to chemical synthesis of antimicrobial agents (Ahmed, 2007). It could improve the discovery of novel antibiotics that act as better chemotherapeutic agent (Kulkorni and Anyicojri, 1995).

Antibiotic production is influenced by several physico-chemical factors including nutrient supply, oxygenation, temperature and pH (Gesheva *et al*., 2005).

The present study describes the production of anti-microbial substances by a local isolate *Streptomyces viridodiastaticus*. Improvement of antibiotic production was achieved by optimization of the cultural conditions. Moreover, isolation, purification and characterization of the antimicrobial substances were studied.

MATERIALS AND METHODS

Organism

Streptomyces viridodiastaticus (NRC1) was isolated from Qalubiya soil of Egypt (Rifaat *et al*., 2006-2007). The strain was identified according to the International *Streptomyces* Project Scheme (Shirling and Gottlieb, 1966) and diagnostic key of Szabo *et al*. (1975).

Media

Streptomyces viridodiastaticus (NRC1) was cultivated on the basal salt liquid medium of Waksman (1961), adjusted to pH 7.0 for the production of antimicrobial substance. The medium contained the following components (g/l): 20.0 starch, 2.0 potassium nitrate, 1.0 dipotassium hydrogen phosphate, 0.5 magnesium sulphate, 0.5 sodium chloride, 3.0 calcium carbonate and 0.01 ferrous sulphate. The fermentation was carried out in 250 ml triple-baffled Erlenmeyer flasks containing 50 ml of medium and

*Corresponding author email: halamohamed6@yahoo.com

incubated at 28ºC for 7 days on a rotary shaker at 200 rpm.

Antimicrobial activity

The antimicrobial spectrum of *Streptomyces viridodiastaticus* was determined against test organisms obtained from Faculty of Agriculture, Cairo University namely Gram +ve bacteria (*Staphylococcus aureus*, *Streptococcus pyogenes*, *Bacillus cereus* and *Bacillus subtilis*), a Gram – ve bacterium (*Escherichia coli*), yeasts (*Candida albicans*, *Saccharomyces cerevisiae*, *Candida pseudotropicalis*) and filamentous fungi (*Macrophomina phaseoli*, *Helminthosporium turcicum*, *Aspergillus niger*, *Aspergillus flavus*, *Aspergillus terreus*, *Fusarium oxysporum* and *Botrytis allii*). The antimicrobial activity was determined by a conventional agar diffusion method (Wu, 1984) using nutrient, yeast-malt extract and Czapek's Dox agar for bacteria, yeasts and fungi respectively (Waksman, 1961). The diameter of inhibition zone was measured after incubation for one day for bacteria and two days for yeasts and fungi at 28ºC.

Optimization conditions for antimicrobial production

Carbohydrates (D-glucose, D-galactose, D-fructose, D-mannitol, L-arabinose, L-rhamnose, xylose, sucrose, maltose, lactose, mannose, starch and cellulose) were tested for their ability to support the production of the antimicrobial substance from *Streptomyces viridodiastaticus*.

The addition of various compounds of nitrogen sources was also studied. Potassium nitrate in the medium was replaced by various nitrogen sources with equimolar amounts such as sodium nitrate, ammonium nitrate, ammonium oxalate, ammonium sulphate, ammonium dihydrogen phosphate, diammonium hydrogen phosphate or triammonium phosphate.

The phosphate in the medium was also replaced by various phosphate sources with equimolar amounts. Potassium dihydrogen phosphate, dipotassium hydrogen phosphate, ammonium dihydrogen phosphate, diammonium hydrogen phosphate, triammonium phosphate, sodium dihydrogen phosphate, disodium hydrogen phosphate and trisodium phosphate were tested.

The *Streptomyces viridodiastaticus* (NRC1) was also incubated at different pH values from 5.0 to 9.0 to determine the optimum pH for highest antimicrobial production.

The time course of antibiotic production from 1 to 10 days was tested in shake flasks to determine the appropriate period of incubation for optimum antimicrobial production.

Extraction and purification of the antimicrobial substance

Three different methods were used to extract the antimicrobial substances namely, solvent-solvent extraction, adsorption and precipitation (Edwards, 1969). In solvent-solvent extraction method, the use of different solvents with different polarities was tested for their ability to extract the antimicrobial substance from the supernatant at different pH values 3, 7 and 9. Diethyl ether, ethyl acetate, butyl acetate, butanol, chloroform, petroleum ether and benzene were added to the concentrated broth (v/v) and shaken in separating funnel.

The adsorption of the antimicrobial substance from the supernatant of the culture broth was tested by shaking with alumina, silica gel or charcoal (2.5 % w/v).

Aqueous solution such as ethyl alcohol, methyl alcohol, acetone, calcium chloride and ammonium sulphate were tested for their ability to precipitate the antimicrobial substances from the supernatant at different pH values 3, 7 and 9.

In order to purify the antimicrobial substance, 20 litres culture broth was centrifuged to remove the cells. The supernatant was bioassayed by the agar diffusion method using test organism *Streptococcus pyogenes* and the active substance was extracted with equal volume of acidic diethyl ether three times. The diethyl ether layer was bioassayed. The extract was concentrated under vacuum and then performed on a Sephadex G-100 chromatographic column (25 x 400 mm) and eluted using 0.1-0.5 M NaCl. The high active fractions of the antimicrobial substances were collected and mixed with equal volume of acidic diethyl ether for further studies.

Physico-chemical properties of the antimicrobial substance

The retention factor (R_f) of the extracted antibiotic was calculated according to the method of Blinov and Khokhlov (1970). The solvent systems used were petroleum ether, benzene, chloroform, carbon tetrachloride, acetone, diethyl ether, ethyl acetate, butyl acetate, amyl alcohol, n-butanol, water saturated with n-butanol, n-butanol-acetic acid-water (2:1:1), n-butanol-pyridine-water (2:0.6:1) and 3% ammonium chloride in water.

Elemental analysis of carbon, hydrogen, nitrogen and oxygen as well as Infrared (I.R.), U.V. and mass spectra of the partially purified antibiotic were estimated using Vario Elementar, Fourier Transform 300 E infrared spectrophotometer, U.V./Vis/NIR 570v spectro-photometer and Finnigan Mat- SSQ 7000 respectively at the National Research Centre, Cairo, Egypt.

RESULTS AND DISCUSSION

Antimicrobial activity

Streptomycetes have been recognized as the potential producers of metabolites such as antibiotics. The antimicrobial substances produced by *Streptomyces viridodiastaticus* (NRC1) (Table 1) showed activity against Gram +ve bacteria (*Streptococcus pyogenes* and *Bacillus subtilis*) as well as fungi (*Aspergillus niger* and *Botrytis allii*). Bioxalomycins, which is a complex of a broad spectrum antibiotic, were isolated from fermentations of *Streptomyces viridodiastaticus*, exhibit excellent activity against Gram +ve bacteria and less active against Gram –ve bacteria (Singh *et al*., 1994). The obtained results suggest that *Streptomyces viridodiastaticus* (NRC1) could produce different antimicrobial substances.

Table 1. Antimicrobial spectrum of *Streptomyces viridodiastaticus*

Test organisms	Inhibition zone (mm)
Staphylococcus aureus	0
Streptococcus pyogenes	24
Bacillus cereus	0
Bacillus subtilis	20
Escherichia coli	0
Candida albicans	0
Saccharomyces cerevisiae	0
Candida pseudotropicalis	0
Macrophomina phaseoli	0
Helminthosporium turcicum	0
Aspergillus niger	28
Aspergillus flavus	0
Aspergillus terreus	0
Fusarium oxysporum	0
Botrytis allii	22

Factors affecting the production of antibiotic substance

Antibiotics production varies with the constituents of the media. The secondary metabolites accumulate only after the growth phase, i.e. when the culture attains a specific growth rate.

The antibiotic substance was detected on the second day of incubation and increased gradually to reach a maximum on the 7th day after which it decreased till the 10th day (Fig. 1). This observation was in agreement with Hassan *et al*. (2001**)** who found that antibiotic production by *Streptomyces violatus* in synthetic media reached the maximum on the 7th day. They mentioned that the highest yield of antibiotic production was obtained in the late exponential and the stationary phases.

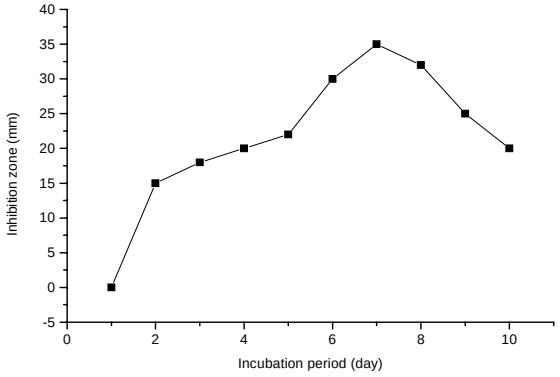

Fig. 1. Effect of incubation period on the production of the antimicrobial substances produced by *Streptomyces viridodiastaticus*.

The pH values of the culture showed a significant influence on the maximum productivity of antibiotic (Haque *et al*., 1995). The highest level of production of the antimicrobial substance produced by *Streptomyces viridodiastaticus* was detected with pH 7.0 (Fig. 2). Similarly, actinorhodin, a blue pigment antibiotic was produced in *Streptomyces coelicolar* culture at pH value around 7 (Bystrykh *et al*., 1996).

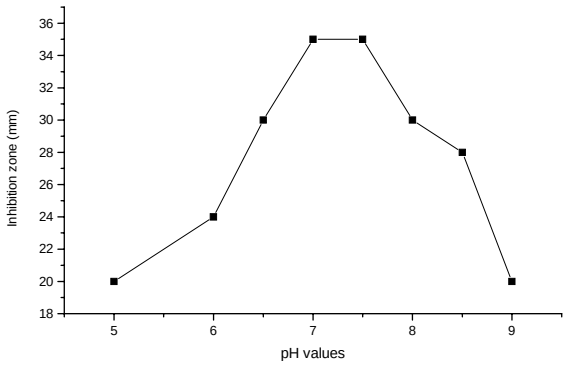

Fig. 2. Effect of different pH values on the production of the antimicrobial substance produced by *Streptomyces viridodiastaticus*

In an earlier study, the medium constituents and the process parameters were optimized by single factor optimization keeping the other factors constant (Elibol and Mavituna, 1998).

Starch supported the highest level of antibiotic production followed by L-arabinose and glucose (Fig. 3). Lower level of production was recorded with mannose, maltose, fructose, mannitol, lactose and sucrose. No production was detected with galactose, rhamnose, xylose and cellulose. Similarly, Sengupta and Paul (1992) detected a high level of antimicrobial substance produced by *Streptomyces* species on starch. The utilization of starch

by *Streptomyces viridodiastaticus* for production of antibiotic indicates the presence of an active uptake system for their substances.

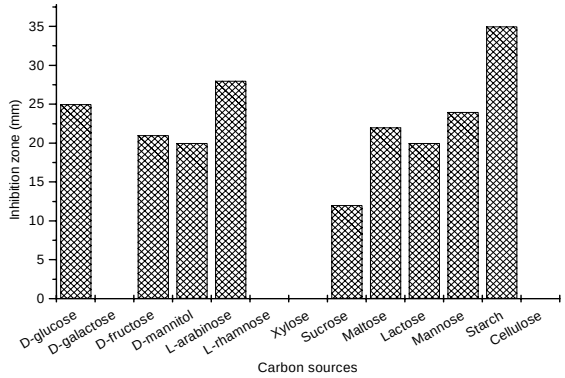

Fig. 3. Effect of different carbon sources on the production of antimicrobial substance produced by *Streptomyces viridiastaticus*

Potassium nitrate encouraged the production of antibiotic followed by sodium nitrate and ammonium sulphate (Fig. 4). Ammonium oxalate showed the lowest level of antibiotic production. The results revealed that the level of antibiotic production may be influenced by the type of nitrogen source supplied in the culture medium. Similar observations have been reported by Khaoua *et al.* (1991) and Mansour *et al*. (1996). It was noted by El-Tayeb *et al.* (2004) that potassium nitrate are superior to sodium nitrate for rifamycin production. For rapamycin, ammonium sulphate was the best nitrogen source (Lee *et al*., 1997).

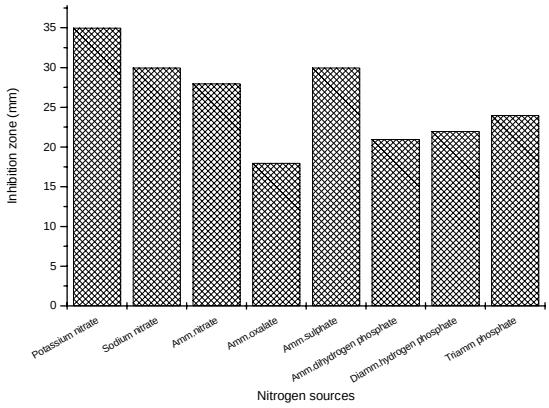

Fig. 4. Effect of different nitrogen sources on the production of antimicrobial substance produced by *Streptomyces viridiastaticus*

The level of production of the antimicrobial substance was greatly affected by the type of the used phosphate sources. In general, dibasic potassium, sodium or ammonium phosphates were more favourable than the mono- or tri-basic ones. Dipotassium hydrogen phosphate was the most favourable salt for antibiotic production (Fig. 5). These results are in agreement with those reported by other investigators (Harold, 1966 and Kishimoto *et al*., 1996). Phosphate was considered as a factor in the synthesis of a wide range of antibiotic (Martin and Demain, 1980).

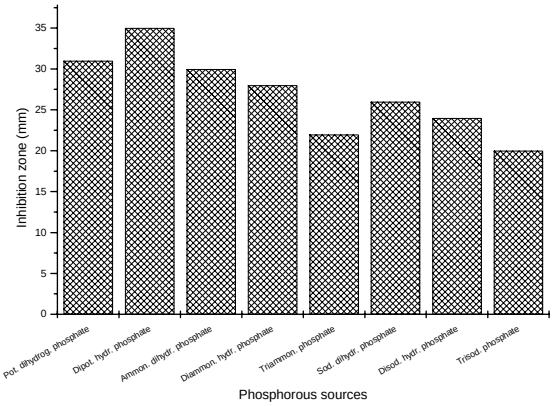

Fig. 5. Effect of different phosphorous sources on the production of antimicrobial substance produced by *Streptomyces viridiastaticus*

In this respect, Young *et al.* (1985) found that while nitrogen and phosphate salts were required for growth, they had negative effects on antibiotic synthesis while Farid *et al*. (2000) confirmed that only ammonium sulphate, sodium nitrate or beef extract were the suitable nitrogen sources in supporting natamycin production by *Streptomyces natalensis*.

Extraction of the antimicrobial substances

The antimicrobial substances produced by *Streptomyces viridodiastaticus* were best extracted by diethyl ether at acidic pH value (pH 3), followed by acidic ethyl acetate. Petroleum ether and benzene failed to extract the antimicrobial substance (Fig. 6). The same method of extraction for antimicrobial substances was performed by some workers (Hosokawa *et al*., 1996 and Kimura *et al*., 1997) however, most antimicrobial substances are extracted using ethyl acetate (Franco and Countinho, 1991).

The antimicrobial substance was completely adsorbed on alumina, silica gel and charcoal at various pH values except alkaline alumina (Table 2).

Results in Figure 7 indicate that the antimicrobial substance was highly precipitated by ethyl alcohol at acidic pH value, followed by acidic acetone and methanol. Calcium chloride and ammonium sulphate showed minor precipitate of the antimicrobial substance.

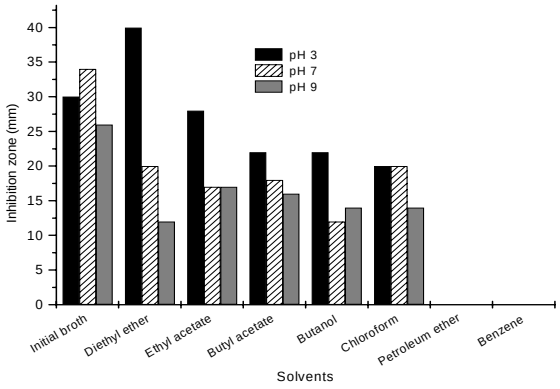

Fig. 6. Effect of different solvents on the extraction of antimicrobial substance produced by *Streptomyces viridodiastaticus* at different pH values

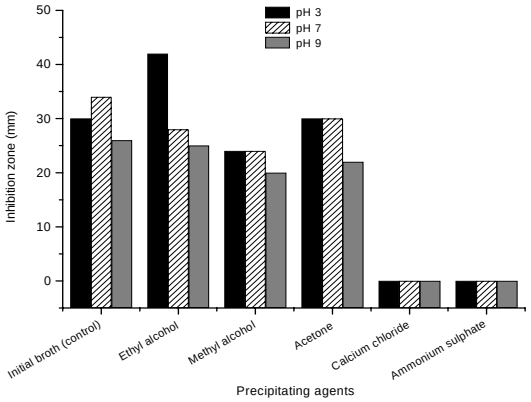

Fig. 7. Suitability to different precipitating agents at various pH values for the precipitation of the antimicrobial substance produced by *Streptomyces viridodiastaticus.*

Table 2. Suitability of alumina, silica gel and charcoal to adsorb antimicrobial substances produced by *Streptomyces viridodiastaticus* at various pH values

Adsorbent	Inhibition zone (mm)		
	pH 3	pH 7	pH 9
Initial broth	30	34	26
Alumina	00	00	20
Silica gel	00	00	00
Charcoal	00	00	00

Characterization of the antimicrobial substances

The antimicrobial substances showed high R_f values with n-butanol-pyridine-water, n-butanol-acetic acid-water, ethyl acetate, acetone, 3% ammonium chloride in water, diethyl ether and chloroform. The rest of solvents used showed lower R_f values (Fig. 8).

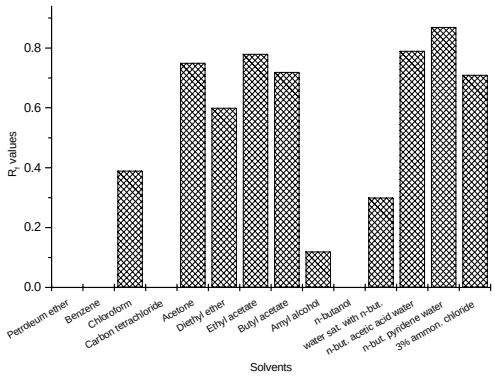

Fig. 8. R_f values of the antimicrobial substance produced by *Streptomyces viridodiastaticus* in different solvent systems

Structure of the antimicrobial substances

From Sephadex G-100 column separation, two fractions of the active antimicrobial substances were obtained (A and B). The substance (A) has yellowish brown colour, while substance (B) was colourless.

The elemental analysis of the two fractions reveals absence of nitrogen. The first fraction contained 72.76% carbon, 13.37% hydrogen and 13.87% oxygen. The second fraction contained 66.62% carbon, 7.81% hydrogen and 25.57% oxygen.

The I.R. spectrum of fraction A showed bands at 3432, 2925, 2855, 1719, 1589, 1459, 1266 and 1381 cm^{-1} which indicate the presence of hydrogen bond, methyl group, carbon hydrogen bond of methyl group, carbonyl group, diketones, aliphatic compound, alkene and hydroxyl group. However, fraction B showed bands at 3406, 2922, 2852, 1709, 1602, 1514, 1496 and 1456 cm^{-1} which indicate the presence of hydrogen bond, carbon hydrogen bond of methyl group, carbonyl group, diketones, aliphatic compound, alkene, and methyl group.

The U.V. absorption of the two fractions of the purified antimicrobial substances was detected at 278.5 and 280.5 nm. The mass spectra of fractions A and B showed M^+ ion at 460 and 402 m/z respectively.

The empirical formulas are $C_6H_{13}O$ and C_5H_7O and molecular formulas may be $C_{30}H_{65}O_5$ and $C_{20}H_{28}O_4$ for the antimicrobial substances A and B respectively.

REFERENCES

Ahmed, AA. 2007. Production of antimicrobial agents by *Streptomyces violachromogenes*. Saudi Journal of Biological Sciences. 14:7-16.

Blinov, NO. and Khokhlov, AS. 1970. Paper chromatography of antibiotics. Nauka. Moscow USSR:24-57.

Bull, AT., Goodfellow, M. and Slater, JW. 1992. Biodiversity as a source of innovation in biotechnology. Annual Review of Microbiology. 46:219-252.

Bystrykh, LV., Fernander-Moreno, MA., Herremo, JK., Malportida, F., Hopwood, DA. and Dijkhuizenen, L. 1996. Production of actinorhodin-related blue pigments by *Streptomyces coelicolor*. Journal of Bacteriology. 178:2238-2244.

Demain, AL. 1999. Pharmaceutically active secondary metabolites of microorganisms. Applied Microbiology and Biotechnology. 52:455-463.

Dworkin, M., Fulkow, S., Rosenberg, E., Schleifer, KH. and Stackebrandt, E. 2006. The Prokaryotes, (3rd ed.), A handbook on the biology of bacteria: Archaea, Bacteria: Firmicetes, Actinomycetes. Springer Science, New York, USA.

Edwards, VH. 1969. The discovery and purification of biochemicals. Advances in Applied Microbiology. 11:159-210.

Elibol, M. and Mavituna, F. 1998. Effect of sucrose on actinorhodin production by *Streptomyces coelicolor*. Process in Biochemistry. 33:307-311.

El-Tayeb, OM., Salama, AA., Hussein, MMM. and El-Sedawy, HF. 2004. Optimization of industrial production of rifamycin B by *Amycolatopsis maditerranei*. The role of colony, morphology and nitrogen sources in productivity. African Journal of Biotechnology. 3:266-272.

Farid, MA., El-Enshasy, HA., El-Diwany, AL. and El-Sayed, SA. 2000. Optimization of the cultivation medium for natamycin production by *Streptomyces natalensis*. Journal of Basic Microbiology. 40:157-160.

Franco, MMC. and Countinho, LEL. 1991. Detection of novel secondary metabolites. Critical Review of Biotechnology. 11:193-276.

Gesheva, V., Ivanova, V. and Gesheva, R. 2005. Effects of nutrients on the production of Ak-111-81 macrolide antibiotics by *Streptomyces hygroscopiccus*. Microbiological Research. 160:243-248.

Haque, SF., Sen, SK. and Pal, SC. 1995. Nutrient optimization for production of broad spectrum antibiotics by *Streptomyces antibioticus*. Acta Microbiologica Hungarica. 42:155-162.

Harold, FM. 1966. Inorganic polyphosphates in biology: structure, metabolism and function. Bacteriological Review. 30:772.

Hassan, MA., El-Naggar, MY. and Said, WY. 2001. Physiological factor affecting the production of an antimicrobial substance by *Streptomyces violatus* in batch cultures. Egyptian Journal of Biology. 3:1-10.

Hosokawa, N., Naganawa, H., Hamada, M. and Takeuchi, T. 1996. Hydroxymycotrieniuns A and B, new ansamycin group antibiotics. Journal of Antibiotics. 49:425-431.

Innes, CMJ. and Allan, EJ. 2001. Induction, growth and antibiotic production of *Streptomyces viridifaciens* L-form bacteria. Journal of Applied Microbiology. 90:301-308.

Khaoua, S., Libricihi, A., Germain, P. and Lefebvre, G. 1991. Cephamycin C biosynthesis in *Streptomyces cattleya*: nitrogen source regulation. Journal of Applied Microbiology and Biotechnology. 35:253-257.

Kimura, KI., Kanou, F., Koshino, H., Uramoto, M. and Yoshihama, M. 1997. SNA-8073-B, a new isoltetracenone antibiotic inhibits prolyl endopeptidase. 1-Fermentation, isolation and biological properties. Journal of Antibiotics. 50:291-296.

Kishimoto, K., Park, YS., Okabe, M. and Akiyama, S. 1996. Effect of phosphate ion on mildiomycin production by *Streptoverticillium rimofaciens*. Journal of Antibiotics. 49: 775-780.

Krassilinikov, NA. 1970. Ray-fungi. Higher form. Nauka, Moscow, USSR.

Kulkorni, Y. and Anyicojri, Y. 1995. Isolation and characterization of actinomycetes and optimization of its production. M. Sc. Thesis, Dept. of Microbiology, University of Pune. India.

Lee, MC., Kojima, J and Demian, AL. 1997. Effect of nitrogen source on biosynthesis of rapamycin by *Streptomyces hygroscopicus*. Journal of Indian Microbiology and Biotechnology. 19:83-86.

Mansour, FA., El-Shirbiny, SA. and El-Metwaly, NA. 1996. Dimethyltetracycline biosynthesis by *Streptomyces aureofaciens* subspecies *viredulans* as influenced by medium composition. Egyptian Journal of Biology. 31:221-235.

Martin, JF. and Demain, AL. 1980. Control of antibiotic biosynthesis. Microbiological Review. 44:230-251.

Omura, S. 1992. Trends in the search for bioactive microbial metabolites. Journal of Indian Microbiology. 10:135-156.

Pelczar, MJ., Chan, ECS., Krieg, NR. and Pelczar, MF. 1986. Microbiology, (5th ed.), McGraw-Hill Book Company, New York, USA.

Rifaat, HM., Abd El Naser, NH. and Helmy, SM. 2006-2007. Taxonomical studies on certain streptomycetes

isolated from Egyptian soils exhibiting antimicrobial activity. Journal of Culture Collections. 5:25-34.

Sengupta, S. and Paul, AK. 1992. Nutritional conditions for the germination of *Streptomyces albus* 5ME-13 spores. Acta Biotechnology. 12:225-228.

Shirling, EB. and Gottlieb, D. 1966. Methods for characterisation of *Streptomyces* species. International Journal of Systematic Bacteriology. 16:313-340.

Silver, LL. and Bostian, KA. 1993. Discovery and development of new antibiotics: the problems of resistance. Antimicrobial Agents and Chemotherapy. 37:337-383.

Singh, MP., Petersen, PJ., Jacobus, NV., Maiese, WM., Greenstein, M. and Steinberg, DA. 1994. Mechanistic studies and biological activity of bioxalomycin alpha 2, a noval antibiotic produced by *Streptomyces viridodiastaticus*. Antimicrobial Agents and Chemotherapy. 38:1808-1812.

Szabo, IM., Marton, M., Buti, I. and Fernades, C. 1975. A diagnostic key for the identification of species *Streptomyces* and *Streptoverticillum* included in the International *Streptomyces* Project. Acta Botanica Academiae Scientiarum Hungaricae. 21:387-418.

Waksman, SA. 1959. The actinomycetes, Vol. I, Nature, occurrence and activities. The Williams and Wilkins Co., Baltimore, USA.

Waksman, SA. 1961. The actinomycetes, Vol. II Classification, identification and description of genera and species. The Williams and Wilkins Co., Baltimore, USA.

Wu, RY. 1984**.** Studies on the *Streptomyces* SC4. II-Taxonomical and biological characteristics of *Streptomyces* strain SC4. Botany Bulletin Academic Science. 25: 111-123.

Young, MD., Kempe, LL. and Bader, FG. 1985. Effect of phosphate, glucose and ammonium on growth and lincomycin production by *Streptomyces lincolnensis* in chemically defined media. Biotechnology and Bioengineering. 27:327-333.

Received: August 1, 2009; Revised: Nov 1, 2009; Accepted Nov 10, 2009

SENRA Academic Publishers, Burnaby, British Columbia
Vol. 4, No. 1, pp. 1053-1071, 2010
ISSN: 1715-9997

Canadian Journal of pure&applied sciences

DISTRIBUTION, POPULATION STATUS AND ENVIRONMENTAL IMPACTS ON REPTILES IN MANORA, SANDSPIT, HAWKESBAY AND CAPE MONZE AREAS OF KARACHI COAST

*M Zaheer Khan, Babar Hussain, Syed Ali Ghalib, Afsheen Zehra and Nazia Mahmood
Department of Zoology – Wildlife and Fisheries, University of Karachi, Karachi-75270

ABSTRACT

In this study, total twenty seven reptilian species including three turtle species, Green Turtle (*Chelonia mydas*), Olive Ridley (*Lepidochelys olivacea*), and Hawksbill Turtle (*Eretmochelys imbricata*), nine lizard species such as Common Tree Lizard (C*alotes versicolor versicolor*), Spotted Barn Gecko (*Hemidactylus brooki*), Yellow Bellied Common House Gecko (*Hemidactylus flaviviridis*), Persian House Gecko (*Hemidactylus persicus*), Blotched House Gecko (*Hamidactylus triedrus*), Mediterranean House Gecko (H*amidactylus turcicus*), Blue Tail Sand Lizard (*Acanthodactylus cantoris*), Spotted Lacerta (*Mesalina watsonana*), and Bengal Monitor (*Varanus bengalensis*) were recorded from Manora, Sandspit, Hawksbay and Cape Monze areas during 2001-2009. Fifteen snakes species viz Beaked Sea Snake (*Enhydrina schistosa*), Blue Green Sea Snake (*Hydrophis caerulescens*), Annulated Sea Snake (*Hydrophis cyanocinctus*), Persian Sea Snake (*Hydrophis lapemoides*), Broad Band Sea Snake (*Hydrophis mamillaris*), Reef Sea Snake (*Hydrophis ornatus*), Yellow Sea Snake (*Hydrophis spiralis*), Pygmy Sea Snake (*Lapemis curtus*), Spotted Small Headed Sea Snake (*Microcephalophis cantrois*), Pelagic Sea Snake (*Pelamis platurus*), Spotted Viperine Sea Snake (*Praescutata viperina*), and Blotched Diadem Snake (*Sphalerosophis diadema diadema*) were recorded, while three species Cliff Racer (*Platyceps rhodorachis*), Saw-scaled Viper (*Echis carinatus*) and Black Cobra (*Naja naja*) were recorded from Manora, Hawkesbay and Cape Monze area only. There are several habitat degradation threats especially to marine turtles, Lizards are also affected by habitat degradation and disturbance, but it is a very minor threat. There is some mortality of Bengal Monitor during the road crossing. Human activities that directly or indirectly threaten marine turtles include the exploitation of eggs and turtles, fishery-related mortality, inappropriate management practices, destruction or modification of habitats, pollution, and recreation activities.

Keywords: Karachi coast, reptilian fauna, distribution, status.

INTRODUCTION

Asia is rich in habitats and biodiversity, and correspondingly rich in turtle species. Asia's highest turtle diversity occurs in four hotspot regions, the Indo-Gangetic Plain, mainland Southeast Asia, the South China coastal region, and New Guinea, but almost any area outside the extreme deserts and the altitude and latitude regions is home to some turtle species. At least 100 species of tortoises and freshwater turtles are native to Asia, and new species continue to be described (Van Dijk and Palasuwan, 2000).

According to IUCN (2009), there are now 1,677 reptiles species have been included on the IUCN Red List, with 293 added in 2009. In total, 469 are threatened with extinction and 22 are already Extinct or Extinct in the wild.

Pakistan derives its marine resources from the Arabian Sea, which has a coastline of 1050km and lying in the Sindh and Balochistan provinces (Fig. 1). The part of the coast in Sindh is 250km, while the one in Balochistan is 800km. Sindh and Balochistan coasts have different physical and climatic characteristics. The coast of Sindh is the tail end of the southwest monsoon, and the coast of Balochistan has a Mediterranean climate (IUCN, 2004). Karachi coast is an important area for reptiles. It has the marine, muddy, sandy and rocky habitats having special significance in the distinct natural environment in the tropical region of' southern Pakistan. The important sites on this coast for the reptiles are Manora, Sandspit, Hawkesbay and Cape Monze areas.

Pakistan has 179 species of reptilian fauna consisting of turtles, tortoises, crocodile, gavial, lizards and snakes (Rehman and Iffat, 1997). Six families of Lizards are found in Pakistan viz. Geckonidae, Agamidae, Chameleonidae, Scincidae, Lacertidae and Varanidae. Auffenberg *et al.* (1989, 1991), Boulenger (1890), Ghalib *et al.* (1981), Iffat and Auffenberg (1988), Khan (2006), Khan and Mirza (1977), Khan and Nazia (2003), Khan *et al.* (2005), Mertens (1969), Minton (1966), Rahman *et al.* (2002), Rahman and Papenfuss (2005) and Iffat (2006, 2009) have been contributed some work in the field of herpetofauna of Pakistan.

*Corresponding author email: zaheerk2k@yahoo.com

Pakistan has long been known to support a large population of Green Turtles (*Chelonia mydas*) with a lesser number of Olive ridleys (*Lepidochelys olivacea*), nesting primarily at Hawkes Bay and Sandspit near Karachi, Sindh province (Ghalib and Zaidi, 1976; Kabraji and Firdous, 1984). In 1976 Pakistan became a signatory to the Convention of International Trade in Endangered Species of Fauna and Flora (CITES), which lists all sea turtles on its Appendix 1, which includes species prohibited from international trade (Firdous, 2005). Seventy four species of snakes have been recorded in Pakistan, out of which 26 species are poisonous comprising 14 species of Sea Snakes and 12 species of Land Snakes, while 48 species are non- poisonous. Of 55 species of the sea Snakes distributed in the world, 14 species has been recorded from the coasts of Pakistan, while two species *Hydrophis faciatus* (Schneider) and *Astrotia stokesi* (Grey) have not been collected in Pakistan since their original records. The objective of the present study was to investigate the distribution, population status and environmental impacts on reptiles in the Manora, Sandspit, Hawkesbay, and Cape Monze areas of Karachi coast.

MATERIALS AND METHODS

Study Sites

Along Karachi coastal sites viz. Manora, Sandspit, Hawkesbay, and Cape Monze (Table 1) were selected as study areas (Fig. 2). The observations were recorded quarterly on the four sites during the years 2001 to 2009. During each visit to the study areas, the population of each species of reptiles was recorded. Identification of the reptilian species in the field was carried out with the help of field guides Minton (1966) and Khan (2006).

COUNTING METHODS

A. DIRECT METHODS

1. Habitat Searching /Transact Method

At each site several hours search was carried out to detect as many reptiles as possible with in a circular central zone along the coastal habitat at each site. This searching consists of approximately 20ha. (within a 250m radius of the observation/ sampling points). This method is very suitable for counting the number of reptiles. At first a suitable place with suitable habitat was chosen. Nearly 100m above the high tide mark was taken up for study of the coastal fauna. It was noted that the lizards are mostly active at day time, while the terrestrial snakes are seen both in the days as well as at night. Female marine turtles are observed at night, visiting or nesting at the beach.

Track counts along with direct observations were made on the beaches of Karachi coast for marine turtles which species is nesting of which species returned without laying eggs, as different turtle species have different types of track sign / crawls made in the sand when they emerge to nest or only for strolling.

2. Incidental Sightings

Incidental sightings are also helpful to determine the presence and population status of the species. In this way number of species, date, time, location and habitat types was recorded on data sheet.

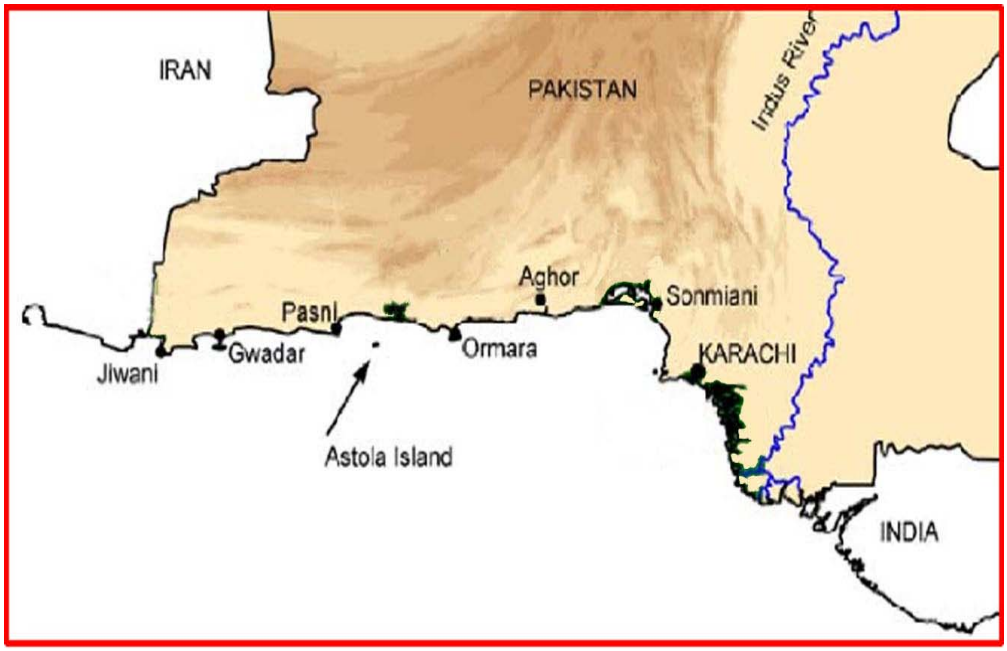

Fig. 1. Coastal areas of Pakistan.

Direct method

3. Hand Capturing

Hand Capturing was used for small terrestrial snakes, lizards and turtles. The simplest method used to capture lizards is to search intensively in micro-habitats which they are known to frequent, and to catch them by hand. Small lizards are found most easily by looking in potential shelter, for example by turning over rocks, or by stripping bark from trees. A small hand –held torch was used for looking into cracks or holes in search of reptiles at night. Reptiles were also searched for in holes and crevices.

Many lizards and snakes were counted or captured during this study period. For many diurnal species, mid- morning was a good time to search, while the reptiles were basking to elevate its body temperature. Nocturnal species were often found by torchlight.

Having located a lizard, the easiest way to catch it is simply to pounce on it with an open, cuffed hand, taking care not to crush it. Care should also be taken with species that practice to drop their tails. When a venomous snake was located, it was caught by pinning it behind the head, using a Y- shaped stick with some padding in the fork. The snake is then picked up, with the neck held firmly. "Snake tongs" 'large forceps manipulated by a trigger-grip' is also useful when catching snakes.

4. Noosing

Noosing is used to catch most of the lizards. Many lizards are most visible when they are active. However, they are wary when approached, and evade hand- capture by running away. Also, some lizards, such as varanids, and agamas, may sleep or bask in places that are difficult to reach, such as in the canopy and large stones, or in burrows. In these situations, a noose may be used to capture lizards without having to approach the lizards too closely. Nooses consist of a long pole, with a loop of string at the tip, which can be tightened around the neck of lizard and pulled tight in order to capture the animal.

5. Trapping

Trapping was used to catch many small reptiles. For terrestrial reptiles, the most commonly used trap is a pitfall trap, consisting of a bucket sunk into the ground so that the lip is flush with the surface. A small layer of leaf-litter or some other cover should be provided for animals that fall in. This also has the benefit of attracting arthropods to the trap, which can act as bait for lizards.

Marine snakes were sometimes observed, both during day and night at the edge of water and in back waters of Sandspit. The lizards were seen moving or resting just near shelters and they became alert to see the observers, some of them ran away very fast and were lost in the burrows of sand. But finally were caught with the help of two or three persons. This practice was done at least for one hour to find the different species of lizards. All species were counted and identified in the field. This method also helped to determine the distribution and occurrence of species. Similarly night surveys were done using the search lights and torches.

B. INDIRECT COUNTING METHODS

1. Information from different sources

Information was collected from the field staff of Sindh Wildlife Department, local fishermen, boatmen and members of local community/ villagers of different villages.

2. Presence of signs like tracks and footprints etc

Impressions of finger or foot prints, track, or tails, were observed for finding the existence, range and rough population of the species and range of the species.

The study was based mainly on direct observation and results calculated by the following formula:

$$P = \frac{AZ}{2YX}$$

P population
A total area
Z number observed
Y average flushing distance
X length of strip

RESULTS AND DISCUSSION

In Pakistan, reptiles are a blend of Palearctic, Indo-Malayan and Ethiopian forms (Fatima, 2008). During the present study, 2001-2009, total twenty seven reptilian species was recorded including 3 turtles, 9 lizards and 15 snakes.

Turtles

Three turtles species were found on Karachi coast, Green Turtle (*Chelonia mydas*) was recorded from all the four study sites Manora, Sandspit, Hawkesbay and Cape Monze, while Hawksbill Turtle (*Eretmochelys imbricata*) was recorded from Cape Monze area only, and Olive Ridley (*Lepidochelys olivacea*) was recorded from Sandspit only.

Green Turtle (*C. mydas*) was rated as common throughout study period i.e. 2001-2009 at Karachi coast (see Fig. 3), while Hawksbill Turtle (*E. imbricata*), and Olive Ridley (*L. olivacea*) were rated as rare. Olive Ridley (*L. olivacea*) was not found during years 2005 – 2009, while Hawksbill Turtle (*E. imbricata*) was recorded only in 2001 and 2003 from Cape Monze area, and after in the year 2003, it was not seen on Karachi coast.

Based on data of 2001, Green Turtle was rated as 30.06%, Hawksbill Turtle 0.02%, and Olive Ridley 0.02% (see Table 2). In year 2002, Green Turtle rated as 31.06%, Hawksbill Turtle 0%, Olive Ridley 0.02% (see Table 3).

In year 2003, Green Turtle rated as 30.32%, Hawksbill Turtle 0.02%, Olive Ridley 0.02% (see Table 4). In year 2004, Green Turtle rated as 30.42%, Hawksbill Turtle 0%, Olive Ridley 0.02% (see Table 5). In year 2005, Green Turtle rated as 28.92%, Hawksbill Turtle 0%, Olive Ridley 0% (see Table 6). In year 2006, Green Turtle rated as 28.37%, Hawksbill Turtle 0%, Olive Ridley 0% (see Table 7). In year 2007, Green Turtle rated as 27.80%, Hawksbill Turtle 0%, Olive Ridley 0% (see Table 8). In year 2008, Green Turtle rated as 27.20%, Hawksbill Turtle 0%, Olive Ridley 0% (see Table 9). In year 2009, Green Turtle rated as 27.56%, Hawksbill Turtle 0%, Olive Ridley 0% (see Table 10).

Lizards

Nine lizard species viz. Common Tree Lizard (C*alotes versicolor versicolor*), Spotted Barn Gecko (*Hemidactylus brooki*), Yellow Bellied Common House Gecko (*Hemidactylus flaviviridis*), Persian House Gecko (*Hemidactylus persicus*), Blotched House Gecko (*Hamidactylus triedrus*), Mediterranean House Gecko (H*amidactylus turcicus*), Blue Tail Sand Lizard (*Acanthodactylus cantoris*), Spotted Lacerta (*Mesalina watsonana*), and Bengal Monitor (*Varanus bengalensis*) were recorded from Manora, Sandspit, Hawkesbay and Cape Monze (see Fig. 4).

During 2001-2009, Blue Tail Sand Lizard (*Acanthodactylus cantoris*) was rated as common, Spotted Barn Gecko (*Hemidactylus brooki*), Yellow Bellied Common House Gecko (*Hemidactylus flaviviridis*), Persian House Gecko (*Hemidactylus persicus*), Spotted Lacerta (*Mesalina watsonana*) were rated as less common, while Bengal Monitor (*Varanus bengalensis*), Common Tree Lizard (C*alotes versicolor*), Mediterranean House Gecko (H*amidactylus turcicus*), and Blotched House Gecko (*Hamidactylus triedrus*) were rated as rare. In year 2002 and 2003, Common Tree Lizard (C*alotes versicolor*) was not recorded from Hawkes Bay area.

Table 1. Study areas of Karachi Coast with GPS position and habitat types.

S. No.	Location	GPS Position	Approx. Area of Surveyed (Km)	Habitat
1.	Manora	N 24 47 547 E 066 58 592	5	Sandy and Rocky Area
2.	Sandspit	N 24 50 723 E 066 54 104	5	Sandy Area
3.	Hawkes-bay	N 24 51 288 E 066 52 726	5	Sandy Area
4.	Cape monze	N 24 50 091 E 066 39 393	5	Rocky and Sandy Area

Based on data during 2001, Common Tree Lizard (*C. versicolor*) was rated as 5.29%, Spotted Barn Gecko (*H. brookii*) 5.83%, Yellow-bellied Common House Gecko (*H. flaviviridis*) 6.17%, Persian House Gecko (*H. persicus*) 4.31%, Blotched House Gecko (*H. triedrus*) 4.36%, Mediterranean House Gecko (*H. turcicus*) 4.75%, Blue Tail Sand Lizard (*A. cantoris*) 17.03%, Spotted Lacerta (*M. watsonana*) 15.55%, and Bengal Monitor (*V. bengalensis*) 1.47 % (see Table 2).

In the year 2002, Common Tree Lizard was rated as 5.22%, Spotted Barn Gecko 6.55%, Yellow-bellied Common House Gecko 6.41%, Persian House Gecko 4.40%, Blotched House Gecko 4.42%, Mediterranean House Gecko 4.89%, Blue Tail Sand Lizard 16.09%, Spotted Lacerta 16.59%, and Bengal Monitor 1.49% (see Table 3).

In the year 2003, Common Tree Lizard was rated as 5.08%, Spotted Barn Gecko 6.55%, Yellow-bellied Common House Gecko 6.41%, Persian House Gecko 0.51%, Blotched House Gecko 4.55%, Mediterranean House Gecko 5.20%, Blue Tail Sand Lizard 16.26%, Spotted Lacerta 15.68%, and Bengal Monitor recorded 1.51% (see Table 4).

In the year 2004, Common Tree Lizard was rated as 5.35%, Spotted Barn Gecko 6.53%, Yellow-bellied Common House Gecko 6.44%, Persian House Gecko 4.20%, Blotched House Gecko 4.72%, Mediterranean House Gecko 5.42%, Blue Tail Sand Lizard 16.04%, Spotted Lacerta 15.75%, and Bengal Monitor 1.22 % (see Table 5).

In the year 2005, Common Tree Lizard was rated as 5.19%, Spotted Barn Gecko 6.82%, Yellow-bellied Common House Gecko 6.71%, Persian House Gecko 4.46%, Blotched House Gecko 4.95%, Mediterranean House Gecko 5.28%, Blue Tail Sand Lizard 16.06%, Spotted Lacerta 15.95%, and Bengal Monitor 1.45% (see Table 6).

In the year 2006, Common Tree Lizard was rated as 5.11%, Spotted Barn Gecko 5.79%, Yellow-bellied Common House Gecko 6.95%, Persian House Gecko 4.37%, Blotched House Gecko 4.96%, Mediterranean House Gecko 5.37%, Blue Tail Sand Lizard 17.56%, Spotted Lacerta 15.58%, and Bengal Monitor 1.51% (see Table 7).

In the year 2007, Common Tree Lizard was rated as 4.88%, Spotted Barn Gecko 6.44%, Yellow-bellied Common House Gecko 6.87%, Persian House Gecko 4.56 %, Blotched House Gecko 1.17%, Mediterranean House Gecko 5.05%, Blue Tail Sand Lizard 17.45%, Spotted Lacerta 15.21%, and Bengal Monitor 1.75% (see Table 8).

Table 2. Population of Reptiles at Karachi Coast in 2001.

S. No.	Scientific name	Common name	Manora	Sandspit	Hawkes-bay	Cape monze	Total	%
1	*Chelonia mydas*	Green Turtle	20	881	309	18	1228	30.06
2	*Eretmochelys imbricate*	Hawksbill Turtle	0	0	0	1	1	0.02
3	*Lepidochelys olivacea*	Olive Ridley	0	1	0	0	1	0.02
4	*Calotes versicolor versicolor*	Common Tree Lizard	158	2	0	56	216	5.29
5	*Hemidactylus brookii*	Spotted Barn Gecko	153	35	47	3	238	5.83
6	*Hemidactylus flaviviridis*	Yellow-belly Common House Gecko	147	41	53	11	252	6.17
7	*Hemidactylus persicus*	Persian House Gecko	119	29	11	17	176	4.31
8	*Hemidactylus triedrus*	Blotched House Gecko	127	21	19	11	178	4.36
9	*Hemidactylus turcicus*	Mediterranean House Gecko	128	31	14	21	194	4.75
10	*Acanthodactylus cantoris*	Blue-Tail Sand Lizard	146	167	179	203	695	17.03
11	*Mesalina watsonana*	Spotted Lacerta	177	176`	133	149	635	15.55
12	*Varanus bengalensis*	Bengal Monitor	19	9	15	17	60	1.47
13	*Platyceps rhodorachis*	Cliff Racer	0	0	0	0	0	0
14	*Sphalerosophis diadema diadema*	Blotched Diadem Snake	3	0	0	0	3	0.06
15	*Naja naja*	Black Cobra	0	0	1	0	1	0.02
16	*Echis carinatus*	Saw-scaled Viper	2	0	0	0	2	0.04
17	*Enhydrina schistosa*	Beaked Sea Snake	5	2	1	9	17	0.41
18	*Hydrophis caerulescens*	Blue Green Sea Snake	3	2	1	10	16	0.39
19	*Hydrophis cyanocinctus*	Annulated Sea Snake	8	3	2	11	24	0.58
20	*Hydrophis lapemoides*	Persian Sea Snake	3	2	2	1	8	0.19
21	*Hydrophis mamillaris*	Broad Band Sea Snake	2	0	0	11	13	0.31
22	*Hydrophis ornatus*	Reef Sea Snake	8	3	1	17	29	0.71
23	*Hydrophis spiralis*	Yellow Sea Snake	7	9	8	11	35	0.85
24	*Lapemis curtus*	Pygmy Sea Snake	2	1	0	5	8	0.19
25	*Microcephalophis cantrois*	Spotted Small Headed Sea Snake	3	2	2	7	14	0.34
26	*Pelamis platurus*	Pelagic Sea Snake	3	1	0	9	13	0.31
27	*Praescutata viperina*	Spotted Viperine Sea Snake	8	3	1	12	24	0.58
	Total		1251	1421	799	610	4081	

In the year 2008, Common Tree Lizard was rated as 4.93%, Spotted Barn Gecko 6.49%, Yellow-bellied Common House Gecko 6.92%, Persian House Gecko 4.60%, Blotched House Gecko 5.11%, Mediterranean House Gecko 5.09%, Blue Tail Sand Lizard 17.60%, Spotted Lacerta 15.34%, and Bengal Monitor 1.77% (see Table 9).

In the year 2009, Common Tree Lizard was rated as 4.90%, Spotted Barn Gecko 6.46%, Yellow-bellied Common House Gecko 6.89%, Persian House Gecko 4.58%, Blotched House Gecko 5.08%, Mediterranean House Gecko 5.06%, Blue Tail Sand Lizard 17.51%, Spotted Lacerta 15.26%, and Bengal Monitor 1.76% (see Table 10).

Snakes

Out of the 15 species of sea snake rated from the Karachi coast, 12 species viz. Beaked Sea Snake (*Enhydrina schistosa*), Blue Green Sea Snake (*Hydrophis caerulescens*), Annulated Sea Snake (*Hydrophis cyanocinctus*), Persian Sea Snake (*Hydrophis lapemoides*), Broad Band Sea Snake (*Hydrophis mamillaris*), Reef Sea Snake (*Hydrophis ornatus*), Yellow Sea Snake (*Hydrophis spiralis*), Pygmy Sea Snake (*Lapemis curtus*), Spotted Small Headed Sea Snake (*Microcephalophis cantrois*), Pelagic Sea Snake (*Pelamis platurus*), Spotted Viperine Sea Snake (*Praescutata viperina*), and Blotched Diadem Snake (*Sphalerosophis diadema diadema*) were recorded from all the four study sites viz. Manora, Sandspit, Hawkesbay and Cape Monze areas and all were rated as rare (see Fig. 5).

Table 3. Population of Reptiles at Karachi Coast in 2002.

S. No.	Scientific name	Common name	Manora	Sandspit	Hawkes-bay	Cape monze	Total	%
1	*Chelonia mydas*	Green Turtle	25	948	319	21	1313	31.06
2	*Eretmochelys imbricate*	Hawksbill Turtle	0	0	0	0	0	0
3	*Lepidochelys olivacea*	Olive Ridley	0	1	0	0	1	0.02
4	*Calotes versicolor versicolor*	Common Tree Lizard	156	3	0	62	221	5.22
5	*Hemidactylus brookii*	Spotted Barn Gecko	150	59	48	20	277	6.55
6	*Hemidactylus flaviviridis*	Yellow-belly Common House Gecko	151	46	57	17	271	6.41
7	*Hemidactylus persicus*	Persian House Gecko	123	31	13	19	186	4.40
8	*Hemidactylus triedrus*	Blotched House Gecko	129	23	21	14	187	4.42
9	*Hemidactylus turcicus*	Mediterranean House Gecko	132	35	16	24	207	4.89
10	*Acanthodactylus cantoris*	Blue-Tail Sand Lizard	146	163	174	197	680	16.09
11	*Mesalina watsonana*	Spotted Lacerta	186	148	139	159	632	14.59
12	*Varanus bengalensis*	Bengal Monitor	21	11	13	18	63	1.49
13	*Platyceps rhodorachis*	Cliff Racer	0	0	0	0	0	0
14	*Sphalerosophis diadema diadema*	Blotched Diadem Snake	3	0	0	0	3	0.06
15	*Naja naja*	Black Cobra	0	0	0	0	0	0
16	*Echis carinatus*	Saw-scaled Viper	1	0	0	0	1	0.02
17	*Enhydrina schistosa*	Beaked Sea Snake	3	1	1	11	16	0.37
18	*Hydrophis caerulescens*	Blue Green Sea Snake	2	4	1	5	12	0.28
19	*Hydrophis cyanocinctus*	Annulated Sea Snake	4	2	3	14	23	0.54
20	*Hydrophis lapemoides*	Persian Sea Snake	2	2	0	1	5	0.11
21	*Hydrophis mamillaris*	Broad Band Sea Snake	1	0	0	9	10	0.23
22	*Hydrophis ornatus*	Reef Sea Snake	3	1	2	15	21	0.49
23	*Hydrophis spiralis*	Yellow Sea Snake	3	6	7	12	28	0.66
24	*Lapemis curtus*	Pygmy Sea Snake	2	2	0	3	7	0.16
25	*Microcephalophis cantrois*	Spotted Small Headed Sea Snake	4	3	2	9	18	0.42
26	*Pelamis platurus*	Pelagic Sea Snake	2	2	1	11	16	0.37
27	*Praescutata viperina*	Spotted Viperine Sea Snake	9	2	2	15	28	0.66
	Total		1258	1493	819	656	4226	

Three species of terrestrial snakes viz. Cliff Racer (*Platyceps rhodorachis*) Saw-scaled Viper (*Echis carinatus*) and Black Cobra (*Naja naja*) were recorded from Manora, Hawkesbay and Cape Monze area only. The main reason for their absence from Sandspit seems to be large scale disturbance due to human population and visitors in the area.

During 2001-2009, Persian Sea Snake, Annulated Sea Snake, Blotched Diadem Snake, Yellow Sea Snake, Blue Green Sea Snake, Reef Sea Snake, Broad Band Sea Snake, Beaked Sea Snake, Pygmy Sea Snake, Spotted Viperine Sea Snake, Spotted Small Headed Sea Snake, and Pelagic Sea Snake were rated as rare, and Saw-scaled Viper was rated as rare during 2001, 2002, 2005 to 2007, while in years 2003 - 2004, it was not recorded. Black Cobra was rated as rare in year 2001, 2005 to 2009, but in year 2002 to 2004, it was not observed. Cliff Racer was not recorded during 2001 and 2002, while during 2003 to 2009 at Cape Monze, and in year 2006, at Monera and Sandspit, it was rated as rare.

In the year 2001 Cliff Racer was rated as 0%, Blotched Diadem Snake 0.06%, Black Cobra 0.02%, Saw-scaled Viper 0.04%, Beaked Sea Snake 0.41%, Blue Green Sea Snake 0.39%, Annulated Sea Snake 0.58%, Persian Sea Snake 0.19%, Broad Band Sea Snake 0.31% , Reef Sea Snake 0.71%, Yellow Sea Snake 0.85%, Pygmy Sea

Table 4. Population of Reptiles at Karachi Coast in 2003.

S. No.	Scientific name	Common name	Manora	Sandspit	Hawkes-bay	Cape monze	Total	%
1	*Chelonia mydas*	Green Turtle	27	931	325	22	1305	30.32
2	*Eretmochelys imbricate*	Hawksbill Turtle	0	0	0	1	1	0.02
3	*Lepidochelys olivacea*	Olive Ridley	0	1	0	0	1	0.02
4	*Calotes versicolor versicolor*	Common Tree Lizard	147	1	0	71	219	5.08
5	*Hemidactylus brookii*	Spotted Barn Gecko	153	61	47	21	282	6.55
6	*Hemidactylus flaviviridis*	Yellow-belly Common House Gecko	149	49	59	19	276	6.41
7	*Hemidactylus persicus*	Persian House Gecko	127	33	15	22	197	0.51
8	*Hemidactylus triedrus*	Blotched House Gecko	131	27	23	15	196	4.55
9	*Hemidactylus turcicus*	Mediterranean House Gecko	136	38	21	29	224	5.20
10	*Acanthodactylus cantoris*	Blue- Tail Sand Lizard	142	177	185	196	700	16.26
11	*Mesalina watsonana*	Spotted Lacerta	202	164	144	165	675	15.68
12	*Varanus bengalensis*	Bengal Monitor	18	8	15	24	65	1.51
13	*Platyceps rhodorachis*	Cliff Racer	0	0	0	1	1	0.02
14	*Sphalerosophis diadema diadema*	Blotched Diadem Snake	2	0	0	3	5	0.11
15	*Naja naja*	Black Cobra	0	0	0	0	0	0
16	*Echis carinatus*	Saw-scaled Viper	0	0	0	0	0	0
17	*Enhydrina schistosa*	Beaked Sea Snake	1	0	0	9	10	0.23
18	*Hydrophis caerulescens*	Blue Green Sea Snake	3	2	1	7	13	0.30
189	*Hydrophis cyanocinctus*	Annulated Sea Snake	3	1	3	12	19	0.44
20	*Hydrophis lapemoides*	Persian Sea Snake	3	1	1	1	6	0.13
21	*Hydrophis mamillaris*	Broad Band Sea Snake	0	0	0	9	9	0.20
22	*Hydrophis ornatus*	Reef Sea Snake	2	1	1	13	17	0.39
23	*Hydrophis spiralis*	Yellow Sea Snake	4	5	3	15	27	0.62
24	*Lapemis curtus*	Pygmy Sea Snake	1	0	0	5	6	0.13
25	*Microcephalophis cantrois*	Spotted Small Headed Sea Snake	2	2	1	4	9	0.20
26	*Pelamis platurus*	Pelagic Sea Snake	6	3	1	12	22	0.51
27	*Praescutata viperina*	Spotted Viperine Sea Snake	5	0	0	13	18	0.41
	Total		1264	1505	845	689	4303	

Snake 0.19%, Spotted Small Headed Sea Snake 0.34%, Pelagic Sea Snake 0.31%, and Spotted Viperine Sea Snake 0.58% (see Table 2).

In the year 2002, Cliff Racer was rated as 0%, Blotched Diadem Snake 0.06%, Black Cobra 0%, Saw-scaled Viper 0.02%, Beaked Sea Snake 0.37%, Blue Green Sea Snake 0.28%, Annulated Sea Snake 0.54%, Persian Sea Snake as 0.11%, Broad Band Sea Snake 0.23%, Reef Sea Snake 0.49%, Yellow Sea Snake 0.66%, Pygmy Sea Snake 0.16%, Spotted Small Headed Sea Snake 0.42%, Pelagic Sea Snake 0.37%, and Spotted Viperine Sea Snake recorded 0.66% (see Table 3)

In the year 2003, Cliff Racer was rated as 0.02%, Blotched Diadem Snake 0.11%, Black Cobra 0%, Saw-scaled Viper 0%, Beaked Sea Snake 0.23%, Blue Green Sea Snake 0.30%, Annulated Sea Snake 0.44%, Persian Sea Snake 0.13%, Broad Band Sea Snake 0.20%, Reef Sea Snake 0.39%, Yellow Sea Snake 0.62%, Pygmy Sea Snake 0.13%, Spotted Small Headed Sea Snake 0.20%, Pelagic Sea Snake 0.51%, and Spotted Viperine Sea Snake 0.41% (see Table 4).

In the year 2004, Cliff Racer was rated as 0.06%, Blotched Diadem Snake 0.18%, Black Cobra 0%, Saw-scaled Viper 0%, Beaked Sea Snake 0.13%, Blue Green Sea Snake 0.31%, Annulated Sea Snake 0.15%, Persian Sea Snake 0.13%, Broad Band Sea Snake 0.33%, Reef Sea Snake 0.49%, Yellow Sea Snake 0.47%, Pygmy Sea Snake 0.24%, Spotted Small Headed Sea Snake 0.27%,

Table 5. Population of Reptiles at Karachi Coast in 2004.

S. No.	Scientific name	Common name	Manora	Sandspit	Hawkes-bay	Cape monze	Total	%
1	*Chelonia mydas*	Green Turtle	30	955	340	21	1346	30.42
2	*Eretmochelys imbricate*	Hawksbill Turtle	0	0	0	0	0	0
3	*Lepidochelys olivacea*	Olive Ridley	0	1	0	0	1	0.02
4	*Calotes versicolor versicolor*	Common Tree Lizard	150	3	1	83	237	5.35
5	*Hemidactylus brookii*	Spotted Barn Gecko	145	65	56	23	289	6.53
6	*Hemidactylus flaviviridis*	Yellow-belly Common House Gecko	153	52	57	23	285	6.44
7	*Hemidactylus persicus*	Persian House Gecko	118	27	18	23	186	4.20
8	*Hemidactylus triedrus*	Blotched House Gecko	134	32	26	17	209	4.72
9	*Hemidactylus turcicus*	Mediterranean House Gecko	141	42	25	32	240	5.42
10	*Acanthodactylus cantoris*	Blue-Tail Sand Lizard	153	175	183	199	710	16.04
11	*Mesalina watsonana*	Spotted Lacerta	209	152	152	184	697	15.75
12	*Varanus bengalensis*	Bengal Monitor	15	5	13	21	54	1.22
13	*Platyceps rhodorachis*	Cliff Racer	0	0	0	3	3	0.06
14	*Sphalerosophis diadema diadema*	Blotched Diadem Snake	3	0	1	4	8	0.18
15	*Naja naja*	Black Cobra	0	0	0	0	0	0
16	*Echis carinatus*	Saw-scaled Viper	0	0	0	0	0	0
17	*Enhydrina schistosa*	Beaked Sea Snake	0	0	1	5	6	0.13
18	*Hydrophis caerulescens*	Blue Green Sea Snake	2	1	2	9	14	0.31
19	*Hydrophis cyanocinctus*	Annulated Sea Snake	2	0	1	4	7	0.15
20	*Hydrophis lapemoides*	Persian Sea Snake	2	1	1	2	6	0.13
21	*Hydrophis mamillaris*	Broad Band Sea Snake	1	0	1	13	15	0.33
22	*Hydrophis ornatus*	Reef Sea Snake	3	2	2	15	22	0.49
23	*Hydrophis spiralis*	Yellow Sea Snake	2	5	3	11	21	0.47
24	*Lapemis curtus*	Pygmy Sea Snake	2	1	0	8	11	0.24
25	*Microcephalophis cantrois*	Spotted Small Headed Sea Snake	3	1	1	7	12	0.27
26	*Pelamis platurus*	Pelagic Sea Snake	5	2	3	16	26	0.58
27	*Praescutata viperina*	Spotted Viperine Sea Snake	3	1	0	15	19	0.42
	Total		1276	1523	887	738	4424	

Pelagic Sea Snake 0.58%, and Spotted Viperine Sea Snake 0.42% (see Table 5).

In the year 2005, Cliff Racer was rated as 0.08%, Blotched Diadem Snake 0.15%, Black Cobra 0.02%, Saw-scaled Viper 0.06%, Beaked Sea Snake 0.17%, Blue Green Sea Snake 0.37%, Annulated Sea Snake 0.19%, Persian Sea Snake 0.17%, Broad Band Sea Snake 0.39%, Reef Sea Snake as 0.48%, Yellow Sea Snake as 0.39%, Pygmy Sea Snake 0.28%, Spotted Small Headed Sea Snake 0.28%, Pelagic Sea Snake 0.59%, and Spotted Viperine Sea Snake 0.46% (see Table 6).

In the year 2006, Cliff Racer was rated as 0.10%, Blotched Diadem Snake 0.21%, Black Cobra 0.02%, Saw-scaled Viper 0.21%, Beaked Sea Snake 0.12%, Blue Green Sea Snake 0.42%, Annulated Sea Snake 0.23%, Persian Sea Snake 0.12%, Broad Band Sea Snake 0.51%, Reef Sea Snake 0.49%, Yellow Sea Snake 0.38%, Pygmy Sea Snake 0.31%, Spotted Small Headed Sea Snake 0.23%, Pelagic Sea Snake 0.38%, and Spotted Viperine Sea Snake 0.57% (see Table 7).

In the year 2007, Cliff Racer was rated as 0.10%, Blotched Diadem Snake 0.20%, Black Cobra 0.16%, Saw-scaled Viper 0.14%, Beaked Sea Snake 0.42%, Blue Green Sea Snake 0.48%, Annulated Sea Snake 0.24%, Persian Sea Snake 0.14%, Broad Band Sea Snake 0.42%, Reef Sea Snake 0.52%, Yellow Sea Snake 0.42%, Pygmy Sea Snake 0.36%, Spotted Small Headed Sea Snake 0.36 %, Pelagic Sea Snake 0.50%, and Spotted Viperine Sea Snake 0.46% (see Table 8).

Table 6. Population of Reptiles at Karachi Coast in 2005.

S. No.	Scientific name	Common name	Manora	Sandspit	Hawkes-bay	Cape monze	Total	%
1	*Chelonia mydas*	Green Turtle	29	935	331	19	1314	28.92
2	*Eretmochelys imbricate*	Hawksbill Turtle	0	0	0	0	0	0
3	*Lepidochelys olivacea*	Olive Ridley	0	0	0	0	0	0
4	*Calotes versicolor versicolor*	Common Tree Lizard	148	2	5	81	236	5.19
5	*Hemidactylus brookii*	Spotted Barn Gecko	142	72	66	30	310	6.82
6	*Hemidactylus flaviviridis*	Yellow-belly Common House Gecko	159	57	61	28	305	6.71
7	*Hemidactylus persicus*	Persian House Gecko	121	29	27	26	203	4.46
8	*Hemidactylus triedrus*	Blotched House Gecko	137	36	29	23	225	4.95
9	*Hemidactylus turcicus*	Mediterranean House Gecko	131	45	27	37	240	5.28
10	*Acanthodactylus cantoris*	Blue- Tail Sand Lizard	170	178	182	200	730	16.06
11	*Mesalina watsonana*	Spotted Lacerta	214	158	156	197	726	15.95
12	*Varanus bengalensis*	Bengal Monitor	18	8	17	23	66	1.45
13	*Platyceps rhodorachis*	Cliff Racer	0	0	0	4	4	0.08
14	*Sphalerosophis diadema diadema*	Blotched Diadem Snake	1	0	1	5	7	0.15
15	*Naja naja*	Black Cobra	0	0	0	1	1	0.02
16	*Echis carinatus*	Saw-scaled Viper	0	0	0	3	3	0.06
17	*Enhydrina schistosa*	Beaked Sea Snake	1	0	1	6	8	0.17
18	*Hydrophis caerulescens*	Blue Green Sea Snake	2	3	1	11	17	0.37
19	*Hydrophis cyanocinctus*	Annulated Sea Snake	3	1	0	5	9	0.19
20	*Hydrophis lapemoides*	Persian Sea Snake	3	2	2	1	8	0.17
21	*Hydrophis mamillaris*	Broad Band Sea Snake	2	1	0	15	18	0.39
22	*Hydrophis ornatus*	Reef Sea Snake	2	1	2	17	22	0.48
23	*Hydrophis spiralis*	Yellow Sea Snake	1	3	1	13	18	0.39
24	*Lapemis curtus*	Pygmy Sea Snake	1	1	2	9	13	0.28
25	*Microcephalophis cantoris*	Spotted Small Headed Sea Snake	1	2	1	9	13	0.28
26	*Pelamis platurus*	Pelagic Sea Snake	3	3	4	17	27	0.59
27	*Praescutata viperina*	Spotted Viperine Sea Snake	2	2	0	17	21	0.46
	Total		1291	1539	916	797	4543	

In the year 2008, Cliff Racer was rated as 0.10%, Blotched Diadem Snake 0.20%, Black Cobra 0.16%, Saw-scaled Viper 0.14%, Beaked Sea Snake 0.42%, Blue Green Sea Snake 0.48%, Annulated Sea Snake 0.24%, Persian Sea Snake 0.14%, Broad Band Sea Snake 0.42%, Reef Sea Snake 0.52%, Yellow Sea Snake 0.42%, Pygmy Sea Snake 0.36%, Spotted Small Headed Sea Snake 0.36 %, Pelagic Sea Snake 0.50%, and Spotted Viperine Sea Snake 0.46% (see Table 9).

In the year 2009, Cliff Racer was rated as 0.10%, Blotched Diadem Snake 0.20%, Black Cobra 0.16%, Saw-scaled Viper 0.14%, Beaked Sea Snake 0.42%, Blue Green Sea Snake 0.48%, Annulated Sea Snake 0.24%, Persian Sea Snake 0.14%, Broad Band Sea Snake 0.42%, Reef Sea Snake 0.52%, Yellow Sea Snake 0.42%, Pygmy Sea Snake 0.36%, Spotted Small Headed Sea Snake 0.36 %, Pelagic Sea Snake 0.50%, and Spotted Viperine Sea Snake 0.46% (see Table 10). The population of reptiles at Manora, Sandspit, Hawkesbay, and Cape Monze has been also summarized in appendix 1-4.

Environmental Impacts

Habitat Degradation

According to field surveys during 2002 – 2009, serious threats especially to marine turtles have been observed, while lizards are also affected by habitat degradation and disturbance, but it is a very minor threat. There are instances of some mortality of Bengal Monitor during the road crossing. Sea snakes are least affected by these factors as they are seldom encountered along the sea

Table 7. Population of Reptiles at Karachi Coast in 2006.

S. No.	Scientific name	Common name	Manora	Sands-pit	Hawkes bay	Cape monze	Total	%
1	*Chelonia mydas*	Green Turtle	32	937	341	21	1331	28.37
2	*Eretmochelys imbricate*	Hawksbill Turtle	0	0	0	0	0	0
3	*Lepidochelys olivacea*	Olive Ridley	0	0	0	0	0	0
4	*Calotes versicolor versicolor*	Common Tree Lizard	146	3	2	89	240	5.11
5	*Hemidactylus brookii*	Spotted Barn Gecko	136	59	56	21	272	5.79
6	*Hemidactylus flaviviridis*	Yellow-belly Common House Gecko	165	63	65	33	326	6.95
7	*Hemidactylus persicus*	Persian House Gecko	118	31	29	27	205	4.37
8	*Hemidactylus triedrus*	Blotched House Gecko	141	32	26	34	233	4.96
9	*Hemidactylus turcicus*	Mediterranean House Gecko	149	48	23	32	252	5.37
10	*Acanthodactylus cantoris*	Blue-Tail Sand Lizard	177	203	209	235	824	17.56
11	*Mesalina watsonana*	Spotted Lacerta	217	152	157	205	731	15.58
12	*Varanus bengalensis*	Bengal Monitor	21	11	14	25	71	1.51
13	*Platyceps rhodorachis*	Cliff Racer	1	0	1	3	5	0.10
14	*Sphalerosophis diadema diadema*	Blotched Diadem Snake	1	2	0	7	10	0.21
15	*Naja naja*	Black Cobra	0	0	1	0	1	0.02
16	*Echis carinatus*	Saw-scaled Viper	2	0	0	8	10	0.21
17	*Enhydrina schistosa*	Beaked Sea Snake	1	0	0	5	6	0.12
18	*Hydrophis caerulescens*	Blue Green Sea Snake	1	4	0	15	20	0.42
19	*Hydrophis cyanocinctus*	Annulated Sea Snake	4	0	1	6	11	0.23
20	*Hydrophis lapemoides*	Persian Sea Snake	2	2	1	1	6	0.12
21	*Hydrophis mamillaris*	Broad Band Sea Snake	0	2	1	21	24	0.51
22	*Hydrophis ornatus*	Reef Sea Snake	1	0	3	19	23	0.49
23	*Hydrophis spiralis*	Yellow Sea Snake	1	0	2	15	18	0.38
24	*Lapemis curtus*	Pygmy Sea Snake	1	0	1	13	15	0.31
25	*Microcephalophis cantoris*	Spotted Small Headed Sea Snake	2	1	1	7	11	0.23
26	*Pelamis platurus*	Pelagic Sea Snake	2	1	0	15	18	0.38
27	*Praescutata viperina*	Spotted Viperine Sea Snake	1	0	2	24	27	0.57
	Total		1322	1551	936	881	4690	

coast. They are entangled in fishermen nets but are released when found in fish catch.

Human activities that directly or indirectly threaten marine turtles include the exploitation of eggs and turtles, fishery-related mortality, inappropriate management practices, destruction or modification of habitats, pollution, and recreation activities. Khan *et al*. (2009) conducted a baseline study to evaluate the estrogenic activities using *in-vitro* yeast estrogenic screen in selected Ramsar sites and Creek areas, and reported that highest estrogenic activity has been recorded at creek area. The sewage discharge from Malir and Layri Rivers is causing big loss to fish nursery ground and the mangrove forest.

Table 8. Population of Reptiles at Karachi Coast in 2007.

S. No.	Scientific name	Common name	Manora	Sandspit	Hawkes-bay	Cape monze	Total	%
1	*Chelonia mydas*	Green Turtle	47	951	351	27	1376	27.80
2	*Eretmochelys imbricate*	Hawksbill Turtle	0	0	0	0	0	0
3	*Lepidochelys olivacea*	Olive Ridley	0	0	0	0	0	0
4	*Calotes versicolor versicolor*	Common Tree Lizard	151	2	3	86	242	4.88
5	*Hemidactylus brookii*	Spotted Barn Gecko	135	64	65	55	319	6.44
6	*Hemidactylus flaviviridis*	Yellow-belly Common House Gecko	167	67	67	39	340	6.87
7	*Hemidactylus persicus*	Persian House Gecko	124	35	33	34	226	4.56
8	*Hemidactylus triedrus*	Blotched House Gecko	138	35	29	44	251	1.17
9	*Hemidactylus turcicus*	Mediterranean House Gecko	140	32	48	30	250	5.05
10	*Acanthodactylus cantoris*	Blue-Tail Sand Lizard	185	215	219	245	864	17.45
11	*Mesalina watsonana*	Spotted Lacerta	215	172	165	201	753	15.21
12	*Varanus bengalensis*	Bengal Monitor	30	8	12	37	87	1.75
13	*Platyceps rhodorachis*	Cliff Racer	0	0	0	5	5	0.10
14	*Sphalerosophis diadema diadema*	Blotched Diadem Snake	1	1	0	8	10	0.20
15	*Naja naja*	Black Cobra	1	0	0	7	8	0.16
16	*Echis carinatus*	Saw-scaled Viper	0	0	1	6	7	0.14
17	*Enhydrina schistosa*	Beaked Sea Snake	8	0	1	12	21	0.42
18	*Hydrophis caerulescens*	Blue Green Sea Snake	1	2	1	20	24	0.48
19	*Hydrophis cyanocinctus*	Annulated Sea Snake	2	1	0	9	12	0.24
20	*Hydrophis lapemoides*	Persian Sea Snake	3	2	1	1	7	0.14
21	*Hydrophis mamillaris*	Broad Band Sea Snake	1	1	0	19	21	0.42
22	*Hydrophis ornatus*	Reef Sea Snake	2	1	0	23	26	0.52
23	*Hydrophis spiralis*	Yellow Sea Snake	2	0	1	18	21	0.42
24	*Lapemis curtus*	Pygmy Sea Snake	2	0	1	15	18	0.36
25	*Microcephalophis cantoris*	Spotted Small Headed Sea Snake	3	2	2	11	18	0.36
26	*Pelamis platurus*	Pelagic Sea Snake	3	2	3	17	25	0.50
27	*Praescutata viperina*	Spotted Viperine Sea Snake	2	0	2	19	23	0.46
	Total		1363	1593	1005	988	4949	

Industrial pollutants are also discharged in the marine water, which produce high concentration of lead and iron in water and fishes. The oil spills with increased oil tankers traffic, spills caused by negligence and marine transport in the area pose dangerous state to our marine biodiversity.

The Hawkesbay and Sandspit beaches, concentrated along 5km stretch represent the largest nesting habitat for marine turtles in Pakistan. Due to various recreational activities and construction of huts, this habitat is now threatened. In the absence of any effective and regular beach cleanup and garbage disposal system, beaches often contain large amounts of beach litter. Green turtles eat a wide variety of marine litter such as plastic bags, plastic styro-foam pieces, balloons and plastic pellets. Effects of consumption include interference in metabolism or gut function, even at low levels of ingestion as well as absorption of toxic by-products. In addition, garbage attracts predators like dogs and crows/gulls in large numbers that then pose a direct threat to the turtle eggs / hatchlings.

Presently, beachfront development is limited to the construction of beach huts. However, land use violations have been observed with a number of huts exceeding the limits of land usage as described in law. This is resulting in the reduction of available nesting habitat of Green

Table 9. Population of Reptiles at Karachi Coast in 2008.

S. No.	Scientific name	Common name	Manora	Sandspit	Hawkes-bay	Cape monze	Total	%
1	*Chelonia mydas*	Green Turtle	31	939	344	21	1335	27.20
2	*Eretmochelys imbricate*	Hawksbill Turtle	0	0	0	0	0	0
3	*Lepidochelys olivacea*	Olive Ridley	0	0	0	0	0	0
4	*Calotes versicolor versicolor*	Common Tree Lizard	151	2	3	86	242	4.93
5	*Hemidactylus brookii*	Spotted Barn Gecko	135	64	65	55	319	6.49
6	*Hemidactylus flaviviridis*	Yellow-belly Common House Gecko	167	67	67	39	340	6.92
7	*Hemidactylus persicus*	Persian House Gecko	124	35	33	34	226	4.60
8	*Hemidactylus triedrus*	Blotched House Gecko	138	35	29	44	251	5.11
9	*Hemidactylus turcicus*	Mediterranean House Gecko	140	32	48	30	250	5.09
10	*Acanthodactylus cantoris*	Blue-Tail Sand Lizard	185	215	219	245	864	17.60
11	*Mesalina watsonana*	Spotted Lacerta	215	172	165	201	753	15.34
12	*Varanus bengalensis*	Bengal Monitor	30	8	12	37	87	1.77
13	*Platyceps rhodorachis*	Cliff Racer	0	0	0	5	5	0.10
14	*Sphalerosophis diadema diadema*	Blotched Diadem Snake	1	1	0	8	10	0.20
15	*Naja naja*	Black Cobra	1	0	0	7	8	0.16
16	*Echis carinatus*	Saw-scaled Viper	0	0	1	6	7	0.14
17	*Enhydrina schistosa*	Beaked Sea Snake	8	0	1	12	21	0.42
18	*Hydrophis caerulescens*	Blue Green Sea Snake	1	2	1	20	24	0.48
19	*Hydrophis cyanocinctus*	Annulated Sea Snake	2	1	0	9	12	0.24
20	*Hydrophis lapemoides*	Persian Sea Snake	3	2	1	1	7	0.14
21	*Hydrophis mamillaris*	Broad Band Sea Snake	1	1	0	19	21	0.42
22	*Hydrophis ornatus*	Reef Sea Snake	2	1	0	23	26	0.52
23	*Hydrophis spiralis*	Yellow Sea Snake	2	0	1	18	21	0.42
24	*Lapemis curtus*	Pygmy Sea Snake	2	0	1	15	18	0.36
25	*Microcephalophis cantoris*	Spotted Small Headed Sea Snake	3	2	2	11	18	0.36
26	*Pelamis platurus*	Pelagic Sea Snake	3	2	3	17	25	0.50
27	*Praescutata viperina*	Spotted Viperina Sea Snake	2	0	2	19	23	0.46
	Total		1347	1581	998	982	4908	

turtles. Most of the land previously used by turtles for nesting has been built upon and hence space for turtle nesting is now severely restricted. Night use of beach huts is common in Karachi coast. Use of lightening in the night discourages females from nesting and cause hatchlings to become disoriented because they intensively head towards the brightest horizon, which should be the moonlit ocean. Beach front lightening instead cause them to disorient and wander inland, where they often die of dehydration or predation.

Of great concern these days is the issue of construction debris from newly constructed and unused/unprotected huts that has been noticed at various locations on the beaches. The debris can alter the beach habitat, hamper or deter nesting attempts as well as interfere with the incubation of eggs and the emergence of hatchlings. Sand excavated during the process also has shown that when beaches are nourished by pumping, trucking or otherwise depositing sand on a beach to replace what has been lost due to natural erosion process or physical removal, it can negatively impact sea turtles. If the sand is too compacted for the turtles to nest in or if the sand imported is drastically different from native beach sediments, the nest-site selection, digging behavior, incubation, temperature and the moisture content of nests is affected. Therefore, it is felt that activities such as sand removal could have irreversible adverse impacts on the turtle nesting habitat at the Haweksbay and Sandspit beaches. These land use practices are also affecting the lizards of the area, but this is a minor threat as the lizards are more restricted to landward site. The population of reptiles on

Table 10. Population of Reptiles at Karachi Coast in 2009.

S. No.	Scientific name	Common name	Manora	Sandspit	Hawkes-bay	Cape monze	Total	%
1	*Chelonia mydas*	Green Turtle	43	953	339	25	1360	27.56
2	*Eretmochelys imbricate*	Hawksbill Turtle	0	0	0	0	0	0
3	*Lepidochelys olivacea*	Olive Ridley	0	0	0	0	0	0
4	*Calotes versicolor versicolor*	Common Tree Lizard	151	2	3	86	242	4.90
5	*Hemidactylus brookii*	Spotted Barn Gecko	135	64	65	55	319	6.46
6	*Hemidactylus flaviviridis*	Yellow-belly Common House Gecko	167	67	67	39	340	6.89
7	*Hemidactylus persicus*	Persian House Gecko	124	35	33	34	226	4.58
8	*Hemidactylus triedrus*	Blotched House Gecko	138	35	29	44	251	5.08
9	*Hemidactylus turcicus*	Mediterranean House Gecko	140	32	48	30	250	5.06
10	*Acanthodactylus cantoris*	Blue-Tail Sand Lizard	185	215	219	245	864	17.51
11	*Mesalina watsonana*	Spotted Lacerta	215	172	165	201	753	15.26
12	*Varanus bengalensis*	Bengal Monitor	30	8	12	37	87	1.76
13	*Platyceps rhodorachis*	Cliff Racer	0	0	0	5	5	0.10
14	*Sphalerosophis diadema diadema*	Blotched Diadem Snake	1	1	0	8	10	0.20
15	*Naja naja*	Black Cobra	1	0	0	7	8	0.16
16	*Echis carinatus*	Saw-scaled Viper	0	0	1	6	7	0.14
17	*Enhydrina schistosa*	Beaked Sea Snake	8	0	1	12	21	0.42
18	*Hydrophis caerulescens*	Blue Green Sea Snake	1	2	1	20	24	0.48
19	*Hydrophis cyanocinctus*	Annulated Sea Snake	2	1	0	9	12	0.24
20	*Hydrophis lapemoides*	Persian Sea Snake	3	2	1	1	7	0.14
21	*Hydrophis mamillaris*	Broad Band Sea Snake	1	1	0	19	21	0.42
22	*Hydrophis ornatus*	Reef Sea Snake	2	1	0	23	26	0.52
23	*Hydrophis spiralis*	Yellow Sea Snake	2	0	1	18	21	0.42
24	*Lapemis curtus*	Pygmy Sea Snake	2	0	1	15	18	0.36
25	*Microcephalophis cantoris*	Spotted Small Headed Sea Snake	3	2	2	11	18	0.36
26	*Pelamis platurus*	Pelagic Sea Snake	3	2	3	17	25	0.50
27	*Praescutata viperina*	Spotted Viperine Sea Snake	2	0	2	19	23	0.46
	Total		1359	1595	993	986	4933	

the Karachi coast is more or less stable except that of Olive Ridley Turtle which has not been recorded from 2005 and onwards.

Appendix 1. Population of Reptiles at Manora, Karachi Coast in 2001 to 2009.

S. No.	Scientific name	Common name	2001	02	03	04	05	06	07	08	09	Total
1	*Chelonia mydas*	Green Turtle	20	25	27	30	29	32	47	31	43	284
2	*Eretmochelys imbricata*	Hawksbill Turtle	0	0	0	0	0	0	0	0	0	0
3	*Lepidochelys olivacea*	Olive Ridley	0	0	0	0	0	0	0	0	0	0
4	*Calotes versicolor versicolor*	Common Tree Lizard	158	156	147	150	148	146	151	151	151	1358
5	*Hemidactylus brookii*	Spotted Barn Gecko	153	150	153	145	142	136	135	135	135	1284
6	*Hemidactylus flaviviridis*	Yellow-belly Common House Gecko	147	151	149	153	159	165	167	167	167	1425
7	*Hemidactylus persicus*	Persian House Gecko	119	123	127	118	121	118	124	124	124	1098
8	*Hemidactylus triedrus*	Blotched House Gecko	127	129	131	134	137	141	138	138	138	1213
9	*Hemidactylus turcicus*	Mediterranean House Gecko	128	132	136	141	131	149	140	140	140	1237
10	*Acanthodactylus cantoris*	Blue-Tail Sand Lizard	146	146	142	153	170	177	185	185	185	1489
11	*Mesalina watsonana*	Spotted Lacerta	177	186	202	209	214	217	215	215	215	1850
12	*Varanus bengalensis*	Bengal Monitor	19	21	18	15	18	21	30	30	30	202
13	*Platyceps rhodorachis*	Cliff Racer	0	0	0	0	0	1	0	0	0	1
14	*Sphalerosophis diadema diadema*	Blotched Diadem Snake	3	3	2	3	1	1	1	1	1	16
15	*Naja naja*	Black Cobra	0	0	0	0	0	0	1	1	1	3
16	*Echis carinatus*	Saw-scaled Viper	2	1	0	0	0	2	0	0	0	5
17	*Enhydrina schistosa*	Beaked Sea Snake	5	3	1	0	1	1	8	8	8	35
18	*Hydrophis caerulescens*	Blue Green Sea Snake	3	2	3	2	2	1	1	1	1	16
19	*Hydrophis cyanocinctus*	Annulated Sea Snake	8	4	3	2	3	4	2	2	2	32
20	*Hydrophis lapemoides*	Persian Sea Snake	3	2	3	2	3	2	3	3	3	24
21	*Hydrophis mamillaris*	Broad Band Sea Snake	2	1	0	1	2	0	1	1	1	9
22	*Hydrophis ornatus*	Reef Sea Snake	8	3	2	3	2	1	2	2	2	25
23	*Hydrophis spiralis*	Yellow Sea Snake	7	3	4	2	1	1	2	2	2	24
24	*Lapemis curtus*	Pygmy Sea Snake	2	2	1	2	1	1	2	2	2	15
25	*Microcephalophis cantrois*	Spotted Small Headed Sea Snake	3	4	2	3	1	2	3	3	3	24
26	*Pelamis platurus*	Pelagic Sea Snake	3	2	6	5	3	2	3	3	3	30
27	*Praescutata viperina*	Spotted Viperine Sea Snake	8	9	5	3	2	1	2	2	2	34
	Total		1251	1258	1264	1276	1291	1322	1363	1347	1359	11731

Appendix 2. Population of Reptiles at Sandspit, Karachi Coast in 2001 to 2009.

S. No.	Scientific name	Common name	2001	02	03	04	05	06	07	08	09	Total
1	*Chelonia mydas*	Green Turtle	881	948	931	955	935	937	951	939	953	8430
2	*Eretmochelys imbricata*	Hawksbill Turtle	0	0	0	0	0	0	0	0	0	0
3	*Lepidochelys olivacea*	Olive Ridley	1	1	1	1	0	0	0	0	0	4
4	*Calotes versicolor versicolor*	Common Tree Lizard	2	3	1	3	2	3	2	2	2	20
5	*Hemidactylus brookii*	Spotted Barn Gecko	35	59	61	65	72	59	64	64	64	543
6	*Hemidactylus flaviviridis*	Yellow-belly Common House Gecko	41	46	49	52	57	63	67	67	67	509
7	*Hemidactylus persicus*	Persian House Gecko	29	31	33	27	29	31	35	35	35	285
8	*Hemidactylus triedrus*	Blotched House Gecko	21	23	27	32	36	32	35	35	35	276

Continued….

Continued….

S. No.	Scientific name	Common name	2001	02	03	04	05	06	07	08	09	Total
9	*Hemidactylus turcicus*	Mediterranean House Gecko	31	35	38	42	45	48	32	32	32	335
10	*Acanthodactylus cantoris*	Blue-Tail Sand Lizard	167	163	177	175	178	203	215	215	215	1708
11	*Mesalina watsonana*	Spotted Lacerta	176`	148	164	152	158	152	172	172	172	1290
12	*Varanus bengalensis*	Bengal Monitor	9	11	8	5	8	11	8	8	8	76
13	*Platyceps rhodorachis*	Cliff Racer	0	0	0	0	0	0	0	0	0	0
14	*Sphalerosophis diadema diadema*	Blotched Diadem Snake	0	0	0	0	0	2	1	1	1	5
15	*Naja naja*	Black Cobra	0	0	0	0	0	0	0	0	0	0
16	*Echis carinatus*	Saw-scaled Viper	0	0	0	0	0	0	0	0	0	0
17	*Enhydrina schistosa*	Beaked Sea Snake	2	1	0	0	0	0	0	0	0	3
18	*Hydrophis caerulescens*	Blue Green Sea Snake	2	4	2	1	3	4	2	2	2	22
19	*Hydrophis cyanocinctus*	Annulated Sea Snake	3	2	1	0	1	0	1	1	1	10
20	*Hydrophis lapemoides*	Persian Sea Snake	2	2	1	1	2	2	2	2	2	16
21	*Hydrophis mamillaris*	Broad Band Sea Snake	0	0	0	0	1	2	1	1	1	6
22	*Hydrophis ornatus*	Reef Sea Snake	3	1	1	2	1	0	1	1	1	11
23	*Hydrophis spiralis*	Yellow Sea Snake	9	6	5	5	3	0	0	0	0	28
24	*Lapemis curtus*	Pygmy Sea Snake	1	2	0	1	1	0	0	0	0	5
25	*Microcephalophis cantrois*	Spotted Small Headed Sea Snake	2	3	2	1	2	1	2	2	2	17
26	*Pelamis platurus*	Pelagic Sea Snake	1	2	3	2	3	1	2	2	2	18
27	*Praescutata viperina*	Spotted Viperine Sea Snake	3	2	0	1	2	0	0	0	0	8
	Total		1421	1493	1505	1523	1539	1551	1593	1581	1595	13801

Appendix 3. Population of Reptiles at Hawkesbay, Karachi Coast in 2001 to 2009.

S. No.	Scientific name	Common name	2001	02	03	04	05	06	07	08	09	Total
1	*Chelonia mydas*	Green Turtle	309	319	325	340	331	341	351	344	339	2999
2	*Eretmochelys imbricata*	Hawksbill Turtle	0	0	0	0	0	0	0	0	0	0
3	*Lepidochelys olivacea*	Olive Ridley	0	0	0	0	0	0	0	0	0	0
4	*Calotes versicolor versicolor*	Common Tree Lizard	0	0	0	1	5	2	3	3	3	17
5	*Hemidactylus brookii*	Spotted Barn Gecko	47	48	47	56	66	56	65	65	65	515
6	*Hemidactylus flaviviridis*	Yellow-belly Common House Gecko	53	57	59	57	61	65	67	67	67	553
7	*Hemidactylus persicus*	Persian House Gecko	11	13	15	18	27	29	33	33	33	212
8	*Hemidactylus triedrus*	Blotched House Gecko	19	21	23	26	29	26	29	29	29	231
9	*Hemidactylus turcicus*	Mediterranean House Gecko	14	16	21	25	27	23	48	48	48	270
10	*Acanthodactylus cantoris*	Blue-Tail Sand Lizard	179	174	185	183	182	209	219	219	219	1769
11	*Mesalina watsonana*	Spotted Lacerta	133	139	144	152	156	157	165	165	165	1376
12	*Varanus bengalensis*	Bengal Monitor	15	13	15	13	17	14	12	12	12	123
13	*Platyceps rhodorachis*	Cliff Racer	0	0	0	0	0	1	0	0	0	1
14	*Sphalerosophis diadema diadema*	Blotched Diadem Snake	0	0	0	1	1	0	0	0	0	2
15	*Naja naja*	Black Cobra	1	0	0	0	0	1	0	0	0	2
16	*Echis carinatus*	Saw-scaled Viper	0	0	0	0	0	0	1	1	1	3
17	*Enhydrina schistosa*	Beaked Sea Snake	1	1	0	1	1	0	1	1	1	7

Continued….

Continued….

S. No.	Scientific name	Common name	2001	02	03	04	05	06	07	08	09	Total
18	*Hydrophis caerulescens*	Blue Green Sea Snake	1	1	1	2	1	0	1	1	1	9
19	*Hydrophis cyanocinctus*	Annulated Sea Snake	2	3	3	1	0	1	0	0	0	10
20	*Hydrophis lapemoides*	Persian Sea Snake	2	0	1	1	2	1	1	1	1	10
21	*Hydrophis mamillaris*	Broad Band Sea Snake	0	0	0	1	0	1	0	0	0	2
22	*Hydrophis ornatus*	Reef Sea Snake	1	2	1	2	2	3	0	0	0	11
23	*Hydrophis spiralis*	Yellow Sea Snake	8	7	3	3	1	2	1	1	1	27
24	*Lapemis curtus*	Pygmy Sea Snake	0	0	0	0	2	1	1	1	1	6
25	*Microcephalophis cantrois*	Spotted Small Headed Sea Snake	2	2	1	1	1	1	2	2	2	14
26	*Pelamis platurus*	Pelagic Sea Snake	0	1	1	3	4	0	3	3	3	18
27	*Praescutata viperina*	Spotted Viperine Sea Snake	1	2	0	0	0	2	2	2	2	11
	Total		799	819	845	887	916	936	1005	998	993	8198

Appendix 4. Population of Reptiles at Cape Monze, Karachi Coast in 2001 to 2009.

S. No.	Scientific name	Common name	2001	02	03	04	05	06	07	08	09	Total
1	*Chelonia mydas*	Green Turtle	18	21	22	21	19	21	27	21	25	195
2	*Eretmochelys imbricata*	Hawksbill Turtle	1	0	1	0	0	0	0	0	0	2
3	*Lepidochelys olivacea*	Olive Ridley	0	0	0	0	0	0	0	0	0	0
4	*Calotes versicolor versicolor*	Common Tree Lizard	56	62	71	83	81	89	86	86	86	700
5	*Hemidactylus brookii*	Spotted Barn Gecko	3	20	21	23	30	21	55	55	55	283
6	*Hemidactylus flaviviridis*	Yellow-belly Common House Gecko	11	17	19	23	28	33	39	39	39	248
7	*Hemidactylus persicus*	Persian House Gecko	17	19	22	23	26	27	34	34	34	236
8	*Hemidactylus triedrus*	Blotched House Gecko	11	14	15	17	23	34	44	44	44	246
9	*Hemidactylus turcicus*	Mediterranean House Gecko	21	24	29	32	37	32	30	30	30	205
10	*Acanthodactylus cantoris*	Blue-Tail Sand Lizard	203	197	196	199	200	235	245	245	245	1965
11	*Mesalina watsonana*	Spotted Lacerta	149	159	165	184	197	205	201	201	201	1662
12	*Varanus bengalensis*	Bengal Monitor	17	18	24	21	23	25	37	37	37	239
13	*Platyceps rhodorachis*	Cliff Racer	0	0	1	3	4	3	5	5	5	26
14	*Sphalerosophis diadema diadema*	Blotched Diadem Snake	0	0	3	4	5	7	8	8	8	43
15	*Naja naja*	Black Cobra	0	0	0	0	1	0	7	7	7	22
16	*Echis carinatus*	Saw-scaled Viper	0	0	0	0	3	8	6	6	6	29
17	*Enhydrina schistosa*	Beaked Sea Snake	9	11	9	5	6	5	12	12	12	81
18	*Hydrophis caerulescens*	Blue Green Sea Snake	10	5	7	9	11	15	20	20	20	117
19	*Hydrophis cyanocinctus*	Annulated Sea Snake	11	14	12	4	5	6	9	9	9	79
20	*Hydrophis lapemoides*	Persian Sea Snake	1	1	1	2	1	1	1	1	1	10
21	*Hydrophis mamillaris*	Broad Band Sea Snake	11	9	9	13	15	21	19	19	19	135
22	*Hydrophis ornatus*	Reef Sea Snake	17	15	13	15	17	19	23	23	23	165
23	*Hydrophis spiralis*	Yellow Sea Snake	11	12	15	11	13	15	18	18	18	131
24	*Lapemis curtus*	Pygmy Sea Snake	5	3	5	8	9	13	15	15	15	88

Continued

Continued….

S. No.	Scientific name	Common name	2001	02	03	04	05	06	07	08	09	Total
25	*Microcephalophis cantrois*	Spotted Small Headed Sea Snake	7	9	4	7	9	7	11	11	11	76
26	*Pelamis platurus*	Pelagic Sea Snake	9	11	12	16	17	15	17	17	17	131
27	*Praescutata viperina*	Spotted Viperine Sea Snake	12	15	13	15	17	24	19	19	19	153
	Total		610	656	689	738	797	881	988	982	986	7327

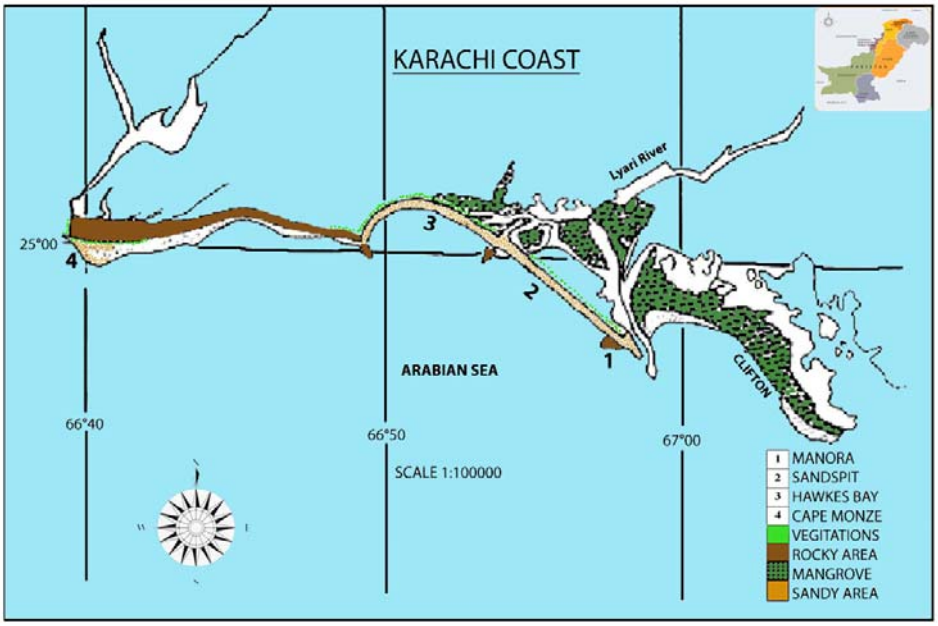

Fig. 2. Study areas of Reptiles on Karachi Coast.

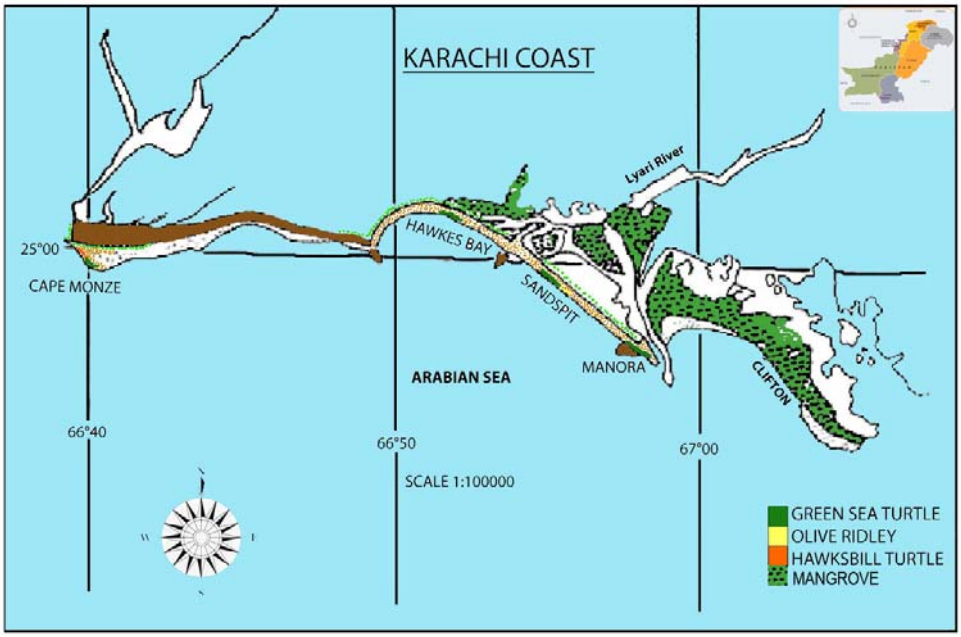

Fig. 3. Distribution of Marine Turtles at Karachi Coast.

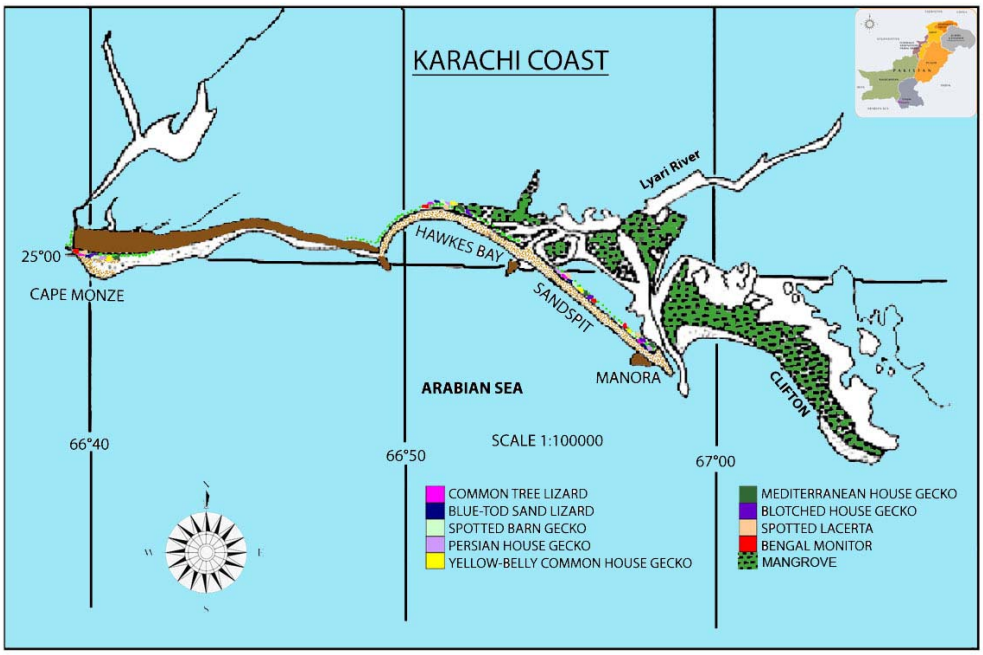

Fig. 4. Distribution of Lizards at Karachi Coast.

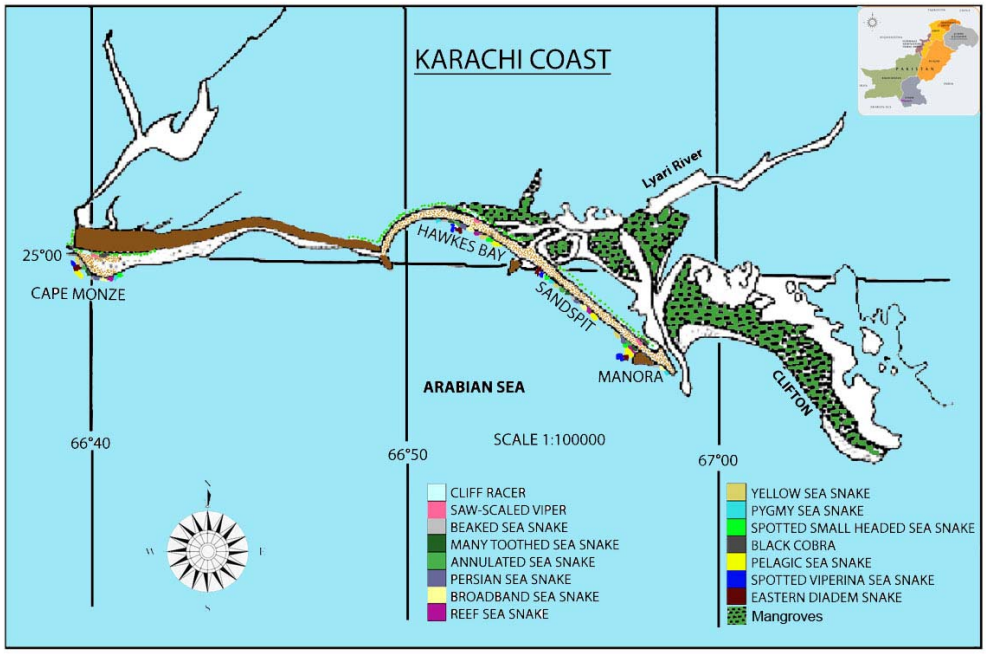

Fig. 5. Distribution of Snakes at Karachi Coast.

REFERENCES

Auffenberg, W., Rahman, H., Iffat, F. and Perveen, Z. 1989. A study of *Varanus flavescens* (Sauria Varanidae). Bombay Nat. Hist. Soc. 86:286-307.

Auffenberg, W. and Rahman, H. 1991. Studies on Pakistan Reptiles. Pt. I. The genus *Echis* (Viperidae). Bull. Florida Mus. Nat. Hist. 35 (5):263-314.

Boulenger, GA. 1890. Fauna of British India, including Ceylon and Burma: Reptile and Batrichia, London.

Firdous, F. 2005. Turtles Conservation and Education in Karachi, Pakistan. pp 1-8. (unpublished report).

Ghalib, SA. and Zaidi, SSH. 1976. Observations on the Survey and Breeding of Marine Turtle on Karachi Coast. Agricultural Pakistan. 27 (1):87-96.

Ghalib, SA., Rahman, H., Iffat, F. and Hasnain, SA. 1981. A Checklist of Reptiles of Pakistan. Rec. Zool. Surv. Pakistan. 8:37-59.

Iffat, F. and Auffenberg, W. 1988. New Reptile Records for Pakistan, *Agama minor*. Sauria. 19:61.

Iffat, F. 2006. On the Lizards of Karachi Coast. Rec. Zool. Surv. Pakistan. 17:37- 40.

Iffat, F. 2009. Marine Turtles. Zoological Survey Department, Govt. of Pakistan, Islamabad. pp. 33.

IUCN. 2004. Sindh State of Environment and Development. IUCN Sindh Program Office. Xxvii + pp. 423.

IUCN. 2009. Extinction Crisis Continues Apace.

Kabraji, AM. and Firdous, F. 1984. Conservation of Turtle. Hawksbay and Sandspit, Pakistan , World Wildlife Fund Project 1451. (unpublished report). WWF International and Sindh Wildlife Management Board. pp. 52.

Khan, MS. 2006. Amphibians and Reptiles of Pakistan. Kriegar Publishing Company, Malabar, Florida. pp. 311.

Khan, MS. and Mirza, MR. 1977. An annotated Checklist and key to the Reptiles of Pakistan Part II: Sauria (Lacertilia). Biologia. 23:41-64.

Khan, MZ. and Nazia, M. 2003. Current Population Status of Diurnal Lizards of Karachi, Pakistan. Russian Journal of Herpetology. 10 (3):207-210.

Khan, MZ., Hussain, B. and Ghalib, SA. 2005. Current Status of the Reptilian Fauna along Karachi Coast with Special Reference to Marine Turtles. J. nat. hist. wildl. 4(2):127-130.

Khan, MZ., Law, FCP., Nelson, J., Walter, L. and Hao-Feng (Howie), Lai. 2009. A Baseline Study to Evaluate the Estrogenic Activities using *In-Vitro* Yeast Estrogenic Screen in the Selected Ramsar Sites and Creek areas. Canadian Journal of Pure and Applied Sciences. 3(1):629-635.

Mertens, R. 1969. Die Amphibian and reptilian, West Pakistan. Stuttgarter Beiter Natur Kunde. 197:1-96.

Minton, SA.1966. A Contribution to the Herpetology of West Pakistan. Bull. Amer. Mus. Nat. Hist. 134:24-184.

Rehman, H. and Iffat, F. 1997. A Revised Checklist of Reptiles of Pakistan. Records Zool. Surv. Pak. 13:1-7.

Rehman, H., Ahmad, SI. and Fakhri, S. 2002. Home Range and Growth Rate of Fringe toad Sand Lizard (*Acanthodactylus cantoris*) at Hawksbay area, Karachi. Rec. Zool. Surv. Pakistan. 14:49-54.

Rehman, H. and Papenfuss, TJ. 2005. An up-to-date Checklist of Reptilian Fauna of Balochistan. J. nat. hist. wildl. 4:131-136.

Van Dijk, PP. and Palasuwan, T. 2000. Conservation Status, Trade and Management of Tortoises and Freshwater Turtles in Thailand. Chelonia Research Monograph. 2.

Received: Oct 2, 2009; Revised: Dec 16, 2009; Accepted: Jan 22, 2010

SENRA Academic Publishers, Burnaby, British Columbia
Vol. 4, No. 1, pp. 1073-1079, 2010
ISSN: 1715-9997

Canadian Journal of pure&applied sciences

SOME STATIC SPHERICAL CLASSICAL SOLUTIONS INCLUDING THE COSMOLOGICAL TERM

Ling Man Tsang
Department of Physics, Trent University, Peterborough, ONT K9J 7B8 Canada

ABSTRACT

The general static spherical potential in the form of $\phi = \frac{A}{r} + \frac{B}{r^2} + \frac{1}{2}kr^2$ is proposed. The first term is the usual Newton's law. The second term refers to the negative field energy of the source which is rather small when comparing with the first term. The last term relates to a spring constant k of the source which acts as a repulsive force against the gravitational one. We point out that the spring effect has a limit distance depending on individual sources. Furthermore, the spring force acting against the gravitational one can be regarded as the fifth force. The spring theory is also applied in short range interaction.

Keywords: Classical electrostatics, general relativity and gravitational fifth force, short range interaction.

INTRODUCTION

When a source is placed in space, its external field is occupied by 2 constituents, namely, the negative energy of the source and tentacles (or springs) attaching to the source. The latter have a range limit, as they will break when being extended to a certain distance. Later in this paper we will investigate the properties of these two constituents. We start with the Yang's pure space equations of (Yang, 1974)

$$R_{\mu\nu}\,;\lambda = R_{\mu\lambda}\,;\nu \quad . \tag{1}$$

We try not to call (1) the vacuum equations. In spite of many unphysical conditions, Pavelle (1974, 1975) pointed out that there exists a possible solution if the cosmological constant $\Lambda \neq 0$ in Einstein's equations, or

$$R_{\mu\nu} - \frac{1}{2} g_{\mu\nu} R + \Lambda g_{\mu\nu} = 0 \quad . \tag{2}$$

In case of spherical static symmetry, the line element is written as

$$ds^2 = e^{\nu(r)} dt^2 - e^{\lambda(r)} dr^2 - r^2 d\theta^2 - r^2 \sin^2\theta \, d\varphi^2 \quad , \tag{3}$$

where $e^{\nu} = e^{-\lambda} = 1 + \frac{2A}{rc^2} + \frac{\Lambda r^2}{3}$ (4)

In case of a non-vacuum exterior solution as we mentioned previously, (2) become

$$R_{\mu\nu} - \frac{1}{2} g_{\mu\nu} R + \Lambda g_{\mu\nu} = T_{\mu\nu} \tag{5}$$

*Corresponding author email: lmtsang05@hotmail.com

and

$$e^{\nu} = e^{-\lambda} = 1 + \frac{2A}{rc^2} + \frac{2B}{r^2c^4} + \frac{\Lambda r^2}{3} \quad , \tag{6}$$

which has the same form as Reisner-Nőrdstrom (Adler, 1975) where A, B, Λ (Λ is replaced by a spring term k) are constants to be determined. In fact, the non-zero cosmological term is nothing new to the physicists (Kottler metric, 1918). However, it cannot be regarded as a universal constant but a spring term relating to different sources.

The potential is $\phi = \frac{A}{r} + \frac{B}{r^2c^2} + \frac{1}{2}kr^2$, (7)

where the second term involves the exterior field of the source.

The following sections will deduce the values of A and B of (7) classically.

ELECTRIC FIELD

The electric field energy density surrounding a charge q is proportional to the square of the field intensity E, or

$$W \propto E^2 \quad . \tag{8}$$

Since a charge is always accompanied by its electromagnetic mass δm,
its mass becomes total rest mass $M =$ mechanical mass + electromagnetic mass

$$\delta m \tag{9}$$

The above two masses on the right side of (9) are non-separable from each other. The surrounding field of this charge possesses a total mass of $-\delta m$ as shown in (13).

Eq (8) can be modified as

$$\nabla \cdot E = 4\pi \rho_e = \alpha E^2 , \tag{10}$$

in which α is a constant to be determined.

Upon integration,

$$E = \frac{A}{r^2}(1+\frac{B}{r})^{-1} , \tag{11}$$

where A, B are the constant of integration.

By setting $A =$ charge q, (8) becomes

$$W = \frac{E^2}{8\pi} = \frac{q^2}{8\pi r^4}(1+\frac{B}{r})^{-2} . \tag{12}$$

The total electric field energy over the whole space is

$$W\ total = \frac{q^2}{2}\int_0^\infty \frac{1}{r^2}(1+\frac{B}{r})^{-2} dr = -\delta m c^2 . \tag{13}$$

We consider the field energy to be negative. Thus,

$$B = \frac{-q^2}{2\delta m c^2} . \tag{14}$$

The field intensity becomes

$$E = \frac{q}{r^2}(1-\frac{q^2}{2\delta m c^2 r})^{-1} . \tag{15}$$

Obviously, for $\delta m \to 0, E \to 0$, indicating that δm always accompanies with the charge. The potential can be written in the form

$$\phi = \frac{q}{r} + \frac{q^3}{4\delta m c^2 r^2} . \tag{16}$$

Bohr's theory of an orbiting electron seems to allow no rooms for the spring term k as well as for the electromagnetic mass δm term. If (13) fails, this section will be totally meaningless. To investigate the property of δm, we compare Newton's law with that of Coulomb's to obtain

$$\delta m = \frac{ie}{(4\pi\varepsilon_0 G)^{\frac{1}{2}}} \tag{18}$$

Thus, the 2nd term of (16) is complex and so a charged particle as described by (9) refers to a composite particle of real and complex parts. The energy-momentum tensor of (5) can be written as

$$T^{\mu\nu} = -\{\frac{\rho + \frac{i\rho_e}{(4\pi\varepsilon_0 G)^{\frac{1}{2}}}}{}\}U^\mu U^\nu \tag{19}$$

where ρ is the mass density and ρ_e is the charge density same as (10). The above (19) can be a good attempt to combine electromagnetic field into general relativity. Moreover, we suspect that the second term of (19) may be related to the dark matter.

GRAVITATIONAL FIELD

Since Newton's law is analogous to that of the Coulombs, (13) in gravitation can be written as, by changing q into $\sqrt{G}$ M for unit purpose (Treder, 1975):

$$\frac{GM^2}{2}\int_0^\infty \frac{1}{r^2}(1+\frac{B}{r})^{-2} d r = -M c^2 , \tag{20}$$

where $-Mc^2$ is the negative energy of the field surrounding the source M. Hence , the result gives

$$B = -\frac{GM}{2c^2} . \tag{21}$$

It is interesting to know that the sum of the source M and its surrounding field –M is zero, showing that our universe is in fact "nothing" when sum up all the real and negative matters! Moreover, M and –M do not attract each other to avoid a true vacuum formed in the exterior of the source.

The gravitational force acting on a particle m becomes

$$\frac{GMm}{r^2} + \frac{G^2M^2m}{2r^3c^2} = ma . \tag{22}$$

A spring force kr needs to be added into (22) eventhough we cannot derive it classically. That is:

field intensity E + or - spring term (kr) = acceleration

.which is different from the traditional concept of field intensity equals acceleration. The plus or minus sign depends on whether the object is falling towards or darting away from the source. It needs to point out that k is not a universal constant but depending on individual sources. To estimate the value of k for the earth, we take the radius of the earth $R = 6.4\times10^6$ m, $a = 9.679$ m/s^2 (see appendix 1) and mass of the earth $M = 6\times10^{24}$ kg. Hence,

$$a = \frac{GM}{r^2} + \frac{G^2M^2}{2r^3c^2} - kr = 9.679 \quad \text{m/s}^2 \tag{23}$$

which yields the value of

$$k \text{ of earth} \sim 10^{-8}/\text{s}^2 \tag{24}$$

Substitute (24) into (23) and set $a = 0$, we obtain r = 10^7 m. Once exceeding this critical distance, only the Newtonian inverse square law remains effective whereas the $G^2M^2/2r^3c^2$ term is too small to be considered. Since the earth-moon distance is 10^8m but the critical distance for the spring is 10^7m. the spring breaks beyond this range and hence, the moon is influenced mainly by the inverse square law .

THE FIFTH FORCE

The fifth force has a potential of the form (Fischbach, 1986, 1992)

$$\phi = \frac{GM}{r}(1 + \alpha e^{-r/\lambda}) \quad , \tag{25}$$

in which

$$\alpha = -(7.2 \pm 3.6) \times 10^{-3} \quad , \quad \lambda = 200 \pm 50 \text{ m}.$$

We find that the distance r is negative where there is no acceleration to any falling object, or a = 0 **.** This is because (25) is only an empirical formula. Moreover, there are still experimental difficulties to detect the true nature of this additional exponential term. Some papers even criticized the existence, that included Thieberger (1987); Cowsik *et al*. (1988); Fitch *et al*. (1988); Adelberger (1988); Bennet (1986); Nelson,Graham and Newman (1990); Stubbs *et al*. (1989); Mannheim (1991) and a more detail one by Franklin (1993). In spite of the difficulties in the experimental search for the fifth force, the theories do exist Kaluza-Klein (1921); Brans-Dicke (1961); Ramanand (1988) and Farrad-Rosen (2007). From (23), the so-called fifth force or the spring force kr in our theory is a repulsive force which is not only effective on earth but also affecting any heavenly object up to the critical distance. The Newtonian inverse square term GM/r^2 of (23) of a planet must be greater than its gravity acceleration in order to obtain a positive k. In the case of Jupiter , GM/r^2 24.79 m/s^2,

$$k \text{ for Jupiter} = 3.2\text{x } 10^{-9}/\text{s}^2 \tag{26}.$$

For other planets , GM/r^2 □a (M = mass of the planet) , which is difficult for us to calculate the value k of these planets (Abell, 1987).

The orbit of a planet

The usual Binet´s equation is of the form

$$\frac{d^2u}{d\varphi^2} + u = \frac{p}{h^2u^2} \quad ,$$

where p is the central force per unit mass. Since there are two additional terms in (23), this Binet's equation should be re-written

$$\frac{d^2u}{d\varphi^2} + u = \frac{GM}{h^2} + \frac{G^2M^2u}{2h^2c^2} - \frac{k}{h^2u^3} \tag{27}$$

To solve for the above (27), we follow the same procedures as in Adler *et al*. (1975) [page 206-209]: rewrite (27) as

$$u'' + bu = H - \frac{k}{h^2u^3} \tag{28}$$

where $H = \frac{GM}{h^2}$ □ $b = 1 - \frac{G^2M^2}{2h^2c^2}$ (28a)

and assume a solution of the form

$$u(\varphi) = u_0(\varphi) + kv(\varphi) + O(k^2) \tag{29}$$

To find $u_0(\varphi)$ and $v(\varphi)$. (29) is substituted into (28),

$$u_0'' + kv'' + bu_0 + kbv = H - \frac{k}{h^2u_0^3} + O(k^2) \tag{29a}$$

Neglecting all terms containing k, we have a simple case of $u_0'' + bu_0 = H$ (29b)

The solution is easily cheeked to be

$$u_0 = \frac{H}{b} + kDCos(\sqrt{b}\varphi + \gamma) \tag{30}$$

where D and γ are arbitrary constants. By an appropriate orientation of the axes we may make γ equal to zero, the familiar equation of an ellipse becomes,

$$u_0 = \frac{H}{b} + kDCos(\sqrt{b}\varphi) \tag{30a}$$

Similarly, equating the first-order k terms in (29a), we obtain

$$v'' + bv = -\frac{1}{h^2u_0^3} \tag{31}$$

Substituting (30a) into (31);

$$v'' + bv = -\frac{b^3}{h^2H^3} + \frac{3b^4kD}{h^2H^4}Cos\sqrt{b}\varphi + O(k^2) \tag{31a}$$

Now v can be the sum $v = v_1 + v_2$, where v_1 and v_2 are solutions of the equations

$$v_1'' + bv_1 = -\frac{b^3}{h^2H^3} \qquad v_2'' + bv_2 = \frac{3b^4kD}{h^2H^4}Cos\sqrt{b}\varphi \tag{31b}$$

whose solutions are

$$v_1 = -\frac{b^2}{h^2 H^3} \quad v_2 = \frac{3b^{\frac{7}{2}} kD}{2h^2 H^4}\varphi Sin\sqrt{b}\varphi \tag{31c}$$

Thus,

$$v = v_1 + v_2 = -\frac{b^2}{h^2 H^3} + \frac{3b^{\frac{7}{2}} kD}{2h^2 H^4}\varphi Sin\sqrt{b}\varphi \tag{32}$$

and we get

$$kv = -\frac{kb^2}{h^2 H^3} + O(k^2) \tag{32a}$$

Combining this with (30a), the entire solution for the orbit to first order in k appears as

$$u = u_0 + kv = \frac{\mathrm{H}}{b} + kDCos\sqrt{b}\varphi - \frac{kb^2}{h^2 H^3} \tag{32b}$$

Substituting H and b of (28a) into (32b) to obtain

$$u = \frac{GM}{h^2(1-\frac{G^2M^2}{2h^2c^2})} + kDCos\sqrt{1-\frac{G^2M^2}{2h^2c^2}}\varphi - \frac{k(1-\frac{G^2M^2}{2h^2c^2})^2 h^4}{G^3M^3} \tag{33}$$

The perihelion shift is given by

$$\delta\varphi = 2\pi(1+\frac{\mathrm{G}^2\mathrm{M}^2}{4h^2c^2}) \tag{34}$$

The spring constant does not appear in (34) but it affects the radial distance. The second term on the right-hand side of (27) affects both the perihelion shift as well as the radial periodic variations. Unfortunately, the latter is very hard to be observed. To estimate the value of the sun's k, we consider the cosine term in (33) be zero and set the following table 1 (Roman, 1989):

Table 1. Mass M for sun□2×10^{30}kg, h □$2\pi r^2/T$

	Mercury	Venus	Earth	Mars	Jupiter
Distance r (10^9 m)	58	108	149	224.9	778.34
Period T(days)	89	224.7	365.25	686.98	4332.59
k of sun (sec^{-2})	10^{-16}	10^{-16}	10^{-16}	10^{-16}	10^{-19}
	Saturn	Uranus	Neptune	Pluto	
Distance r (10^9 m)	1427	2869.6	4496.67	5900.2	
Period T(days)	10759.2	30684.9	60190.3	90470	
k of sun (sec^{-2})	10^{-21}	10^{-21}	10^{-21}	10^{-20}	

The sun's k □10^{-16} sec^{-2} to $10^{-21}sec^{-2}$. (35)

Discrepancies appearing in (35) are expected. One reason is that the spring loses its elasticity at very large distances. Moreover,(33) is not an accurate solution of (27). Taking the value 10^{-21} sec^{-2}, $a = 0$, the sun's spring effective range can be obtained from (23) ;

$r = 10^{13}$ m (36)

The bending of light under the sun's gravitational field

Let the sun's location at x□y□0. Light path is traveling from .x□+∞ to x□−∞. The closest distance from the sun is at x□0, y = r_o and r is the distance between the light and the sun. The deflection δ is the angle between the light path and the horizontal line y = r_0, Light path should be described as the motion of an ordinary particle and hence the v_1 and v_o denote different light speeds. The work done by a photon can be calculated in this way:

$$dW = f \cdot dr = ma \cdot dr = m\frac{dv}{dt} \cdot dr = mv \cdot dv$$

$$W = \int_{r_0}^{r_1} dW = \int_{r_0}^{r_1} mv \cdot dv = \frac{1}{2}mv_1^{\,2} - \frac{1}{2}mv_0^{\,2} = \Delta E$$

We select only the first and third terms of (23),

$$W = \int_{\infty}^{r_0} Fdr = \int_{\infty}^{r_0} (\frac{GMm}{r^2} - mkr)dr$$

As $r \to \infty,\ k = 0$, we get the potential

$$\phi = -\frac{GM}{r_0} - \frac{1}{2}kr_0^{\,2} \tag{37}$$

The change of kinetic energy per unit mass is

$$\Delta E = \frac{1}{2}c^2 - \frac{1}{2}v_1^{\,2} \tag{38}$$

To estimate the approximate value of v_1, we ignore the spring term in (37) and compare with Newton's result of $\delta = -\frac{GM}{c^2 r_0}$ to obtain, from (38)

$$v_1 = c(1-2\delta)^{1/2}$$

which seems to be reasonable but we need to point out that the speed of light in (38) is not c since there is no vacuum due to the second term of (23) [see appendix 2]. With the presence of a spring term,

$$\delta = \frac{GM}{c^2 r_0} + \frac{kr_0^{\,2}}{2c^2} \tag{39}$$

The first term is only half the result of general relativity as expected but there is an additional term containing the spring .The total deflection of the light ray or the angle between the asymptotes is

$$\Delta = 2\delta = \frac{2GM}{r_0 c^2} + \frac{kr_0^2}{c^2}$$

Using the results of (36), once light is so far away such that at $r = 10^{13}$ m, the spring breaks but light continues to bend due to Newton's effect only.

Spring theory in short range interaction

The basic assumption of Spring theory is that when a source is placed in space, its external field is occupied by 2 constituents, namely, the negative energy of the source and tentacles (or springs) attaching to the source. The latter have a range limit, as they will break once being extended to a certain distance. The external field of negative energy is governed by (20)

$$\frac{GM^2}{2}\int_0^{\infty}\frac{1}{r^2}\left(1+\frac{B}{r}\right)^{-2} dr = -Mc^2 \tag{20}$$

DISCUSSION

Treder (1975) pointed out that once the mass M is reduced to $M = (hc/G)^{1/2} = 10^{-8}$ kg, gravitation will be converted into a short range strong interaction. In this case, the Newton format on the left side of (20) can be converted into the quantum format, i.e. convert GM^2 into hc.

In the case of short range, integration takes place from zero to λ inside a small domain instead of from zero to ∞.

The right side of (20) can be written as $Mc^2 = hc/\lambda$. The negative sign disappears since interaction takes place inside the domain of range λ, but not the external field of the source

Axiom:

"If the mass of each of the two interacting particles is less than 10^{-8} kg, Newton's inverse square law GMm/r^2 should be replaced by the quantum gravity format of hc/λ^2, where M, m each is less than 10^{-8} kg and λ is a short range".

Eq(20) can now be re-written as

$$\frac{hc}{2}\int_0^{\lambda}\frac{1}{r^2}\left(1+\frac{B}{r}\right)^{-2} dr = hc/\lambda \tag{40}$$

and upon integration, the constant $B = 0.366\lambda$.

As previously mentioned, the acceleration of a falling object under the influence of both the field intensity plus the spring force of the source is in the form of

$$\frac{GM}{r^2}\left(1+\frac{B}{r}\right)^{-1} - kr = \text{acceleration} \tag{41}$$

where k is the spring constant of the source, for instance, the proton. However, in short range, there is no acceleration as the interacting particles are confined in a small domain. Using the obtained value of $B = 0.366\lambda$, the above equation can be reduced to

$$k = \frac{\sqrt{hcG}}{1.366\lambda^3}\sec^{-2}$$

Since

total energy = potential energy + (strain energy of the spring $\frac{1}{2}Mkr^2$),

with the help of (41)

total energy

$$= \frac{hc}{0.366\lambda}\ln\left(1+\frac{B}{\lambda}\right) + \frac{1}{2}\sqrt{\frac{hc}{G}}\frac{\sqrt{hcG}}{1.366\lambda^3}\lambda^2 \tag{42}$$

The above yields the total energy stored inside the domain = 1.3 GeV for a short range of, say, 1.1 fm.

The second term of (42) represents the harmonic oscillating energy of a meson which equals $m_\pi c^2$. Therefore, the energy of the Yukawa π meson is found to be 370 MeV using λ = 1.1 fm.

Appendix 1

.Eq(23) can also be modified as (Amots, 2007)

$$\frac{GMm}{r^2}+\frac{G^2M^2m}{2r^3c^2}-krm=\frac{d\left(mc^2\right)}{dr}. \quad (43)$$

The following equation will explain the gravitational red-shift:

$$\frac{d\left(mc^2\right)}{dr}=\frac{h\cdot d\nu}{dr}. \quad (44)$$

The Jefferson Physical Laboratory at Harvard used a ^{57}Fe source being placed at a height of 22.6m above the detector. Gamma photons dropped to the detector. The original purpose was to demonstrate the Mőssbauer effect (see the famous Pound -Rebka experiment).The data were

ΔE □the energy gain 3.5×10^{-11}eV

Δr □height dropped 22.6m

E □the source energy 14.4keV

Hence,

$$\frac{c^2\Delta E}{E\Delta r}=9.679 \text{ m/s}^2$$

Appendix 2

Using the same experiment as in appendix 1, we re-calculate the earth's gravity based on the condition that light speed varies along the gravity distance. In fact, some physicists suggested that mass of a photon is non-zero and light speed may not be constant everywhere. They included Jackson (1987,1999); Goldhaber (1971); Ugarov (1979) and Kan (2008). Based on their proposals, like any other particles, a falling photon changes its frequency and velocity in the form of

$$h\nu_0\ (1-v^2/c^2)^{-1/2}=h\nu, \quad (45)$$

and the acceleration

$$a = v\ dv/dr \quad (46)$$

Solving the above two equations, we obtain

$$a = (c^2/2\Delta r)\ [\nu_0^2/\nu^2-1] \quad (47)$$

where $\nu-\nu_0$ = change of frequency after the drop as given in appendix 1. The maximum speed of light is $c = 3 \times 10^8$ m. The rest mass of a photon cannot be zero, indicating ν_0 is non-zero. Furthermore, no photon can reach its maximum speed c. Hence, using the experimental data from appendix 1 and substitute into(47),we obtain

$a = 9.679$ m/s^2

the same result as in appendix 1.

CONCLUSION

We admit that it is difficult to calculate the exact value of the spring term for each source, especially the sun. By comparing (24), (26) and (35), we discover that the larger the mass, the lesser the value of k .The cosmological spring term as abandoned must be extremely small (Weinberg, 1987): 10^{-35} sec^{-2}, or 10^{-47}GeV^4, or 10^{-26} kg/m^3 (Tegmark, 2004). This also explains why the spring inside the quark confinement is so strong. We have no intention to abandon relativity but to suggest that this cosmological (or spring) term needs to be restored. Eq (19) is an attempt to combine electromagnetism into general relativity by splitting the energy-momentum tensors of a charged particle into a real plus a complex part. The most striking result is that the effective range of the earth's spring is 10^7m whereas the earth-moon distance is 10^8m. A gravity-free spherical surface is predicted which allows artificial satellites orbiting economically around the earth.

REFERENCES

Abell, GO. 1987. Exploration of the Universe, CBS College Publ. (5th ed.). p. 732.

Adelberger, EG. and Stubbs, CW. 1988. Comments on "a new approach to the question of the fifth force". Phys. Lett. A.132:91-92.

Adler, R., Bazin, M. and Schiffer, M. 1975. Introduction to general relativity. Mcgraw Hill (2nd ed.). pp. 485.

Amots, NB. 2007. Relativistic exponential gravitation and exponential potential of electric charge. Found. Phys. 37:773-787.

Bennet, WR. 1986. Modulated source Eötvös experiments at Little Goose Lock. Phys. Rev. Lett. 62:365-368.

Cowsik, RN., Krishman, SN., Tandor et al. 1988. Limit on the strength of intermediate range force coupling to isospin. Phys. Rev. Lett. 61:2179-2181.

Farrar, G. and Rosen, R. 2007. A new force in the dark sector. Phys. Rev. Lett. 98:171302.

Fiscbach, E., Sudarsky, D., Szafer, A., Talmadge, C. and Aronson, SH. 1986. Reanalysis of the Eötvös experiment. Phys. Rev. Lett. 56:3-6.

Fischbach, E. and Talmadge, C. 1992. Six years of the fifth force, Nature. 356: 207-215.

Fitch, VL., Isaila, MV. and Palmer, MA. 1988. Limits on thre existence of a material dependent intermediate range force. Phys. Rev. Lett. 60:1801-1804.

Franklin, A. 1993.The Rise and Fall of the Fifth Force: Discovery, Pursuit and Justification in Modern Physics, American Institute of Physics.

Goldhaber, AS. and Neto, MM. 1971. Terrestrial and extra-terrestrial limits on the photon mass. Rev. Mod. Phys. 43:277-296.

Jackson, JD. 1999. Classical electrodynamics. John-Wiley & Sons. 600-602.

Jackson, JD. 1987. The impact of special relativity on theoretical physics. Phys. Today. 40:34-42.

Kan, XM. 2008. Photon mass and the lower limit of the velocity of light. Journal of South China Normal University.1:67-70.

Mannheim, P. 1991. General relativity and the fifth force experiment. Astrophys. and Space. Sci.181:55-59.

Nelson, PG., Graham, DM. and Newman. 1990. Search for an intermediate range composition dependent force. Phys. Rev. D. 42:963-976.

Pavelle, R. 1975. Unphysical solutions of Yang's gravitation field Equations. Phys. Rev. Lett. 34:1114.

Pavelle, R. 1974. Yang's gravitational field equations. Phys. Rev. Lett. 33:1461-1463.

Ramanand, Jha. and Sinha, KP. 1988. A possible model for fifth force. Pramana J. Physics (India). 31:93-97.

Ronan, C. 1989. Amateur Astronomy. Hamlyn Publ., England, (4^{th} ed.). pp. 28.

Stubbs, CW., Adelberger, EG. and Heckel, B. 1989. Limits on Composition dependent interactions using; laboratory source: Is there a fifth force? Phys. Rev. Lett. 62:609-612.

Tegmark, M., Strauss. *et al*. 2004. Cosmological parameters from SDSS and WMAP. Phys. Rev. D69:103501.

Thieberger, P. 1987. Search for a substance dependent force with a new differential accelerometer. Phys. Rev. Lett. 58:1066-1069.

Treder, von H J. 1975. Wann kann die Gravitation zu einer starken Wechselwirkung werden? Annnalen der Physik.7 Folge, Band. 32, Heft 3:238-240.

Ugarov, VA. 1979. Special theory of relativity. Moscow Mir Publ. 38-41.

Weinberg, S. 1987. Anthropic bound on the cosmological constant. Phys. Rev. Lett. 59:2607-2610.

Yang, CN. 1974. Integral formalism for the gauge fields. Phys. Rev. Lett. 33:445-447.

Received: Dec 4, 2009; Revised: Dec 29, 2009; Accepted: Dec 30, 2009.

SENRA Academic Publishers, Burnaby, British Columbia
Vol. 4, No. 1, pp. 1081-1085, 2010
ISSN: 1715-9997

Canadian Journal of pure&applied sciences

ABLATIVE LASER DEPTH-PROFILING (ICP-MS) OF RESERVOIR CORES TO EVALUATE HOMOGENEITY OF STRONTIUM AND BARIUM DISTRIBUTIONS LINKED TO SCALE DEPOSITION – PART 1

*****AE Pillay[1], B Ghosh[2], B Senthilmurugan[2], S Stephen[1] and A Abd-Elhameed[1]
[1] Department of Chemistry, [2] Department of Petroleum Engineering,
The Petroleum Institute, PO Box 2533, Abu Dhabi, UAE

ABSTRACT

The thrust of this work demonstrates the unique capability of laser depth-profiling to 'peer' within reservoir cores and reveal anomalies and irregularities associated with sulphate scale deposition. The intrinsic behavior of scale deposition within the pore space of near wellbore formation rock is relatively unexplored, and the essence of this paper concerns the application of an ablative laser technique to study the uniformity of strontium and barium distributions in suitable oil producing reservoir core sections. Information on the spatial and depth distributions of these metal components in side-well core slivers could provide an insight into the location of relevant scale deposits, particularly barium and strontium sulphates. Nucleation and growth on the surface could indicate potentially favorable conditions for precipitation. On the other hand, sporadic ingrained deposits would signal abrupt changes in compositional or physical conditions within the specimen. The investigation was divided into two parts: (i) continuous 'drilling' by the laser at random points to uncover metal distribution at successive depths; and (ii) iterative surface scans at randomly selected areas to evaluate compositional consistency. The laser was attached to a high resolution ICP-MS instrument, and irradiations were conducted with a 213-nm beam of 30% total energy and 100 µm diameter. Following iterative surface scanning, the laser ablated a total depth of 50µm at 10µm-intervals at each point. The study was largely semi-quantitative in the absence of standardization. Characteristic intensities originating from the metals of interest were measured. The experimental results showed distinct inhomogeneity in the distribution of Sr and Ba – declining sharply to negligible levels in some cases, and occurring sporadically at specific depths. Some data revealed that these deposits were markedly absent from some points in the core fragments, distinctly suggesting that specific conditions in the rock matrix are necessary to influence scale formation. The exact mechanism for this irregular behavior is not clear at this stage, and has considerable scope for extended research, including modeling studies. This work is of definite interest to geophysicists and petroleum scientists.

Keywords: Strontium, barium, scale-formation, laser ablation, ICP-MS.

INTRODUCTION

Barium and strontium sulphate scale deposition is a common problem in hydrocarbon producing wells/reservoirs. Seawater (relatively abundant in sulphates) is injected into these reservoirs for pressure maintenance, and co-mingles with formation brines that contain appreciable levels of barium and strontium. Scale formation near wellbore locations is accelerated because of significant and favorable changes of pressure and temperature at these locations (Bamidele *et al*., 2009; Jamailahmadi and Muller-Steinhagen, 2008; Merdah and Yassin, 2007; Ohen *et al*., 2004; Shen and Crosby, 1983; Vetter *et al*., 1982). Progressive and undesirable congestion by scale deposits tend to reduce the production of oil and gas. The distribution of these deposits in the pore space and pore throats of reservoir rock could provide valuable clues to the mechanism of scale formation and the conditions that exist (Ohen *et al*., 2004). Our group has developed an ultrasensitive technique for assessing the distribution of minor metals in reservoir rock samples (that are linked to scale deposits); and pinpointing areas on the surfaces of such rock cores to study spatial dispersion of these metals. Laser ablation depth-profiling (ICP-MS) has the capability of 'drilling' through a core-plug and obtaining relevant information on the distribution of scale deposits. The laser itself is linked to a high-performance ICP-MS instrument. The technique is semi-quantitative and capable of high-resolution detection over a wide range of elemental levels (Jamailahmadi and Muller-Steinhagen, 2008; Jarvis *et al*., 1992; Ohen *et al*., 2004; Robinson *et al*., 2005; Skelley-Frame *et al*., 1998; Ward, 2000). Very few contemporary instrumental methods have the capability to study metal intensity with depth. X-ray methods are useful, but lack the ability to control depth penetration. Nuclear particle irradiation, SEM, SIMS and XPS are equally useful, but such techniques tend to be limited to only a few microns below the surface (Robinson *et al*., 2005). The competence, therefore, of the laser approach to delve to discreet depths below the surface of a sample is attractive for homogeneity studies in bulk materials.

*Corresponding author email: apillay@pi.ac.ae

The aim of this work was to explore the potential of ablative laser technology to rapidly track the profiles of barium and strontium in side-well core sections to examine the uniformity of (sulphate) deposits linked to these elements.

MATERIALS AND METHODS

Instrumentation / Sample handling

Laser ablation technology (coupled to ICP-MS) uses a micro-beam to ablate samples in a special sample chamber (Fig. 1) (Li and Anderson, 2006; Robinson *et al*., 2005; Skelley-Frame *et al*., 1998). The fine ablated material is transported to a hot plasma where it is atomized and converted to ions (characteristic of the elements of the sample), which are subsequently carried to a mass spectrometer for detection. The technique is highly sensitive and can attain a limit of detection of 10^{-6}mg/kg (parts per trillion) for most elements (Skelley-Frame *et al*., 1998; Ward, 2000). Laser ablation technology is capable of depth and surface analysis, displays the elemental intensities in proportion to their levels, and produces an elemental profile.

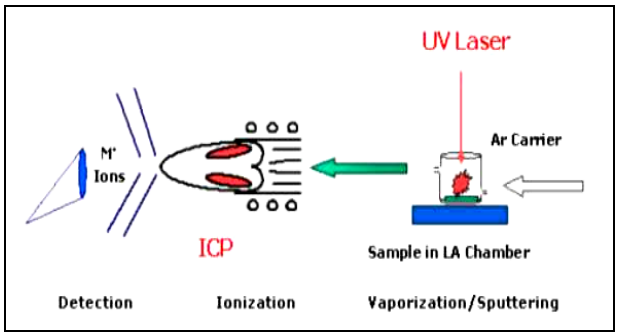

Fig. 1. A schematic of the laser ablation (LA) technique (taken from reference Li and Anderson, 2006).

A side-well core plug (from side-wall coring) containing embedded scale deposits, and collected from a limestone reservoir in the Arabian Gulf region, was slivered with a diamond cutter to produce sections and fragments that were adequate for irradiation (Fig. 2). Specimens were suitably labeled and random points on the top and bottom surfaces were examined with the laser. No serious sample treatment was necessary prior to irradiation. Samples were investigated with a Perkin Elmer SCIEX DRC-e ICP-MS fitted with a New Wave UP-213 laser ablation system. The core-sections were placed in a special sample holder with dimensions 5cm x 5cm. Samples were subjected to 213-nm laser irradiation; the level of the beam energy was 30%, with a beam diameter of 100µm. The laser gas flow was 0.80 L/min. It was programmed to continuously ablate successive depths of 10µm at each point and 'drilled' through the sample to a depth of 50µm. Depth-profiling spectra were recorded for each measurement.

Fig. 2. Cross-sections of core plugs used in this investigation.

Spectral analysis

Characteristic intensities originating from the metals of interest were measured; and valid considerations were given to potential interferences and matrix effects. Prior to each run, the instrument underwent appropriate calibration and correction for background (Robinson *et al*., 2005; Jarvis *et al*., 1992). The study was largely semi-quantitative in the absence of standardization, and for the purposes of comparison, all measurements were conducted under identical experimental conditions. Signal intensities were compared with surface metals and those occurring in the bulk of the sample; and appropriate spectra were produced to observe fluctuations in characteristic metal intensity spatially and with penetration depth. Spatial studies can reveal irregularities by measuring the elemental composition at different points on the surface. Depth profiling has the potential of providing information on the homogeneity of distributions below the surface. Thus detailed analysis of different spots on the sample could provide a valuable insight into the mechanism of scale formation (Ohen *et al*., 2004).

Validation of the technique

Solid standards of matching matrix are generally not available, and the only recourse to validating the analytical performance of the laser technique was to examine an available certified standard, which in our case was a glass bead (NIST, Certificate 613). Repeatability studies with the laser could be affected by accumulation of debris in the crater formed by the laser. This effect is not particularly marked, but its extent has not been established and wider studies are needed to determine exactly how pronounced it is. In addition, imperfect beam spots due to slight perturbations in focusing could lead to significant scatter in the results (Robinson *et al*., 2005). We originally examined the typical analytical performance of the instrument for different isotopes by

Table 1. Typical analytical performance of the ICP-MS as shown by reproducibility measurements (counts/sec) in a NIST 613 glass standard.

Measurement	^{59}Co	^{85}Rb	^{88}Sr	^{138}Ba	^{140}Ce	^{238}U
1	503	718	3688	1618	1023	1805
2	511	736	3672	1624	1141	1814
3	491	735	3587	1620	1036	1792
Mean + RSD	502 ± 1.6%	730 ± 1.1%	3649 ± 1.2%	1621 ± 0.15%	1067 ± 4.95%	1804 ± 0.50%

taking replicate measurements (n = 3) for equivalent counting times at random points on the glass standard. Relative standard deviations of less than 5% were attained (Table 1) indicating that the characteristic performance of the facility was acceptable.

RESULTS AND DISCUSSION

Depth profiling

Laser depth-penetration studies of several core-fragments (core-sections) were undertaken, and typical depth-profiling plots to illustrate the salient features of the investigation appear in figures 3-6. Typical Ba spectra of a suitable fragment appear in figure 3. Each spectrum represents a random point on the same core-section. The laser 'drilled' from the surface into the core. Clearly, the general trend shows that in each spectrum a similar pattern emerges where strong barium peaks occur roughly at a depth of 10μm followed by no deposits up to a depth of about 40μm; and then between 40 and 50μm, deposits are again present. This formation is irregular and could be attributed to general conditions within the core matrix and pore distribution pattern. The data seem to suggest that suitable conditions prevail at certain points (possibly pore spaces) to induce Ba precipitation. This indicates that at significant locations in the interior of the core-section conditions for formation of Ba deposits appear favorable; supporting the view that sporadic distribution of pore spaces could be largely responsible for this. Obviously, such scale formation is invariably linked to chemical composition and temperature oscillations (Bamidele *et al*., 2009; Shen and Crosby, 1983; Vetter *et al*., 1982), and clearly precipitation will occur if conditions support a shift in chemical equilibrium towards solid formation - which seems to be prevalent at particular sites in the core-section.

In the case of Sr, typical depth-profiling spectra of the same core fragment (Fig. 4) clearly show that Sr deposits tend to be more prolific (than Ba), when compared to the barium plot in figure 3. Here again, each spectrum represents a random point on the core-section. The experimental results (Fig. 4) indicate that Sr scales precipitate intermittently, and such formations tend to fade and re-occur at different points in the interior. The experimental data suggest that favorable conditions are replicated at different depths within the core. This finding is interesting from the perspective that if particular conditions of temperature and concentrations fluctuate randomly, the conditions at the low points in the spectra could possibly be mimicked to minimize Sr scale deposition (Bamidele *et al*., 2009). Undoubtedly, replication of the conditions linked to the gaps in the spectra in figure 4 would represent circumstances where Sr deposits are reluctant to form. If the physical (and possibly chemical) conditions of the low points in the spectra could be simulated on a lab-scale, a deeper insight into inhibiting Sr scale formation could be gained (Ohen *et al*., 2004; Shen and Crosby, 1983; Vetter *et al*., 1982).

Deposition trends

It was of interest to know how the elemental profiles would change with the examination of different core fragments. Laser study of another fragment (Fig. 5) delineated a trend which tends to corroborate the view that particular conditions exist intermittently in the core that favor Ba scale formation. The data in the spectrum support the view that circumstances at specific locations induce Ba scale deposition. Inspection of figure 5 shows that Ba is prominent initially in the first 10μm, then fades and re-appears around a depth of 40μm. This trend could provide clues to establish the mechanism of Ba scale formation in reservoir rock. The results imply that certain physical conditions, such as temperature (Bamidele *et al*., 2009), within the core could be favorable for preventing deposition of Ba scales. This is evident from the gaps in the spectrum (which resemble the gaps in figure 3). An extended study would be to simulate these conditions by flooding virgin cores in a lab study with scale-forming solutions to examine deposition trends.

As regards Sr, the experimental evidence indicates that conditions for scale-formation in the core samples are more favorable than those for Ba, but are irregular and tend to vary. Figure 6 represents laser penetration of a third core fragment, at two randomly selected points (shown in the figure as two independent spectra). The intensities of the Sr peaks in the first 10 μm of the depth-profiling spectra (Fig. 6) are not as pronounced as we progress with depth. The trends in both spectra are somewhat consistent (but differ from those in Fig. 4), suggesting that Sr deposits fluctuate in accordance with

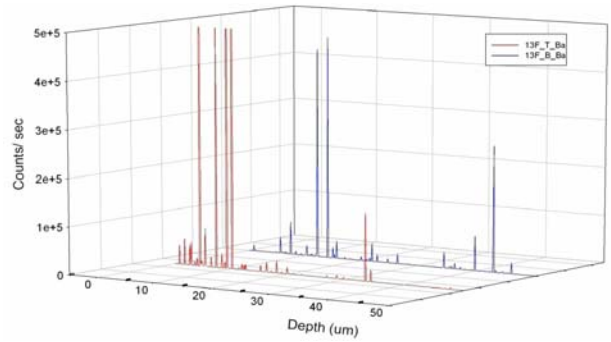

Fig. 3. Depth-profiling plots of Ba (core-fragment #1). Each spectrum represents a random point.

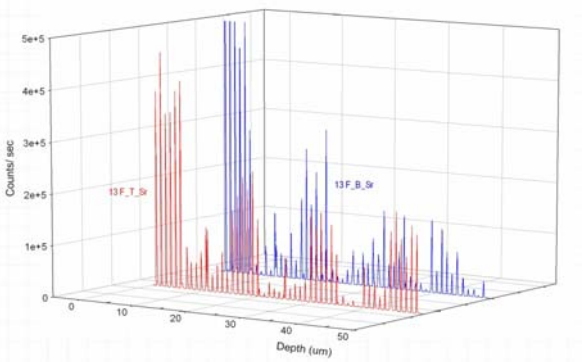

Fig. 4. Depth-profiling plots of Sr (core-fragment #1). Each spectrum represents a random point.

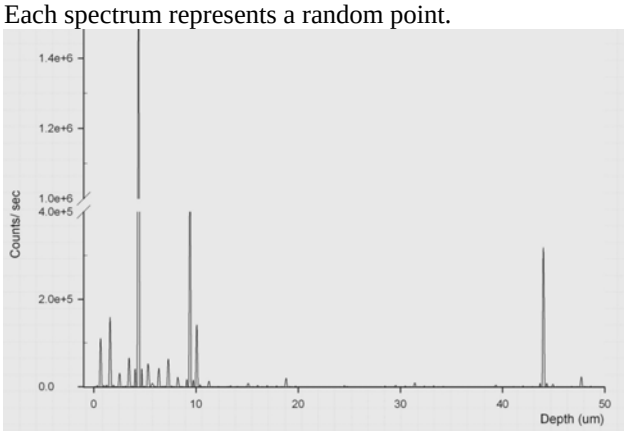

Fig. 5. Interior profile of Ba (core-fragment #2).

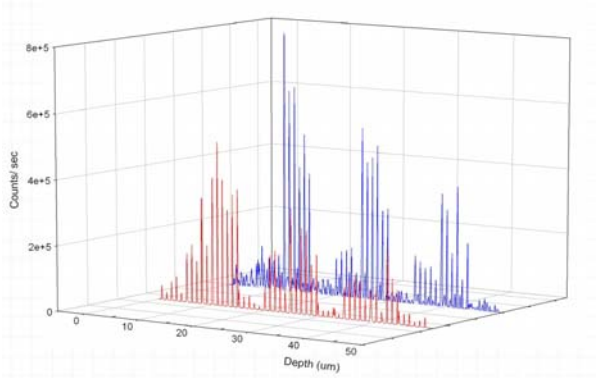

Fig. 6. Interior profile of Sr (core-fragment #3).

circumstances in the core. Unlike Ba, no big gaps appear in the Sr spectra, which proclaim that conditions for Ba and Sr scale deposition differ (as expected). It should be underscored that oscillating conditions in the interior of reservoir rocks are linked to fluctuations in compositional and temperature conditions, which in turn could be affected by permeability, mineral composition and fractures within the matrix structure. Our research represents an indirect method of gaining some insight into changes in physical conditions within the core. These are evident from the abrupt changes in the spectra.

Impact of our findings

The data in figures 3-6 delineate significant 'gaps' in the spectra which suggest that at these points Ba and Sr deposits were absent. Clearly, these gaps further purport that the conditions for Ba/Sr scale formations at such points in the specimen were not favorable and that either (or both) the concentrations of the scale-forming ions were not adequately elevated to exceed the solubility product (and thus precipitate) or the temperature at these points were not conducive to scale formation (Bamidele *et al*., 2009). Clearly two of the most significant factors that would encourage deposition are favorable compositional and temperature conditions; and as stated above these factors are linked to features of the core itself. For example, the dramatic appearance of peaks following a lengthy hiatus in some of the Ba depth-profiling spectra in figures 3 and 5 proclaim that either the laser struck a random crystal of barium, or conditions abruptly changed in the pore spaces and were suddenly favorable for deposition to occur. This further suggests that the interior of the core is possibly prone to sudden cooling and heating (Vetter *et al*., 1982). What brings about these perturbations in temperature is not clear, but it is feasible that voids or the intrinsic characteristic of minerals in the core itself could contribute to such perturbations (Vetter *et al*., 1982). On the other hand, 'bottlenecks' inside the core could affect permeability and create the opportunity for scale-forming ions to 'conglomerate' thus exceeding their solubility properties. Based on this study a robust invasive treatment of core plugs could be devised to unblock the pore spaces, and the samples re-examined with the laser.

Our observations revealed that the frequency of gaps in the Ba spectra are more pronounced than in the Sr spectra, indicating that strontium salts are more 'prone' to scale-formation, which would partially account for the more 'prolific' nature of the Sr spectra. A point to note is that the bulk of the core is comprised of calcite as the matrix material with 'voidages' or pore spaces dispersed sporadically (Ohen *et al*., 2004). Ostensibly, the gaps in the Ba spectra (Figs. 3 and 5) suggest that most of the Ba

precipitation occurred in these sporadic pore spaces – whose dimensions seem difficult to quantify from the spectra themselves - whereas deposition of Sr occurred along with the bulk material (calcite). This observation purports that strontium deposition could be linked to a primary deposition process together with the bulk calcite, whilst Ba deposition is related to a secondary process, largely influenced by conditions in the pore throats and composition of the fluid flow through the porous media. It is also possible that Sr compounds being less bulky than equivalent Ba salts have the advantage of leaching through the calcite matrix - deduced by the abundance of peaks in the Sr spectra (Figs. 4 and 6). Ba deposits, on the other hand, tend to be ensconced in the pore space and less prone to leaching. Accumulated data could be useful for modeling studies (Ohen *et al*., 2004).

CONCLUSIONS

High resolution laser technology has the capability of delineating surface and depth distributions of Ba and Sr in core matrices. It appears that such distributions would depend on several variables such as temperature and chemical concentrations; as well as features such as permeability and mineral composition of the cores. It is not clear at this stage whether these distributions could be treated mathematically and modeled. In the case of all distributions we observed varying trends, indicating that applying modeling statistics to these distributions would be complex. In some cases depth-distributions revealed lack of Ba and Sr scale, whereas in other cases the opposite was observed. It would definitely be useful to implement laser technology more widely for modeling purposes and this particular aspect could be a suitable extension to our study.

ACKNOWLEDGEMENTS

The authors would like to thank the Petroleum Institute for financial assistance.

REFERENCES

Bamidele, OA., Falode, OA. and Omole, O. 2009. Effects of oilfield scale deposition in oil production from horizontal wells. Petroleum and Coal. 51: 91-99.

Jamailahmadi, M. and Muller-Steinhagen, H. 2008. Mechanisms of scale depositions and scale removal in porous media. International Journal of Oil. Gas and Coal Technology. 1:81-108.

Jarvis, KE., Gray, AL. and Houk, RS. 1992. Handbook of ICP-MS, Blackie Publishers, London. UK.

Li, F. and Anderson, S. 2006. An alternate dopant-measurement method for analyzing ULE implant. Solid State Technology. 49:20-24.

Merdah, A. and Yassin, A. 2007. Study of $BaSO_4$ scale formation in oil reservoirs. Journal of Applied Sciences. 21:3198-3207.

Ohen, HA., Williams, LE. Lynn, JD. and Ali, L. 2004. Assessment and diagnosis of inorganic scaling potential using near-infrared technology for effective treatment. SPE Production and Facilities. 19:245-252.

Robinson, JW., Skelly-Frame, EM. and Frame, GM. 2005. Undergraduate Instrumental Analysis, Marcel Dekker, New York, USA.

Shen, J. and Crosby, CC. 1983. Insight into strontium and calcium sulfate scaling mechanisms in a wet producer. J. Petroleum Technology. 35:1249-1255.

Skelley-Frame, EM. and Uzgiris, EE.1998. The determination of gadolinium in biological samples by ICP-AES and ICP-MS in evaluation of the action of MRI agents. Analyst. 123:675-679.

Vetter, JO., Kandarpa, V. and Harouaka, A. 1982. Prediction of scale problems due to injection of incompatible waters. Journal of Petroleum Technology. 33:273 -284.

Ward, NJ. 2000. Environmental Analytical Chemistry, Blackwell Science, Oxford, UK.

Received: August 21, 2009; Accepted: December 17, 2009

SENRA Academic Publishers, Burnaby, British Columbia
Vol. 4, No. 1, pp. 1087-1093, 2010
ISSN: 1715-9997

Canadian Journal of pure&applied sciences

PREPARATION AND CHARACTERIZATIONS OF BARIUM HYDROXYAPATITE AS ION EXCHANGER

Adli A Hanna[1], *Marwa A Sherief[1], Reham MM. Aboelenin[2] and Sahar MA Mousa
[1]Department of Inorganic Chemistry, National Research Centre, Dokki, Cairo
[2]Department of Physical Chemistry, National Research Centre, Dokki, Cairo, Egypt

ABSTRACT

The aim of this study was preparation and characterization of barium hydroxyapatite, $Ba_{10}(PO_4)_6(OH)_2$, BHP, to be used as ion exchanger for removal of some toxic cations from their aqueous solutions. The starting materials were barium hydroxide and phosphoric acid. The effects of the ratio between phosphoric acid and barium hydroxide on the produced hydroxyapatite were studied. X-ray diffraction, IR spectra, Transition electron microscope, and surface area were used for characterization of the produced barium hydroxyapatite. The x-ray patterns indicated the formation of the crystalline barium hydroxyapatite by using 0.02M H_3PO_4, while the other normality gives more than one phase. The IR spectrum exhibits specific absorption peaks at 558.2, 693.28, 1008.11, 1428.99, 1751.53, 1941.97, 3440.87, which characterizes the barium hydroxyapatite. It is observed that the intensity of the specific peaks on the x-ray charts increases with increasing of the acid normality, this indicate that the crystallinity improves by the increase of the acid normality. The TEM showed that: (1) the particle size of the barium hydroxyapatite lies in the scale of nanoparticles (40- 180 nm). (2) the size of the barium hydroxyapatite increases with increasing the ratio of phosphoric acid. (3) the particles have irregular shape and not depend on the ratio of phosphoric acid. (4) The sample produced by using phosphoric acid = 0 .04 M showed a bone structure. The measurements of the surface area indicated that it depends on the morphology of the produced samples which by turn depends on the normality of phosphoric acid. The more suitable sample was used to remove Cu, Cd, Ni, and Zn from their aqueous solutions.

Keywords: Barium hydroxyapatite, preparation, charsacterization, removal, metals.

INTRODUCTION

The objective of this work was preparation and characterization of barium hydroxyapatite, $Ba_{10}(PO_4)_6(OH)_2(BHAP)_2$, to be used as ion exchanger to remove some heavy metals from their aqueous solutions. The more conventional technologies for heavy metal ions removal are chemical precipitation, ion exchange, reverse osmoses, electrochemical treatment, sorption, solvent extraction and filtration. Among these methods, sorption and ion exchange technologies are the most promising methods due to their high efficiency, easy handling, availability of different materials and cost effectiveness. Phosphate minerals have been shown to possess the potential to remove heavy metal ions from aqueous solutions (Monteil – Rivera and Fedoroff, 2002). Of all the inorganic phosphate sources, apatite is most readily available. Different origins of apatite (mineral or synthetic) have been used to remove heavy metal cations (Elouear *et al*., 2008). Peld *et al*. (2004) studied the effects of different factors on removing Cd^{+2}, Zn^{+2}, by some synthetic types of hydroxyapatite. Removal of single, binary and tertiary divalent cations, i.e Pb^{+2}, Cu^{+2}, Cd^{+2} respectively, from their chloride or nitrate aqueous solutions were carried out by using hydroxylapatite. The results indicated that Pb^{+2} were adsorbed on the apatite structure very fast than the other cations **(**Takeuchi and Arai, 1990**)**. Bailliez *et al*. (2004) studied the mechanism of the removal of Pb^{+2}on the structure of hydroxyapatite, and used the chemical analysis and the x-ray techniques for the solution and the solid respectively. They found that the slightly dissolution of HAP is followed by formation of hydroxy pyromorphite, a solid solution of $Pb_{10-x}Ca_x(PO_4)_6(OH)_2$ formula, with Pb ions mostly occupying Ca(II) sites, and that the Ca/P molar ratio of this solid solution decreases continuously. Sugiyanaa *et al*. (2000) identified the formation of lead hydroxyapatite in the solid state after exchange with Pb^{+2}, while no copper analogue of HAP was found. Also, they found that the addition of HCl enhance the exchangeability. It is noteworthy that most of the work was focused on Ca - hydroxyapatite due to its natural occurrence in the rock, bones and teeth, beside the ability of Ca^{+2} in CaHAP to substituted by various other cations. A few works was devoted to the other hydroxyapatite such as SrHAP, BaHAP to study the effect of the atomic radius on the exchangeability (Sugiyanaa *et al*., 2000**;** Sgiyama, 1998). For this reason our work was aimed to prepare barium hydroxyl apatite by simple method and using as ion exchanger agent for removing the more toxics metals such as Cd^{+2}, Zn^{+2}, Cu^{+2} and Ni^{+2} where these cations interaction with the biological apatite

*Corresponding author email: an.mam@hotmail.com

of bones, leading to a disease producing effects similar to osteoporosis (Miyahara, 1980; Christoffersen, 1988). BaHAP have been synthesized by many researchers using solid state reactions (Fowler, 1974, 1974), wet process and sol- gel route (Bigi *et al*., 1984). BaHAP, $Ba_{10}(PO_4)_6(OH)_2$ possesses unique properties as catalysts and immobilization reagents. For example, catalysts activities on BaHAP into metal conversion (Sgiyama and Moffat, 2002) and oxidative dehydration of alkanes (Sgiyama *et al*., 1999, 2001) were reported together with the removal properties of BaHAP with aqueous heavy metals (Bailliez *et al*., 2004).

MATERIALS AND METHODS

Pure grade chemicals were used without further purification. Barium hydroxyapatite, BaHAP, was prepared from $Ba(OH)_2.8H_2O$ and H_3PO_4(85%) according to the procedure reported by (Yasukawa *et al* 1999). 0.2 M of $Ba(OH)_2.8H_2O$ and different molarities of H_3PO_4(0.02, 0.04, 0.06, 0.08, and 0.1 M) were prepared as stock materials. H_3PO_4 solution was added to the barium hydroxide with continuous stirring at 100°C under nitrogen atmosphere. Phosphoric acid was added with low rate (4cm^3/min) to avoid the local depression in the pH of the solution. The resultant white suspensions were aged at 100°C for 16hr. and the formed precipitates were filtered off. The precipitates were washed with di-ionized water and methanol and dried at the room temperature for 16hr. The produced samples were calcinated at 500°C for 4 hr. to study the effect of the calcinations on the structure of the samples (Matsumoto *et al*., 2001). The obtained particles were characterized by various techniques. Infrared absorption spectra (IR) were performed by the KBR disc technique using a Fourier transformer infrared spectrometer (Nexus 670 FTIR, USA) in the range between 400 to 4000 cm-1.X-ray diffraction (XRD) was carried out by using Brukur D8 advance diffractometer (Germany) using CuKα radiation. The surface area of the prepared samples was performed by using Quantachrome Inst., Quantachrome Nova Automated gas sorption system version 1.12.

The dried BHA was used as ion exchanger to remove some divalent cations, Cu, Ni, Cd, and Zn from their aqueous solutions, In this work, 0.4gm of the BaHAP powder were dispersed in 100 cm^3 aqueous solutions containing concentrations of the divalent cations nitrates. The pH value of the solutions were adjusted between 5 to 7 by adding 1 N HNO_3 solution at 30°C. The solutions were left for 60 min to attain the equilibrium state. After this period the solid part were separated by filtration, dried at 70°C. The filtrate was analyzed by using atomic absorption route to determine the remainder amounts of Cu, Ni, Cd, and Zn. The effects of the concentration of the divalent cations between 10^{-4} to 10^{-2} M and the time of immersion between 10 to 75 min were investigated. The efficiency of removing was calculated by using the following formula f % = $(C_o - C) / C_o$ where C_o and C are the initial and the concentration of the divalent cations in the solution after removing respectively.

RESULTS AND DISCUSSION

Figure 1, represents the IR spectra of the five prepared samples (a, b, c, d and e). At all samples, a broad band at ~3425.3 - 3440 cm^{-1} was appeared, this band attributed to the vibration of the OH^- in the lattice as proposed by (Yasukaua *et al*., 1999). The intensity of this band decrease with increasing the concentration of H_3PO_4 and becomes very weak at sample (e), this may due to the presence of some difference in the orientation of OH^- groups through the structure of the lattice (Reisner and Klee, 1982). Also, curve (a) shows a strong band at 1000-1100cm^{-1} beside a week one at ~ 930cm^{-1} due to the stretching vibrations of PO_4^{-3}. Two other sharp bands at ~580 and 558 were specified due to the deformation vibrations of the phosphate ions $(PO_4)^{-3}$ (Baddiel and Berry, 1966). In addition, a sharp band was appeared at ~1420 corresponding to CO_3^{-2} ions incorporated with OH^- sites on the surface hydroxyl apatite. (Cheng *et al*., 1998) suggested that the presence of the CO_3^- group in the lattice of the hydroxyl apatite may due to the atmospheric carbon dioxide. For the other samples (b,c,d, and f), the IR spectrum shows the same character as that proceeded for sample (a) with some shifts which may due to the orientation in the lattice. In general the IR spectrum indicate that the BaHAP is formed in agreement with the previous work (1,2,3). In previous study, the authors found that the CaHAP powder is converted from amorphous state to crystalline phase by increasing the calcinations temperature (El-sayed and Mousa, 2006). According to these results, a sample from the prepared BaHAP was exposed to calcinations at 500°C for 4hr. The results of the X-ray diffraction were presented in fig 2, for the prepared samples by using 0.02, 0.04, 0.06, 0.08, and 0.1 M H_3PO_4. The X-ray patterns of the produced powder showed that only sample (a) which prepared by using 0.02 M of phosphoric acid gives BaHAP (JCPDS 36-0272). For the other four samples (b-e) which prepared by using (0.04-0.1M) of phosphoric acid. The produced phases are BaHAP with traces of $Ba_3(PO_4)_2$, $Ba_3(PO_4)_2$, and a mixture of $Ba_3(PO_4)_2$ and $Ba_2(P_2O_7)$ and $Ba_2(P_2O_7)$, respectively at high molarities of H_3PO_4 due to the formation of pyrophosphate. According to the results of the X-ray diffraction, sample (a) is the preferable one to be used as ion exchanger. The results indicate that the formed BaHAP have a nanoparticle size in the range between 40 and 180 nm. Also it is observed that the particle size of BaHAP increased by increasing the molarities of H_3PO_4, this may due to the crystal growth.

Figure 3, displays TEM images of the prepared samples by using different molarities of H_3PO_4. The average

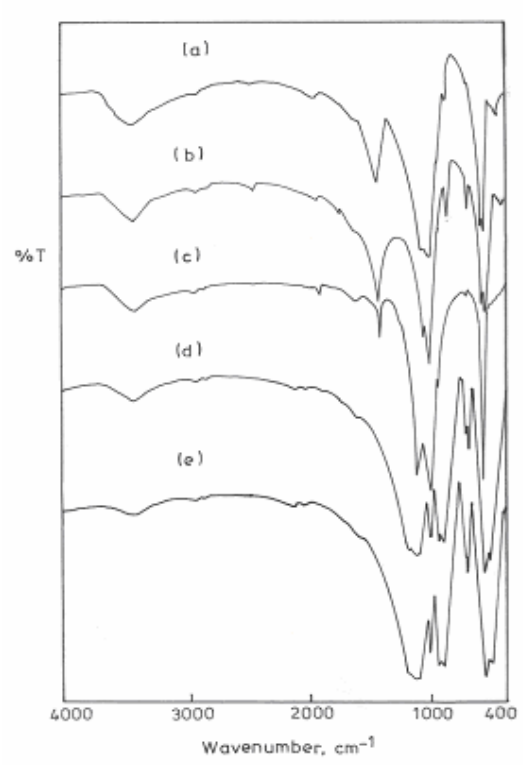

Fig. 1. IR spectrum of prepared samples
a= sample with 0.02 M H_3PO_4
b= sample with 0.04 M H_3PO_4
c= sample with 0.06 M H_3PO_4
d=sample with 0.08 M H_3PO_4
e= sample with 0.1 M H_3PO_4

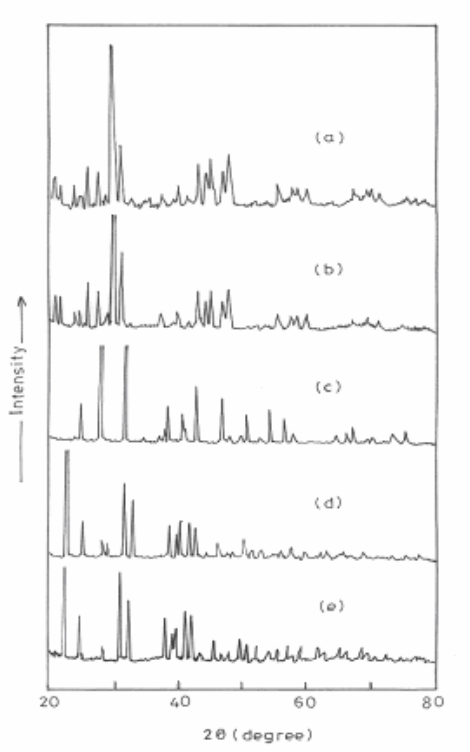

Fig. 2. X-ray diffraction of prepared samples.
a= sample with 0.02 M H_3PO_4
b= sample with 0.04 M H_3PO_4
c= sample with 0.06 M H_3PO_4
d=sample with 0.08 M H_3PO_4
e= sample with 0.1 M H_3PO_4

particle size estimated from the TEM image are increase from 40 to 180nm as the molarities of the used phosphoric acid increases from 0.02 to 0.1. On other hand, it is observed that the short rod particles elongated as the molarities of H_3PO_4 increases. The formed BaHAP are arranged in irregular shape and this increased by increasing the molarities of H_3PO_4 forming a structure lake bone at the high molarities of H_3PO_4 samples (d,f). The results of the measured surface area indicate that the surface area of the produced BaHAP decrease as increasing in the molarities of H_3PO_4 (Table 1). This finding is in agreement with the results of X-ray diffraction, where the crystallinity of the BaHAP increased with the molarities of the acid which leads to decrease in the surface area.

To study the effects of the surface area of BaHAP on the efficiency of removing copper cations with concentration = $5x10^{-4}$ M, was used as example of the divalent cations. The results indicate that the sample with high surface area exhibiting high efficiency to removal the copper from its aqueous solution (Table 2). These results are in agreement with the fundamental bases and the obtained results.

The prepared sample of Barium hdroxyapatite calcinated at 500°C for 4hr with 0.02 M H_3PO_4 was used as ion exchanger to remove some heavy metals M^{+2}(M^{+2} =Zn, Cu, Cd, and Ni). In this study, the batch process was performed, where a certain weight of BaHAP was immersed in nitrate solutions of the divalent cations with continuous stirring to attain the equilibrium. The effect of the pH values at pH = 5,5.5,6 and 7 on the efficiency of the up taking the cations was studied. At the pH values > 7, some problems were observed in performing the experiments such as complex formation or dissolution of the precipitated salts. Also, the effect of the initial concentration C(C =10^{-4}, $5x10^{-3}$, 10^{-3}, $5x10^{-2}$, 10^{-2}) and the time of removing (t), (t=10, 20, 30, 45, 60min) on the efficiency of removing was investigated.

Figure 4, represents the variation of the efficiency to removing the metal cations with the pH values by using sample (a) [prepared from 0.02M H_3PO_4 and having the higher surface area]. For the four cation under investigation, it was observed that the efficiency of removing decreases with increased in the pH values. At low pH value ranges, the decrease in the efficiency is

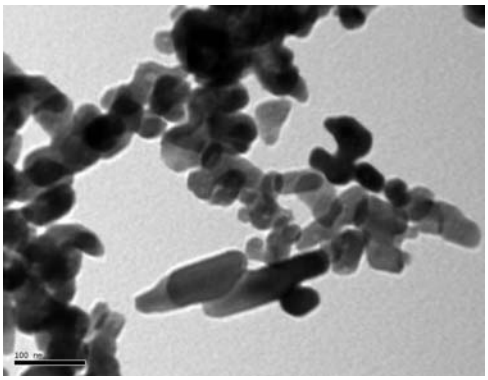

Sample (a)

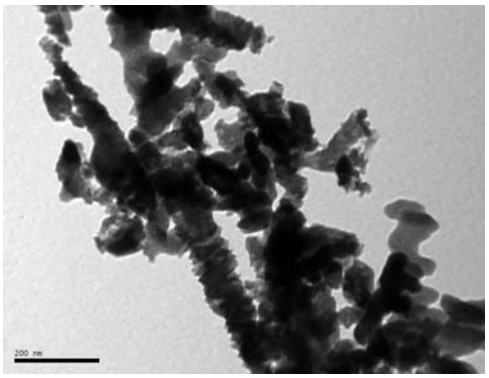

Sample (b)

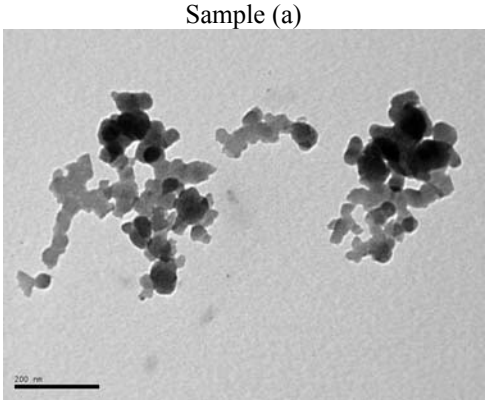

Sample (c)

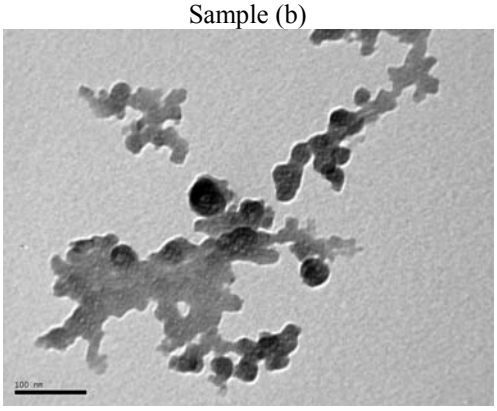

Sample (d)

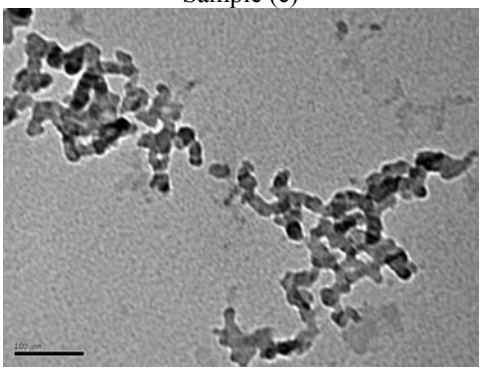

Sample (e)

Fig. 3. TEM of prepared samples.
a= sample with 0.02 M H_3PO_4 b= sample with 0.04 M H_3PO_4
c= sample with 0.06 M H_3PO_4 d=sample with 0.08 M H_3PO_4
e= sample with 0.1 M H_3PO_4

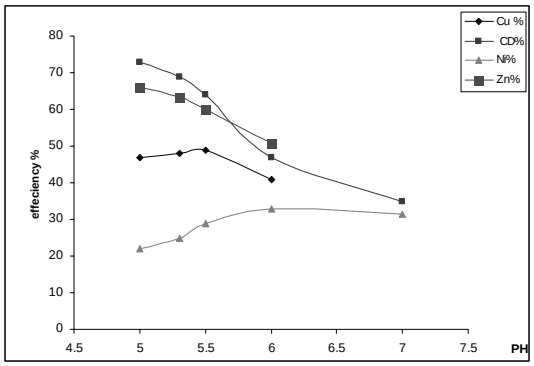

Fig. 4. Effects of pH on adsorption process.

more remarkable than that at high pH value. This behavior is in agreement with the results obtained by (Sgiyama *et al*., 2000), where they observed that the addition of HCl to the medium of solution enhances the up taking of the divalent cations. On other hand, (Suzuki *et al*., 1981) reported that hydroxylapatites are quite suitable as an a desorbent in the acidic medium of the aqueous solution

In general figure 4, shows that the removing of the four cations take place the same trends by the variation of the pH values and following the sequence Cu > Zn > Cd > Ni. This arrangement may depend on the nature of cations such as their electronegativity, ionic radius atc. Literatures indicated that there are two mechanisms for the ability of the hydroxyapatites to take up the cations from their solutions (Lower *et al*., 1998).

1) ion–ion exchange mechanism, where the cations were adsorbed on the solid surface, followed by diffusion into the HAP and release of cations, whatever they are Ca^{+2},Ba^{+2},Sr^{+2} .

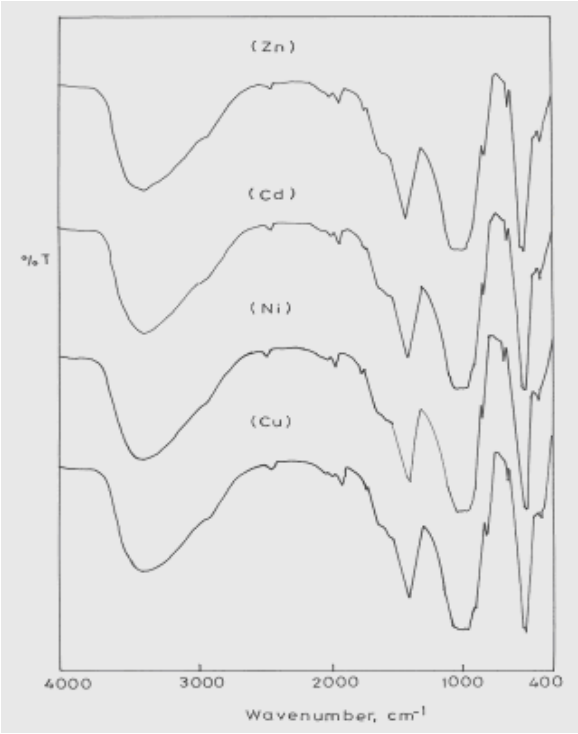

Fig. 5. IR spectrum of produced BaHAP samples after adsorption process.

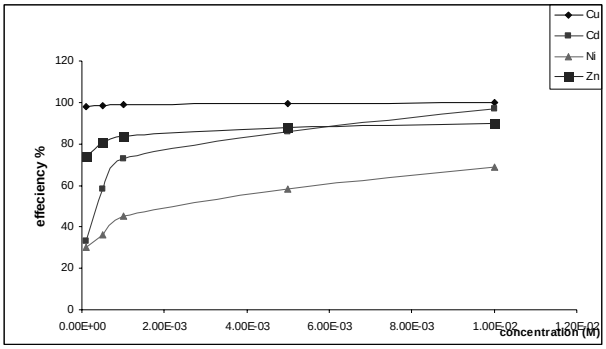

Fig. 6. Effects of the initial concentrations on adsorption process.

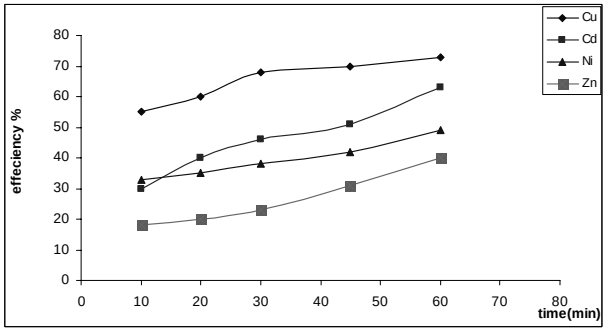

Fig. 7. Effects of the time on adsorption process.

2) Dissolution – precipitation mechanism, where a few amounts of HAP was dissolved in the aqueous solution containing the divalent cations followed by precipitation or coprecipitation.

The mechanism of the removal of divalent cations by hydroxyapatites depends on the nature of these cations such as their ionic radius and the electromotivities as well as the type of the hydroxyapatites whatever it is strontium, calcium, barium. On other hand, the morphology and the structure of the hydroxyapatites affected greatly on the efficiency of the removing for the cations. Because no detection on the formation of the substituted hydroxyapatites on the IR spectrum for the BaHAP after removing, fig. 5, the most acceptable mechanism is the solubility of some barium hydroxyapatites particles from the surface (the coprecipitation mechanism).

The effect of the initial concentration of the divalent cations on the efficiency of up taking was illustrated in fig. 6, In all adsorption cases, the efficiency of absorption increases with the increase the initial concentration of cations, but this increase is more remarkable at the low concentration than that at high concentration. This may due to the low solubility of barium hydroxyapatite and their interaction with the divalent cations. This results are in agreement with the obtained results by (Fedoroff *et al*., 1999)**,** where they observed that no significant difference are noted between experiments performed with initial concentration of $3.96x10^{-3}$ and $3.96x10^{-4}$ $mol.l^{-1}$ of cadmium cation and using CaHAP.

Figure 7, represents the dependence of the efficiency of removing on the time of immersion. In general it is observed that the efficiency increases rapidly at the first stages (>30 min) of removing, and increases slightly with time of immersion between 30-60min. This results support the mechanism of removing which depend on the dissolution and precipitation on the surface of the barium hydroxyl apatite.

CONCLUSION

The preparation of barium hydroxyapatite depends on the normality of H_3PO_4 as well the conditions of preparation and the calcination temperatures. The prepared BaHAP from 0.02M H_3PO_4 and barium hydroxide shows a single phase with higher surface area than the other samples. The up taking of the heavy metals from their aqueous solutions was depended on the initial concentration, time of contact and the pH values.

Table 1. Surface area measurements of BaHAP samples.

Samples	Surface area
a(0.02M) H_3PO_4	89.7 m^2/g
B(0.04M) H_3PO_4	37.9 m^2/g
c(0.06M) H_3PO_4	30.8 m^2/g
d(0.08M) H_3PO_4	33 m^2/g
e(0.1M) H_3PO_4	29 m^2/g

Table 2. the efficiency of removal of Cu metal by BaHAP with different molarities.

Samples of Cu solutions	Samples of BaHAP	Efficiency %
a	a(0.02M) H_3PO_4	35.9
b	b(0.04M) H_3PO_4	28.6
c	c(0.06M) H_3PO_4	5.58
d	d(0.08M) H_3PO_4	4.88
e	e(0.1M) H_3PO_4	3.59

REFERENCES

Baddiel, CB. and Berry, EE. 1966. Spectra structure correlations in hydroxyl and fluoroapatite. Spectrochem. Acta. 22:1407-1420.

Bailliez, S., Nzihou, A., Beche, E. and Flamant, G**.** 2004.Removal of lead (Pb) by hydroxylapatite sorbent. process safety and environmental Protection. 82(2)175-180.

Bigi, A., Foresti, E., Marchetti, F., Ripamonti, A. and Roveri, N. 1984. Barium calcium hydroxyapatite solid solutions. J. Chem. Soc. Dalton Trans. 1091-1094.

Cheng, ZH., Yasukawa, A., Kandori, K. and Ishikawa, T. 1998. FTIR study of Adsorption of Co2 on nonstoichiometric calcium hydroxyapatite. Langmuir. 14:6681- 6686.

Christoffersen, J., Christoffersen, MR., Larsen, R., Rostrup, E., Tingsgaard, P., Andersen,O. and Grandjean, P**.** 1988. Interaction of cadmium ions with calcium hydroxyapaqtite crystals: a possible mechanism contributing to the pathogenesis of cadmium – induced bone diseases. Calcif.Tissue Int. 42:331-339.

Elouear, Z., Bouzid, J., Boujelben,N., Feki, M., Jamoussi,F. and Montil, A. 2008. Heavy metal removal from aqueous solutions by activated phosphate rock. J. of Hazardous Mater. 156(1-3):412-420.

El-sayed, AM. and Mousa, SMA. 2006. Synthesis, heat treatment and characterization of nanocrystalline hydroxyl apatite powders. Egypt. J. Chem. 49(6):699.

Federoff, M., Jeanjean, J., Rouchaud, JC., Mazerolles, L., Trocellier P., Maireles, TP. and .Jones, DJ. 1999. Sorption kinetics and diffusion of cadmium in calcium hydroxyapatites. Solid State Sciences. 1:71.

Fowler, BO. 1974. Influenced studies of apatites. I. Vibrational assignments for calcium strontium, and barium hydroxyapatites utilizing isotopic substitution. Inorg. Chem. 13:194-207.

Fowler, BO. 1974. Influenced studies of apatites.II. Preparation of normal and isotopically substituted calcium strontium, and barium hydroxyapatites and spectra – structure – composition correlations. Inorg.Chem. 13:207-214.

Lower, SK., Maurice, PA., Traina, SJ. and Carson, EH. 1998. Aqueous Pb sorption by hydroxyiapatite: application of atomic force microscopy to dissolution, nucleation, and growth studies. Am. Mineral. 83:147-158.

Matsumoto, H., Sgiyama, S, Ichii, T., Hayashi, H., Hiraga, Y. and Shigemoto, N. 2001. Enhancement of lead – barium exchangeability of barium Hydroxyapatite. J. of Colloid and Interface Science. 238:183-187.

Miyahara,T., Miyakoshi, M., Saito,Y. and Kozuka, H**.** 1980.Influence of poisonous metals on bone metabolism:III. The effect of cadmium on bone resorption in tissue culture. Toxicol. Applied Pharmacol. 55:477-483.

Monteil – Rivera, F. and Fedoroff, M. 2002. Sorption of inorganic species on apatites from aqueous solution. Encyclopedia of Surface and Colloid Science, Marcel Dekker Inc., New York. 1:1-26.

Peld, M.,Tonnsuaadu K. and Bender, V**.** 2004. Sorption and desorption of Cd^{+2} and Zn^{+2} ions in Apatite- Aqueous system. Environ. Sci. Technol. 38(21):5626-5631.

Reisner, I. and Klee,WE. 1982. Temprature dependence on the ν(OH) bands of hydroxyapatite. Spectrochem. Acta. A 38:899-902.

Sugiyama, S**,** Fujii,Y., Abe, K., Hayashi, H. and Moffat, JB**.** 1999. Facile formation of the partial oxidation and oxidative – coupling products from the oxidation of methane on barium hydroxyapayites with tetra chloromethane. Energy Fuels. 13:637-640.

Sugiyama, S., Matsumoto, H., Hayashi, H. and Moffat, JB. 2000 Sorption and ion – exchange properties of barium hydroxyapatite with divalent cations. Colloids Surface, A, Physicochem. Eng. Aspect. 169:17-26.

Sugiyama, S. and Moffat, JB. 2002. Cation effects in the conversion of methanol on calcium, strontium, barium and lead hydroxyapatites. Catal. Lett. 81:77-81.

Sugiyama,S., Nishioka, H., Moriga, T., Hayashi, H. and Moffat, JB. 1998. Ion – exchange properties of strontium hydroxyapatite under acidic Conditions. Sci.Technol. 33:1999 -2007.

Sugiyama, S., Shono, T., Nitta, E. and Hayashi, H. 2001. Effect of gas- and solid –phase additives on oxidative hydrogenation of propane on strontium and barium hydroxyapatites. Appl. Catal. A,211:123-130.

Suzuki, T., Hatsushika, T. and Hayakawa, Y. 1981. Synthetic hydroxyapatites employed as inorganic cation – exchanger. J. Chem. Soc. FaradayTrans. 1 (77):1059-1062.

Takeuchi, Y. and Arai, H**.** 1990. Removal of coexisting Pb^{+2}, Cu^{+2} ions from water by addition of hydroxyl – apatite power. J. of Chem. Engineering of Japan. 23(1):75-80.

Yasukawa, A., Nakajima, M., Kandori, K. and Ishikawa, T. 1999. Preparation and characterization of carbonated barium hydroxyapatites J. of Colloid and Interface Science. 212:220-227.

Received: June 12, 2009; Accepted: Dec. 18, 2009

SENRA Academic Publishers, Burnaby, British Columbia
Vol. 4, No. 1, pp. 1095-1099, 2010
ISSN: 1715-9997

Canadian Journal of pure&applied sciences

THE RELATIONSHIP BETWEEN ELEVATED ALANINE TRANSAMINASE AND BODY MASS INDEX IN COLLEGE STUDENTS POPULATION: A CROSS-SECTIONAL STUDY

Chang-Hung Hung
Department of Leisure Industry Management, National Chin-Yi University of Technology, Taiwan
No.35, Lane 215, Section 1, Chung-Shan Road, Taiping City, Taichung, 411, Taiwan

ABSTRACT

The objective of our study was to evaluate the accuracy of body mass index (BMI) in detecting an elevated alanine transaminase (ALT) level in the college students population. The cross-sectional survey was conducted from 2005 to 2008 based on the health checkup data. A total of 7875 college freshmen were examined. Logistic regression was used to quantify the contribution of BMI to an elevated ALT (40 U/L) level. The Receiver Operating Characteristic (ROC) curve was used to calculate the BMI cut-off points for the risk of elevated ALT. BMI was a significant predictor of elevated ALT in both male (OR=1.30, 95%CI:1.24–1.36) and female (OR=1.21, 95%CI:1.60–1.27). The risk of elevated ALT was 38.79 (95%CI:22.46–67.01) fold higher with obesity in male and 21.96 (95%CI:8.24–58.51) fold in female. According to the data of the ROC curve, the BMI cut-off points for predicting the risk of elevated ALT were 24.1 kg/m^2 in male and 21.7 kg/m^2 in female. BMI is a good predictor of elevated ALT serum activity in the college students population. To identify college students population at high risk of elevated ALT in Taiwan, cut-off points little higher than currently recommended overweight for BMI is needed in male students while lower than overweight for BMI is suggested in female.

Keywords: Alanine transaminase, body mass index, ROC curve, AUC.

INTRODUCTION

With the continual improvement in hygiene and decreasing exposure to health hazards, acute liver damage has become less common. Instead, the growing concern is now for early detection of chronic liver damage (Sia1 *et al*., 2004). Alanine transaminase (ALT) is the most common laboratory tests for the detection of liver diseases. Elevated plasma ALT levels are associated with obesity and metabolic syndrome (Marchesini *et al*., 2005; Oh *et al*., 2006; Shen *et al*., 2005). Body mass index (BMI) is the principal and universal measure of obesity. Studies show that BMI values are associated with elevated ALT levels (Bedogni *et al*., 2003; Lee *et al*., 2001; Okita *et al*., 2001; Pratt and Kaplan, 2000). Overweight and obesity are the most common findings in adolescents with elevated ALT levels (Strauss *et al*., 2000). The prevalence and etiologies of elevated ALT have geographic variations and they are rarely reported in Taiwan, and even fewer reports describing the relationship between BMI and ALT in college students population. In this study, we explored the prevalence of elevated ALT levels and the contribution of BMI to elevated ALT and to determine optimal BMI cut-off points for predicting the risk of elevated ALT in the college students.

*Corresponding author email: hongjh@ncut.edu.tw

METERIALS AND METHODS

Subjects

This cross-sectional investigation was based on a health checkup data from a university in central Taiwan, conducted from 2005 to 2008. A total of 7875 freshmen were examined. The students of this university were from a wide range of locations throughout Taiwan. ALT was measured by common laboratory methods in hospital. BMI was calculated as weight (kg)/height(m)^2. Subjects were classified as under-weight (BMI <18.5 kg/m^2), normal-weight (18.5 BMI<24.0 kg/m^2), over-weight (24.0 BMI<27 kg/m^2) and obesity (BMI 27 kg/m^2) according to the definition recommended by the Department of Health, Executive Yuan, Taiwan (2002). Blood ALT level was used to screen abnormal liver function with a cut-off values of 40 U/L representing a state of acute liver cell damage (Guzzaloni *et al*., 2000). Therefore, elevated ALT was defined as ALT higher than 40 U/L.

Statistical analysis

Continuous variables were presented as mean values and standard deviation. Categorical variables were presented as frequencies. Associations between categorical variables were tested by using of Chi-square test. Continuous variables were tested using the *t*-test. Logistic regression

analysis was used to establish the contribution of BMI to elevated ALT, with elevated ALT serving as the was set to a value of $p<0.05$ for all tests. Statistical analysis was performed using SPSS for Windows.

Table 1. Characteristic of the study subjects.

Variables	Total (*n*=7,875)	Male (*n*=5,586)	Female (*n*=2,289)	*P* value
	Mean ± SD	Mean ± SD	Mean ± SD	
Height (cm)	168.22 ± 8.18	171.77 ± 6.23	159.55 ± 5.46	<0.001
Weight (kg)	62.30 ± 13.98	67.06 ± 13.38	53.01 ± 9.81	<0.001
BMI (kg/m^2)	22.15 ± 4.16	22.71 ± 4.27	20.80 ± 3.54	<0.001
ALT(U/L)	21.66 ± 22.95	24.48 ± 25.52	14.79 ± 12.53	<0.001
	Frequencies (%)	Frequencies (%)	Frequencies (%)	
Obesity (BMI 27.0 kg/m²)	957 (12.2)	810 (14.5)	147 (6.4)	<0.001
Over-weight (24.0<BMI 27.0 kg/m²)	1076 (13.7)	913 (16.3)	163 (15.1)	<0.001
Elevated ALT (ALT>40 U/L)	796 (9.6)	690 (12.4)	69 (3.0)	<0.001

Continuous variables are given as mean ± standard deviation and tested using the *t*-test.
Categorical variables were presented as frequencies (percentage) and tested using Chi-square test.
Abbreviations: BMI, body mass index; ALT, alanine aminotransferase

Table 2. Odds ratios and 95% confidence intervals for the relationship between BMI and elevated ALT.

Elevated ALT	Male			Female		
	OR	95% CI	*P* value	95%CI		*P* value
BMI all	1.30	1.24- 1.36	<0.001	1.21	1.60- 1.27	<0.001
Under- weight	1			1		
Normal-weight	3.05	1.76- 5.29	<0.001	2.91	1.14- 4.81	<0.001
Over-weight	12.52	7.20-21.77	<0.001	4.81	1.51-15.36	<0.001
Obesity	38.79	22.46-67.01	<0.001	21.96	8.24-58.51	<0.001

under-weight (BMI<18.5 kg/m^2); normal-weight (18.5 BMI<24.0 kg/m^2); over-weight (24.0 BMI<27 kg/m^2); obesity (BMI 27 kg/m^2)

Table 3. The AUC and optimal cut-off point of BMI for prediction elevated ALT.

	AUC (95% CI)	*P* AUC	Cut-off (Sen,%; Spec,%)
BMI male	0.81(0.80 - 0.83)	<0.001	24.1 (72.9, 75.8)
BMI female	0.72(0.66 - 0.79)	<0.001	21.7 (62.7, 71.6)

Abbreviations: AUC=area under the curve; Sen=sensitivity; Spec=specificity

dichotomous outcome variable. Odd ratio (OR) and 95% confidence intervals (CI) were computed. We used the Receiver Operating Characteristic (ROC) analysis to ensure the predictive validity, and to find out the optimal cut-off points (Schouw *et al*., 1992). The sensitivity (SN) and specificity (SP) of each model were calculated and ROC curves were drawn by plotting SN vs. 1-SP to determine the BMI cut-off points for the risk of elevated ALT. We defined the best cut-off points as the value with the highest accuracy that maximizes the Youden's index (sensitivity+specificity-1) (Swets, 1973). Sensitivity and specificity have been calculated at all possible cut-off points to find the optimal cut-off points. The areas under receiver operator characteristic curve (AUC) were calculated to assess accuracy. AUC is a measure of the diagnostic power of a test. A perfect test will have an AUC of 1.0 and an AUC equal 0.5 means the test performs no better than chance. Statistical significance

RESULTS

The characteristics of the study subjects are given in table 1. A total of 7875 college freshmen (5586 male students, 2289 female students) attending the university were included in this study. The average BMI of the students was 22.71±4.27 kg/m^2 for male and 20.80±3.54 kg/m^2 for female. The average ALT of the students was 24.48±25.52 U/L for male and 14.79±12.53 U/L for female. ALT level higher than 40 U/L was found in 9.6% (796/7875) of all students (12.4% in male and 3.0% in female). The prevalence of elevated ALT was significantly ($p<0.001$) higher in male than in female. The prevalence of obesity (BMI 27.0 kg/m^2) was 12.2% (14.5% in male and 6.4 % in female).

Odds ratio (OR) of elevated ALT was calculated according to BMI classification compared to the reference

group (Table 2). The results show that BMI was a significant predictor of elevated ALT in both male

Table 4. Statistical indices for a range of cut-off value of BMI.

Male			Female		
Cut-off	Sensitivity (%)	Specificity (%)	Cut-off	Sensitivity (%)	Specificity (%)
20.0	95.4	31.6	19.0	85.3	33.4
21.0	92.1	45.0	20.0	74.7	49.7
22.0	86.7	56.5	21.0	66.7	64.3
23.0	80.1	67.3	21.3	66.7	68.0
23.5	76.0	71.8	21.5	65.3	7.03
23.7	75.1	73.5	**21.7***	62.7	71.6
24.1*	72.9	75.8	22.0	58.7	74.8
24.3	69.6	77.9	22.5	53.3	79.1
24.5	68.2	79.6	23.0	49.3	82.1
25.0	62.8	82.5	24.0	42.7	87.6
26.0	55.0	87.1	26.0	34.7	93.2

* maximum *J*, *J*= Sensitivity+Specificity-100

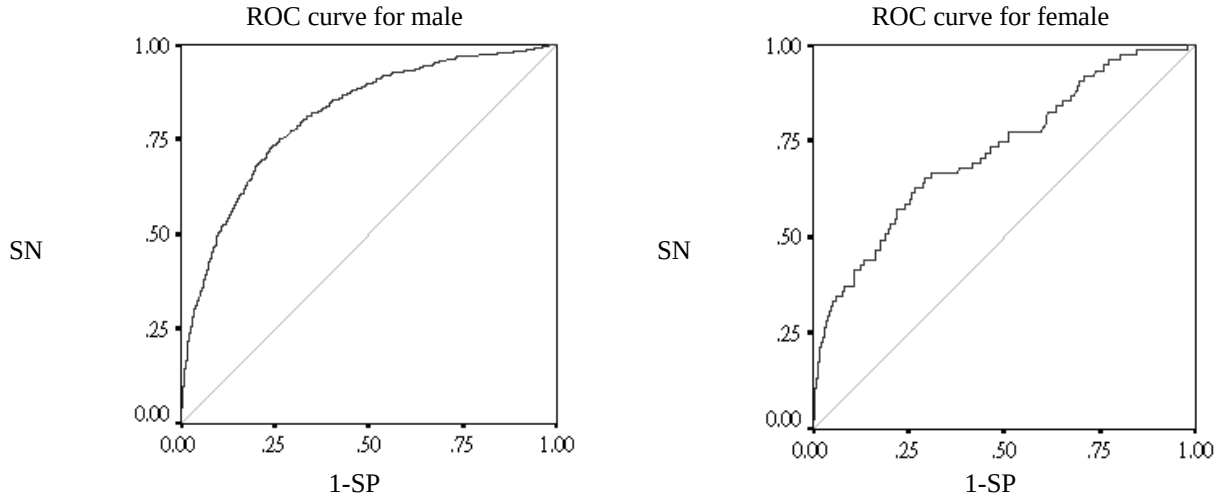

Fig. 1. Accuracy in detecting elevated ALT (40 U/L) by body mass index, Abbreviations: SN=sensitivity; SP=specificity

specificity 75.8%) and 21.7 kg/m^2 in female (sensitivity 62.7%, specificity 71.6%) (Table 4).

(OR=1.30, 95%CI:1.24–1.36) and female (OR=1.21, 95%CI: 1.60–1.27). In male students with over-weight and obesity had 12.52 times (95%CI:7.20–21.77) and 38.79 times (95%CI:22.46–67.01) for elevated ALT. In female students with over-weight and obesity had 4.81 times (95%CI:1.51–15.36) and 21.96 times (95%CI:8.24–58.51) for elevated ALT.

In table 3 shows that AUC was 0.81 (95%CI:0.80–0.83) for male and 0.72 (95%CI:0.66–0.79) for female ($p<0.001$) which were significantly higher than what would be expcted by chance (AUC > 0.5). Thus, as determined by ROC curves, BMI was a good predictor of elevated ALT. ROC curve analysis by sex suggested that BMI is a more sensitive and specific measure of elevated ALT in male than in female (Fig. 1). The ROC curves achieved a maximum Youden's index at BMI cut-off points of 24.1 kg/m^2 in male (sensitivity 72.9%,

DISCUSSION

In our study the prevalence of elevated ALT was 9.6 %, and was more common in male students compared to female students (12.4% vs. 3.0%, $p<0.001$). There was 11.4% of elevated ALT in an adult population in Taiwan and was more common in men compared to women (17.3% vs. 6.1%, $p<0.05$) (Chen *et al*., 2007). It is obvious that the prevalence of elevated ALT was more common in adult population compared to college students in Taiwan.

The present study aimed to establish the relative contribution of BMI to elevated ALT in the college students population. ROC curve analysis has been a useful tool in the study of BMI cut-off points (Do1 *et al*., 2004; Lin *et al*., 2002). In the study, we want to clarify the best BMI values for elevated ALT predicting, and

want to balance the sensitivity and specificity, so we use ROC curve to determine the best BMI cut-off points. Our study shows that the BMI cut-off points for the risk of elevated ALT were 24.1kg/m^2 in male students which were little higher than overweight cut-points (BMI 24 kg/m^2); and 21.7 kg/m^2 in female students which were lower than overweight cut-points, recommended by the Department of Health, Executive Yuan, Taiwan (2002). Therefore, BMI was a significant predictor for the risk of elevated ALT in both genders. The main strength of the present study is that we quantified the association between BMI and ALT in the college students population. Our findings were very similar to recent studies that BMI was strongly associated with ALT (Adsms *et al*., 2007; Bedogni *et al*., 2003) and a good predictor for the risk of elevated ALT in adolescents (Bedogni *et al*., 2004). The accuracy of the prediction in our study (AUC 0.81 for male and 0.72 for female) was higher than the study in Italy adolescents (AUC 0.71) proposed by Bedogni *et al*. (2004). Potential limitation with the present study is that our sample is from a university so the study subjects do not fully reflect the general college population in Taiwan, an issue that can be addressed by a country-wide study in the future. In addition, we did not consider the influence of physical activity, ethanol intake, tobacco use, HbsAg status on elevated ALT.

In conclusion, prevalence of elevated ALT was more common in adult population compared to college students in Taiwan. BMI was a significant predictor for the risk of elevated ALT which was more accurate in male than in female. To identify college students population in Taiwan at risk of elevated ALT, BMI cut-off points little higher than currently recommended overweight is needed in male students while lower than overweight is suggested in female.

REFERENCES

Adsms, LA., Knuiuman, MW., Divitin, ML. and Olynyk, JK. 2007. Body mass index is a stronger predictor of alanine aminotransaminase levels than alcohol consumption. Journal of Gastroenterology and Hepatology. 23(7):1089-1093.

Bedogni, G., Miglioli, L., Battistini, N., Masutti, F., Tiribelli, C. and Bellentani, S. 2003. Body mass index is a good predictor of an elevated alanine transaminase level in the general population: hints from the Dionysos study. Digestive and Liver Disease. 35:648-652.

Bedogni, G., Miglioli, L., Masutti, F., Castiglione, A., Tiribelli, C. and Bellentani, S. 2004. Accuracy of body mass index in detecting an elevated alanine transaminase level in adolescents. Annals of Human Biology. 31(5):570-577.

Chen, CH., Huang, MH., Yang, JC., Nien, CK., Yang, CC., Yeh, YH. and Yueh, SK. 2007. Prevalence and etiology of elevated serum alanine aminotransferase level in an adult population in Taiwan. Journal of Gastroenterology and Hepatology. 22(9):1482-1489.

Department of Health, Executive Yuan, Taiwan. 2002. The definition of obesity and managing principle. Retrieved October 15, 2007, from Web site: http://food.doh.gov.tw/healthbite/eat_health/control_weight01.htm

Do1, TT., Dibley, MJ. and Este, CD. 2004. Receiver operating characteristic analysis of body mass index to detect increased risk of functional morbidity in Vietnamese rural adults. European Journal of Clinical Nutrition. 58:594-1603.

Guzzaloni, G., Grugni, G., Minocci, A., Moro, D. and Morabito, F. 2000. Liver steatosis in juvenile obesity: correlations with lipid profile, hepatic biochemical parameters and glycemic and insulinemic responses to an oral glucose tolerance test. International Journal of Obesity. 24(6):772-776.

Lee, DH., Ha, MH. and Christiani, DC. 2001. Body weight, alcohol consumption and liver enzyme activity a 4-year follow-up study. Interna**t**iona**l** Journal of Epidemiology. 30:766-770.

Lin, WY, Lee, LT., Chen, CY., Lo H., Hsia, HH., Liu, IL., Lin, RS, Shau, WY. and Huang, KC. 2002. Optimal cut-off values for obesity: using simple anthropometric indices to predict cardiovascular risk factors in Taiwan. International Journal of Obesity. 26(9):1232-1238.

Marchesini, G., Avagnina, S., Barantani, EG., Ciccarone, AM., Corica, F., Dall'Aglio, E., Dalle, GR., Morpurgo, PS., Tomasi, F. and Vitacolonna, E. 2005. Aminotransferase and gamma-glutamyltranspeptidase levels in obesity are associated with insulin resistance and the metabolic syndrome. Journal of Endocrinological Investigation. 28(4):333-339.

Oh, SY., Cho, YK., Kang, MS., Yoo, TW., Park, JH., Kim, HJ., Park, DI., Sohn, CI., Jeon, WK. and Kim, BI. 2006. The association between increased alanine aminotransferase activity and metabolic factors in nonalcoholic fatty liver disease. Metabolism. 55(12):1604-1609.

Okita, M., Hayash, M., Sasagawa, T., Takagi, K., Suzuki, K., Kinoyama, S., Ito, T. and Yamada, G. 2001. Effect of a moderately energy-restricted diet on obese patients with fatty liver. Nutrition. 17:542-547.

Pratt, DS. and Kaplan, MS. 2000. Evaluation of abnormal liver-enzyme results in asymptomatic patients. New England Journal of Medicine. 342:1266-1271.

Schouw, YT., Verbeek, ALM. and Ruijs, JHJ. 1992. ROC curves for the initial assessment of new diagnostic tests. Family Practice. 9:506-511.

Shen, YH., Yang, WS., Lee, TH., Lee, LT., Chen, CY. and Huang, KC. 2005. Bright liver and alanine aminotransferase are associated with metabolic syndrome in adults. Obesity research. 13:1238-1245.

Sia1, HK., Wang, JD., Huang, CH. and Huang, CC. 2004. Serum alanine aminotransferase as an annual screening tool for diseases among workers. Changhua Journal of Medicine. 9(1):22-27.

Strauss, RS., Barlow, SE. and Dietz, WH. 2000. Prevelance of abnormal serum aminotransferase values in overweight and obese adolescents. The Journal of Pediatrics. 136(6):727-733.

Swets, JA. 1973. The relative operating characteristics in psychology. Science. 182:990-1000.

Received: Oct 27, 2009; Revised: Jan 4, 2010; Accepted: Jan 5, 2010

SENRA Academic Publishers, Burnaby, British Columbia
Vol. 4, No. 1, pp. 1101-1105, 2010
ISSN: 1715-9997

Canadian Journal of pure&applied sciences

EFFECT OF CONFINEMENT OF GLUONS ON GROUND STATE HEAVY MESON SPECTRUM IN THE RELATIVISTIC HARMONIC MODEL

*KB Vijaya Kumar and K Gopala Krishna Naik
Department of Physics, Mangalore University, Mangalagangothri, Mangalore, 574199, India

ABSTRACT

In the frame work of relativistic harmonic model (RHM), we have investigated the mass spectrum of the S-wave heavy mesons. The full Hamiltonian used in the investigation has Lorentz scalar plus vector harmonic potential and confined one gluon exchange potential (COGEP). The mass of the mesons was obtained by diagonalsing a 5x5 matrix. A good agreement is obtained with the experimental masses of heavy mesons. The role of COGEP is discussed. The limitation of the perturbative treatment of estimating η_c-J/ψ is pointed out.

PACS Nos. 14.40.-n; 14. 40. Aq; 14. 40. Ev; 12.39.-x; 12.39. Ki

Keywords: Quark model, confined-one-gluon-exchange potential, relativistic model, heavy meson spectra.

INTRODUCTION

The meson spectroscopy is a broad subject covering from few hundred MeV masses of the light mesons to the 10 GeV scale of the $b\bar{b}$ system (Namgung and Lichtenberg, 1984). Such a wide energy region allows us to address perturbative and nonperturbative phenomena of the underlying Quantum Chromodynamics (QCD) theory. Though QCD is accepted as the fundamental theory of strong interactions, there exist no exact solutions to the theory in the non-perturbative low energy regime. The QCD is not exactly solvable in the non-perturbative regime which is required to obtain the physical properties of the hadrons. Hence various approximation methods have been employed to solve QCD in the non-perturbative regime. The most promising of these is through lattice gauge theories (Hooft, 1976). The lattice gauge theories involve gigantic computation, hence the progress has been slow and detailed predictions of the hadron properties have not been made. As a consequence, our understanding of hadrons continues to rely on insights obtained from the experiments and QCD motivated models in addition to lattice QCD results. The phenomenological models developed to explain observed properties of hadrons are either non-relativistic quark models (NRQM) (Bhaduri *et al*., 1981; Godfrey and Isgur, 1985; Blask *et al*., 1990; Brau *et al*., 2000; Vijande *et al*., 2005) with suitably chosen potential or relativistic quark models (RQM) (Jena 1983; Khadkikar and Vijaya, 1991; Vinodkumar *et al*., 1992) where the interaction is treated perturbatively. There are successful NRQM and RQM to explain the meson spectra (Vijaya *et al*., 1998; Bhavyshri *et al*., 2005 and 2008). The NRQM usually contain three main ingredients: the kinetic energy, confinement potential and a hyperfine interaction term which has often been taken as an effective one-gluon-exchange potential (OGEP) (De Rujula *et al*., 1975). On the other hand, the relativistic models have a confinement potential which is usually taken to be Lorentz scalar plus vector potential (Khadkikar and Gupta, 1983). There are models both non-relativistic and relativistic employed to explain meson spectra with OGEP (Semay and Silvestre-Brac, 1997, 1999; Takayuki *et al*., 2007).

In the present work, an attempt has been made to obtain the ground state mass of the heavy mesons in the frame work of relativistic harmonic model (RHM) (Khadkikar and Gupta, 1983; Khadkikar and Vijaya, 1991; Vijaya *et al*., 2004). The objective of present study was to obtain the ground state mass of the heavy mesons with minimum number of parameters and to investigate the relativistic effects on the mass spectrum. Infact, the non-relativistic models should work better for heavy quark mesons, since a particle of mass m, localised in a volume of radius R, has a momentum ~ 1/R through the uncertainty relation its kinetic energy $(< T >) << m$ only if $m R >> 1$. In the constituent quark model this is satisfied for the c,b and t quarks. Also, in NRQM the spurious excitation of the centre-of-mass (CM) motion can be eliminated easily. But as has been shown in reference (Rosner, 2007), the non-relativistic description for charmonium is quite crude, whereas it is substantially better for $b\bar{b}$ systems. Hence, to study the S wave spectra of heavy mesons we have made use of the successful RHM in which the confinement potential is a Lorentz scalar plus vector potential. Both scalar and vector potential are harmonic oscillator potentials. The total Hamiltonian has Lorentz scalar plus vector potential along with COGEP. In our model, the effect of confinement of gluons also has been taken into account. In the existing models though the

*Corresponding author email: kbvijayakumar@yahoo.com

effect of confinement of quarks has been taken into account the effect of confinement of gluons has not been taken into account. Hence, a consistent scheme has been employed for the confinement of gluons. For the confinement of gluons, we have made use of the current confinement model (CCM) (Vinodkumar, 1992). The confined gluon propagators (CGP) are derived in CCM has been used to obtain the confined one gluon exchange potential (COGEP). Our present model along with instanton induced interaction has been successful in obtaining the mass spectra of S and P wave light mesons (Vijaya *et al*., 2004, 2009; Bhavyshri *et al*., 2005, 2008).

The Relativistic harmonic model

In RHM (Khadkikar and Gupta 1983; Vijaya *et al*., 2004) quarks in a hadron are confined through the action of a Lorentz scalar plus a vector harmonic-oscillator potential

$$V_{conf}(r) = \frac{1}{2}\left(1+\gamma_0\right)A^2r^2 + M \tag{5}$$

where γ_0 is the Dirac matrix:

$$\gamma_0 = \begin{pmatrix} 1 & 0 \\ 0 & -1 \end{pmatrix}, \tag{6}$$

M is the quark mass and A^2 is the confinement strength. They have a different value for each quark flavour. In RHM, the confined single quark wave function (ψ) is given by:

$$\psi = N\begin{pmatrix} \phi \\ \dfrac{\boldsymbol{\sigma}\cdot\mathbf{P}}{E+M}\phi \end{pmatrix} \tag{7}$$

with the normalization

$$N = \left(\frac{2(E+M)}{3E+M}\right)^{1/2} \tag{8}$$

where E is an eigenvalue of the single particle Dirac equation with the interaction potential given in (1). The lower component is eliminated by performing the similarity transformation,

$$U\psi = \phi \tag{9}$$

Where U is given by,

$$\frac{1}{N\left[1+\dfrac{\mathbf{P}^2}{(E+M)^2}\right]}\begin{pmatrix} \mathbf{1} & \dfrac{\boldsymbol{\sigma}\cdot\mathbf{P}}{E+M} \\ -\dfrac{\boldsymbol{\sigma}\cdot\mathbf{P}}{E+M} & \mathbf{1} \end{pmatrix} \tag{10}$$

Here, U is a momentum and state (E) dependent transformation operator. With this transformation, the upper component ϕ satisfies the harmonic oscillator wave equation.

$$\left[\frac{\mathbf{P}^2}{E+M} + A^2r^2\right]\phi = (E-M)\phi, \tag{11}$$

which is like the three dimensional harmonic oscillator equation with an energy-dependent parameter Ω_n^2:

$$\Omega_n = A\left(E_n+M\right)^{1/2} \tag{12}$$

The eigenvalue of (11) is given by,

$$E_n^2 = M^2 + (2n+1)\Omega_n^2 . \tag{13}$$

Note that eqn. (11) can also be derived by eliminating the lower component of the wave function using the Foldy-Wouthuysen transformation.

Adding the individual contributions of the quarks we obtain the total mass of the hadron. The spurious centre of mass (CM) is corrected by using intrinsic operators for the $\sum_i r_i^2$ and $\sum_i \nabla_i^2$ terms appearing in the Hamiltonian. This amounts to just subtracting the CM motion zero point contribution from the E^2 expression. It should be noted that this method is exact for the 0S-state quarks as the CM motion is also in the 0S state.
In addition, the Hamiltonian has COGEP

The COGEP is obtained from the scattering amplitude (Khadkikar and Vijaya, 1991;Vijaya and Khadkikar, 1993),

$$M_{fi} = \frac{g_s^2}{4\pi}\bar{\psi}_i\gamma^\mu\frac{\lambda_i^a}{2}\psi_i D_{\mu\nu}^{ab}(q)\bar{\psi}_j\gamma^\nu\frac{\lambda_j^b}{2}\psi_j , \tag{14}$$

where, $\bar{\psi} = \psi^+\gamma_0$, $\psi_{i/j}$ are the wave functions of the quarks in the RHM, $D_{\mu\upsilon}^{ab} = \partial_{ab}D_{\mu\upsilon}$ are the CCM gluon propagators in momentum representation, $g_s^2/4\pi$ (= α_s) is the quark-gluon coupling constant and λ_i is the color $SU(3)_c$ generator of the i^{th} quark. Below we give the expressions for the central part of the COGEP.
The central part of COGEP is (Khadkikar and Vijaya Kumar, 1991),

$$V_{COGEP}^{cent}(\vec{r}_{ij}) = \frac{\alpha_s N^4}{4}\boldsymbol{\lambda}_i\cdot\boldsymbol{\lambda}_j\left[D_0(\vec{r}_{ij}) + \frac{1}{(E+M)^2}\left[4\pi\delta^3(\vec{r}_{ij}) - c^4r^2D_1(\vec{r}_{ij})\right]\left[1-2/3\,\boldsymbol{\sigma}_i\cdot\boldsymbol{\sigma}_j\right]\right] \tag{15}$$

To calculate the matrix elements (ME) of COGEP, we have fitted the exact expressions of $D_0(\vec{r})$ and $D_1(\vec{r})$ by Gaussian functions. It is to be noted that the $D_0(\vec{r})$ and

$D_1(\vec{r})$ are different from the usual Coulombic propagators. However, in the asymptotic limit ($\vec{r} \to 0$) they are similar to Columbic propagators and in the infra-red limit ($\vec{r} \to \infty$) they fall like Gaussian. In the above expression the c (fm^{-1}) gives the range of propagation of gluons. The $D_0(r)$ and $D_1(r)$ are given by,

$$D_0(\vec{r}) = \left(\frac{\alpha_1}{r} + \alpha_2\right) \exp\left[\frac{-r^2 c_0^{\,2}}{2}\right]; \qquad D_1(\vec{r}) = \frac{\gamma}{r} \exp\left[\frac{-r^2 c_2^{\,2}}{2}\right]$$

Where α_1 = 1.035994, α_2 = 2.016150, c_0 = $(3.001453)^{1/2}$ fm^{-1} γ = 0.8639336

And $c_2 = (4.367436)^{1/2}$ fm^{-1}. It should be noted that in the limit c $\to$ 0, the central part of the COGEP goes over to the corresponding potential OGEP of the NRQM (Vinodkumar *et al*., 1992).

Fitting Procedure

The parameters in our model are the masses of up (M_u), down (M_d), strange (M_s), charm (M_c) and bottom (M_b) which are taken as parameters. The α_s is fixed by the J/Ψ - η_c mass splitting. The mass difference arises from the colour magnetic term of COGEP. The, A^2 is the confinement strength parameter and Ω (=1/b) is the oscillation size parameter. The b is fixed by minimizing the expectation value of the Hamiltonian for the pseudo scalar mesons. The confinement strength A^2 is fixed by the stability condition for the variation of the mass of the mesons against the size parameter b. The additional parameter c, termed CCM parameter was fitted to iota (1440 MeV), $J^{pc} = 0^{-+}$ (the oldest glue ball candidate) as a digluon glue ball (Vijaya *et al*., 1998). The values of the parameters used in our calculation are listed in table 1.

Table 1.Values of the parameters used in our model.

$M_{u/d}$ (MeV)	160.6
M_s (MeV)	402
M_c (MeV)	847
M_b(MeV)	2156
Ω(fm)	0.77
α_s	0.6
C (fm^{-1})	1.74
A^2 (MeV fm^{-2})	3693

Results of S wave Meson Spectra

In the present study, the product of quark-antiquark oscillator wave functions is expressed in terms of oscillator wave functions corresponding to the relative and CM coordinates. The oscillator quantum number for the CM wave functions are restricted to N_{CM} = 0. The Hilbert space of relative wave functions is truncated at radial quantum number n_{max} = 5. The Hamiltonian matrix is constructed for each meson separately in the basis states of $\left|N_{CM}=0, L_{CM}=0;\ ^{2S+1}L_J\right\rangle$. The masses of the pseudo scalar mesons (PSM) and vector mesons (VM) after diagonalisation for successive values of n_{max} are listed in table 2 and table 3 respectively. We get a very good agreement with the experimental masses (Amsler, 2008) both for PSM and VM. The COGEP is attractive for PSM hence the diagonalisation in the space of radially excited states brings down the value of PSM to their physical mass. For example, with n_{max} = 1, the naive masses of the η_c turned out to be 5039.18 MeV. The colour-electric term of COGEP are attractive both for PSM and VM and contribute significantly to the masses. It is satisfying to note that all the masses converge reasonably well to respective experimental values for the same value of α_s (= 0.6). It is to be noted here that we need to enhance the value of α_s when diagonalisation is carried out in smaller configuration space. For the VM, the range of values over which α_s is tuned is considerably smaller than that for the PSM as the OGEP is repulsive. It is clear from tables 2 and 3 that the difference between the masses of the successive values of n_{max} decreases.

The masses of the PSM and VM after diagonalisation for successive values of n_{max} are listed in table 2 and 3 respectively. With n_{max} = 5, the masses of η_c and J/ψ mesons are found to be 2980.3 MeV and 3097.9 MeV respectively. Further increase of the oscillator basis does not lead to any significant change in the masses. The calculation clearly indicates that masses for both PSM and VM converge to the experimental values when the diagonalisation is carried out in a larger basis, but the convergence is achieved in a smaller basis for VM. The CMP of COGEP has an additional term c^4 r^2 $D_1(r)$ whose overall sign is opposite to the δ(r) term and hence has a repulsive contribution to the masses of PSM. Hence, to obtain the physical mass of the PSM it was sufficient to carry out the diagonalisation in a smaller configuration space truncated at n_{max} = 5.

Summary and conclusions

In our present work, we have investigated the masses of ground state heavy mesons in the frame work of RHM with COGEP. The calculation shows that the computation of mesonic masses and mass splittings using COGEP is adequate for both PSM and VM. Hence, it is justified to use a combination of the COGEP along with a Lorentz scalar plus vector potential to reproduce the masses of

Table 2. The PSM masses (in MeV) for successive values of n_{max} .

n_{max}	$\eta_c(c\bar{c})$	$\eta_b(b\bar{b})$	$D(c\bar{d})$	$D_S^{\pm}(c\bar{s})$	$B(u\bar{b})$	$B_S^0(s\bar{b})$	$B_C^{\pm}(c\bar{b})$
1	5039.18	15988.55	3159.12	3331.74	8889.84	9174.22	10822.42
2	3963.4	12583.13	2486.17	2618.11	7021.07	7152.3	8512.01
3	3337.6	10596.32	2056.23	2204.72	5912.48	6098.16	7168.01
4	3045.56	9669.14	1906.69	2014.81	5395.14	5494.23	6540.81
5	2980.3	9467.84	1873.19	1969.43	5279.08	5378.89	6405.77
Expt.	2980±1.2	9461	1869.3±0.5	1968.5±0.6	5279.0±0.5	5369.6±2.4	6400±0.4

Table 3. The VM masses (in MeV) for successive values of $n_{max.}$

n_{max}	$J/\psi(c\bar{c})$	$\gamma(b\bar{b})$	$D^*(c\bar{d})$	$D_S^{*\pm}(c\bar{s})$	$B^*(u\bar{b})$	$B_S^*(s\bar{b})$
1	3243.91	9872.45	2136.57	2182.11	5500.72	5591.42
2	3134.08	9573.82	2034.12	2137.75	5388.9	5477.75
3	3109.92	9500.03	2018.44	2127.27	5347.36	5435.53
4	3098.77	9465.98	2011.21	2122.03	5328.19	5416.05
5	3097.9	9462.04	2010.89	2117.28	5321.62	5413.88
Expt.	3096.916±0.011	9460.3±0.26	2010.0±0.5	2112.4±0.7	5325.0±0.6	5412.8±1.3

both PSM and VM. For the attractive COGEP for PSM, the contribution from the off-diagonal elements is found to be significant. For the VM, there is no substantial change in the masses by increasing n_{max} as COGEP is repulsive and hence perturbative techniques are adequate and are justified. There is a significant contribution from the colour electric term of COGEP in all the models. The masses for both PSM and VM converge to the experimental values when the diagonalisation is carried out in a larger basis, but the convergence is achieved in a smaller basis for VM for reasons stated earlier. The results show that RHM with COGEP provide a quite a good description of the S wave mesons.

ACKNOWLEDGEMENTS

The author (KBV) acknowledges the DST for funding the project (Sanction No. SR/S2/HEP-14/2006).

REFERENCES

Amsler, C. 2008. PDG Physics Letters. B667:1-42.

Bhaduri, RK., Cohler, LE. and Nogami, Y. 1981. A Unified Potential for Mesons and Baryons. Nuovo Cimento A. 65:376-390.

Bhavyashri., Vijaya Kumar, KB, Hanumaiah, B., Sarangi, S. and Shan-Gui Zhou. 2005. Meson spectrum in a non relativistic model with instanton – induced interaction. Journal of Physics G: Nuclear and Particle Physics. 31:981-986.

Bhavyashri, S., Godfrey., S. and Vijaya, KB. 2008. P wave Meson spectrum in a non relativistic model with instanton induced interaction. Pramana Journal of Physics. 70:G:75-85.

Blask, WH., Bohn, U., Huber, MG., Metsch, B. Ch. and Petry, HR. 1990. Hadron spectroscopy with instanton induced quark forces. Z. Phys. A337:327-335.

Brau, F., Semay, C. and Silvestre- Brac, B. 2000. Semiclassical model of light mesons. Physical Review D62:117501(1-4).

De Rujula, A., Georgi, H. and Glashow, SL. 1975. Hadron masses in a gauge theory. Physical Review. D12:147-162.

Godfrey, S. and Isgur, N. 1985. Mesons in a relativised quark model with chromodynamics Physical Review. D32:189-231.

Jena, SN. 1983. Mass spectra of light and heavy mesons in the Dirac equation with power-law potential Pramana. Journal of Physics. 21:247-255.

Khadkikar, SB. and Gupta, SK. 1983. Magnetic moments of light baryons in harmonic Model. Physics Letters. B124:523-526.

Khadkikar, SB. and Vijaya, KKB. 1991. N-N scattering with exchange of confined gluons. Physics Letters. B254:320-324.

Namgung, W. and Lichtenberg, DB. 1984. Meson spectra in a quark model with relativistic kinematics. Letter Al Nuovo Cimento. 41:597-603.

Rosner, JL. 2007. Heavy Quark Spectroscopy –Theory Overview. Journal of Physics. 69: 012002-012013.

Semay, C. and Silvestre- Brac, B. 1997. Potential models and meson spectra. Nuclear Physics. A618:455-482.

Semay, C. and Silvestre-Brac, B. 1999. Determination of quark- antiquark potentials and meson spectra. Nuclear Physics. A.647:72-96.

Takayuki, M., Toshiyuki, M. and Sudoh, K. 2007. Mass spectra of charmed and bottomed mesons in 1/mq expansion Progress of Theoretical Physics Supplement. 168:219-222.

Hooft, TG. 1976. Computation of the quantum effects due to a four dimensional pseudoparticle. Physical Review. D14:3432-3450.

Vijande, J., Fernandez, F. and Valcarce, A. 2005. Constituent quark model study of the meson spectra. Journal of Physics G: Nuclear and Particle Physics. 31:481-506.

Vijaya, Kumar, KB., and Khadkikar, SB. 1993. N-N interaction in a relativistic harmonic model with confined. Nuclear Physics. A556:396-408.

Vijaya, Kumar, KB., and Khadkikar, SB. 1998. Spin observables of the NN interaction in a relativistic harmonic model with confined gluons and mesons. Pramana- Journal of Physics. 50:149-153.

Vijaya, Kumar, KB., Hanumaiah, B. and Pepin, S. 2004. Meson spectrum in a relativistic harmonic model with instanton- induced interaction. The European Physical Journal. A19:247-250.

Vijaya, Kumar, KB., Bhavyshri, Yong-Ling Ma. and Antony, PM. 2009. P wave meson spectrum in a relativistic model with instanton induced interaction. International Journal of Modern Physics. A22:4209-4220.

Vinodkumar, PC., Vijaya Kumar, KB, and Khadkikar, SB. 1992. Effect of the confined gluons in quark-quark interaction. Pramana-Journal of Physics. 39:47-70.

Received: Oct 23, 2009; Revised: Dec 29, 2009; Accepted: Dec 30, 2009

SENRA Academic Publishers, Burnaby, British Columbia
Vol. 4, No. 1, pp. 1107-1111, 2010
ISSN: 1715-9997

Canadian Journal of pure&applied sciences

TRANSPORT OF VORTICITY IN VISCOELASTIC MAGNETIC FLUID PARTICLE MIXTURES THROUGH POROUS MEDIUM

*Pardeep Kumar[1] and Gursharn Jit Singh[2]
[1]Department of Mathematics, ICDEOL, Himachal Pradesh University, Shimla-171005, India
[2]SCD Govt. College, Ludhiana, Punjab, India

ABSTRACT

The transport of vorticity in viscoelastic Walters B′ fluid in the presence of suspended magnetic particles in porous medium is considered. Equations governing the transport of vorticity in Walters B′ viscoelastic fluid in the presence of suspended magnetic particles in porous medium are obtained from the equations of magnetic fluid flow proposed by Wagh and Jawandhia (1996). From these equations, it follows that the transport of solid vorticity $\vec{\Omega}$ is coupled with the transport of fluid vorticity $\vec{\Omega}_1$ in porous medium. Further, it is found that due to thermo-kinetic process, fluid vorticity may exist in the absence of solid vorticity in porous medium, but when fluid vorticity is zero, then solid vorticity is necessarily zero. A two-dimensional case is also studied.

Keywords: Walters B′ viscoelastic fluid, suspended magnetic particles, vorticity, porous medium.

INTRODUCTION

Magnetic fluids are those fluids in which magnetic particles are suspended in a liquid carrier. Thus, it is a two-phase system, consisting of solid and liquid phases. We shall suppose that the liquid phase is non-magnetic in nature and magnetic force acts only on the magnetic particles. Thus, the magnetic force changes the velocity of the magnetic particles. Consequently, the dragging force acting on the carrier liquid is changed and thus the flow of carrier liquid is also influenced by the magnetic force. Due to the relative velocity between the solid and liquid particles, the net effect of the particles suspended in the fluid is extra dragging force acting on the system. In recent years, there has been considerable interest in the study of magnetic fluids. Saffman (1962) proposed the equations of the flow of suspension of non-magnetic particles. These equations were modified by Wagh (1991) to describe the flow of magnetic fluid, by including the magnetic body force $\mu_0 M \nabla H$. Wagh and Jawandhia (1996) have studied the transport of vorticity in a magnetic fluid. Transport and sedimentation of suspended particles in inertial pressure-driven flow has been considered by Yan and Koplik (2009). With the growing importance of non-Newtonian fluids in modern technology and industries, investigations on such fluids are desirable. Widely used theoretical models (models A and B, respectively) for certain classes of viscoelastic fluids have been proposed by Oldroyd (1958). The thermal instability of Maxwellian viscoelastic fluid in the presence of a uniform rotation has been considered by Bhatia and Steiner (1972), where rotation is found to have a destabilizing effect. This is in contrast to the thermal instability of a Newtonian fluid where rotation has a stabilizing effect. The thermal instability of an Oldroydian viscoelastic fluid acted on by a uniform rotation has been studied by Sharma (1976). An experimental demonstration by Toms and Strawbridge (1953) has revealed that a dilute solution of methyl methacrylate in n-butyl acetate agrees well with the theoretical model of Oldroyd (1958). There are many viscoelastic fluids that cannot be characterized by Maxwell's or Oldroyd's constitutive relations. One such fluid is Walters B′ viscoelastic fluid (1960), having relevance and importance in geophysical fluid dynamics, chemical technology, and petroleum industry. Walters (1962) reported that the mixture of polymethyl methacrylate and pyridine at 25^0C containing 30.5g of polymer per litre with a density of 0.98g/litre behaves very nearly as the Walters B′ viscoelastic fluid. Polymers are used in the manufacture of spacecrafts, aeroplanes, tyres, belt conveyers, ropes, cushions, seats, foams, plastics engineering equipments, contact lens etc. Walters B′ viscoelastic fluid forms the basis for the manufacture of many such important and useful products. Sharma and Kumar (1998) have studied the Rayleigh-Taylor instability of two superposed conducting Walters B′ elastico-viscous fluids in hydromagnetics. Kumar (2001) has studied the effect of rotation on thermal instability in Walters B′ elastico-viscous fluid. In another study, Kumar *et al.* (2006) have studied the stability of two superposed Walters B′ viscoelastic fluids permeated with suspended particles. The medium has been considered to be non-porous in all the above studies. In recent years, the

*Corresponding author email: pkdureja@gmail.com

investigations of flow of fluids through porous media have become an important topic due to the recovery of crude oil from the pores of reservoir rocks. A great number of applications in geophysics may be found in the books by Phillips (1991), Ingham and Pop (1998), and Nield and Bejan (1999). When the fluid permeates a porous material, the gross effect is represented by the Darcy's law. As a result of this macroscopic law, the usual viscous term in the equations of fluid motion is replaced by the resistance term $-\frac{1}{k_1}\left(\mu-\mu'\frac{\partial}{\partial t}\right)\vec{q}$, where μ and μ' are the viscosity and viscoelasticity of the Walters B′ fluid, k_1 is the medium permeability and $\vec{q}$ is the Darcian (filter) velocity of the fluid. The Rayleigh instability of a thermal boundary layer in flow through porous medium has been considered by Wooding (1960). Kumar (1998) has studied the stability of two superposed Walters B′ viscoelastic fluid-particle mixtures in porous medium. Kumar *et al*. (2006) have studied the MHD instability of rotating superposed Walters B′ viscoelastic fluids through a porous medium. Kumar and Singh (2007) have studied the instability of two rotating viscoelastic (Walters B′) superposed fluids with suspended particles in porous medium.

Keeping in mind the importance of non-Newtonian fluids in modern technology and industries and owing to the importance of porous medium in chemical engineering and geophysics, the present paper attempts to study the transport of vorticity in magnetic Walters B′ viscoelastic fluid-particle mixtures in porous medium by using the equations proposed by Wagh and Jawandhia (1996).

DISCUSSION

Basic Assumptions and Magnetic Body Force

Particles of magnetic material are much larger than the size of the molecules of carrier liquid. Accordingly considering the limit of a microscopic volume element in which a fluid can be assumed to be a continuous medium and the magnetic particles must be treated as discrete entities. Now, if one considers a cell of magnetic fluid containing a larger number of magnetic particles then one must consider the microrotation of the cell in addition to its translations as a point mass. Thus, one has to assign average velocity $\vec{q}_d$ and the average angular velocity $\vec{\omega}$ of the cell. But, here as an approximation, we neglect the effect of microrotation. We shall also make the following assumptions:

(i) Most of the ferrofluids are relatively poor conductors and hence free current density $\vec{J}$ is negligible and hence $\vec{J}\times\vec{B}$ is assumed to be insignificant.

(ii) The magnetic field is assumed to be curl free i.e. $\nabla\times\vec{H}=0.$

(iii) In many practical situations liquid compressibility is not important. Hence contribution due to magnetic friction can be neglected. The remaining force of magnetic field is referred as magnetization force.

(iv) All time-dependent magnetization effects in the fluid such as hysteresis are assumed to be negligible and the magnetization $\vec{M}$ is assumed to be collinear with $\vec{H}$.

From electromagnetic theory, the force per unit volume in MKS units on a piece of magnetized material of magnetization $\vec{M}$ (i.e. dipole moment per unit volume) in the field of magnetic intensity $\vec{H}$ is $\mu_0\left(\vec{M}.\nabla\right)\vec{H}$, where μ_0 is the free space permeability. Using assumption (iv)

$\mu_0\left(\vec{M}.\nabla\right)\vec{H}=\frac{\mu_0 M}{H}\left(\vec{H}.\nabla\right)\vec{H}$, where $M=\left|\vec{M}\right|$ and $H=\left|\vec{H}\right|$. (1)

But $\left(\vec{H}.\nabla\right)\vec{H}=\frac{1}{2}\nabla\left(\vec{H}.\vec{H}\right)-\vec{H}\times\left(\nabla\times\vec{H}\right)=\frac{1}{2}\nabla\left(\vec{H}.\vec{H}\right)$

[by assumption (ii)]. (2)

Hence $\mu_0\left(\vec{M}.\nabla\right)\vec{H}=\left(\frac{\mu_0 M}{H}\right)\frac{1}{2}\nabla\left(\vec{H}.\vec{H}\right)=\mu_0 M\nabla H.$

Thus the magnetic body force assumes the form (Rosensweig, 1997)

$$f_m=\mu_0 M\nabla H. \quad (3)$$

Derivation of Equations Governing Transport of Vorticity in Magnetic Viscoelastic Walters B′ Fluid

Wagh (1991) modified the Saffman's equations for flow of suspension to describe the flow of magnetic fluid by including the body force $\mu_0 M\nabla H$ acting on the suspended magnetic particles. Now the equations expressing the flow of suspended magnetic particles and the flow of viscoelastic Walters B′ fluid in which magnetic particles are suspended in porous medium are

$$\frac{mN}{\varepsilon}\left[\frac{\partial\vec{q}_d}{\partial t}+\frac{1}{\varepsilon}\left(\vec{q}_d.\nabla\right)\vec{q}_d\right]=mN\vec{g}+\mu_0 M\nabla H+\frac{KN}{\varepsilon}\left(\vec{q}-\vec{q}_d\right), \quad (4)$$

$$\frac{\rho}{\varepsilon}\left[\frac{\partial\vec{q}}{\partial t}+\frac{1}{\varepsilon}\left(\vec{q}.\nabla\right)\vec{q}\right]=-\nabla P+\rho\vec{g}-\frac{1}{k_1}\left(\mu-\mu'\frac{\partial}{\partial t}\right)\vec{q}+\frac{KN}{\varepsilon}\left(\vec{q}_d-\vec{q}\right), \quad (5)$$

where ε is the medium porosity and is defined as $\varepsilon=\frac{volume\ of\ the\ voids}{total\ volume}$, $(0<\varepsilon<1)$.

For very fluffy foam materials, ε is nearly one and in bed of packed spheres in the range 0.25-0.50.

In the equations of motion for the fluid, the presence of suspended particles adds an extra force term, proportional to the velocity difference between suspended particles and fluid. Since the force exerted by the fluid on the suspended particles is equal and opposite to that exerted by the particles on the fluid, there must be an extra force term, equal in magnitude but opposite in sign, in the equations of motion for the suspended particles.

Making use of the Lagrange's vector identities

$$(\vec{q}_d.\nabla)\vec{q}_d = \frac{1}{2}\nabla q_d^2 - \vec{q}_d \times \vec{\Omega}\,,\ (\vec{q}.\nabla)\vec{q} = \frac{1}{2}\nabla q^2 - \vec{q}\times\vec{\Omega}_1\,, \quad (6)$$

equations (4) and (5) become

$$\frac{mN}{\varepsilon}\left[\frac{\partial \vec{q}_d}{\partial t} - \frac{1}{\varepsilon}\left(\vec{q}_d \times \vec{\Omega}\right)\right] = -mNgz - \frac{1}{2\varepsilon^2} mN\nabla q_d^2 + \mu_0 M\nabla H + \frac{KN}{\varepsilon}(\vec{q} - \vec{q}_d), \quad (7)$$

$$\frac{\rho}{\varepsilon}\left[\frac{\partial \vec{q}}{\partial t} - \frac{1}{\varepsilon}\left(\vec{q}\times\vec{\Omega}_1\right)\right] = -\nabla P - \nabla\rho gz - \frac{1}{2\varepsilon^2}\rho\nabla q^2 - \frac{1}{k_1}\left(\mu - \mu'\frac{\partial}{\partial t}\right)\vec{q} + \frac{KN}{\varepsilon}(\vec{q}_d - \vec{q}), \quad (8)$$

where $\vec{\Omega} = \nabla\times\vec{q}_d$ and $\vec{\Omega}_1 = \nabla\times\vec{q}$ are solid vorticity and fluid vorticity.

Taking the curl of these equations and keeping that the curl of a gradient is identically zero, we have

$$\frac{mN}{\varepsilon}\left[\frac{\partial\vec{\Omega}}{\partial t} - \frac{1}{\varepsilon}\left(\nabla\times\vec{q}_d\times\vec{\Omega}\right)\right] = \mu_0\nabla\times M\nabla H + \frac{KN}{\varepsilon}\left(\vec{\Omega}_1 - \vec{\Omega}\right), \quad (9)$$

$$\frac{\rho}{\varepsilon}\left[\frac{\partial\vec{\Omega}_1}{\partial t} - \frac{1}{\varepsilon}\left(\nabla\times\vec{q}\times\vec{\Omega}_1\right)\right] = -\frac{1}{k_1}\left(\mu - \mu'\frac{\partial}{\partial t}\right)\vec{\Omega}_1 + \frac{KN}{\varepsilon}\left(\vec{\Omega} - \vec{\Omega}_1\right). \quad (10)$$

By making use of the vector identities

$$\nabla\times\left(\vec{q}_d\times\vec{\Omega}\right) = \left(\vec{\Omega}.\nabla\right)\vec{q}_d - \left(\vec{q}_d.\nabla\right)\vec{\Omega} + \vec{q}_d\nabla.\vec{\Omega} - \vec{\Omega}\nabla.\vec{q}_d = \left(\vec{\Omega}.\nabla\right)\vec{q}_d - \left(\vec{q}_d.\nabla\right)\vec{\Omega}\,, \quad (11)$$

$$\nabla\times\left(\vec{q}\times\vec{\Omega}_1\right) = \left(\vec{\Omega}_1.\nabla\right)\vec{q} - \left(\vec{q}.\nabla\right)\vec{\Omega}_1 + \vec{q}\nabla.\vec{\Omega}_1 - \vec{\Omega}_1\nabla.\vec{q} = \left(\vec{\Omega}_1.\nabla\right)\vec{q} - \left(\vec{q}.\nabla\right)\vec{\Omega}_1\,, \quad (12)$$

equations (9) and (10) become

$$\frac{mN}{\varepsilon}\frac{D\vec{\Omega}}{Dt} = \mu_0\nabla\times M\nabla H + \frac{mN}{\varepsilon^2}\left(\vec{\Omega}.\nabla\right)\vec{q}_d + \frac{KN}{\varepsilon}\left(\vec{\Omega}_1 - \vec{\Omega}\right), \quad (13)$$

$$\frac{D\vec{\Omega}_1}{Dt} = -\frac{\varepsilon}{k_1}\left(\nu - \nu'\frac{\partial}{\partial t}\right)\vec{\Omega}_1 + \frac{1}{\varepsilon}\left(\vec{\Omega}_1.\nabla\right)\vec{q} + \frac{KN}{\rho}\left(\vec{\Omega} - \vec{\Omega}_1\right), \quad (14)$$

where ν *and* ν' are kinematic viscosity and kinematic viscoelasticity, respectively and $\frac{D}{Dt} = \frac{\partial}{\partial t} + \frac{1}{\varepsilon}(\vec{q}_d.\nabla)$ is the convective derivative.

In equation (13),

$$\nabla\times\left(M\nabla H\right) = \left(\nabla M\times\nabla H\right) + \left(M\nabla\times\nabla H\right). \quad (15)$$

Since the curl of the gradient is zero, the last term in equation (15) is zero. Also since

$M = M(H,T)$.

Therefore, $\nabla M = \left(\frac{\partial M}{\partial H}\right)\nabla H + \left(\frac{\partial M}{\partial T}\right)\nabla T.$ (16)

By making use of (16), equation (15) becomes

$$\nabla\times\left(M\nabla H\right) = \left(\frac{\partial M}{\partial H}\right)\nabla H\times\nabla H + \left(\frac{\partial M}{\partial T}\right)\nabla T\times\nabla H\,. \quad (17)$$

The first term on the right hand side of this equation is clearly zero, hence we get

$$\nabla\times\left(M\nabla H\right) = \left(\frac{\partial M}{\partial T}\right)\nabla T\times\nabla H\,. \quad (18)$$

Putting this in equation (13), we get

$$\frac{mN}{\varepsilon}\frac{D\vec{\Omega}}{Dt} = \mu_0\left(\frac{\partial M}{\partial T}\right)\nabla T\times\nabla H + \frac{mN}{\varepsilon^2}\left(\vec{\Omega}.\nabla\right)\vec{q}_d + \frac{KN}{\varepsilon}\left(\vec{\Omega}_1 - \vec{\Omega}\right). \quad (19)$$

Here (14) and (19) are the equations governing the transport of vorticity in magnetic viscoelastic Walters B′ fluid-particle mixtures in porous medium.

In equation (19), the first term $\mu_0\left(\frac{\partial M}{\partial T}\right)\nabla T\times\nabla H$ describes the production of vorticity due to thermo-kinetic processes. The last term $\frac{KN}{\varepsilon}\left(\vec{\Omega}_1 - \vec{\Omega}\right)$ gives the change in solid vorticity on account of exchange of vorticity between the liquid and solid in porous medium.

From equations (14) and (19), it follows that the transport of solid vorticity $\vec{\Omega}$ is coupled with the transport of fluid vorticity $\vec{\Omega}_1$ in porous medium.

From equation (19), we see that if solid vorticity $\vec{\Omega}$ is zero, then the fluid vorticity $\vec{\Omega}_1$ is not zero, but it is given by

$$\vec{\Omega}_1 = -\frac{\varepsilon\mu_0}{KN}\left(\frac{\partial M}{\partial T}\right)\nabla T\times\nabla H. \quad (20)$$

This implies that due to thermo-kinetic process, fluid vorticity may exist in the absence of solid vorticity in porous medium. Equation (20) also shows that fluid

vorticity decreases in the presence of porosity. In the absence of porous medium $(\varepsilon = 1)$

$$\vec{\Omega}_1 = -\frac{\mu_0}{KN}\left(\frac{\partial M}{\partial T}\right)\nabla T \times \nabla H. \quad (21)$$

This is in conformity with Wagh and Jawandhia (1996) result.

From equation (14), we find that if $\vec{\Omega}_1$ is zero, then $\vec{\Omega}$ is also zero. This implies that **when fluid vorticity is zero, then solid vorticity is necessarily zero.**

In the absence of suspended magnetic particles, N is zero and magnetization M is also zero, so equation (19) is identically satisfied and equation (14) reduces to

$$\frac{D\vec{\Omega}_1}{Dt} = -\frac{\varepsilon}{k_1}\left(\nu - \nu'\frac{\partial}{\partial t}\right)\vec{\Omega}_1 + \frac{1}{\varepsilon}\left(\vec{\Omega}_1.\nabla\right)\vec{q}. \quad (22)$$

This equation is vorticity transport equation in porous medium. The last term on the right hand side of equation (22) represents the rate at which $\vec{\Omega}_1$ varies for a given particle, when the vortex lines move with the fluid, the strengths of the vortices remaining constant. The first term represents the rate of dissipation of vorticity through friction (resistance) and rate of change of vorticity due to fluid viscoelasticity.

Two-Dimensional Case

Here we consider the two-dimensional case:

Let ,

$$\vec{q}_d = q_{d_x}(x,y)\hat{i} + q_{d_y}(x,y)\hat{j} \ ,$$
$$\vec{q} = q_x(x,y)\hat{i} + q_y(x,y)\hat{j} \quad (23)$$

where components q_{d_x}, q_{d_y} *and* q_x, q_y are functions of x, y *and* t, then

$$\vec{\Omega} = \Omega_z\hat{k} \ , \ \vec{\Omega}_1 = \Omega_{1z}\hat{k} \ . \quad (24)$$

In two-dimensional case, equation (19) becomes

$$\frac{D\Omega_z}{Dt} = \frac{\mu_0\varepsilon}{mN}\left(\frac{\partial M}{\partial T}\right)\left(\frac{\partial T}{\partial x}\frac{\partial H}{\partial y} - \frac{\partial H}{\partial x}\frac{\partial T}{\partial y}\right) + .$$
$$\frac{K}{m}\left(\Omega_{1z} - \Omega_z\right). \quad (25)$$

Similarly, equation (14) becomes

$$\frac{D\Omega_{1z}}{Dt} = -\frac{\varepsilon\nu}{k_1}\Omega_{1z} + \frac{\varepsilon\nu'}{k_1}\frac{\partial}{\partial t}\Omega_{1z} +$$
$$\frac{KN}{\rho}\left(\Omega_z - \Omega_{1z}\right), \quad (26)$$

since it can be easily verified that

$$\left(\vec{\Omega}.\nabla\right)\vec{q}_d = 0 \ and \ \left(\vec{\Omega}_1.\nabla\right)\vec{q} = 0. \quad (27)$$

The first term on the right hand side of equation (26) is the change of fluid vorticity due to internal friction (resistance), the second term is the rate of change of fluid vorticity due to fluid viscoelasticity and the third term is change in fluid vorticity on account of exchange of vorticity between solid and liquid. Equation (26) does not involve explicitly the term representing change of vorticity due to magnetic field gradient and/or temperature gradient. But equation (25) shows that solid vorticity Ω_z depends on these factors. Hence, it follows that **fluid vorticity is indirectly influenced by the temperature and the magnetic field gradient.**

In the absence of magnetic particles, N is zero and magnetization M is also zero, so equation (25) is identically satisfied and equation (26) reduces to classical equation of transport of vorticity for fluid in porous medium. If instead of magnetic field we consider a suspension of non-magnetic particles, then the corresponding equation for the transport of vorticity may be obtained by putting M equal to zero in the equations governing the transport of vorticity in magnetic fluids. If magnetization M of the magnetic particles is independent of temperature, then the first term of equations (19) and (25) vanish and so the equations governing the transport of vorticity in magnetic fluid in porous medium are same as those which govern the transport of vorticity in non-magnetic suspensions in porous medium.

If the temperature gradient ∇T vanishes or if the magnetic field gradient ∇H vanishes or if ∇T is parallel to ∇H, then also the first term of equations (19) and (25) vanish. Thus, we see that in this case also the transport of vorticity in magnetic fluid in porous medium is same as transport of vorticity in non-magnetic suspension in porous medium.

REFERENCES

Bhatia, PK. and Steiner, JM. 1972. Convective instability in a rotating viscoelastic fluid layer. Z. Angew. Math. Mech. 52:321-324.

Ingham, DB. and Pop, I. 1998. Transport phenomena in porous medium. Pergamon Press. Oxford, UK.

Kumar, P. 1998. Stability of two superposed viscoelastic (Walters B′) elastico-viscous fluids in hydromagnetics. Z. Naturforsch., Germany. 54a:343-347.

Kumar, P. 2001. Effect of Rotation on thermal instability in Walters B′ elastico-viscous fluid. Proc. Nat. Acad. Sci. A, Phys. Sci. India. 71A:33-41.

Kumar, P., Mohan, H. and Singh, GJ. 2006. Stability of two superposed viscoelastic fluid-particle mixtures. Z. Angew. Math. Mech. Germany. 86:72-77.

Kumar, P., Lal, R. and Singh, GJ. 2006. MHD instability of rotating superposed Walters B′ viscoelastic fluids through a porous medium. J. Porous Medium. 9(5):463-468.

Kumar, P. and Singh, M. 2007. Instability of two rotating viscoelastic (Walters B′) superposed fluids with suspended particles in porous medium. Thermal Science. 11(1):93-102.

Nield, DA. and Bejan, A. 1999. Convection in porous medium (2nd ed.). Springer Verlag, New York, USA.

Oldroyd, JG. 1958. Non-Newtonian effects in steady motion of some motion idealized elastico-viscous liquids. Proc. Roy. Soc. London. A245:278-279.

Phillips, OM. 1991. Flow and reaction in permeable rocks, Cambridge University Press, Cambridge, UK.

Rosensweig, RE. 1997. Ferrohydrodynamics. Dover Publications. Inc. Mineola, New York.

Saffman, P. 1962. On the stability of a laminar flow of a dusty gas. J. Fluid Mech. 13:120-128.

Sharma, RC. 1976. Effect of rotation on thermal instability of a viscoelastic fluid. Acta Physica Hung. 40:11-17.

Sharma, RC. and Kumar, P. 1998. Rayleigh-Taylor instability of two superposed conducting Walters B' elastico-viscous fluids in hydromagnetics. Proc. Nat. Acad. Sci. India A, Phys. Sci. 68:151-161.

Toms, BA. and Strawbridge, DJ. 1953. Elastic and viscous properties of dilute solutions of polymethyl methacrylate in organic liquids. Trans. Faraday Soc. 49:1225-1232.

Wagh, DK. 1991. A Mathematical model of magnetic fluid considered as two-phase system. Proc. Int. Symp. on Magnetic Fluids, held at REC Kurukshetra, India, during Sept. 21:23-182.

Wagh, DK. and Jawandhia, A. 1996. Transport of vorticity in magnetic fluid. Indian J. Pure Appl. Phys. India. 34:338-340.

Walters, K. 1960. The motion of elastico-viscous liquid contained between coaxial cylinders. J. Mech. Appl. Math. 13:444-453.

Walters, K. 1962. The solution of flow problems in case of materials with memory. J. Mecanique. 1:469-479.

Wooding, RA. 1960. Rayleigh instability of a thermal boundary layer in flow through a porous medium. J. Fluid Mech. 9:183-192.

Yan, Y. and Koplik, J. 2009. Transport and sedimentation of suspended particles in inertial pressure-driven flow. Phys. Fluids. 21:013301.

Received: Aug 14, 2009; Revised: Jan 4, 2010; Accepted: Jan 8, 2010

SENRA Academic Publishers, Burnaby, British Columbia
Vol. 4, No. 1, pp. 1113-1117, 2010
ISSN: 1715-9997

Canadian Journal of pure&applied sciences

NEUTRON ACTIVATION AND FLAME ATOMIC ABSORPTION ELEMENTAL ANALYSES OF SELECTED HAIR DYES

Margaret A Briggs-Kamara[1], Alaiyi G Warmate[1], *Yehuwdah E Chad-Umoren[2] and Chukwuemeka M Ibechedor[1]
[1]Department of Physics, Rivers State University of Science and Technology, PMB- 5080, Port Harcourt, Nigeria
[2]Department of Physics, University of Port Harcourt, PMB- 5323 Port Harcourt, Nigeria

ABSTRACT

In this study, two hair dye types, one liquid and the other solid, were analyzed to determine their elemental compositions and possible radioactivity. The liquid dye sample was analyzed using Flame Atomic Absorption Spectroscopy and based on the American Standard Test Method (ASTM), five ions namely: Fe^{2+}, Pb^{2+}, Cd^{2+}, S^{2-}, and SO_4^{2-} were detected with concentrations of 0.702, 0.002, 0.003, 0.044, and 0.059mg.l^{-1} respectively. The solid hair dye sample was analyzed using the Neutron Activation Analysis technique. Eighteen elements (Al, Ti, K, Fe, Na, V, Mn, Sb, La, Sm, Sc, Cs, Eu, Br, Ce, and Th) were measured. Six of the elements (Al, Na, Eu, Br, Ce, and Th) were found in trace concentrations of 31.9± 5.4, 40.6 ± 5.9, 0.16 ± 0.05, 0.18 ± 0.04, 0.37 ± 0.08, and 0.13± 0.02 ppm respectively. Ce and Eu presently have no known negative effect on humans, while Pb, Cd, and Fe cannot easily get into the body through skin absorption. Hence the application of dyes containing these elements may not bring about effects associated with the intake of these elements, unless the dye mistakenly finds its way into food. The presence of Al, Na, Br, Th, S, and SO_4 could result to those adverse effects associated with each element. In addition, the major active ingredient; Paraphelylene diamine (1, 4-diaminobenzene) has cancerous effects usually directed at the bladder.

Keywords: Hair dye, elemental composition, flame atomic absorption spectroscopy, neutron activation, trace concentrations, cancerous effects.

INTRODUCTION

Due to adverse environmental conditions in recent times which include enhanced green house effect, excessive air and water pollution, noise (vibration), and thermal pollution, man is faced with untimely ageing with such symptoms as the wrinkling of the skin and the emergence of grey hair (Lind *et al*., 2005). As a result, there is need for man to device means of improving his looks. One of these means is the application of hair dye by some individuals, especially the middle-aged group.

Hair dyes are those chemicals used to darken or change the color of human or animal hair to a desired colour. The change is due to the ability of the dye to emit only light whose wavelength is that of the desired colour, while all other wavelengths are absorbed (Sadaji *et al*., 1982). Based on their duration or persistency, hair dyes can be grouped into three main types: permanent, semi-permanent, and temporary dyes. Temporary dyes can be removed in just one washing. They are mainly used for festive purposes and then washed off after the activity. Temporary dyes do not change the natural underlying colour of the hair. The risk associated with the use of temporary dyes is negligible. Semi-permanent dyes are mostly organic and do not involve developers like hydrogen peroxide, to fix the color in the hair fiber. They can survive through several washings before being depleted. How long the dye lasts depends on the active ingredients, the frequency of hair washing, and also the frequency of exposure to environmental modifiers like sunlight, and chemicals in the air (Vann, 2000). The permanent dye gives the most dramatic color change. Users of this dye usually have visible roots as their hair grows. These dye types have very high affinity for hair fibers, hence cannot be removed by washing (Lind *et al*., 2005).

Hair dye analysis is essential as many of the available formulations are known to be unsuitable for human use (Allan, 2005; Hans and Tlaytmas, 2000; Lind *et al*., 2005; Sϕoted *et al*., 2004; Vann, 2000). Some constituents have been found to be carcinogenic and there have been suspected cases of breast and duodenal cancer after prolonged use of certain hair dyes (Andrew, 2000). Furthermore, there is now a growing risk of occupational skin diseases among hair dressers from exposure to skin irritants and sensitizers (Lind *et al*., 2005). Severe allergic contact dermatitis has been observed in hairdressers, their clients and home users of permanent hair dyes (Sϕoted *et al*., 2004; Lind *et al*., 2005).

Most of these dyes change to the required color on exposure to ultra-violet radiation from the sun, which is also a carcinogen. When the skin is exposed to UV

*Corresponding author email: echadumoren@yahoo.com

radiation, it acts directly on the skin cells, causing changes in the cell DNA. This effect may result to skin cancer if the body repair mechanism is slow. Some active ingredients in hair dyes exert their effect about twenty years or more after initial use (Allan, 2005) while continuous use produces more effects in later years. Hair dye studies often focus on analyzing the organic compound constituents of the dye. Sadaji *et al*. (1982) have used high performance liquid chromatography (HPLC) to determine the organic compounds present in commercial oxidative hair dyes. Using the same HPLC approach Vincent *et al*. (1999) have studied the effect of matrix compounds on the analysis of the organic compounds in hair dyes. The work of Shih *et al*. (2004) employed a screen – printed electrode to evaluate the toxic lead level in hair dyes.

In this present study, we seek to determine the elements that are present in hair dyes. To do this we use two techniques, viz flame atomic absorption spectroscopy (FAAS) and neutron activation analysis (NAA). We further investigate the possible presence of radioactivity in hair dyes as a result of the presence of radioactive elements in the dyes.

Atomic Absorption is based on the measurement of light irradiation absorbed by unexcited ground state atom of analyte. If the atoms are produced by a flame, it is called Flame Atomic Absorption Spectroscopy (FAAS). If the atoms are produced by other means, for example electrical, it is called non-flame or flameless atomic absorption. The flame is known as the atom cell or the atomizer. The outlay consists of a light source, usually a hollow cathode lamp. This light source is usually made up of the material of the analyte, that is, the material to be determined, for example a nickel or lead lamp. The lamp is followed by the monochromator (usually made of a filter, prism or grating) and a detecting device (usually a micro-processor or a moving coil galvanometer, or stripe chart recorder). The absorption technique is used for the determination of several elements in several environmental samples like soil, rock, water, plant, clinical, cosmetics, and food (Schrenk, 1975). They are not used for potassium, sodium, calcium, because they are soft metals (that is alkali and alkaline earth metals).

Neutron activation analysis is a sensitive analytical technique used for both qualitative and quantitative multi-element analysis of major, minor and trace elements. To determine the concentration of elements in a given sample, both the sample and a comparator standard containing a known amount of the element of interest are irradiated within the reactor. The mass of an element in the sample relative to the comparator standard is then given by:

$$\frac{A_{sam}}{A_{std}} = \frac{M_{sam}}{M_{std}} \frac{\left(e^{-\lambda T_d}\right)_{sam}}{\left(e^{-\lambda T_d}\right)_{std}} \quad (1)$$

where A_{sam}, A_{std} are the activity of the sample and the activity of the standard respectively; M mass of the element; λ decay constant of the isotope and T_d decay time (Akaho and Nyarko, 2002).

For short irradiations, the irradiation, decay and counting times have the same fixed value for both sample and standard so that the time-dependent factor cancels and eq (1) then becomes:

$$C_{sam} = C_{std} \frac{W_{std}}{W_{sam}} \frac{A_{sam}}{A_{std}} \quad (2)$$

where C_{is} the concentration of the element and W is the weight of the sample and the standard.

The sensitivity for NAA depends on the irradiation parameters (neutron flux, irradiation and decay times); measurement conditions (measurement time, detector efficiency) and nuclear parameters of the element being measured (isotope abundance, neutron cross – section and half-life).

Health effects associated with elements identified in the two analyses (NAA and FAAS) include: damage to central nervous system; dementia; loss of memory; restlessness and severe trembling; disturbances in genetic materials; cancer; damage to the lungs and kidneys (David and Norman, 2005); diarrhea; stomach pains and severe vomiting; anaemia; loss of appetite; abdominal pain; constipation; fatigue, headache and kidney problems; skin, eyes, nose and throat irritation causing sneezing and coughing; difficulty in breathing and chemical bronchitis; disturbance of blood circulation; heart damage; reproductive failure; damage to liver and kidney functions. Apart from serving as a medium for further sensitizing hair dye users, this work will also serve as a reminder to hair dye manufacturers of the need to use human friendly elements in their products and formulations.

MATERIALS AND METHODS

Three methods were used in carrying out the analysis. The first was the use of questionnaires to get the responses of hair dye users on the kind of dyes they use as well as any unexplained medical condition they encounter. Flame Atomic Absorption Spectroscopy (FAAS) was used to analyze the liquid dye sample selected through the information realized from the questionnaire, while

Neutron Activation Analysis (NAA) was used to analyze the solid dye sample.

This questionnaire was designed to have three parts. The first part revealed the name and form of dyes used. The second part was on the frequency and number of years of usage. The third part dealt with unexplained medical history: Respondents had to select from a list of illnesses (stomach upset, vomiting, diarrhea, headache, nausea, and weakness, loss of appetite, body pains, urinary problems, and indigestion) or specify any not in the list.

The FAAS (carried out at the Central Research Laboratory, University of Uyo, Akwa Ibom State, Nigeria**)**, a standard solution of the analyte (the liquid dye) using distilled water was prepared. A stock solution was prepared, followed by a serial dilution of the stock solution. The instrument was switched on and allowed to run for about 30minutes to warm up. The gas was turned on and the flow rate adjusted until a blue flame (2- layer distinct) was observed. A premixed gas with a laminar flow was used. The instrument was zeroed with the zero adjustable knobs. The clamp which unlocks the read out device was removed. The instrument was checked for full scale deflection. The blank solution (de-ionized water) was aspirated and the instrument zeroed. The maximum standard was aspirated and the instrument adjusted to give full scale reading at 100. Blank and maximum standard were rechecked thrice. Each standard solution was aspirated and the instrument scale reading obtained. A calibration graph was plotted. In addition to all the steps already presented, it is necessary to add that a concentration step was required generally for water sample. A known volume of about 500 ml of the water sample was taken, and extracted in the extraction flask. Two important extracts are usually used like Ammonium Pyroline Dithio-Carbamate (APDC) and Methyl Isobutyl Ketone (MIBK). They are called chelating agents. During extraction process, two layers were observed in the extraction flask because water and APDC do not mix. The water layer is drained off through the tap. All the metals were concentrated in the APDC layer but MIBK was added to the APDC to concentrate the metals before aspiration to Atomic absorption instrument. All the elements analyzed for are suspected chemical carcinogens. Part of the sample used to analyze for trace metals was digested with nitric acid to remove organic matter and to dissolve the metals.

The Nigerian Research Reactor 1 (NIRR-I) was used for the NAA. The analysis was done at the Centre for Energy Research and Training, Ahmadu Bello University, Zaria, Nigeria. It is a miniature neutron source reactor (MNSR) and has a tank-in-pool structural configuration with a nominal thermal power rating of 31KW. NIRR-1 is specifically designed for neutron activation analysis and it has enhanced the capability for the analyses of trace minor and major elements in different sample matrices. The neutron flux parameters of MNS reactors are known to be very stable, thus permitting the use of semi-absolute NAA method (Akaho and Nyarko, 2002; Jonah *et al*., 2006). The procedures involved include minimum sample preparation, two irradiation regimes and four counting strategies, which have been adopted on the basis of the half-life of product radionuclide and the neutron spectrum parameters in the inner and outer irradiation channels. The NIRR-1 has highly enriched uranium as fuel, light water as moderator and Beryllium as reflector. The associated facility for radioactive measurement is a gamma-ray data acquisition system. It consists of a horizontal, deep-stick high purity germanium (HPGe) detector with a relative efficiency of 10% at 1332.5KeV gamma ray line, the MAESTRO emulation software compatible with the ADCAM^{R} multi-channel analyzer (MCA) card. There are also associated electronic modules, all made by EG&G ORTEC and a personal computer. The efficiency curves of the detector system at near and far source detector geometrics have been determined by standard gamma ray sources in the energy range of 59.5-2254KeV and were extended to 4000KeV by a semi-empirical method. For data processing, the gamma-ray spectrum analysis software; WINSPAN2004 (Liyu, 2004) is used. It is software developed at CIAE, Beijing, China. On the basis of a well known activation equation, the software requires that calibration factor be pre-determined by a multi-element standard reference material for elements of interest using adopted irradiation and counting regimes. In addition to NAA calculations, WINSPAN2004 performs peak analysis, remote-control of the MCA and other auxiliary functions such as efficiency calibration and nuclear data generation.

RESULTS AND DISCUSSION

Seventy-eight percent of questionnaires given out were substantially filled. The responses showed that the most commonly used solid dye was Paraphenyleme Diamine (PPD) and the liquid dye was “Youth hair” dye. A theoretical survey of the constituents of these dyes showed that all the dye brands comprised of azonium compounds. Results obtained from the questionnaire showed that the longer the usage time, the more the unexplained medical conditions. The medical conditions are shown in figure 1. Those with significant percentage occurrence were headache (16%), body pains and stomach upset (15.5%), and weakness (15%). Next to these were urinary problems (9.5%), indigestion (8.5%) and loss of appetite (6%). It should however be noted that, some interfering habits like smoking, snuff intake and drinking of alcohol may present symptoms similar to those suspected to be caused by hair dye usage.

The result of the analysis from Flame Atomic Absorption Spectroscopy (FAAS) is tabulated in table 1. The result is

Table 1. Sample Parameters in mg/l for the liquid hair dye using FAAS.

S/N	SAMPLE ID	ASTM D3539 Fe^{2+}	ASTM D3557 Pb^{2+}	ASTM D516 Cd^{2+}	ASTM D4658 S^{2-}	ASTM D4658 SO_4^{2-}
1	A	0.702	0.002	0.003	0.044	0.059

based on the American Standard Test Method (ASTM). Five ions namely: Fe^{2+}, Pb^{2+}, Cd^{2+}, S^{2-}, and SO_4^{2-} were detected with concentrations of 0.702, 0.002, 0.003, 0.044, and 0.059mg.l^{-1} respectively. No permissible limits have been quoted specifically in hair by any regulatory authority for any of the ions. However, permitted Dietary Reference Intake level for Fe^{2+} in the human body is 45mg/kg. Permissible levels for Pb are 1.5µg/m^3 (United States Environmental Protection Agency) and 50µg/m^3 (United States Occupational Safety and Health Administration). In air the permissible levels for Cd are 5ppb (United States Environmental Protection Agency). Though the metals observed in the sample are in traces, there is a high tendency for accumulation due to regular use of these dyes which may lead to the hazardous effects associated with each of the identified elements.

Results from Neutron Activation Analysis (NAA) are shown in table 2. The six elements found to be present are Al, Na, Eu, Br, Ce, and Th, in trace concentrations of 31.9± 5.4, 40.6 ± 5.9, 0.16 ± 0.05, 0.18 ± 0.04, 0.37 ± 0.08, and 0.13± 0.02ppm respectively. Here also no permissible limits have been quoted specifically in hair by any Regulatory Authority for Na, Eu, Ce or Th. However, permitted level in the human body for Al is 10mg/m^3 (United States National Institute for Occupational Safety and Health) and for Br is 1ppm (United States Occupational Safety and Health Administration). Since the solid dye sample is the main constituent used in the manufacture of most other permanent hair dyes, this result is valid for all the dye brands used in this work, unless there were processes aimed at extracting these elements from the parent substance.

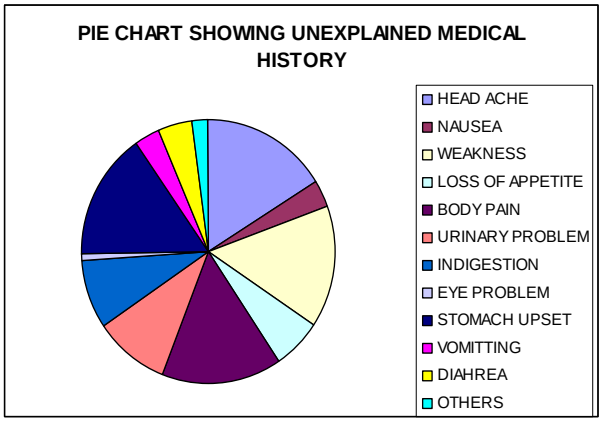

Fig. 1. Pie chart showing unexplained medical conditions.

Table 2. Result for the solid hair dye from NAA.

Elements	Symbol	Concentration (ppm)
Aluminum	Al	31.9 ± 5.4
Titanium	Ti	BDL
Calcium	Ca	BDL
Magnesium	Mg	BDL
Potassium	K	BDL
Iron	Fe	BDL
Sodium	Na	40.6 ± 5.9
Vanadium	V	BDL
Manganese	Mn	BDL
Antimony	Sb	BDL
Lanthanum	La	BDL
Samarium	Sm	BDL
Scandium	Sc	BDL
Cesium	Cs	BDL
Europium	Eu	0.16 ± 0.05
Bromine	Br	0.18 ± 0.04
Cerium	Ce	0.37 ± 0.08
Thorium	Th	0.13 ± 0.02

BDL = below detection limit

The presence of the radioactive isotope, thorium (Th), even tough in trace amounts and bromine (Br) serve as potential carcinogens. Whether the effects associated with all the elements detected are synergistic or antagonistic is yet to be proven with information available at present. In addition to elements present in the dyes analyzed, the major active ingredient; Paraphelylene diamine (PPD; IUPAC name- 1, 4-diaminobenzene) has its own cancerous effects. PPD is also the most widely used primary intermediate in hair dye formulation. Most of its cancerous effects are directed towards the bladder. The Aryl group present in PPD has high affinity for DNA.

CONCLUSIONS

The liquid dye sample, which was analyzed using Flame Atomic Absorption Spectroscopy, had five ions detected namely Fe^{2+}, Pb^{2+}, Cd^{2+}, S^{2-}, and SO_4^{2-} with concentrations of 0.702, 0.002, 0.003, 0.044 and 0.059 mg.l^{-1} respectively. The solid hair dye sample, which was analyzed using the Neutron Activation Analysis technique, had six elements (Al, Na, Eu, Br, Ce, and Th) in trace concentrations of 31.9± 5.4, 40.6 ± 5.9, 0.16 ± 0.05, 0.18 ± 0.04, 0.37 ± 0.08, and 0.13± 0.02ppm respectively. Twelve other elements (Ti, Ca, Mg, K, Fe,

V, Mn, Sb, La, Sm, Sc and Cs) were below the detection limit. No permissible limits have been quoted specifically in hair by regulatory authorities for any of the ions or elements hence comparison with such values was not possible. Consequently, these results would be taken as baseline data for future work. The presence of radioactive isotopes could serve as a possible explanation for the observation that the negative health impact of certain hair dyes is felt many years after initial use (Allan, 2005).

REFERENCES

Akaho, EHK., and Nyarko, BJB. 2002. Characterization of Neutron Flux Spectra in Irradiation Sites of MNSR Reactor using the WESCOTT Formalism for the K_o Neutron Activation Analysis Method. Accra Ghana: G.A.E.A., p. 265-273.

Allan, P. 2005. United States World Health Report on Harmful/Toxic Toiletries and Cancer Causing Chemicals. Washington DC, Jonsson Cancer Centre. p. 1-4.

Andrew, HK. 2000. Cancer of the Pancreas. American Journal of Pathology. 5:1-9.

David, RL. and Norman, EH. 2005. Handbook of Chemistry and Physics, C.R.C Press, Bocca Recton, Florida.

Hans, FM. and Tlaytmas, AM. 2000. N-acetylation of Paraphenylene Diamine in Human skin and kerainocytes. American Journal of Pharmacology and Experimental Therapeutics. 292:150-155.

Jonah, SA., Umar, IM., Oladipo, MOA., Balogun, GI. and Adeyemo, DJ. 2006. Applied Radiation and Isotopes. Zaria Nigeria, Elservier Press. p. 818-822.

Lind, ML., Boman, A., Sollenberg, J., Johnsson, S., Hagelthorn, G. and Meding, B. 2005. Occupational Deceimal Exposure to Permanent Hair Dyes Among Hairdressers. Annals of Occupational Hygiene. 49: 473-480.

Sadaji, Y., Harumi, O., Naoki, N., Junko, H. and Keiichi, U, 1982. Analysis of Hair Dyes. II Determination of Hair Dye Ingredients by High performance Liquid Chromatography. Japanese Journal of Toxicology and Environmental Health. 28:335-340.

Schrenk, WG. 1975. Analytical Atomic Spectroscopy, Plenium Press, New York. pp. 1-8.

Shih, Y., Zen, JM., Kumar, KS., Lee, YC. and Hurng, HR. 2004. Determination of the Toxic Lead Level in Cosmetic – Hair Dye Formulations Using a Screen – Printed Silver Electrode. Bulletin of the Chemical Society of Japan. 77:311-312.

Sϕoted, H., Rastogi, SC., Andersen, KE., Johansen, JD. and Menne, T. 2004. Hair Dye Contact Allergy: Quantitative Exposure Assessment of Selected Products and Clinical Cases. Contact Dermatitis. 50:344-348.

Liyu WA. 2004. Multipurpose Gamma-ray spectrum Analysis software. Beijing China: CIAE. pp. 1-6.

Vann, D. 2000. Direct Hair Dyes: Uses and Effects. American Journal of Pharmacology and Experimental Therapeutics. 292:76-81.

Vincent, U., Bordin, G. and Rodriguez, AR. 1999. Influence of Matrix Compounds on the Analysis of Oxidative Hair Dyes by HPLC. Journal of Cosmetic Science. 50:231-248.

Received: Oct 2, 2009; Accepted: Dec : 23, 2009

SENRA Academic Publishers, Burnaby, British Columbia
Vol. 4, No. 1, pp. 1119-1126, 2010
ISSN: 1715-9997

Canadian Journal of pure&applied sciences

PREDICTION OF MACHINABILITY OF SINTERED IRON COMPONENT USING RESPONSE SURFACE METHOD

*PK Bardhan[1], S Patra[2] and G Sutradhar[3]
[1] Department of Mechanical Engineering, JIS College of Engineering, Kalyani - 741235, West Bengal
[2]IIT Kharagpur - 721302, West Bengal
[3]Department of Mechanical Engineering, Jadavpur University, Kolkata-700032, India

ABSTRACT

In the present study an attempt has been made to investigate the machinability of Powder Metallurgy components. According to the literature review on this topic it has been found that very little effort has been expended so far on studying the effect of machining parameters and process variables on the machinability of Powder Metallurgy components. So it was felt necessary to carry out a systematic study of the above parameters and processes of Powder Metallurgy components. These investigations were based on Design of Experiments Technique in order to achieve optimum machinability of such components. Compacting pressure, sintering temperature and sintering time are considered as the controllable process parameters and cutting forces as the response variable. A second order response surface model (RSM) has been used to develop a predicting equation of cutting force based on the data collected by a statistical design of experiments known as central composite design (CCD). The analysis of variance (ANOVA) shows that the observed data fits well into the assumed second order responses surface model.

Keywords: Sintered components, response surface, central composite design.

INTRODUCTION

The Powder Metallurgy process has created an immense interest in many parts of the world as an economic method of producing components from metal powders (Ferguson, 1983; German, 1994). Normally it eliminates the need of secondary operations like turning, milling etc. However, to produce certain geometrical features like transverse holes, undercuts etc, some machining operations like turning and drilling are indispensable. As the use P/M materials are increasing day by day and to increase the productivity, the study of their machinability has become important (Salak *et al*., 2005). There is ample evidence from test on a wide variety of materials that machinability depends on work piece, tool material properties, cutting parameters, rigidity of the machine tools (Bothyord, 1987). It has been reported that cutting characteristics of work piece material are controlled by the alterations of the microstructure through changes in chemical compositions, additional free machining additives or by a variety of mechanical treatments (Anderson and Hirschhorn, 1977; Smith, 1990; Agapiou and Devries, 1988). Very little investigation has been carried out on the machinability of sintered P/M components (Engstrom, 1983; Salak *et al*., 2006). Moreover, machinability could not be predicted solely from the knowledge of the work piece and cutting tool properties but it is commonly determined through machining tests Measurement of cutting forces during machining processes is very important parameter and basic step to determine the machinability and performance of the workpiece. Therefore it is being felt necessary to study the effect of different process parameters on the machinability of iron P/M components. The difference of machining behavior of the P/M components with wrought products may be a subject of interest to the researchers as well as to the practicing engineers. In the present study, P/M preforms produced at different process parameters and examined the changes of Tangential cutting force during machining of the preforms at different cutting speeds. A 2^3 full factorial design of experiments (DOE) have been used to perform statistical analysis about the influence of various process parameters on the machinability of iron P/M components and a second order response surface method (RSM) have been used to developed the predicting equations of cutting forces at different cutting speed of the developed component with the variation of process parameters (Chatterjee *et al*., 2007; Boxes *et al*., 1987; Montgomery, 1991).

Experimental procedures

The iron powder used for the present investigation has been provided by Kawasaki Steel Corporation Chiba Works, Chiba, Japan. The chemical analysis and powder particle size distribution was provided by the said company as given in table 1.

Corresponding author email: pkbardhan@yahoo.com

Table 1. Chemical Analysis of iron powder (weight %).

C	Si	Mn	P	S	O	Total. Fe
0.001	0.02	0.17	0.013	0.010	0.129	Balance

Powder Properties:

Apparent Density (gm/cc): 2.94
Flow (50gm/s) : 24.7

Sieve Distribution:

Sieve Number	Size	Cumulative wt%
+ 100#	> 150 um	8.5
+ 150#	> 106 um	20.1
+ 200#	> 75 um	22.9
+ 250#	> 63 um	9.5
+ 325#	> 45 um	16.8
- 325#	< 45 um	22.2

The iron powder was compacted in a closed cylindrical die using 120 Ton hydraulic press (Lawrence & Mayo) for manufacturing of green samples (Fig. 10). Before compaction, the die and punch were lubricated with Z*n*-stearate. The sintering process was carried out in vacuum furnace (1450°C) using argon as an inert ambient (Fig. 11). The objective of present study is to throw light on the machinability of the compacted sintered samples under different processing conditions. In this context 60 different P/M components (25mm diameter) were produced as per the design of experiment (DOE). Related machining parameter like cutting forces during machining of these samples were studied against the variation of controllable input process variables like compaction pressure, sintering time and sintering temperature. In this experiment three different cutting speeds were used to find out the tangential cutting forces under constant depth of cut (0.50mm) and feed (0.1 mm/rev). The use of low feed minimizes the effect of temperature influence on the work piece. Cutting forces were measured in the lathe tool dynamometer (Strain gauge type, Syscon Instruments Pvt. Ltd., Bangalore, India) and relevant cutting tool (tungsten carbide) used was TCMX 11 03 04 - WF12 grade supplied by Sandvik India Ltd. The results obtained through the experiments are given in table 2 and all the available data have been analyzed using response surface method and using Minitab software (Version 14).

Effect of process parameters on machinability is illustrated below.

In order to perform test of significance for individual process parameters as well as their interactions, the following standard equation is considered.

$$R2 = \beta_o + \beta_1 x_1 + \beta_2 x_2 + \beta_3 x_3 + \beta_{12} x_1 x_2 + \beta_{13} x_1 x_3 + \beta_{23} x_2 x_3 + \beta_{123} x_1 x_2 x_3 + \varepsilon, \quad (1)$$

The corresponding fitted equation can be expressed as follows:

$$\acute{R}2 = E(R2 - \varepsilon) = \hat{\beta}_o + \hat{\beta}_1 x_1 + \hat{\beta}_2 x_2 + \hat{\beta}_3 x_3 + \hat{\beta}_{12} x_1 x_2 + \hat{\beta}_{13} x_1 x_3 + \hat{\beta}_{23} x_2 x_3 + \hat{\beta}_{123} x_1 x_2 x_3. \quad (2)$$

Table 2 shows the parameter settings for performing statistical test on the degree of significance of process parameters and their interactions. For any factor z_i, the transformation from actual to coded values has been performed considering the equations (3) – (5) as given below:

$$z_i^o = \frac{z_i^{\max} + z_i^{\min}}{2}, \quad (3)$$

$$\Delta z_i = \frac{z_i^{\max} - z_i^{\min}}{2}, \quad (4)$$

$$x_i = \frac{z_i - z_i^o}{\Delta z_i}. \quad (5)$$

A full factorial experimental design (l^k) with six additional central points (n_c) has been considered for performing the statistical analysis. The six additional central points give an estimate of experimental error. Table 2 gives the observed data for different settings of process parameters. The data have been collected conducting the experiments in a random order of run numbers and equation (1) has been developed using observed data obtain from the experiment using MINITAB software (Version 14). The coefficients of the fitted equations can be obtained from equation (6) as given below [16].

$$\mathbf{B_1} = (\mathbf{X}^T \mathbf{X})^{-1} \mathbf{X}^T \mathbf{T_f}, \quad (6)$$

where

$\mathbf{B_1} = [\hat{\beta}_0 \ \hat{\beta}_1 \ \hat{\beta}_2 \ \hat{\beta}_3 \ \hat{\beta}_{12} \ \hat{\beta}_{13} \ \hat{\beta}_{23} \ \hat{\beta}_{123}]^T$,

$\mathbf{X} = [\mathbf{x_0} \ \mathbf{x_1} \ \mathbf{x_2} \ \mathbf{x_3} \ \mathbf{x_{12}} \ \mathbf{x_{13}} \ \mathbf{x_{23}} \ \mathbf{x_{123}}]$,

$\mathbf{x_o} = [1 \ 1 \ 1 \ 1 \ 1 \ 1 \ 1 \ 1]^T$,

$\mathbf{x_1} = [-1 \ 1 \ -1 \ 1 \ -1 \ 1 \ -1 \ 1]^T$,

$\mathbf{x_2} = [-1 \ -1 \ 1 \ 1 \ -1 \ -1 \ 1 \ 1]^T$,

$\mathbf{x_3} = [-1 \ -1 \ -1 \ -1 \ 1 \ 1 \ 1 \ 1]^T$

$\mathbf{x_{12}} = [1 \ -1 \ -1 \ 1 \ 1 \ -1 \ -1 \ 1]^T$,

$\mathbf{x_{13}} = [1 \ -1 \ 1 \ -1 \ -1 \ 1 \ -1 \ 1]^T$,

$\mathbf{x_{23}} = [1 \ 1 \ -1 \ -1 \ -1 \ -1 \ 1 \ 1]^T$,

$\mathbf{x_{123}} = [-1 \ 1 \ 1 \ -1 \ 1 \ -1 \ -1 \ 1]^T$,

In order to get the regression equations of Tangential cutting force (R_2) using the data of table 2, we have used the Minitab statistical software to get the desire result more precisely.

The following ANOVA observations were done at 3 different cutting speeds.

Table 2. Observed Tangential cutting forces at different cutting speed – values for different settings of process parameters based on 2^3 full factorial designs.

Sl. No.	Coded Value of Parameters			Actual Value of Parameters			Response variables Tangential Cutting Forces. (Kgf.)		
	x_1	x_2	x_3	Compaction Ton	Sintering. Temp °c	Sintering. Time hour	R2 (@ cutting speed 4.24 m/min.)	R2 (@ cutting speed 18.37m/min)	R2 (@ cutting speed 27.95 m/min)
1	-1	-1	-1	17.66	975	1	14	16	15
2	1	-1	-1	26.49	975	1	18	21	18
3	-1	1	-1	17.66	1125	1	12	15	16
4	1	1	-1	26.49	1125	1	19	20	18
5	-1	-1	1	17.66	975	2	17	18	16
6	1	-1	1	26.49	975	2	19	20	18
7	-1	1	1	17.66	1125	2	13	15	14
8	1	1	1	26.49	1125	2	22	21	18
9	-1.6818	0	0	14.6499	1050	1.5	11	15	11
10	1.68179	0	0	29.5001	1050	1.5	27	23	20
11	0	-1.6818	0	22.075	923.87	1.5	16	17	16
12	0	1.68179	0	22.075	1176.13	1.5	19	18	17
13	0	0	-1.6818	22.075	1050	0.6591	16	16	16
14	0	0	1.68179	22.075	1050	2.3409	16	18	17
15	0	0	0	22.075	1050	1.5	18	16	14
16	0	0	0	22.075	1050	1.5	17	16	15
17	0	0	0	22.075	1050	1.5	19	18	16
18	0	0	0	22.075	1050	1.5	18	18	16
19	0	0	0	22.075	1050	1.5	17	17	16
20	0	0	0	22.075	1050	1.5	15	18	15
21	-1	-1	-1	17.66	975	1	13	15	14
22	1	-1	-1	26.49	975	1	18	20	17
23	-1	1	-1	17.66	1125	1	14	16	16
24	1	1	-1	26.49	1125	1	18	21	18
25	-1	-1	1	17.66	975	2	16	17	15
26	1	-1	1	26.49	975	2	19	21	19
27	-1	1	1	17.66	1125	2	14	16	15
28	1	1	1	26.49	1125	2	21	20	19
29	-1.6818	0	0	14.6499	1050	1.5	10	15	10
30	1.68179	0	0	29.5001	1050	1.5	26	24	19
31	0	-1.6818	0	22.075	923.87	1.5	17	18	17
32	0	1.68179	0	22.075	1176.13	1.5	18	19	17
33	0	0	-1.6818	22.075	1050	0.6591	17	16	16
34	0	0	1.68179	22.075	1050	2.3409	16	17	17
35	0	0	0	22.075	1050	1.5	17	17	16
36	0	0	0	22.075	1050	1.5	17	18	16
37	0	0	0	22.075	1050	1.5	18	17	17
38	0	0	0	22.075	1050	1.5	19	18	17
39	0	0	0	22.075	1050	1.5	18	18	16
40	0	0	0	22.075	1050	1.5	16	17	16
41	-1	-1	-1	17.66	975	1	14	16	16
42	1	-1	-1	26.49	975	1	19	20	19
43	-1	1	-1	17.66	1125	1	14	17	15
44	1	1	-1	26.49	1125	1	19	21	18
45	-1	-1	1	17.66	975	2	16	18	16
46	1	-1	1	26.49	975	2	20	21	17
47	-1	1	1	17.66	1125	2	15	16	13
48	1	1	1	26.49	1125	2	21	21	19
49	-1.6818	0	0	14.6499	1050	1.5	12	14	11
50	1.68179	0	0	29.5001	1050	1.5	28	23	21
51	0	-1.6818	0	22.075	923.87	1.5	17	17	17
52	0	1.68179	0	22.075	1176.13	1.5	20	18	18
53	0	0	-1.6818	22.075	1050	0.6591	16	17	16
54	0	0	1.68179	22.075	1050	2.3409	18	19	17
55	0	0	0	22.075	1050	1.5	17	17	15
56	0	0	0	22.075	1050	1.5	18	18	16
57	0	0	0	22.075	1050	1.5	20	19	16
58	0	0	0	22.075	1050	1.5	17	18	17

Table 3. Analysis of variance (ANOVA).

For cutting speed 4.24m/min.
Analysis of Variance for R2 (Tangential Cutting Force)

Source	DF	Seq SS	Adj SS	Adj MS	F	P
Regression	9	534.881	534.881	59.4312	25.52	0.000
Linear	3	505.651	9.516	3.1719	1.36	0.065
Square	3	19.772	19.772	6.5907	2.83	0.048
Interaction	3	9.458	9.458	3.1528	1.35	0.068
Residual Error	50	116.452	116.452	2.3290		
Lack-of-Fit	5	73.286	73.286	14.6572	15.28	0.000
Pure Error	45	43.167	43.167	0.9593		
Total	59	651.333				

R-Sq = 85.1%

For cutting speed 18.37m/min.
Analysis of Variance for R2 (Tangential Cutting Force)

Source	DF	Seq SS	Adj SS	Adj MS	F	P
Regression	9	249.182	249.182	27.6869	43.71	0.000
Linear	3	228.757	228.757	76.2523	120.39	0.000
Square	3	15.592	15.592	5.1973	8.21	0.000
Interaction	3	4.833	4.833	1.6111	2.54	0.067
Residual Error	50	31.668	31.668	0.6334		
Lack-of-Fit	5	7.390	7.390	1.4780	2.74	0.030
Pure Error	45	24.278	24.278	0.5395		
Total	59	280.850				

R-Sq = 88.7%

For cutting speed 27.95m/min.
Analysis of Variance for R2 (Tangential Cutting Force)

Source	DF	Seq SS	Adj SS	Adj MS	F	P
Regression	9	189.612	189.612	21.0680	23.42	0.000
Linear	3	173.127	9.744	3.2481	3.61	0.019
Square	3	13.360	13.360	4.4535	4.95	0.004
Interaction	3	3.125	3.125	1.0417	1.16	0.335
Residual Error	50	44.988	44.988	0.8998		
Lack-of-Fit	5	21.210	21.210	4.2420	8.03	0.000
Pure Error	45	23.778	23.778	0.5284		
Total	59	234.600				

equations of tangential cutting force for different cutting speed.

(i) The equation for tangential cutting force at cutting speed 4.24 m/min is represented as R2 = 26.0572 – 1.9883X1 – 0.008X2 + 8.4286X3 – $2.19X3^2$ + 0.0019X1X2 + 0.0189X1X3 – 0.0011X2X3

(ii) The equation for tangential cutting force at cutting speed 18.37 m/min R2 = 17.5984 + 2.3365X1 + 0.0235X2 + 0.3517X3 + $0.574X1^2$ + $0.1625X2^2$ – $0.742X3^2$ + 0.25X1X2 - 0.6617X1X3 – 0.3338X2X3

(iii) The equation for tangential cutting force at cutting speed 27.95 m/min R2 = 103.208 – 0.047X1 - 0.177X2 + 0.535X3 – $0.007X1^2$ + $1.137X3^2$ + 0.001X1X2 + 0.094X1X3 – 0.006X2X3

From these equations we can predict the tangential cutting force at different cutting speeds and against the input process parameters, compaction (X1), sintering temperature (X2) & sintering time (X3).

RESULTS AND DISCUSSION

Studies on machinability of sintered P/M components have attracted substantial research interest in contemporary manufacturing technology. This issue has been addressed in a number of previous communications. Some of the researchers investigated machinability in porous iron components (Šalak *et al.*,2005). In the present study we focus on machinability of sintered P/M components through the measurement of cutting forces at

various cutting speeds. At the cutting speed of 4.24m/min the nature of variation of Tangential cutting force (R2) is illustrated in (Figs. 1-3). The tangential cutting force is strongly influenced by the variation of compaction (X1), sintering time (X3) and sintering temperature (X2). When the cutting speed is increased to 18.37m/min. the nature of variation (Figs. 4–6) of tangential cutting force against compaction and sintering temperature remains similar to that obtained at the cutting speed of 4.24m/min. This features are compared in figures 1 and 4. However, variation of tangential cutting force against simultaneous variation of sintering time and sintering temperature (Fig. 5) are different from that observed at cutting speed 4.24m/min. Similarly, the response parameter like tangential cutting force shows almost consistent behavior when the sintering time and compaction are chosen as variables (Fig. 6). In this perspective, it is worth mentioning that in each cutting speed, tangential cutting force is also influenced by all the three parameters.

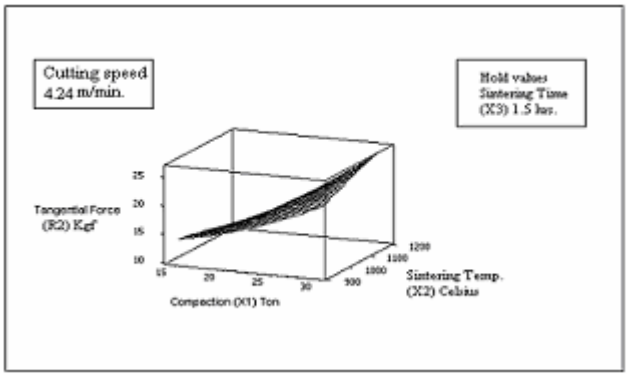

Fig.1. Surface Plot of Tangential Force R2vs Sintering Temp.(X2), Compaction(X1).

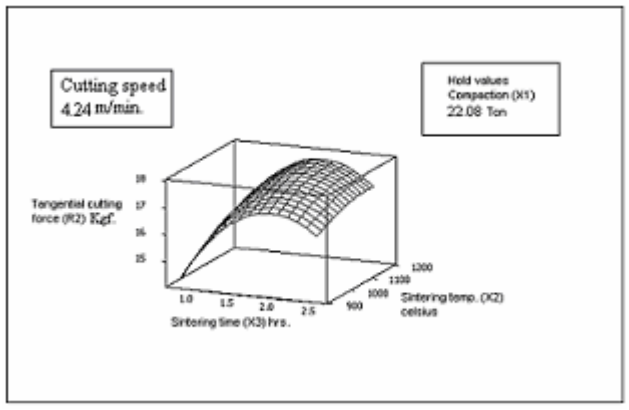

Fig. 2. Surface Plot of Tangential Force R2vs Sintering Temp.(X2), Sintering time(X3).

We notice some intriguing feature in the variation of tangential cutting force against compaction load (X1), sintering temperature (X2) and sintering time (X3). The cutting force gradually increases with the increase in compacting load (X1) and sintering temp (X2). In addition, we noticed that in general, samples sintered at lower sintering time (X3) produces higher cutting force under relatively higher sintering temperature. Moreover, tangential cutting force shows increasing tendency with the simultaneous increase of sintering time and compaction load.

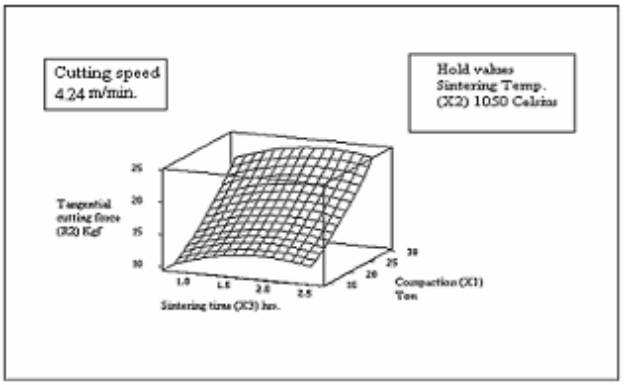

Fig. 3. Surface Plot of Tangential Force R2vs Compaction (X1), Sintering time (X3).

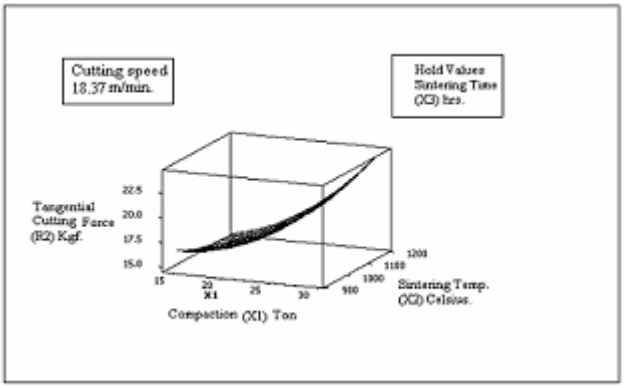

Fig. 4. Surface Plot of Tangential Force R2vs Sintering Temp. (X2), Compaction(X1).

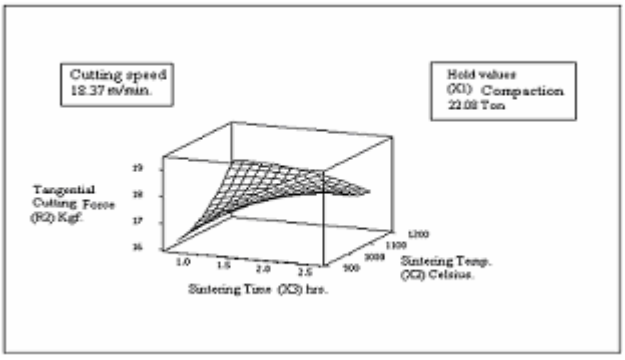

Fig. 5. Surface Plot of Tangential Force R2vs Sintering Temp. (X2), Sintering Time (X3).

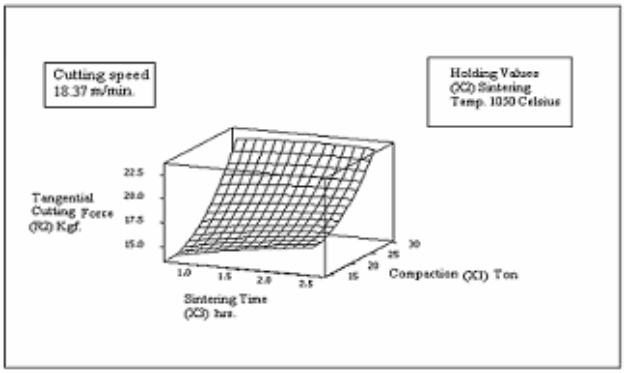

Fig. 6. Surface Plot of Tangential Force, R2vs Compaction (X1), Sintering time (X3).

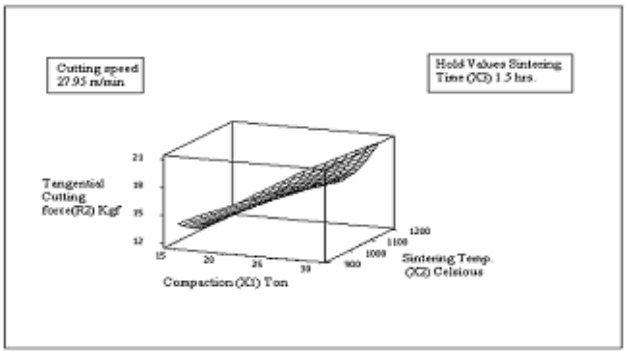

Fig. 7. Surface Plot of Tangential Force R2vs Sintering Temp. (X2), Compaction (X1).

Nature of variation of tangential cutting force at the cutting speed of 27.95 m/min. is depicted in (Figs. 7-9). The figure illustrates a gradual increase in tangential cutting force due to increase of compaction load and temperature. The nature of variation of tangential cutting force against sintering time and compaction load are analogous to that of (Fig. 7). However, it is observed that completely distinct behavior in the variation of tangential cutting force against sintering time and temperature.

A systematic experimental study was performed on the machinability of 60 different sintered P/M iron samples based on DOE. The tangential cutting force was measured during the machining of the above samples under various cutting speeds. Results obtained during experimentation have been analyzed through response surface methodology. Our study reveals that at each cutting speeds, the tangential cutting force is strongly influenced by the variations of sintering temperature, sintering time and compaction. These studies have also revealed that during machining sintered P/M components, the magnitude of tangential cutting force is determined by different external features like compaction load, sintering temperature and sintering time. The Table 3 presents the ANOVA (Analysis of variances) for the second order response surface equations, which quite clearly show that second order response surface model fit well into the observed data. This is evident from the findings that co-efficient of determination (R^2) values are between 82 and 88%. Hence, it may be concluded that the prediction made by this developed model corroborates well with experimental observations. It is expected that the present study will of great importance to the professionals as well as the academicians working in this area.

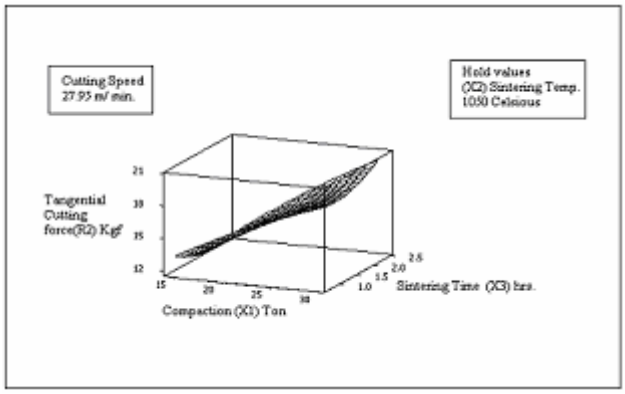

Fig. 8. Surface Plot of Tangential Force R2vs Sintering Time (X3), Compaction (X1).

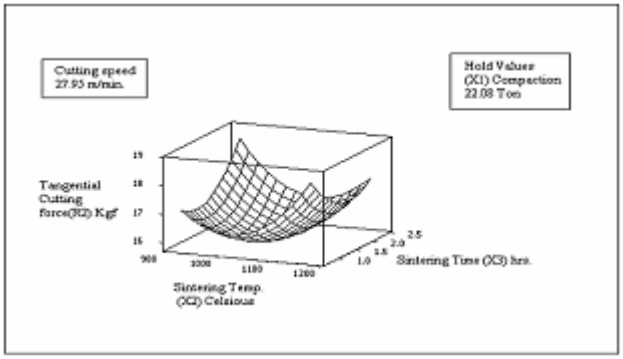

Fig. 9. Surface Plot of Tangential Force R2vs Sintering Time (X3), Sintering Temp.(X2).

CONCLUSIONS

A 2^3 full factorial design of experiments (DOE) have been used to perform statistical analysis of the effect of various process parameters on the machinability of sintered iron P/M component. Second order response surface method (RSM) have been used to develop the predicting equations of cutting force based on the data collected using a statistical design of experiments known as central composite design (CCD) for different cutting speeds. Analysis of variance (ANOVA) presented in Table 3 show that the observed data fits well into the assumed second order RSM model. The surface plots of response surfaces show the existence of optimum values of process parameter for different cutting force of sintered iron components. For the same cutting speed the tangential cutting force is influenced by all the three input processes

parameters (X1, X2 & X3). At a relatively higher cutting speed also the tangential cutting force shows similar behavior as in the case of simultaneous variation of compaction, sintering temperature & sintering time. It is worth mentioning that the overall development of new P/M components also requires a thorough analysis of hardness of material against the external variables which we plan to report in our future communication.

Fig. 10. Hydraulic press (120 Ton).

Fig. 11. Tubular vacuum furnace (1450°C).

Fig. 12. Lathe with Tool dynamometer Force display unit.

ACKNOWLEDGEMENTS

Authors are very much grateful to All India Council for Technical Education, New Delhi [F-No. 8021 /RID/NPROJ/R&D-174/2002-03/ (Revalidated 2003-2004)] for funding this Project. Authors also like to acknowledge their sincere thanks to M/S Kawasaki Steel Corporation Chiba Works, Chiba, Japan for sending 4 Kg iron Powder along with the certificate of chemical analysis free of cost for this study.

Nomenclature

α distance from the centre point of the design to a star point (*star arm*)

$\mathbf{B_1}$ $[\hat{\beta}_o \ \hat{\beta}_1 \ \hat{\beta}_2 \ \hat{\beta}_3 \ \hat{\beta}_{12} \ \hat{\beta}_{13} \ \hat{\beta}_{23} \ \hat{\beta}_{123}]^T$

$\mathbf{B_2}$ $[\hat{\beta}_o \ \hat{\beta}_1 \ \hat{\beta}_2 \ \hat{\beta}_3 \ \hat{\beta}_{11} \ \hat{\beta}_{22} \ \hat{\beta}_{33} \ \hat{\beta}_{12} \ \hat{\beta}_{13} \ \hat{\beta}_{23}]^T$

β_o *free term* of the regression equation

β_i regression coefficient of *i*th process parameter (*linear terms*)

β_{ij} regression coefficient of interaction between *i*th and *j*th process parameters (*interaction terms*)

β_{ii} regression coefficient of self interaction of *i*th process parameter (*quadratic terms*)
β_{ijk} regression coefficient of interaction among *i*th, *j*th and *k*th process parameters
$\hat{\beta}_o$ estimated value of β_o
$\hat{\beta}_i$ estimated value of β_i
$\hat{\beta}_{ij}$ estimated value of β_{ij}
$\hat{\beta}_{ii}$ estimated value of β_{ii}
$\hat{\beta}_{ijk}$ estimated value of β_{ijk}
$E(x)$ mathematical expectation of the variable x
E an error component
$R2$ Tangential Cutting Force
Ŕ2 Average value of Tangential Cutting Force
K number of controllable process parameters
l number of levels for each process parameter
m number of coefficients in the regression equation
N total number of design points = $n_f + n_a + n_c$
n_a number of axial points = $2k$
n_c number of central points
n_f number of points used in factorial positions = 2^k
σ_{β}^2 variance of regression coefficients
σ_{res}^2 residual variance
σ_e^2 estimate of error (replication variance)
$t_{estimated}$ estimated t value
$t_{\alpha_s,\nu}$ value of Students t distribution for α_s level of significance and ν degrees of freedom
$\mathbf{X}$ a matrix formed by column vector $\mathbf{x_o}$, $\mathbf{x_1}$, $\mathbf{x_2}$, $\mathbf{x_3}$,…..etc
$\mathbf{X^T}$ transpose of the matrix $\mathbf{X}$
x_i coded value of *i*th process parameter
$\mathbf{x_o}$ column vector of dummy variable i.e column of 1' s
$\mathbf{x_i}$ column vector of coded values for process parameter x_i
$\mathbf{x_{ij}}$ [scalar product of column vectors $\mathbf{x_i}$ and $\mathbf{x_j}$]
$\mathbf{x_{ijk}}$ [scalar product of column vectors $\mathbf{x_i}$, $\mathbf{x_j}$ and $\mathbf{x_k}$]
z_i actual value of *i*th process parameter
z_i^{max} maximum actual value of the *i*th process parameter
z_i^{min} minimum actual value of the *i*th process parameter
z_i^o centre point of the design or the basic level of the *i*th process parameter
Δz_i unit or interval of variation on the z_i axis for the *i*th process parameter.

REFERENCES

Agapiou, JS. and Devries, MF. 1988. Machinability of Powder Metallurgy Materials. The International Journal of powder Metallurgy. 24(10):47-56.

Anderson, PJ.and Hirschhorn, JS. 1977. Use of Additives to improve the machinability of sintered steel. Modern developments in Powder metallurgy. 10:477-490.

Boxes, GEP. and Hunter, JS. 1957. Multifactor Experimental Designs for Exploring Response Surfaces. Annals of Mathematical Statistics. 28:195-242.

Boxes, GEP. and Draper, NR. 1987. Empirical Model Building and Response Surfaces. Wiley, New York.

Bothyord, G. 1987. Fundamental of Metal Machining and Machine Tools. McGraw-Hill Book Company, Singapore.

Chatterjee, D., Oraon, B., Sutradhar, G. and Bose, PK. 2007. Prediction of hardness for sintered HSS components using response surface method. Journal of Material Processing Technology. 190:123-129.

Engstrom. U. 1983. Machinability of Sintered Steels. Powder metallurgy. 26 (3):137-143.

Ferguson, BL. 1983. Ferrous Powder Metallurgy. Part II, American Powder Metallurgy Institute, New York.

German, RM. 1994. Powder metallurgy Science. Metal Powder Industries Federation. Prinston, USA.

Muthukrishnan, N. and Davim, JP. 2009. Optimization of machining parameters of AL/Sic-MNC with ANOVA and ANN analysis. Materials processing Technology. 209:225-232.

Montgomery, DC.1991. Design and Analysis of Experiments. John Wiley & Sons.

Salak, A., Vasilko, K., Selecka, M. and Danninger, H. 2006. New short time face turning method for testing the machinability of PM Steel. Journal of Materials Processing Technology. 176:62-69.

Smith, GT. 1990. Powder metallurgy secondary machining operations and resulting surface integrity. Surface Topography. 3:25-42.

Šalak, A., Selecka, M. and Danninger, H. 2005. Machinability of powder metallurgy steels. Cambridge International Science Publishing.

Received: Oct 27, 2009; Revised: Jan 6, 2010; Accepted: Jan 7, 2010